Vol. 269, No. 2, November 20, 1992
Completing Volume 269

ISSN 0003-2670

ANALYTICA CHIMICA ACTA

An international journal devoted to all branches of analytical chemistry

ELSEVIER

ANALYTICA CHIMICA ACTA

Scope. *Analytica Chimica Acta* publishes original papers, preliminary communications and reviews dealing with every aspect of modern analytical chemistry. Reviews are normally written by invitation of the editors, who welcome suggestions for subjects. Preliminary communications of important urgent work can be printed within four months of submission, if the authors are prepared to forego proofs.

Submission of Papers

Americas

Prof. Harry L. Pardue
Department of Chemistry
1393 BRWN Bldg, Purdue University
West Lafayette, IN 47907-1393
USA
Tel:(+1-317) 494 5320
Fax:(+1-317) 496 1200

Computer Techniques

Prof. J.T. Clerc
Universität Bern
Pharmazeutisches Institut
Baltzerstrasse 5, CH-3012 Bern
Switzerland
Tel:(+41-31) 654171
Fax:(+41-31) 654198

Other Papers

Prof. Alan Townshend
Department of Chemistry
The University
Hull HU6 7RX
Great Britain

Tel:(+44-482) 465027
Fax:(+44-482) 466410

Prof. Willem E. van der Linden
Laboratory for Chemical Analysis
Department of Chemical Technology
Twente University of Technology
P.O. Box 217, 7500 AE Enschede
The Netherlands
Tel:(+31-53) 892629
Fax:(+31-53) 356024

Prof. Paul Worsfold
Dept. of Environmental Sciences
University of Plymouth
Plymouth PL4 8AA
Great Britain

Tel:(+44-752) 233006
Fax:(+44-752) 233009

Submission of an article is understood to imply that the article is original and unpublished and is not being considered for publication elsewhere. *Anal. Chim. Acta* accepts papers in English only. There are no page charges. Manuscripts should conform in layout and style to the papers published in this issue. See inside back cover for "Information for Authors".

Publication. *Analytica Chimica Acta* appears in 14 volumes in 1993. The subscription price for 1993 (Vols. 267–280) is Dfl. 4214.00 plus Dfl. 462.00 (p.p.h.) (total approx. US$ 2816.75). *Vibrational Spectroscopy* appears in 2 volumes in 1993. The subscription price for *Vibrational Spectroscopy* (Vols. 4 and 5) is Dfl. 700.00 plus Dfl. 66.00 (p.p.h.) (total approx. US$ 461.50). The price of a combined subscription (*Anal. Chim. Acta* and *Vib. Spectrosc.*) is Dfl. 4592.00 plus Dfl. 528.00 (p.p.h.) (total approx. US$ 3084.25). All earlier volumes (Vols. 1–266) except Vols. 23 and 28 are available at Dfl. 259.50 (US$ 156.25), plus Dfl. 18.00 (US$ 10.75) p.p.h., per volume. The Dutch guilder price is definitive. The U.S. dollar price is subject to exchange-rate fluctuations and is given only as a guide. Subscriptions are accepted on a prepaid basis only, unless different terms have been previously agreed upon.
Our p.p.h. (postage, packing and handling) charge includes surface delivery of all issues, except to subscribers in the U.S.A., Canada, Australia, New Zealand, China, India, Israel, South Africa, Malaysia, Thailand, Singapore, South Korea, Taiwan, Pakistan, Hong Kong, Brazil, Argentina and Mexico, who receive all issues by air delivery (S.A.L.–Surface Air Lifted) at no extra cost. For Japan, air delivery requires 25% additional charge of the normal postage and handling charge; for all other countries airmail and S.A.L. charges are available upon request.

Subscription orders. Subscription orders can be entered only by calendar year and should be sent to: Elsevier Science Publishers B.V., Journals Department, P.O. Box 211, 1000 AE Amsterdam, The Netherlands. Tel: (+31-20) 5803 642, Telex: 18582, Telefax: (+31-20) 5803598, to which requests for sample copies can also be sent. Claims for issues not received should be made within six months of publication of the issues. If not they cannot be honoured free of charge. Readers in the U.S.A. and Canada can contact the following address: Elsevier Science Publishing Co. Inc., Journal Information Center, 655 Avenue of the Americas, New York, NY 10010, U.S.A. Tel: (+1-212) 6333750, Telefax: (+1-212) 6333990, for further information, or a free sample copy of this or any other Elsevier Science Publishers journal.
Advertisements. Advertisement rates are available from the publisher on request.

Detailed "Instructions to Authors" for *Analytica Chimica Acta* was published in Volume 256, No. 2, pp. 373–376. Free reprints of the "Instructions to Authors" of *Analytica Chimica Acta* and *Vibrational Spectroscopy* are available from the Editors or from: Elsevier Science Publishers B.V., P.O. Box 330, 1000 AH Amsterdam, The Netherlands. Telefax: (+31-20) 5862845.

US mailing notice – Analytica Chimica Acta (ISSN 0003-2670) is published biweekly by Elsevier Science Publishers (Molenwerf 1, Postbus 211, 1000 AE Amsterdam). Annual subscription price in the USA US$ 2816.75 (subject to change), including air speed delivery. Application to mail at second class postage rate is pending at Jamaica, NY 11431. *USA Postmasters*: Send address changes to Anal. Chim. Acta, Publications Expediting, Inc., 200 Meacham Av., Elmont, NY 11003. Airfreight and mailing in the USA by Publication Expediting.

ANALYTICA CHIMICA ACTA

An international journal devoted to all branches of analytical chemistry

(Full texts are incorporated in CJELSEVIER, a file in the Chemical Journals Online database available on STN International; Abstracted, indexed in: Aluminum Abstracts; Anal. Abstr.; Biol. Abstr.; BIOSIS; Chem. Abstr.; Curr. Contents Phys. Chem. Earth Sci.; Engineered Materials Abstracts; Excerpta Medica; Index Med.; Life Sci.; Mass Spectrom. Bull.; Material Business Alerts; Metals Abstracts; Sci. Citation Index)

VOL. 269 NO. 2 CONTENTS NOVEMBER 20, 1992

(Continued overleaf)

Contents (continued)

Analytica Chimica Acta, 269 (1992) 167–175
Elsevier Science Publishers B.V., Amsterdam

Thickness-shear mode acoustic wave sensors and flow-injection analysis

Mengsu Yang and Michael Thompson

Department of Chemistry, University of Toronto, 80 St. George Street, Toronto, Ontario M5S 1A1 (Canada)

(Received 11th May 1992; revised manuscript received 8th July 1992)

Abstract

A feasibility study of the combination of the flow-injection analysis (FIA) technique with the piezoelectric acoustic wave sensor (thickness-shear mode, TSM) is described. Flow-injection systems provide a method to relate the hydrodynamic response of the sensor to the concentration–time profile of the analyte produced by the dispersion behaviour of sample zones. Network analysis of the TSM sensor generates multi-dimensional information on the bulk properties of the liquid sample and surface properties at the liquid/solid interface. The relationship between acoustic energy transmission and the interfacial structure, viscosity, density and dielectric constant of the analyte is discussed. The FIA–TSM system provides a rapid, reproducible detection method with enhanced sensitivity and scope.

Keywords: Acoustic methods; Flow injection; Piezoelectric sensors; Acoustic wave sensor

Thickness-shear mode (TSM) piezoelectric acoustic wave devices have been used as a microbalance in the gas phase based on the observation of Sauerbrey [1] that changes in the resonant frequency of the device are proportional to mass changes on the piezoelectric crystal. In recent times, increasing attention has been paid to the operation and application of the TSM sensors in the liquid phase [2]. Studies have been made in areas including liquid chromatographic detection [3], immunoassay [4], liquid-phase properties [5] and the electrochemical microbalance [6]. In addition, several attempts have been made to provide theories for coupling of the oscillating sensor surface to a liquid medium [7–11]. These have been reviewed recently [2].

Previous studies of TSM devices in liquids have almost exclusively used the oscillator method. In this method the quartz crystal is part of an oscillator circuit. It is connected between the output and input of the oscillator amplifier and provides positive feedback to cause oscillation of the circuit. The resonant frequency of the quartz crystal is measured by a standard frequency counter. There are some serious limitations associated with the oscillator method: as the series resonant frequency is the sole parameter measured, the method only partially characterizes the device; the resonant frequency depends on the components of the oscillator circuit; and the oscillator will not function in certain situations, notably when the crystal is in a liquid of high viscosity. More recently, the network analysis method has been developed to characterize completely a TSM acoustic wave device [12]. This technique provides the characteristic parameters to more completely describe the behaviour of the TSM device in the liquid phase. The prominent parameters obtained from the impedance measurements are the resonant frequencies, the

Correspondence to: M. Thompson, Department of Chemistry, University of Toronto, 80 St. George Street, Toronto, Ontario M5S 1A1 (Canada).

phases and magnitudes of the impedances and the equivalent electrical circuit elements. All the quantities can be related to physical properties of the quartz and surrounding environments through electromechanical analysis [12,13].

In this paper the use of network analysis of the TSM quartz crystal sensor in combination with the flow-injection technique is reported. Flow-injection analysis (FIA) is a well known and widely used technique, especially in the field of process monitoring, owing to its relative simplicity and high precision [14]. The application of gradient techniques, the versatility of manifold design and the use of FIA as a sample transport system have also made FIA an attractive tool in the field of clinical analysis and biotechnology [15,16]. Combination of FIA and the TSM acoustic wave sensor will provide new opportunities for detection capability in automated analysis. The purpose of the work described here was to evaluate the feasibility of coupling a flow-injection system to a TSM sensor and to identify the analytical features of the combination.

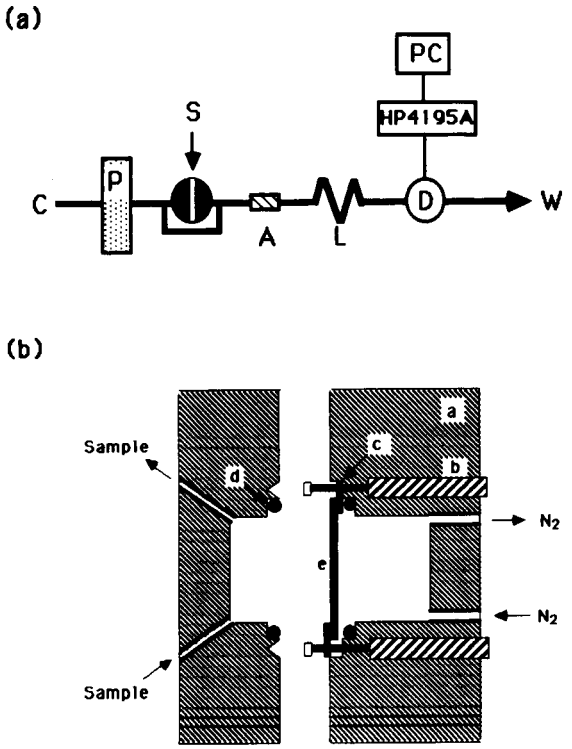

Fig. 1. (a) Single-line manifold for the FIA–TSM system. The sample (S) is injected into a carrier stream (C) and then passed through an air trap (A) and mixing coil (L) before reaching the TSM acoustic wave detector (D). (b) Flow cell: a = plexiglas blocks; b = screws and springs leading to network analyser; c = gold leads; d = O-rings; e = piezoelectric crystal. The two blocks are held together with a clamp. The diagram is not to scale.

EXPERIMENTAL

Reagents

Glycerol (Fisher), potassium chloride (BDH), sodium chloride (BDH) and lithium chloride (Alfa Inorganics) were dissolved in doubly distilled water to prepare standard solutions. Hexadecanethiol (Aldrich) was used as received. All other chemicals were of analytical-reagent grade. Doubly distilled water was used as the carrier.

Apparatus

A single-line FIA manifold (Fig. 1a) was used in all experiments. A four-channel EVA-Pump Model 1000 peristaltic pump (Eppendorf) was adapted and combined with a EVA-Valve Model 2000 injector valve (Eppendorf). The PTFE tubing for the sample loop had an i.d. of 0.5 mm and all other tubing had an i.d. of 0.8 mm.

The 9-MHz AT-cut quartz piezoelectric crystals coated with either gold or silver electrodes were supplied by International Crystal Manufacturing (Oklahoma City, OK). The instrument used to characterize the quartz crystal was an HP 4195A Network/Spectrum Analyser (Hewlett-Packard). The HP 41951A impedance test kit and HP 16092A spring clip fixture were used to make impedance measurements directly. The values of the equivalent circuit elements of the quartz crystal are calculated internally by the HP 4195A from the measured data.

The electrodes of the quartz crystals were cleaned in a PD-3XG plasma cleaner (Harrick) to generate a hydrophilic surface. The hydrophobic surfaces were prepared by self-assembly of hexadecanethiol on to the gold or silver electrodes following a published procedure [17]. A Remy-Hart goniometer was used to measure the ad-

vancing contact angles of water on various surfaces.

Flow cell

The design of the flow cell is shown in Fig. 1b. The two Plexiglas blocks are held together with a clamp to give a cell volume of about 10 μl for the liquid flow. The other side of the crystal was under nitrogen in order to reduce the interference from the atmosphere. The electrodes of the crystal held in the flow cell are connected with two gold leads, which are fixed with screws on the block. Two springs are connected to the screws and lead to the HP 16092A fixture with a cable.

Procedures

The HP 4195A network analyser was calibrated at a centre frequency of 9 MHz (with 120 kHz band width). The instrument scans 100 points across the frequency range in 0.5 s. A user program was edited to scan the frequency range and collect the characteristic parameters continuously. The acquisition time for each set of parameters can be controlled from less than 1 s to 10 min. It was adjusted at 2.3 s per set for all the experiments unless specified otherwise.

RESULTS AND DISCUSSION

Network analysis method

Detailed theories to describe the behaviour of the piezoelectric crystal have been derived by Cady [18] and Bottom [19]. The analysis of the coupling between mechanical displacement and electrical potential in the piezoelectric quartz crystal results in a complex quantity as a function of the properties of quartz and frequency. The complex quantity, defined as the electrical impedance (the reciprocal of admittance), is the ratio of the voltage across the crystal to the current flowing through the crystal. The complex quantity can be interpreted as an electrical circuit, which responds to an applied voltage in the same way as the quartz crystal itself.

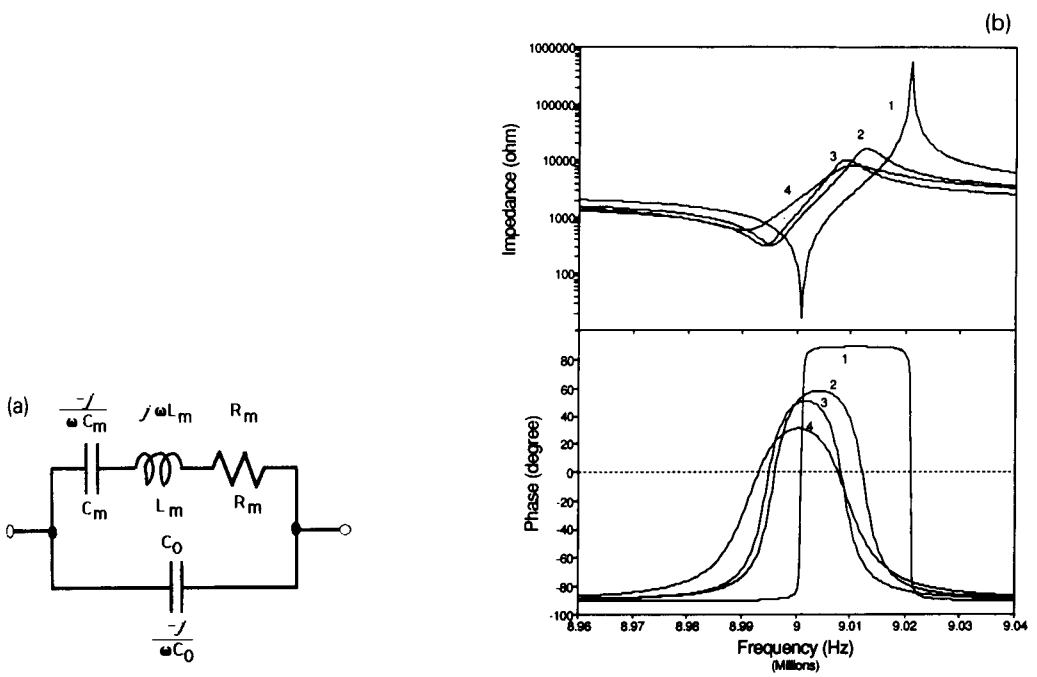

Fig. 2. Circuit elements and respective impedances of the equivalent electrical circuit of the TSM sensor. (b) Typical measurements of the magnitudes and phase angles of the impedances of the TSM sensor with one side in contact with: (1) air; (2) water; (3) 0.1 M KCl; (4) 36% (w/w) glycerol.

The equivalent circuit of the quartz crystal is shown in Fig. 2a. The parallel ("static") capacitance C_0 is the capacitance between the two parallel electrodes on the quartz surfaces. The "motional arm" of the circuit (resistance R_m, inductance L_m and capacitance C_m) arises from the electromechanical motion caused by the piezoelectric effect in the resonant region. The impedance of each circuit element is also given, where $\omega = 2\pi f$ and f is the frequency.

The impedance of the equivalent circuit, Z, is the impedance of the series combination of R_m, L_m and C_m in parallel with the impedance of C_0:

$$Z = R + jX \quad (1)$$

Both R and X are functions of the four circuit elements and the frequency. The magnitude and phase angle of the impedance Z are

$$|Z| = (R^2 + X^2)^{\frac{1}{2}} \quad (2)$$

and

$$\theta = \tan^{-1}(X/R) \quad (3)$$

In practice, sinusoidal voltages incident on and reflected from the quartz crystal are measured for a large number of frequencies in the resonant frequency range. The experimental values of the magnitude and phase of impedance can be calculated at each frequency from the measured voltages and currents, and characteristic quantities can be found from the impedance–frequency curves. Typical impedance measurements of a 9-MHz TSM quartz crystal under different conditions are given in Fig. 2b, where the frequency span covers the entire resonance region (fundamental mode). Several characteristic quantities can be extracted from the magnitude and phase curves of the impedance measurement. They can be classified into three groups based on their characteristic properties: frequency characteristics, including frequencies at zero phase, series resonant frequency f_s and parallel resonant frequency f_p; impedance characteristics, including maximum impedance Z_{max}, minimum impedance Z_{min} and maximum phase angle θ_{max}; and equivalent circuit parameters, C_0, R_m, L_m and C_m. All the quantities measured from the impedance and phase curves and calculated from the equivalent circuit are listed in Table 1 for a 9-MHz gold electrode quartz crystal under different surrounding environments.

FIA–TSM system

There are two frequencies at which the phase angle of the impedance is zero: series resonant frequency f_s is the low frequency of zero phase, and parallel resonant frequency f_p is the high frequency of zero phase. The theoretical expressions for f_s and f_p are obtained by solving the quadratic function of frequency at zero phase (actually the effect of dissipation of energy is neglected):

$$f_s = \frac{1}{2\pi}\left(\frac{1}{L_m C_m}\right)^{1/2} \quad (4)$$

$$f_p = \frac{1}{2\pi}\left(\frac{1}{L_m C_m} + \frac{1}{L_m C_0}\right)^{1/2} \quad (5)$$

The series resonant frequency is the only quantity measured by the oscillator method.

Figure 3 shows FIA profiles of the responses of the series and parallel resonant frequencies for an electrolyte solution, 0.1 M KCl, and a viscous

TABLE 1

Network analysis of a thickness-shear mode bulk acoustic wave sensor under different conditions (20°C)

Condition [a]	f_s (Hz)	f_p (Hz)	θ_{max} (degree)	Z_{min} (ohm)	Z_{max} (kohm)	R_m (ohm)	L_m (mH)	C_m (fF)	C_0 (pF)
Air	9000970	9021083	88.81	16.88	522.73	15.84	12.04	25.97	5.81
Water	8995183	9011309	58.35	316.99	16.37	322.98	10.78	29.03	7.76
0.1 M KCl	8994977	9008301	50.84	310.84	10.42	320.24	10.05	31.15	9.82
36% (w/w) glycerol	8993052	9007675	30.77	574.20	8.20	627.23	9.72	32.23	8.14

[a] 9-MHz gold electrode TSM device. One side in contact with the liquid, the other protected by nitrogen.

organic solution, 36% (w/w) glycerol in water. The baseline noise observed was significant and periodic, especially in the case of the series resonant frequency. This behaviour is attributed to the fluctuating pressure caused by the peristaltic pump. The magnitude of the noise can be reduced by incorporating a pulse damping device in the FIA system or using a long coil. The periodic fluctuation can also be smoothed by a simple Fourier transform treatment. Rather than use either of the above correction methods, the original manifold was retained in some experiments in order to compare the effect of pulsation on the different characteristic parameters.

The injection of the glycerol solution (dotted lines in Fig. 3) results in a decrease in both the series and parallel resonant frequencies due to viscous damping of the TSM device. The viscous nature of this sample (viscosity $\eta = 3.089$ g ms^{-1}, density $\rho = 1.088$ g cm^{-3}) also causes broadening of the FIA concentration profiles. Electrolyte injection (solid lines in Fig. 3) results in only a slight change in f_s. This result is not surprising,

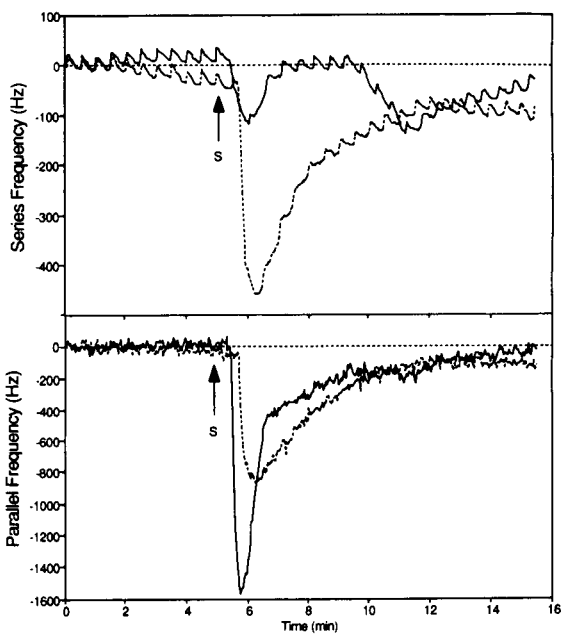

Fig. 3. FIA profiles of the series and parallel resonant frequency responses of the TSM sensor for 0.1 M KCl (solid line) and 36% (w/w) glycerol (dotted lines). Flow-rate, 0.4 ml min^{-1}; injection volume, 30 μl; coil length, 30 cm.

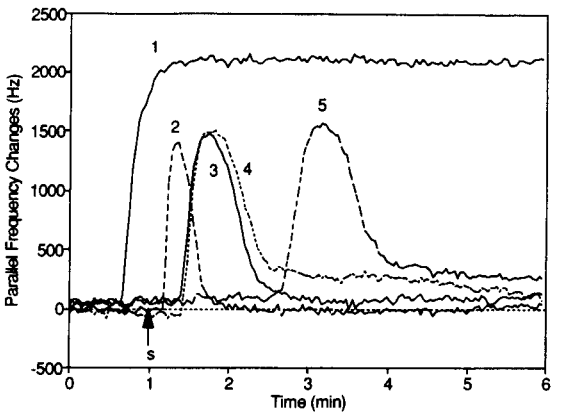

Fig. 4. FIA profiles of the parallel resonant frequency responses of the TSM sensor for 0.1 M KCl: (1) steady state; (2) flow-rate, 0.8 ml min^{-1} (injection volume 30 μl, coil length 30 cm); (3) 0.4 ml min^{-1} (30 μl, 30 cm); (4) 0.4 ml min^{-1} (50 μl, 30 cm); (5) 0.4 ml min^{-1} (30 μl, 150 cm).

as 0.1 M KCl has almost the same viscosity and density as the carrier water. Interestingly, however, the response of the parallel frequency, f_p, is significantly shifted from the values for both pure carrier and glycerol. The electrolyte condition is certainly expected to affect the "static" capacitance, C_0, in view of the relationship of this parameter to f_p (Eqn. 5). Presumably this occurs through the formation of an electrical double layer at the sensor electrode surface. In summary, the resonant frequencies are sensitive to a number of properties of the liquid, but it is difficult to distinguish the effects of these from one another. A similar observation was made by Martin et al. [13], who noted that when only the resonant frequency is monitored, it is impossible to differentiate changes in surface mass from liquid properties.

The intensity and shape of an FIA peak depend on a number of parameters. The effects of flow-rate, sample injection volume and coil length were studied. Figure 4 shows the parallel frequency responses of the TSM sensor on injection of KCl under different manifold conditions. The f_p decrease is plotted as a positive signal to yield a conventional FIA profile. Curve 1 in Fig. 4 is a steady-state signal generated by pumping 0.1 M KCl solution through the detector cell continuously. The time delay before any signal is ob-

served (curves 2–5 in Fig. 4) is the time required for the sample to travel from the injector valve to the detector. Increasing the flow-rate reduces the time lag and peak broadening (curve 2), but the magnitude of the baseline noise is also increased owing to the peristaltic action of the pump. A larger sample injection volume does not increase the peak height greatly (curve 4), but broadens it. A 30-μl injection gives a reasonable intensity with less peak broadening (curve 3). A longer coil results in both a longer time delay and peak broadening with little improvement in peak height (curve 5).

Acoustic energy dissipation

The total energy of the acoustic wave quartz device equals the maximum kinetic energy of the quartz plate plus the maximum kinetic energy of the surrounding media. There are both internal and external losses of electrical energy in the quartz crystal. Electrical energy is converted into thermal energy in the quartz as a result of internal friction in the crystal lattice and energy radiation into the bulk material at the edges of the plate. The external energy dissipation arises from both viscous damping and acoustic radiation. The external energy loss depends on the bulk properties of the fluid and the nature of the interaction between the fluid and the surface of the sensor.

The motional resistance R_m represents the dissipation of electrical energy in the quartz crystal. Figure 5 shows the responses of R_m under different sample injections. As the concentration of the glycerol increases, the viscosity and density of the contacting liquid increases, which results in an increase in energy dissipation, and thus in an increase of R_m (solid curves 1–3 in Fig. 5)

The injection of 0.1 M KCl solution displays a different profile (solid curve 4). At high concentration gradients, a decrease in R_m is observed, but at low concentration gradients, a slight increase in R_m is observed. The response of R_m on a separate injection of dilute KCl (0.01 M) only results in an increase in R_m (not shown). It appears that KCl of high concentration reduces the energy dissipation whereas that of low concentration increases the same parameter relative to water. The viscosity and density of KCl solu-

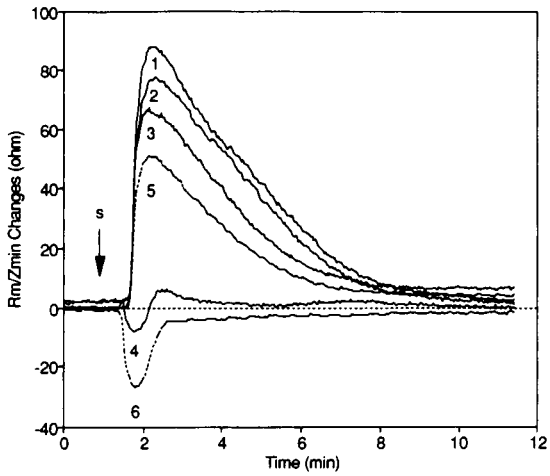

Fig. 5. Variation of equivalent circuit resistance R_m (solid curves 1–4) and minimum impedance Z_{min} (dotted curves 5 and 6). (1) 69% (w/w) glycerol; (2) 56% (w/w) glycerol; (3 and 5). 36% (w/w) glycerol; (4 and 6). 0.1 M KCl. Flow-rate, 0.4 ml min^{-1}; injection volume, 30 μl; coil length, 30 cm.

tions in the concentration range 0.01–0.1 M are similar to those of water. A possible explanation is that different interfacial structures of the electrolyte at the electrode surface may affect the coupling and radiation of the acoustic wave towards the liquid media. The behaviour of the TSM sensor response under electrolytic solutions is currently under investigation.

Another characteristic quantity, which is comparable to R_m, is the minimum magnitude of impedance, Z_{min}. This is measured directly from the impedance frequency curve. Z_{min} also responds to the energy dissipation of the system. At low viscosity, Z_{min} and R_m have the same magnitude. However, Z_{min} also depends on other equivalent circuit parameters. Thus it may account for the total energy fluctuation in the system caused by various energy loss mechanisms. The difference between Z_{min} and R_m is shown in Fig. 5. In the case of glycerol injection, Z_{min} (dotted curve 3) had the same FIA profile as R_m with lower intensity. When KCl is injected, Z_{min} has a stronger signal than R_m, whereas at low concentration gradients, Z_{min} shows and insignificant reversed response compared with R_m.

Static capacitance C_0

At frequencies far from the resonant frequency, the quartz crystal plate is equivalent to a simple parallel-plate capacitor having a capacitance given by

$$C_0 = k\epsilon_0 A/e \quad (6)$$

where A is the area of the electrodes, e is the thickness of the plate, k is the dielectric constant of the quartz and ϵ_0 the permittivity of space. In an actual experimental configuration C_0 also includes the capacitance contribution from the cell and wires.

Because only one side of the TSM device is in contact with liquid, the conduction current between the two electrodes is not considered. However, the conductive properties of the contacting liquid will result in a change in C_0. Figure 6 shows the responses of C_0 under different sample injections. Whereas there is no change for glycerol injection (curve 1), C_0 increases as the electrolyte solutions of LiCl, NaCl, and KCl (curves 2–4) are injected, probably owing to fringing of the electrical field. Although the concentrations and specific conductances of these three solutions are the same, the differences in the peak heights and the dispersion profiles of C_0 changes suggest that C_0 also depends on other factors such as the interfacial liquid structure and interactions due to ionic adsorption.

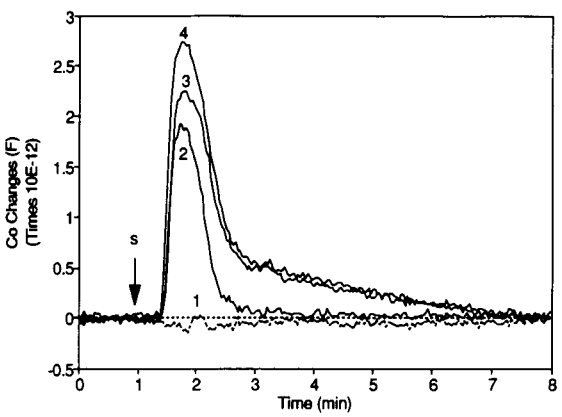

Fig. 6. Variation of static equivalent circuit capacitance C_0: (1) 36% (w/w) glycerol; (2) 0.1 M LiCl; (3) 0.1 M NaCl; (4) 0.1 M KCl. Same manifold as in Fig. 5.

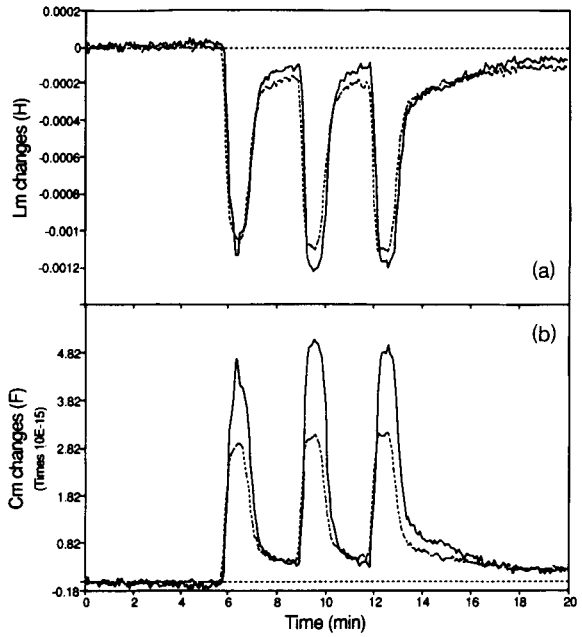

Fig. 7. Effect of surface wettability of the TSM sensor on (a) the equivalent circuit inductance L_m and (b) the motional capacitance C_m using 0.1 M KCl. Solid line, hydrophilic surface; dotted line, hydrophobic surface. Flow-rate, 0.4 ml min^{-1}; injection volume, 30 μl; coil length, 50 cm; data acquisition time, 5 s per set.

Inductance L_m and capacitance C_m

The effect of interfacial properties on the response of the TSM device in the liquid phase has been examined by Thompson and co-workers [4,11,20,21]. The motional inductance L_m represents the mass of the quartz plate, including the coating on its surface and the effect of the liquid loading. The motional capacitance C_m represents the elastic properties of the quartz. Whereas L_m determines the mass loading on the quartz crystal and the energy transfer due to viscous damping, C_m determines the efficiency of electromechanical coupling between the quartz surface and contacting liquid.

Figure 7 illustrates the responses of L_m and C_m on injection of KCl with controlled conditions on the electrode surfaces of the TSM device. The gold electrodes of the quartz crystal were plasma cleaned to give a hydrophilic surface (advancing contact angle of water $< 10°$), or treated with a long-chain thiol species [hexadecanethiol, CH_3-

$(CH_2)_{15}SH$] to generate a close-packed molecular configuration yielding a hydrophobic surface (contact angle $> 110°$). Although no significant difference is observed on the response of L_m (Fig. 7a), the response of C_m is greater for the hydrophilic than for the hydrophobic surface (Fig. 7b), suggesting a different degree of electromechanical coupling. On the other hand, the similar response of L_m for different surfaces indicates that the discrepancy of frequency responses on different surfaces is not caused by different mass loading.

Conclusions

It is emphasized that this study was intended to outline the versatility of the network analysis method for the study of the thickness-shear mode acoustic wave sensor and to examine the feasibility of the combination of the flow injection technique with a TSM device. No attempt was made to optimize the system and to relate explicitly the characteristic quantities to physical properties of the quartz crystal, contacting liquid and the interfacial properties at the liquid/solid interface. Systematic studies to optimize both the flow cell and manifold design should lead to significant improvement in detection limit and dynamic range and the elimination of baseline noise. The network analysis method completely characterizes the TSM quartz crystal sensor for all conditions of the crystal. The impedance measurement provides multi-dimensional information in studying the bulk properties of the surrounding media and the interfacial structure. The development of an electromechanical model for the TSM acoustic wave sensor from first principles will determine the physical significance of the characteristic quantities.

The applicability of the FIA–TSM combination is greater than the sum of the separate applications of FIA and the TSM sensor. Flow-injection systems can provide rapid, reproducible chemistry with its speed; simplicity and economy. The versatility of the TSM sensor in studying the mass loading, liquid properties and interfacial parameters will allow wide applications of this technique, which is still in an early developmental stage.

Potential applications of this technique lie in the field of continuous monitoring of chemical and biochemical processes. The ability of the TSM detector to measure the viscosity and density of liquids can be used for the control of industrial fermentation and downstream processing. The immobilization of selective binding agents on TSM surfaces, combined with the abilities of sample pretreatment of FIA (filtration, dilution, preconcentration, affinity column, enzyme reactor, etc.), will allow the development of automatic immunoassay and enzyme assays and the study of drug–receptor interactions and DNA hybridization.

The authors are grateful to the Natural Science and Engineering Research Council of Canada for support of this work.

REFERENCES

1 G. Sauerbrey, Z. Phys., 155 (1959) 206.
2 M. Thompson, A. Kipling, W.C. Duncan-Hewitt, L.V. Rajaković and B.A. Ĉavić-Vlasak, Analyst, 116 (1991) 881.
3 P.K. Konash and G.J. Bastiaans, Anal. Chem., 52 (1980) 1929.
4 M. Thompson, G.K. Dhaliwal, C.L. Arthur and G.S. Calabrese, IEEE Trans. Ultrason. Ferroelec. Freq. Control., UFFC-34 (1987) 128.
5 S.-Z. Yao and T.-A. Zhou, Anal. Chim. Acta, 212 (1988) 61.
6 M.D. Ward and D.A. Buttry, Science, 249 (1990) 1000.
7 K.K. Kanazawa and J.G. Gordon, Anal. Chim. Acta, 175 (1985) 99.
8 S. Bruckenstein and M. Shay, Electrochim. Acta, 30 (1985) 1295.
9 H.E. Hager, Chem. Eng. Commun., 43 (1986) 25.
10 R. Schumacher, Angew. Chem., Int. Ed. Engl., 29 (1990) 329.
11 W.C. Duncan-Hewitt and M. Thompson, Anal. Chem., 64 (1992) 94.
12 A.L. Kipling and M. Thompson, Anal. Chem., 62 (1990) 1514.
13 S.J. Martin, V.E. Granstaff and G.C. Frye, Anal. Chem., 63 (1991) 2272.
14 J. Ruzicka and E.H. Hansen, Flow Injection Analysis, Wiley-Interscience, New York, 2nd edn., 1988.
15 R.D. Schmid and W. Kuennecke, J. Biotechnol., 14 (1990) 3.
16 I. Ogbomo, U. Prinzing and H.-L. Schmidt, J. Biotechnol., 14 (1990) 63.

17 C.D. Bain, J. Evall and G.M. Whitesides, J. Am. Chem. Soc., 11 (1989) 7155.
18 W.G. Cady, Piezoelectricity, Dover, New York, 1964.
19 V.E. Bottom, Introduction to Quartz Crystal Unit Design, Van Nostrand Reinhold, New York, 1982.
20 L.V. Rajaković, B.A. Ĉavić-Vlasak, V. Ghaemmaghami, K.M.R. Kallury, A.L. Kipling and M. Thompson, Anal. Chem., 63 (1991) 615.
21 M. Yang, M. Thompson and W.C. Duncan-Hewitt, Langmuir, submitted for publication.

Analytica Chimica Acta, 269 (1992) 177–185
Elsevier Science Publishers B.V., Amsterdam

Determination of nanomole amounts of sulphur dioxide in air by flow-injection conductimetry with on-line preconcentration

I. Gács [1] and R. Ferraroli

Environment Division, CISE, P.O. Box 12081, 20134 Milan (Italy)

(Received 14th April 1992; revised manuscript received 14th July 1992)

Abstract

A simple and sensitive flow-injection technique for measuring nanomole amounts of sulphur dioxide in gaseous atmospheres is presented. The samples are passed through 0.2 M sulphamic acid solution to eliminate constituents interfering with the final electrolytic conductivity measurement. Sulphur dioxide is preconcentrated from the carrier gas stream by absorption in a capillary denuder tube coated with 0.02 M hydrogen peroxide solution. The sulphuric acid formed in the liquid film is then eluted with a stream of the absorbent circulated through an electrolytic conductivity microdetector. The change in specific conductance due to the presence of the sulphuric acid in the effluent stream is linearly related to the amount of sulphur dioxide in the sample (up to 55 nmol). The method can also be applied to the analysis of aqueous sulphite solutions. In this case the samples are injected into the sulphamic acid, and the acidic solution is then stripped with a stream of nitrogen. The limit of detection for aqueous samples is 1 $\mu g\ l^{-1}$ and for air samples 4 $\mu g\ m^{-3}$. A simple determination, including sample preparation, takes 7 min. The precision is better than 5% ($P = 95\%$) for 2.5–50 nmol of sulphur dioxide. The selectivity of the system with respect to nitrogen oxides, ammonia, hydrogen chloride and hydrogen sulphide was also examined.

Keywords: Conductimetry; Flow injection; Air; Preconcentration; Sulphur dioxide

Sulphur dioxide is a pollutant causing widespread concern. Assessment of the deleterious effects on the ecosystem necessitates the determination of sulphur dioxide at trace levels. With the advent of flow-injection analysis (FIA) utilizing either a so-called "diffusion scrubber" [1] or a "sniffer" tube [2], FIA has proved to be a useful technique for monitoring atmospheric sulphur dioxide in the $\mu g\ m^{-3}$ range [3–5]. Enhancement of sensitivity and selectivity was achieved via linking the addition product of sulphur dioxide with formaldehyde to a fluorogenic maleimide [4], or converting the analyte into electrochemically detectable hydrogen peroxide by an immobilized enzyme [5]. It has also been demonstrated that a denuder interface can provide a simple means for the introduction of a highly dispersed gaseous analyte into a flow system via on-line preconcentration [6,7]. Consequently, the formation of this type of interface in the system may facilitate quantitative collection of sulphur dioxide even from large amounts of samples if the analyte can be trapped in the form of a non-volatile substance such as sulphuric acid. In order to achieve desirable simplicity in the configuration of the analytical system, however, the interface should be coupled with a sample preparation unit

Correspondence to: I. Gács, Environment Division, CISE, P.O. Box 12081, 20134 Milan (Italy).

[1] On leave from Central Research Institute for Chemistry, Hungarian Academy of Sciences, P.O. Box 17, 1525-Budapest, Hungary.

that is capable of removing potentially interfering constituents, thus allowing the simple electrolytic conductivity detection of the analyte trapped in various measurement situations, compensating for evaporation loss of the absorbent in the denuder tube and handling aqueous solutions, thus allowing the use of a simple calibration procedure and the measurement of sulphur dioxide in aqueous solutions. Therefore, the use of a rapid gas stripping technique [6] for on-line sample preparation is considered to be advantageous.

Electrolytic conductivity detection has been applied succesfully to the determination of atmospheric sulphur dioxide [8–10]. Provided that a low and reliable blank can be ensured, preconcentration leads to an improvement in the detection limit for the flow-through type of conductivity detector, which, in comparison with other electrochemical [5,11–15] or optical [4,16–18], detectors, has a substantially simpler construction and is easier to operate and maintain. The response of the flow cell is primarily determined by background conductance (baseline) and dispersion, the dissociation constant and the equivalent conductance of the absorbed analyte (e.g., sulphuric acid). As a conductivity solvent (absorbent), the use of a dilute solution of hydrogen peroxide is advantageous, because its properties can simultaneously meet the requirements imposed by the detection and the interface units of the proposed system.

With this in mind, the method presented here was developed, and its suitability for the determination of sulphur dioxide in air is discussed. The selectivity of the system with respect to nitrogen oxides, ammonia, hydrogen chloride and hydrogen sulphide is also reported. The applicability of the technique to the determination of sulphite in some aqueous solutions (e.g., boiler feedwater, polluted natural waters and waste waters) was assessed by the analysis of standard sulphite solutions.

The principle of the method is as follows. An aqueous sample containing sulphite is added to 0.2 M sulphamic acid solution and the acidic solution is then purged with nitrogen. The gaseous samples are led through the same acidic medium. The sulphamic acid removes nitrogen dioxide [19–21] and retains ammonia and, up to a concentration of about 0.7 mg m^{-3}, hydrogen chloride. If a 0.03 M lead nitrate solution of the 0.2 M aqueous sulphamic acid is used, the hydrogen chloride can be removed completely prior to the preconcentration step even at an HCl concentration of about 7 mg m^{-3}. The sulphur dioxide is collected from the carrier gas streams as sulphuric acid in a capillary denuder tube coated with a thin layer of a 0.01–0.03 M hydrogen peroxide solution of 0.05 mM sulphuric acid; meanwhile, carbon dioxide, nitrogen monoxide and hydrogen sulphide are removed with the carrier gas passing through the tube. The film containing the sulphuric acid is eluted with a circulating stream of the absorbent and is passed through a conical plate electrolytic conductivity micro flow cell [22–24]. The otherwise low specific conductance of the absorbent increases significantly in the presence of the acid. The elution pattern obtained via a conductivity meter as a d.c. voltage signal shows a sharp peak corresponding to the change in conductivity. The peak height of the signal can be linearly related to the amount of sulphur dioxide present in the sample.

EXPERIMENTAL

Reagents

All chemicals were of analytical-reagent grade and solutions were prepared with water purified with a Milli-Q system (Millipore). The recirculated absorbent was obtained by addition of 2 cm^3 of hydrogen peroxide (30%, w/w) (Carlo Erba) to 1000 cm^3 of 0.05 mM sulphuric acid degassed prior to use. Standard sulphite solution was prepared by dissolving 12.61 mg of anhydrous sodium sulphite in 1000 cm^3 of 0.04 M potassium tetrachloromercurate [25] purged with purified nitrogen. Standard gas samples were obtained by using a dynamic gas calibration system (Model 146, Thermo Environmental Instruments, Franklin, MA) containing sulphur dioxide and nitrogen oxide permeation devices (Vici Metronics, Santa Clara, CA). The permeation rate of sulphur dioxide was 1912 ng min^{-1} (at 35°C), corresponding to a concentration of 1912 $\mu g\ m^{-3}$ in the carrier

gas stream (air) at a flow-rate of 1.0 l min^{-1}. Final concentration levels of sulphur dioxide were achieved by adjusting the flow-rate of the source air ("zero gas") to the desired values. Nitrogen dioxide and nitrogen monoxide concentration levels in the air stream were generated by mixing known amounts of nitrogen monoxide from a cylinder with ozone (gas-phase titration). The decrease in the nitrogen oxide level (increase in the nitrogen dioxide level) was determined by using a chemiluminescence NO analyser (APNA-350E Ambient NO_x Monitor; Horiba, Kyoto).

Apparatus

Figure 1 is a schematic diagram of the flow-injection system. The sample preparation unit is coupled to the flow system via a six-port, two-position rotary valve (made of PTFE) by means of a PTFE-lined stainless-steel tube (20 cm × 2 mm i.d.) (Alltech, Deerfield, IL). Other parts of the equipment are linked via stainless-steel capillary tubing (1.6 mm o.d., 0.8 mm i.d.). Nitrogen (inlet pressure 1.5 atm) utilized as a gas source for the sample preparation unit is purified using granulated manganese dioxide [8] and ascarite (both from Merck) in glass absorption tubes (25 cm × 2.5 cm o.d.). The configuration of the unit is adapted to the analytical task to be performed (Fig. 2).

The denuder tube (CL in Fig. 1) is a stainless-steel capillary (50 cm × 1.6 mm o.d. × 0.8 mm i.d.). The capacity of the denuder tube for sulphur dioxide and the unretained fraction of the gaseous analyte was determined by liquid scintillation counting (LSC) of the sulphur dioxide passed through the tube during gas stripping of known amounts of aqueous sodium [^{35}S]sulphite solution injected into 0.2 M sulphamic acid in the sample preparation unit shown in Fig. 2a. Trapping of the non-retained fraction by the absorbent and the subsequent LSC measurement of the dilute [^{35}S]sulphuric acid obtained were performed as described previously [26].

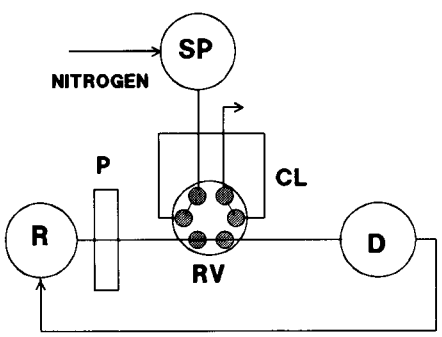

Fig. 1. Schematic diagram of the flow-injection system. CL = capillary denuder tube; D = detector; P = pump; R = 0.02 M hydrogen peroxide solution; RV = six-port, two-position rotary valve made of PTFE; SP = sample preparation unit.

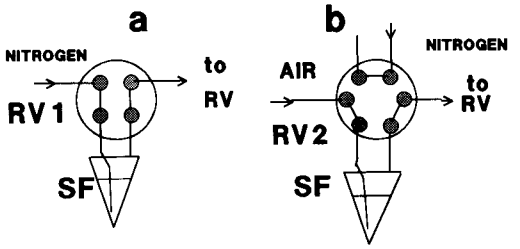

Fig. 2. Configuration of the sample preparation unit for the determination of sulphur dioxide in aqueous and gaseous samples. RV1 = four-port, two-position rotary valve made of PTFE; RV2 = six-port, two-position rotary valve made of PTFE; SF = sulphamic acid solution. (a) Configuration for liquid samples; (b) configuration for gaseous samples.

The absorbent stream (flow-rate 2 cm^3 min^{-1}) is circulated via the conductivity flow cell with an LC pump (SP8800; Spectra-Physics). In accordance with previous observations [6,7,23], no thermostating of the cell is needed. The circulating absorbent ensures sufficient thermal stability of the system. A 1-l volume of fresh absorbent can be used for several days. The detector is connected to a conductivity meter (Model 101, measuring frequency 3 kHz; Orion Research) and the d.c. voltage signal is registered with a recorder (SR 6255; Watanabe Instruments).

The selectivity of the system with respect to potential interference from nitrogen oxides, was examined by means of the sample preparation unit shown in Fig. 3. A simple gas stripping device [6] was applied for purging of the aqueous sulphite solutions and generating of hydrogen chloride, ammonia and hydrogen sulphide to establish their effects and the "filtering" properties of the sulphamic acid solution.

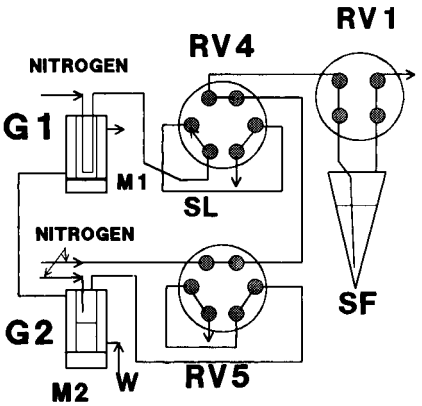

Fig. 3. Configuration of the sample preparation unit for the investigation of the effects of nitrogen oxides: G1 = sulphur dioxide generator; G2 = nitrogen oxides generator; M1, M2 = magnetic stirrers; SF = sulphamic acid solution; SL = sample loop; RV1 = four-port, two-position rotary valve; RV4, RV5 = six-port, two-position rotary valve; W = water from a thermostat.

A stream of nitrogen (flow-rate 130 cm^3 min^{-1}) with a low concentration of sulphur dioxide (2.2 mg m^{-3}) was obtained by means of a simple laboratory generator [27] (G_1 in Fig. 3). The concentration of sodium hydrogensulphite in the generation solution was 30 mg cm^{-3} and a silicone-rubber permeation tube with a length of 10 cm (2 mm o.d., 1 mm i.d) was fitted into the device. The stream of nitrogen containing the sulphur dioxide was sampled with a loop (SL in Fig. 3; made of glass, 15.5 $cm^3 \times 9$ mm i.d.) allowing the introduction of 34.5 ng of sulphur dioxide into a stream of nitrogen-containing nitrogen oxides. A laboratory generator [28] (G_2 in Fig. 3) was applied also for the preparation of a stream of nitrogen (flow-rate 300 cm^3 min^{-1}) containing trace amounts of nitrogen oxides. The concentration of sodium nitrite in the generation solution was 0.5 mg cm^{-3}. The ratio of the concentration of NO to NO_2 in the generated gas was set to ca. 1:10 and 1:1 by adjusting the pH of the solution to pH 5 and 5.9, respectively [28]. At these pH values the total concentration of the nitrogen oxides could be assumed to be 1.2 and 0.4 cm^3 m^{-3}, respectively [28].

During field measurement of sulphur dioxide in urban air, prior to the analysis with the system shown in Figs. 1 and 2b, the sample was passed through a PTFE filter identical with that applied for a UV fluorescence instrument (APSA-350 Ambient SO_2 Monitor; Horiba) operating simultaneously. A common sampling unit was used for both instruments.

Procedure

Performance characteristics were established in two types of analytical experiments by determining sulphur dioxide in aqueous solutions and gaseous samples (nitrogen and air). These analytical procedures obviously vary only in the operation of the sample preparation unit.

Between successive runs, the absorbent is circulated through the denuder tube and the detector. Prior to initiating the analytical cycle, the passage of the absorbent stream is changed by turning the six-port rotary valve (RV in Fig. 1) and (if an aqueous solution is being analysed) the sample is injected into the sulphamic acid solution (1–5 cm^3) in the gas stripping unit (SF in Fig 2a). After the bulk of the absorbent has been driven out of the denuder tube by nitrogen (30 s), the analytical process is initiated. The alternative routes for this are as follows: the four-port, two-position valve RV1 is turned and the acidified aqueous sample in the gas stripping device is purged with purified nitrogen (flow-rate 300 cm^3 min^{-1}) to transfer the sulphur dioxide into the capillary denuder (Fig. 2a); the six-port, two-position rotary valve (RV2 in Fig. 2b) is turned and the gaseous sample (flow-rate 300 cm^3 min^{-1}) is introduced into the denuder via the sulphamic acid solution. After 6 min the absorbent stream is again led through the denuder tube (valve RV in Fig. 1 is turned) and the sharp signal corresponding to the change in electrolytic conductivity is registered. The next analytical operational cycle can then be started.

The study of the effects of nitrogen oxides and the examination of the "filtering" properties of the sulphamic acid solution were accomplished via analyses of gaseous samples containing nitrogen oxides in known concentrations. In order to establish the retention properties of the sulphamic acid solution with regard to hydrogen chloride, known volumes of nitrogen passing

through a gas stripping device containing hydrochloric acid (1–2 M) was led into the denuder tube directly or via the "filter" solution. The amount of the hydrogen chloride transferred into the nitrogen carrier stream was calculated on the basis of its vapour pressure over the hydrochloric acid [29]. Ammonia and hydrogen sulphide could be introduced into a stream of nitrogen via the addition of ammonia solution (0.1 M) to sodium hydroxide (7.5 M) and sodium sulphide (0.01 M) to sulphuric acid (0.2 M), respectively.

The system blank was checked by using only sulphamic acid solution in the sample purging device. The detector response was determined with standard aqueous and gaseous samples. Standard samples can be prepared, e.g., by consecutive addition of aliquots of a standard sulphite solution to the already stripped sulphamic acid.

RESULTS AND DISCUSSION

Operational parameters

The volume of the carrier gas, led through the denuder tube at a flow-rate chosen on the basis of previous investigations [6,7], was determined experimentally. With a 6 min stripping time no memory effect could be observed. An additional 5 min did not influence the recovery, thus verifying the formation of non-volatile sulphuric acid. Naturally, recovery depends on the dimensions of the denuder tube [30]. The use of a 50-cm tube with a radius of 0.4 mm proved to be the most favourable. As shown in Fig. 4, within the linear range of detection almost quantitative trapping of the sulphur dioxide is ensured. The flow-rate of the carrier gas (e.g., air), however, must not exceed 300 cm^3 min^{-1}, because at higher flow-rates the trapping efficiency gradually decreases (Fig. 5) compared with the value obtained at 300 cm^3 min^{-1}. Figure 6 illustrates the effect of hydrogen peroxide on the signal measured.

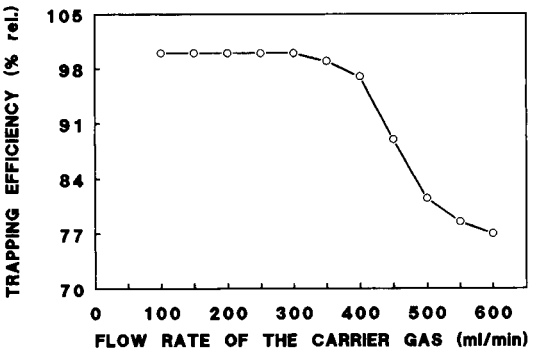

Fig. 5. Trapping efficiency as a function of flow-rate.

The detector response is linear up to 55 nmol of sulphur dioxide. This line follows the equation $y = mx + a$, for which $m = 0.52$, $a = 5.68 \times 10^{-3}$, $s_m = 1.3 \times 10^{-3}$, $s_a = 5.21 \times 10^{-2}$, $s_{xy} = 8.6 \times 10^{-2}$, $n = 22$ and $r^2 = 0.999$, where m is the slope (mV neq^{-1}), a is the intercept, s_m is the standard deviation of the slope, s_a is the standard deviation of the intercept, s_{xy} is the standard

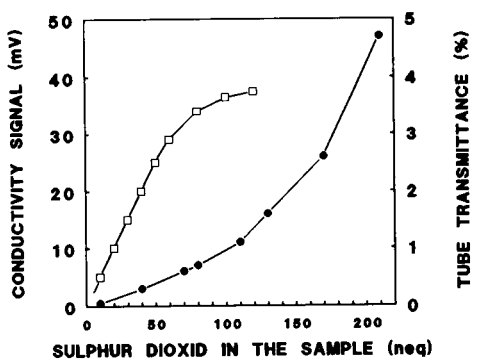

Fig. 4. Conductivity signal and unretained fraction as functions of the amount of sulphur dioxide in the sample. □ = Conductivity signal; ● = unretained fraction.

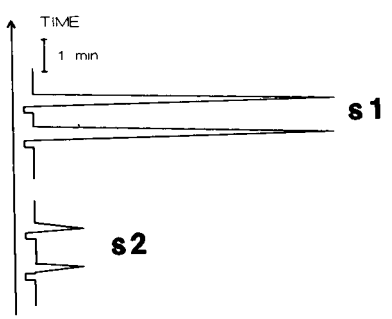

Fig. 6. Recorder traces illustrating the effect of hydrogen peroxide in the absorbent solution: s1 = signals of 5 neq of sulphur dioxide; s2 = signals of 5 neq of sulphur dioxide if hydrogen peroxide is omitted from the solution.

TABLE 1

Operational data at various concentration levels

Set measuring range [a] of recorder (mV)	Maximum sulphur dioxide content [b] (nmol)	Measurable maximum concentration in sample		Blank [c] as a fraction of recorder full-scale (%)
		Gaseous [c] (μmol m^{-3})	Water [d] (10^2 μmol l^{-1})	
1	1.6	0.8	1.6	10.0 [f,g]
2	3.4	1.8	3.4	5.0
5	8.8	4.8	8.8	2.0
10	17.8	9.8	17.8	1.0
20	35.8	19.8	35.8	0.5
50	89.8 [h]	30.5	55.0	0.2

[a] Range of the conductivity meter = 10 mS. [b] Linear range of detection = 0.11–55 nmol. [c] If sample volume = 1.8 l. [d] If sample volume = 10 μl. [f] $\mu_{blank} = 13 \pm 0.7$ ng ($P = 99\%$, $n = 10$); $\mu = \bar{X} \pm ts/n^{1/2}$, where μ = mean value, $\bar{X}$ = arithmetic mean value, s = standard deviation of the set, n = number of measurement, t = Student's numerical factor referring to the level and degree of freedom. [g] Limit of detection [31] = 0.11 nmol. [h] Outside the linear range of detection.

error of the estimate, r is the regression coefficient and n is the number of determinations. Operational data for various concentration levels are summarized in Table 1.

The signal values from Table 2 indicate that the effects of the interfering constituents can be eliminated completely by using the sulphamic acid solution. It can also be observed that the nitrogen oxide at levels in excess of the analyte yielded no change in response for the detector (see also Table 3). Apart from the response which may be attributed to a slight contamination of the sodium sulphide, the same can be stated with regard to the effect of the hydrogen sulphide. The relatively slight influence of the nitrogen dioxide on the detector response (if the sulphamic acid solution is in an off-line position) is considered to be due to its low solubility under the experimental conditions and to the pH dependence of aqueous phase oxidation of nitrous acid by hydrogen peroxide [32]. When the "filter" solution is not in the on-line position, the ammonia produces a nega-

TABLE 2

Elimination of the effects of various potentially interfering constituents by using an on-line 0.2 M sulphamic acid filter solution

Constituents of sample [a] (nmol)						Signal [b] (mV)		Sulphur dioxide found (nmol)
SO_2	NO	NO_2	H_2S	NH_3	HCl	Sulphamic acid		
						Off-line	On-line	
0.54						0.28	0.28	0.54
	15	15				0.17	–	–
0.54	15	15				N [c]	0.28	0.54
	8	82				0.35	–	–
0.54	8	82				N [c]	0.28	0.54
			50			0.15	0.15 [e]	0.29 [f]
			200			0.60 [d]	0.60 [e]	1.15 [f]
				5000		−1.25 [d]	–	–
					40	0.10	–	–
					197	3.25	– [e]	–

[a] Volume = 1.8 l. [b] Mean of five measurements. [c] N = not measured. [d] Smell at the outlet. [e] Filter solution = 0.03 M lead nitrate solution of the 0.2 M sulphamic acid. [f] As the detector response could not be decreased or eliminated even if the filter solution containing lead nitrate was used, these values are attributed to slight contamination of the sodium sulphide reagent.

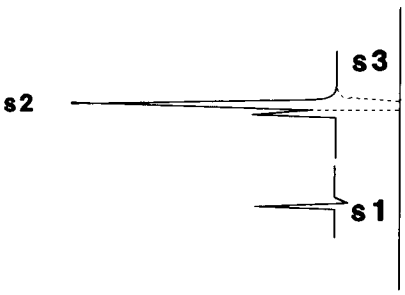

Fig. 7. Recorder traces illustrating the potential effect of ammonia: s1 = blank; s2 = signal attributed to the effect of 5 nmol of ammonia; s3 = location of the sulphur dioxide signal.

tive response on the detector (Fig. 7). This can be attributed to the formation of the corresponding salt, thus decreasing the conductivity.

Determination of sulphur dioxide

Tables 3 and 4 show that the method is suitable for the determination of sulphur dioxide in air. In comparison with the standard UV fluorescence technique, the results in Table 4 suggest that the proposed flow-injection method is equally applicable to the evaluation of air pollution due to sulphur dioxide, provided that the change in concentration is sufficiently resolved by the successive measurement of 6-min mean values. Figure 8 indicates that the change can be followed by FIA quantitatively, even if the relevant time interval is less than 1 h. Both the hourly and the 6-min mean values obtained by the two techniques (see Table 4 and Fig. 8) are in good agreement. These facts, with a knowledge of the composition of both the standard and the urban air samples (see Tables 3 and 4), support the results of the experiments that were performed to establish the effect of potentially interfering substances.

The volume of the sample in the field experiments was limited to 1.8 l. It is believed, however, that the present method can handle larger volumes, thus allowing the measurement of even lower concentration levels. As the samples are passed through the on-line aqueous sulphamic acid solution and because the background con-

TABLE 3

Results for determination of sulphur dioxide in standard air samples

Sample composition [a] (μg m^{-3})			Sulphur dioxide in sample (nmol)	Signal [b,c] (mV)	Sulphur dioxide found	
SO_2	NO	NO_2			nmol [d]	μg m^{-3} [e]
191.2			5.38	2.69 ± 0.05 [f]	5.17 ± 0.10	184.2 ± 3.6
191.2	458.8	862.5	5.38	2.68 ± 0.07 [f]	5.16 ± 0.13	183.7 ± 4.6
382.4			10.76	5.35 ± 0.09 [g]	10.29 ± 0.17	366.2 ± 6.1
382.4	825.5	258.8	10.76	5.36 ± 0.10 [g]	10.30 ± 0.19	366.6 ± 6.8

[a] Volume = 1.8 l. [b] Signal minus blank. [c] Expressed as $\bar{x} \pm ts/n^{1/2}$ ($n = 9$, $P = 95\%$). Symbols are defined in Table 1. [d] SO_2 (nmol) = signal/m, where m (mV nmol^{-1}) = 0.52. [e] SO_2 (μg m^{-3}) = nmol × M/1.8, where M = molar mass. [f] Set measuring range = 5 mV, 10 mS. [g] Set measuring range = 10 mV, 10 mS.

TABLE 4

Results for comparative measurement of sulphur dioxide in urban air

Measuring technique	Concentration found [a] (μl m^{-3}) [b]				X(μl m^{-3}) [c,d]
UV fluorescence	21.62	22.20	24.27	23.54	22.68
	24.25	23.09	21.02		
FIA [e]	21.54	20.51	22.31	21.30	22.51
	24.62	25.72	21.54		

[a] Successively measured 6-min mean values. [b] μl m^{-3} = ppbv. [c] Hourly mean value. [d] Other components measured: NO_x = 136.03 μl m^{-3}, HCl = 22.0 μl m^{-3} (24 h average), O_3 = 11.66 μl m^{-3}, total hydrocarbons = 3210 μl m^{-3}. [e] Concentration = (signal × V_m)/(mV), where m (mV nmol^{-1}) = 0.52, V (l) = sample volume = 1.8, V_m (l) = molar volume = 24.

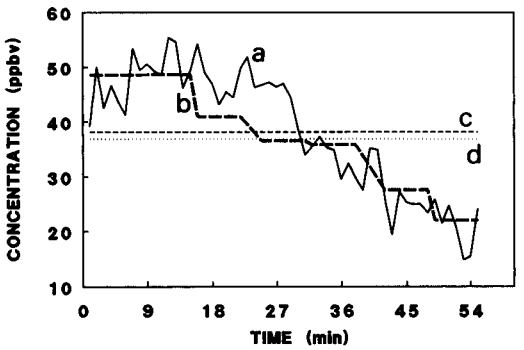

Fig. 8. Determination of sulphur dioxide in urban air. a = Concentration measured with UV fluorescence monitor; b = concentration measured by FIA; c = hourly mean value obtained by the UV fluorescence technique; d = hourly mean value obtained by the FIA technique.

ductance is low, variation in the blank (which might be due to the effect of relative humidity of the sample air on the evaporation loss of the scrubber film) becomes negligible.

Table 5 indicates that the method may be suitable for the determination of sulphur dioxide (sulphite) in some types of aqueous solutions (e.g., polluted natural waters, boiler feed water). It should be noted, however, that samples stabilized with formaldehyde could not be analysed by the proposed method, because the concentrations of the free S(IV) species available for removal are minimal at the pH of the sulphamic acid solution [33]. Similarly, the capability of the method for the determination of sulphite in brine containing chlorate under alkaline conditions [34] should be established before use.

TABLE 5

Results for triplicate determination of sulphur dioxide in water samples

Sample [a]		Signal [b] (mV)	Sulphur dioxide found ($\mu g\ SO_2\ l^{-1}$)
Concentration ($\mu g\ SO_2\ l^{-1}$)	Amount of standard solution (μl)		
12.81	10	0.53	13.06
		0.51	12.56
		0.54	13.30
64.06	50	2.63	64.80
		2.55	62.83
		2.65	65.30
128.12	100	5.20	128.13
		5.15	126.90
		5.30	130.60

[a] Standard sodium sulphite solution (0.1 nmol $SO_2\ \mu l^{-1}$) was added to 5 cm^3 of purged aqueous acid solution. [b] Signal minus blank.

The authors express their thanks to Dr. A. Negri for helpful discussions and for providing the facilities for field experiments.

REFERENCES

1 P.K. Dasgupta, Atmos. Environ., 18 (1984) 1593.
2 D.M. Pranitis and M.E. Meyerhoff, Anal. Chem., 53 (1987) 2354.
3 P.K. Dasgupta, W.L. McDowell and J.S. Rhee, Analyst, 111 (1986) 87.
4 P.H. Dasgupta, S. Dong, H. Hwang, H.C. Yang and Z. Genfa, Atmos. Environ., 22 (1988) 949.
5 W. Matuszewski and M.E. Meyerhoff, Anal. Chim. Acta, 248 (1991) 379.
6 I. Gács and K. Payer, Anal. Chim. Acta, 220 (1989) 1.
7 I. Gács and K. Payer, Anal. Chim. Acta, 241 (1990) 71.
8 F. Opekar and A. Trojánek, Anal. Chim. Acta, 203 (1987) 1.
9 J.S. Symansky and S. Bruckenstein, Anal. Chem., 58 (1986) 1171.
10 P.K. Simon, P.K. Dasgupta and Z. Veĉeřa, Anal. Chem., 63 (1991) 1237.
11 G.B. Marshall and D. Midgley, Analyst, 108 (1983) 701.
12 M. Masoom and A. Townshend, Anal. Chim. Acta, 179 (1986) 399.
13 M. Granados, S. Mashpoch and M. Blanco, Anal. Chim. Acta, 179 (1986) 445.
14 A. Rios, M.D. Luque de Castro, M. Valcárcel and H.A. Mottola, Anal. Chem., 59 (1987) 666.
15 G. Schiavon, G. Zotti, R. Toniolo and G. Bontempelli, Analyst, 116 (1991) 797.
16 S.M. Ramasamy and H.A. Mottola, Anal. Chem., 54 (1982) 283.
17 P. Linares, M.D. Luque de Castro and M. Valcárcel, Anal. Chim. Acta, 225 (1989) 443.
18 J.L. Burguera and M. Burguera, Anal. Chim. Acta, 214 (1988) 429.
19 P.W. West and F.E. Ordoveza, Anal. Chem., 34 (1962) 1324.
20 R.M. Harrison and R. Perry (Eds.), Handbook of Air Pollution Analysis, Chapman and Hall, London, 2nd edn., 1986, p. 294.
21 A. Bhatt and V.K. Gupta, Analyst, 108 (1983) 374.
22 J.F. Alder, P.K.P. Drew and P.R. Fielden, J. Chromatogr., 212 (1981) 167.

23 J.F. Alder, P.K.P. Drew and P.R. Fielden, Anal. Chem. 55 (1983) 256.
24 J.F. Alder, P.R. Fielden and A.J. Clark, Anal. Chem., 56 (1984) 985.
25 American Public Health Association, American Water Works Association and Water Pollution Control Federation, Standard Methods for the Examination of Water and Wastewater, APHA, Washington, DC, 16th edn., 1985, p. 481.
26 I. Gács, Z. Vargay, E. Dobis, S. Dombi, K. Payer and L. Ötvös, J. Radioanal. Chem., 68 (1982) 93.
27 J. Langmaier and F. Opekar, Anal. Chim. Acta, 166 (1984) 305.
28 Y. Hashimoto and S. Tanaka, Environ. Sci. Technol., 14 (1980) 413.
29 Gmelins Handbuch der Anorganischen Chemie, Chlor, System-Nummer 6, Verlag Chemie, Berlin, 1927, pp. 144–145.
30 D.M. Murphy and D.W. Fahey, Anal. Chem., 59 (1987) 2753.
31 G.L. Long and J.D. Winefordner, Anal. Chem., 55 (1983) 713A.
32 Y.-N. Lee and J.A. Lind, J. Geophys. Res., 91 (1986) 2793.
33 P.K. Dasgupta and H.-C. Yang, Anal. Chem., 58 (1986) 2839.
34 P. MacLaurin, K.S. Parker, A. Townshend, P.J. Worsfold, N.W. Barnett and M. Crane, Anal. Chim. Acta, 238 (1990) 171.

Analytica Chimica Acta, 269 (1992) 187–191
Elsevier Science Publishers B.V., Amsterdam

Flow-injection determination of glucose in serum with an immobilized pyranose oxidase reactor

Nobutoshi Kiba, Fumito Ueda and Motohisa Furusawa

Department of Applied Chemistry and Biotechnology, Faculty of Engineering, Yamanashi University, Kofu 400 (Japan)

Takeshi Yamane

Department of Chemistry, Faculty of Education, Yamanashi University, Kofu 400 (Japan)

(Received 21st May 1992; revised manuscript received 15th July 1992)

Abstract

A flow-injection system for the chemiluminometric determination of D-glucose in serum with an immobilized pyranose oxidase reactor is described. Pyranose oxidase is immobilized on controlled-pore glass beads and packed into a stainless-steel column. Serum (100 nl) is diluted 1000-fold with water. Sample solution (10 μl) is injected into the carrier stream. The hydrogen peroxide produced is detected by measuring the chemiluminescence emitted on admixing with luminol and potassium hexacyanoferrate(III). The maximum sample throughput is 60 h^{-1}. The calibration graph is linear from 0.2 to 500 μM glucose; the detection limit is 0.05 μM. The immobilized enzyme reactor is stable for at least 2 months.

Keywords: Chemiluminescence; Enzymatic methods; Flow injection; Glucose; Serum

The determination of glucose is essential in clinical analysis for the diagnosis of disorders of metabolism (e.g., diabetes). Flow-injection analysis (FIA) combined both with an immobilized glucose oxidase (E.C. 1.1.3.4) (GOD) reactor and with chemiluminescence is suitable for the rapid and sensitive analysis of large numbers of samples [1–4]. In this system hydrogen peroxide is produced in the immobilized GOD reactor according to the following reaction:

β-D-glucose + O_2 + H_2O →
D-gluconic acid + H_2O_2

The hydrogen peroxide produced is determined by reaction with luminol in the presence of potassium hexacyanoferrate(III) to produce light:

H_2O_2 + luminol + $2OH^-$ →
3-aminophthalate + N_2 + $h\nu$

D-Glucose is known to be present in aqueous solution as a mixture of isomers. At mutarotation equilibrium, more than 35% of D-glucose occurs as the corresponding α-anomer, which is not oxidizable by GOD. The equilibrium composition varies strongly with temperature and pH, and is also affected by the presence of anions [5–7].

Pyranose oxidase (pyranose : oxygen 2-oxidoreductase, E.C. 1.1.3.10) (PyrOD) catalyses the oxidation of the hydroxyl group at the C-2 position of pyranose ring of glucose to glucosone and hydrogen peroxide in the presence of molecular oxygen:

D-glucose + O_2 → D-glucosone + H_2O_2

Correspondence to: N. Kiba, Department of Applied Chemistry and Biotechnology, Faculty of Engineering, Yamanashi University, Takeda-4, Kofu 400 (Japan).

PyrOD oxidizes α- and β-anomers of D-glucose to the same extent and shows excellent stability [8–10]. PyrOD has been immobilized on glass beads and used as a reactor for the determination of monosaccharides in continuous-flow analysis [11].

In this work, immobilized PyrOD and GOD reactors in a flow system were compared in terms of specificity, stability and sensitivity. This paper describes a flow-injection system for chemiluminometric determination of glucose with an immobilized PyrOD reactor. This method was applied to the determination of glucose in serum.

EXPERIMENTAL

Reagents

Saccharides were obtained from Nacalai Tesque (Kyoto). PyrOD (from *Coriolus versicolor*, 1160 U ml^{-1}) and GOD (from *Aspergillus* sp., 150 U ml^{-1}) were purchased from Kyowa Hakko Kogyo (Tokyo) and Toyobo (Osaka), respectively. Aminopropyl-controlled-pore glass (CPG) (mean pore diameter 59 nm, amount of amine 76 μmol g^{-1}, particle size 200–400 mesh) was supplied by CPG (Fairfield, NJ). All other reagents were of analytical-reagent grade.

A stock solution of D-glucose (10 mM) was prepared in water and stored in a refrigerator. McIlvaine buffer (pH 4.5) was prepared from 0.1 M sodium monohydrogenphosphate and 0.05 M citric acid.

Apparatus

A schematic diagram of the flow system is shown in Fig. 1. The carrier [McIlvaine buffer (pH 4.5)] was pumped (Hitachi L6000 pump) at a flow-rate of 1.0 ml min^{-1}. The sample was introduced with an injection valve (Sanuki SV1-SU7) with a 10-μl loop. The enzyme reactor (5 cm × 4 mm i.d.) was kept at 40°C. Luminol solution [0.7 mM luminol in 0.3 M carbonate buffer (pH 10.5)] and 20 mM potassium hexacyanoferrate(III) solution were pumped by a double-plunger pump (Kyowa Seimitsu KHU-W-52) at a total flow-rate of 1.0 ml min^{-1}. The magnitude of chemiluminescence based on the H_2O_2 produced was measured with a luminometer (Niti-ON Lumiflow LF-800) with a flow-through cell (70 μl), connected to a data processor (System Instrument Chromatocorder II).

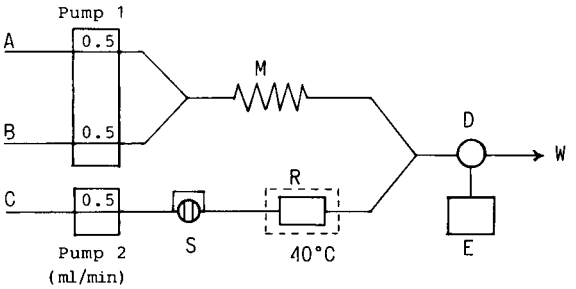

Fig. 1. Flow diagram of the chemiluminometric flow-injection system for the determination of glucose using an immobilized pyranose oxidase reactor. A = luminol solution; B = potassium hexacyanoferrate(III) solution; C = carrier solution; S = injection valve with a loop; M = mixing coil (3 m × 0.5 mm i.d.); R = immobilized PyrOD reactor, maintained at 40°C; D = luminescence detector; E = data processor; W = waste.

Preparation of enzyme reactors

CPG beads were packed into a stainless-steel column (5 cm × 4 mm i.d.) by the slurry-packing method. Glutaraldehyde solution (2%) in 0.1 M phosphate buffer (pH 7.0) was pumped through the column for 2 h at a flow-rate of 0.2 ml min^{-1} and the column was washed with deaerated water for 15 min at a flow-rate of 0.6 ml min^{-1}. Enzyme solution [1000 U of PyrOD or GOD in 10 ml of 0.05 M phosphate buffer solution (pH 7.0)] was circulated through the column at a flow-rate of 0.2 ml min^{-1} for 3 h at room temperature. The enzyme activity in the solution was measured spectrophotometrically with D-glucose as substrate in the presence of peroxidase and *o*-dianisidine [12]. PyrOD and GOD were immobilized with 72% and 90% yields, respectively.

RESULTS AND DISCUSSION

Evaluation of enzyme reactors

The properties of immobilized PyrOD and GOD were first compared in terms of reaction conditions (pH and temperature), substrate specificity, operational and storage stabilities and sensitivity.

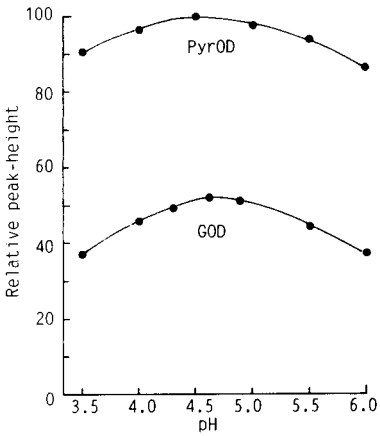

Fig. 2. Effect of pH on the activity of the immobilized enzymes. PyrOD = immobilized pyranose oxidase reactor; GOD = immobilized glucose oxidase reactor.

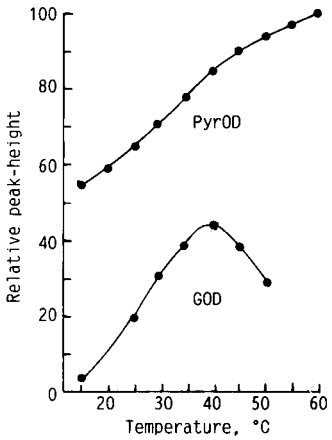

Fig. 3. Effect of temperature on the activity of the immobilized enzyme. PyrOD = immobilized pyranose oxidase; GOD = immobilized glucose oxidase.

To test the activities of the reactors, the system shown in Fig. 1 was used and measurements were made to establish the optimum pH with McIlvaine buffer between pH 3.5 and 6.0. Figure 2 shows the effect of pH on peak height. Maximum responses for PyrOD and GOD were obtained at pH 4.5 and 4.6, respectively. Compared with the free enzymes (the optimum pH values for PyrOD and GOD are 5.8 and 5.0, respectively), the pH maxima for the immobilized PyrOD and GOD are ca. 1.3 and 0.4 pH units more acidic, respectively.

The effect of temperature on the activity was examined over the range 15–60°C. The immobilized GOD exhibited maximum activity at 40°C and the activity was considerably dependent on temperature, as shown in Fig. 3. At 40°C, glucose (5 μM) was converted in a 41% yield. For immobilized PyrOD higher temperatures resulted in higher activities up to at least 60°C, although the activity was not strongly influenced by the reaction temperature. Rapid deactivation was observed above 68°C. The conversion efficiencies of glucose (5 μM) at 40 and 60°C were 78 and 91%, respectively.

The relative activities of the immobilized enzymes for various saccharides and alcohols were measured under the conditions in Fig. 1 and the results are given in Table 1. GOD is specific for

TABLE 1

Specificities of immobilized PyrOD and GOD

Substrate	Relative activity [a]	
	PyrOd	GOD
β-D-Glucose	100	100
α-D-Glucose	100	0
D-Xylose	106	0
L-Xylose	4	0
L-Sorbose	67	0
D-Galactose	54	0
L-Xylose	4	0
Maltose	2	0
Melibiose	3	0
Cellobiose	2	0
2-Deoxy-D-glucose	0	7
1,5-Anhydroglucitol	76	0
Sorbitol	4	0
Inositol	2	0
Ethylene glycol	65	0
Glycerol	44	0
Butanediol	9	0
Propylene glycol	8	0
Methanol	9	0
Ethanol	4	0
1-Butanol	8	0

[a] PyrOD and GOD did not oxidize D-mannose, D-fructose, L-fucose, L-arabinose, D-ribose, sucrose, lactose, raffinose, stachyose, xylitol, D-ribitol, galactitol, D-arabinitol and D-mannitol.

β-D-glucose and 2-deoxyglucose, but PyrOD exhibits low specificity for pyranoses and polyols.

The operational stability of the immobilized enzymes was evaluated over a period of 8 weeks. The reactors were used for 4 h per day (240 injections of 5 μM glucose) and stored in a refrigerator when not in use. The results are shown in Fig. 4. Immobilized PyrOD was stable and after 8 weeks (about 9500 injections) the activity was 90% of the initial value. The immobilized enzymes were lyophilized and stored at −15°C in the presence of sucrose (500 mg g^{-1} enzyme). Immobilized PyrOD and GOD retained 95 and 70%, respectively, of their original activities after 8 months.

Under the conditions in Fig. 1, peak heights were plotted against D-glucose concentration. The calibration graphs for immobilized PyrOD and GOD were linear over the ranges 0.2–500 and 0.5–1000 μM glucose, respectively. Four calibration graphs were prepared by using immobilized PyrOD, covering the ranges 0.2–2.0, 1.0–10, 10–100 and 100–500 μM. The least-squares calibration equation for the concentration range 1.0–10 μM ws $y = 20.95x + 0.21$, where y is peak height (mm) and x is glucose concentration (μM), with a linear correlation coefficient of $r = 0.998$ (11 data points). In the same concentration range, the calibration equation for immobilized GOD was $y = 11.03x + 0.14$, with $r = 0.996$ (11 data points). The detection limits (signal-to-noise ratio = 3) for immobilized PyrOD and GOD were 0.05 μM (0.1) and 0.1 μM glucose (0.2 ng in a 10-μl injection), respectively.

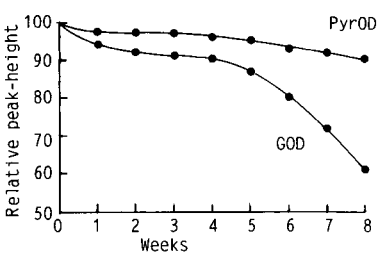

Fig. 4. Operational stabilities of immobilized enzymes. PyrOD = immobilized pyranose oxidase; GOD = immobilized glucose oxidase. For each reactor the peak height on the first day was taken as 100.

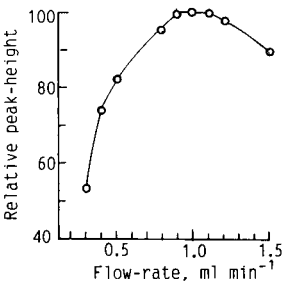

Fig. 5. Effect of flow-rate on peak height.

The effect of the flow-rate of the carrier on the peak height was studied over the range 0.3–1.5 ml min^{-1} by using the immobilized PyrOD reactor. The flow-rates of both the luminol solution and potassium hexacyanoferrate(III) solution were kept constant at 0.5 ml min^{-1}. The results are shown in Fig. 5. As the flow-rate was decreased, the peak height decreased but the peak width increased, owing to the dilution of sample and the H_2O_2, although the peak area remained constant below 0.5 ml min^{-1} (the reaction efficiency was 100%). The peak height was constant from 0.9 to 1.1 ml min^{-1} because the decrease in reaction efficiency compensates for the increase in the peak sharpness. At higher flow-rates, on account of the decrease in reaction efficiency, the peak height decreased with increasing flow-rate, whereas the time for baseline reversion decreased. A flow-rate of 1.0 ml min^{-1} was chosen for a compromise between sensitivity and sample throughput.

Application

The flow-injection system shown in Fig. 1 was applied to the determination of glucose in serum samples. As the concentrations of the substrates for PyrOD in serum are normally far lower than that of glucose, this method is not subject to interferences from such compounds. Serum (100 nl) was diluted 1000-fold with water because of the interference with the chemiluminescence reaction from proteins at concentrations > 3 g l^{-1} and of the low solubility of oxygen in aqueous solution (8 mg l^{-1} at 25°C in contact with air). The diluted serum sample (10 μl) was injected into the carrier stream. The reactor was kept at

TABLE 2

Results for glucose in serum sample by the flow-injection method with an immobilized PyrOD reactor

Glucose concentration (mM) [a]	Relative standard deviation (%)	
	Within	Day-to-day
7.44 ± 0.087	1.2	
7.61 ± 0.103		1.4

[a] Mean ± standard deviation. Values are means of nine determinations.

40°C in a thermostat in order to obtain precise data. The results were compared with those obtained with a Hitachi 736 automatic analyser with soluble hexokinase–glucose-6-phosphate dehydrogenase. The calculated linear regression and correlation coefficient were $y = 0.987x - 0.002$ and $r = 0.995$, respectively.

Normal pooled serum was repeatedly analysed for 4 weeks with the immobilized PyrOD reactor. As shown in Table 2, the proposed method gave satisfactorily reproducible results. The presence of an equimolar concentration of L-ascorbate lowered the peak height of glucose by 27%.

It is concluded that this flow-injection system with an immobilized PyrOD reactor is useful for the sensitive and reliable measurement of glucose. It was expected that, if the enzymatic reactions go to completion, the method with immobilized PyrOD would be about 1.5 times more sensitive than that with immobilized GOD. However, the sensitivity for the proposed method was about twice that for the method with immobilized GOD. This difference shows that the flow-injection methods are kinetically controlled and that the reaction rate for PyrOD is greater than that for GOD. The immobilized PyrOD was stable enough to permit about 9500 measurements during 2 months.

REFERENCES

1 D.T. Bostick and D.M. Hercules, Anal. Chem., 47 (1975) 447.
2 M. Tabata, C. Fukunaga, M. Ohyabu and T. Murachi, J. Appl. Biochem., 6 (1984) 251.
3 C.A. Swinlehurst and T.A. Nieman, Anal. Chim. Acta, 205 (1988) 195.
4 B.A. Petersson, Anal. Lett., 22 (1989) 83.
5 A.S. Keson and R. Brandt, Anal. Biochem., 6 (1963) 461.
6 J. Okuda and I. Miwa, Anal. Biochem., 43 (1971) 312.
7 J. Okuda, I. Miwa, K. Maeda and K. Tokui, Carbohydr. Res., 58 (1977) 267.
8 H.W. Ruelius, R.M. Kerwin and F.W. Janssen, Biochim. Biophys. Acta, 167 (1968) 493.
9 F.W. Janssen and H.W. Ruelius, Biochim. Biophys. Acta, 167 (1968) 501.
10 Y. Machida and T. Nakanishi, Agric. Biol. Chem., 48 (1984) 2463.
11 L. Olsson, C.F. Mandenius and J. Velc, Anal. Chem., 62 (1990) 2688.
12 H.U. Bergmeyer, M. Grassl and H.-E. Walter, in H.U. Bergmeyer, J. Bergmeyer and M. Grassl, Methods of Enzymatic Analysis, Vol. II, Verlag Chemie, Weinheim, 3rd edn., 1983, pp. 201–202.

Analytica Chimica Acta, 269 (1992) 193–198
Elsevier Science Publishers B.V., Amsterdam

Flow-injection determination of sulphonamides with fluorimetric or photochemical–fluorimetric detection

M.C. Mahedero

Department of Analytical Chemistry, Faculty of Sciences, University of Extremadura, Badajoz (Spain)

J.J. Aaron

Institut de Topologie et de Dynamique des Systèmes de l'Université Paris 7, associé au CNRS, 1 rue Guy de la Brosse, 75005 Paris (France)

(Received 23rd April 1992; revised manuscript received 3rd July 1992)

Abstract

A flow-injection method with photochemically induced fluorescence (PF) or native fluorescence (NF) detection was developed for the determination of four sulphonamides. Sulphamethazine was determined using PF and sulphanilamide, sulphaguanidine and sulphacetamide using NF. Linear calibration graphs were obtained over a concentration range of one order of magnitude. The relative standard deviations were within the range 0.4–5%. Limits of detection were between 0.015 and 0.12 μg ml^{-1}. The method was applied to the determination of sulphonamides in milk and pharmaceutical preparations.

Keywords: Flow injection; Fluorimetry; Milk; Pharmaceuticals; Sulphonamides

Sulphonamides are extensively used in medicine and veterinary practice as antibacterial drugs. A variety of methods have been developed for determining sulphonamides. Ultraviolet (UV) and visible spectrophotometry [1–9], liquid chromatography (LC) [10–23], flow-injection analysis (FIA) [24–27] and, less frequently, spectrofluorimetry [28,29] have been reported. Several of these methods are not very sensitive, such as the classical spectrophotometric Bratton–Marshall procedure [1], or are time consuming, such as spectrofluorimetry, which involves chemical derivatization of sulphadiazine by the fluorescamine reaction [28].

Correspondence to: J.J. Aaron, Institut de Topologie et de Dynamique des Systèmes de l'Université Paris 7, associé au CNRS, 1 rue Guy de la Brosse, 75005 Paris (France).

Recently, it has been established that the UV irradiation of photoreactive drugs led to the formation of species that could be detected by fluorescence [30–38]. However, until now, such photochemical–fluorescence detectors have been mainly applied to LC [30,35]; they have been used only rarely for improving the fluorescence detection of analytes in simple hydrodynamic systems such as FIA [36–38].

The photochemistry of sulphonamides was investigated a few years ago [39,40]. Ahmad [39] proposed a general scheme for the photodegradation pathways of sulphacetamide in aqueous solution. Tammilehto and Lehtonen [40] separated by high-performance thin-layer chromatography several products resulting from the photolysis of sulphacetamide. Also, recently it was shown that the photochemically induced fluorescence of sev-

eral heterocyclic sulphonamides could be used for determining these compounds in batch aqueous solution [29].

In this paper, a new method based on FIA coupled to photochemically induced fluorescence (PF) or native fluorescence (NF) is described for the determination of several sulphonamides. The PF method was applied to the determination of sulphamethazine and the NF method to that of sulphanilamide, sulphaguanidine and sulphacetamide. These sulphonamides were also determined in authentic samples.

EXPERIMENTAL

Apparatus

A schematic diagram of the FIA photochemical–fluorescence system is shown in Fig. 1. The experimental set-up consisted of an Ismatec IPN-4 peristaltic pump, a rotary injection valve, a 254-nm low-pressure mercury lamp irradiating a PTFE reactor (0.5 mm i.d.) and a Kontron SFM-25 spectrofluorimeter equipped with an LC fluorescence cell accessory and a Sefram Servotrace Type PE chart recorder.

The injected samples were propelled with an aqueous carrier and were irradiated in the PTFE photoreactor before fluorimetric detection. The effect of PTFE photoreactor length, flow-rates through the reactor, residence times and volumes injected on the fluorescence signals were examined for several concentrations of sulphonamides and optimized to provide maximum responses and minimum band broadening.

Reagents

Sulphanilamide (SAN), sulphaguanidine (SG), sulphacetamide (SAC) and sulphamethazine (SMT) were purchased from Sigma. Pharmaceutical preparations of sulphonamides were donated by various manufactuers (Canidiarix, from Therapeutique Vétérinaire Moderne, Lempdes; Antebor from Lab. Biologique Ile-de-France, Paris; Vitaseptine from Lab. M. Faure, Annonay; and Sulphadimerazine 33% Noé from Lab. Noé-Socopharm, Château-Thierry). Standard solutions of sulphonamides (2×10^{-3} M) were prepared from the corresponding compounds by dissolving them in ethanol (Aldrich, analytical-reagent grade) or deionized water.

Procedure

The carrier used was water in all instances. Fluorescence measurements of sulphonamides were performed in two operating modes, according to the photochemical behaviour of the compounds [29], i.e., UV lamp off (native fluorescence detection) for SAN, SG and SAC, or UV lamp on (photochemically induced fluorescence detection) for SMT. Triplicate measurements

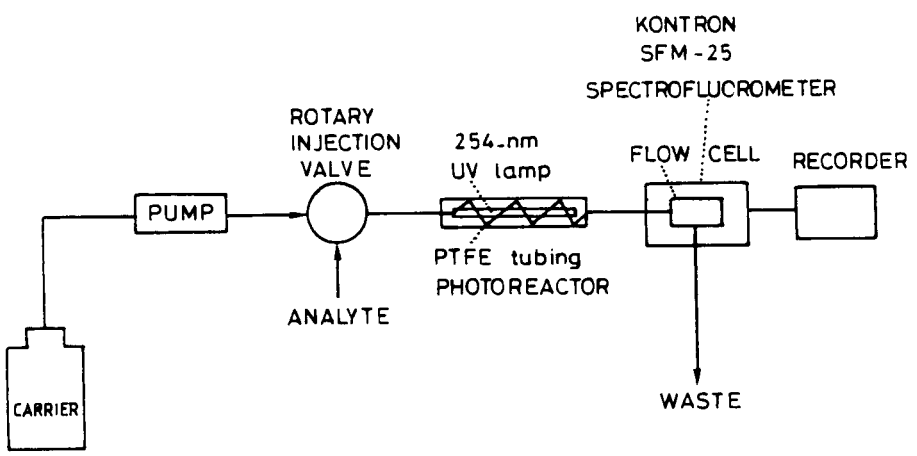

Fig. 1. Schematic diagram of the experimental set-up.

TABLE 1

Analytical parameters for the flow-injection fluorimetric and photochemical–fluorimetric determination of sulphonamides

Compound	λ(ex/em) (nm) [a]	Flow-rate (ml min^{-1})	Volume injected (μl)	Reactor length (cm)	UV irradiation [c]
SAN	260/345	5.0	140	20 [b]	N
SGN	260/345	5.0	104	20 [b]	N
SAC	260/345	5.0	104	20 [b]	N
SMT	284/350	5.0	104	100	Y

[a] Analytical excitation and emission wavelengths. [b] Minimum length of the reactor required for operating the rotary injection valve. [c] N means that the UV lamp was off and Y that the UV lamp was on for these measurements.

were made to evaluate the reproducibility for each analyte. All sulphonamides were detected at constant excitation and emission wavelengths (listed in Table 1). Analytical figures of merit were obtained in the range 0.04–3.0 μg ml^{-1} for the sulphonamide standard solutions. Recoveries from authentic samples (milk and pharmaceutical preparations) were evaluated by using the standard addition procedure.

RESULTS AND DISCUSSION

Effect of variables

The effects of several variables on the intensity and the width of the flow-injection peaks of sulphonamides were studied. It was found that the volume injected, the flow-rate and the reactor length produced significant changes of the fluorescence signals. Figure 2 shows that the highest peaks were obtained for volumes injected larger than 100 μl, when native fluorescence detection was used. Changes in flow-rate also led to a variation of the fluorescence intensity; for SMT, the curves in Fig. 3 demonstrate a decrease in the fluorescence signal when the flow-rate is increased because of a decreased time of exposure to the UV source. The strongest signal for SMT was achieved with a reactor length of 100 cm (Fig. 3). A reactor tube is not necessary for native fluorescence detection, so a 20 cm length gave the highest peaks, for the other sulphonamides. Table 1 summarizes the optimum values of the variables selected for FIA–fluorescence determination of sulphonamides. A typical set of peaks, obtained under the optimum conditions, is given for SMT in Fig. 4, showing the excellent precision of the triplicate measurements.

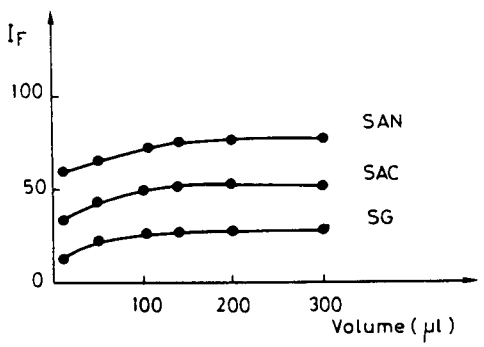

Fig. 2. Effect of sample injection volumes on the fluorescence signals of sulphanilamide ([SAN] = 1.0 μg ml^{-1}), sulphacetamide ([SAC] = 0.4 μg ml^{-1}) and sulphaguanidine ([SG] = 1.0 μg ml^{-1}). Flow-rate, 5 ml min^{-1}; reactor length, 16 cm.

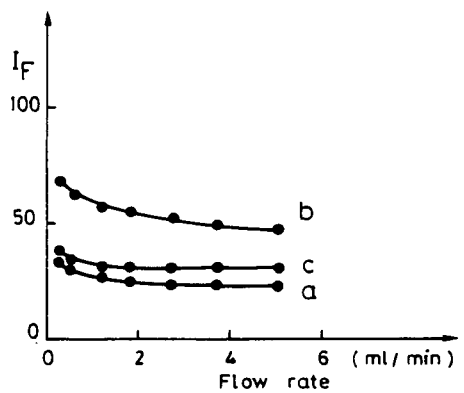

Fig. 3. Effect of flow-rate on the fluorescence signal of 1.25 μg ml^{-1} sulphamethazine for reactor lengths of (a) 50, (b) 100 and (c) 200 cm. Sample volume injected, 104 μl.

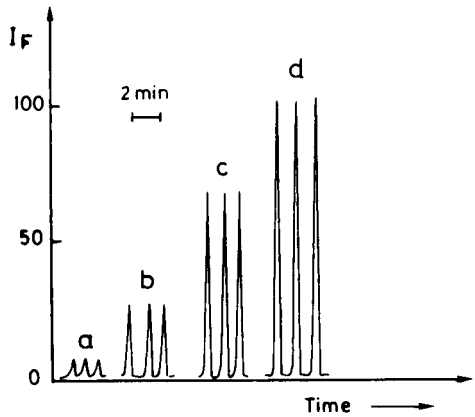

Fig. 4. Influence of concentration of sulphamethazine on the FIA–PF peak: (a) 0.4; (b) 1.0; (c) 2.0; (d) 3.0 μg ml^{-1}. Sample volume injected, 104 μl; flow-rate, 5 ml min^{-1}; reactor length, 100 cm.

TABLE 3

Effect of other sulphonamides on the determination of the sulphonamides

Foreign species	Maximum tolerated level [b] (μg ml^{-1})			
	SAN [c]	SG [d]	SAC [e]	SMT [f]
Sulphamethazine	1.0	1.0	1.0	–
Sulphamerazine	2.0	0.8	0.6	0.06
Sulphadiazine	1.2	1.0	1.0	0.06
Sulphapyridine	2.0	0.8	0.6	0.06
Sulphaguanine	0.2	–	0.08	0.1
Sulphanilamide	–	0.2	0.08	0.06
Sulphacetamide	0.5	0.2	–	0.02

[a] Study performed under the conditions given in Table 1. [b] Defined as the concentration of foreign species at which the variation of the measured fluorescence signal is greater than ±5%. [c] [SAN] = 1.0 μg ml^{-1}. [d] [SG] = 0.6 μg ml^{-1}. [e] [SAC] = 0.08 μg ml^{-1}. [f] [SMT] = 2.0 μg ml^{-1}.

Analytical figures of merit

The analytical figures of merit for the determination of the four sulphonamides are given in Table 2. These figures were obtained from at least 4–6 measurements at various concentrations. Typical calibration graphs for these analytes were linear over a concentration range of at least one order of magnitude.

Interferences

Because of the possible simultaneous presence of several sulphonamides either in pharmaceutical compounds or in natural food products, the influence of other sulphonamides (acting as foreign species) on the determination of the four sulphonamides under study was evaluated (Table 3). The experiments were performed by adding specific amounts of interferent to various concentrations of analyte. Sulphamerazine, sulphadiazine and sulphapyridine were tolerated at the 0.6–2 μg ml^{-1} level for the determination of sulphanilamide, sulphaguanidine and sulphacetamide, whereas these same compounds interfered in the determination of sulphamethazine at the 0.06 μg ml^{-1} level. Also, sulphaguanidine interfered at the 0.08–0.2 μg ml^{-1} level in the determination of sulphanilamide, sulphacetamide and sulphamethazine. These interferences at relatively low levels can be attributed to the very similar values of the fluorescence excitation and emission wavelengths of these compounds.

TABLE 2

Analytical figures of merit for the flow-injection fluorimetric and photochemical–fluorimetric determination of sulphonamides

Compound	Detection [a]	Concentration range (μg ml^{-1})	Regression equation [b]	Correlation coefficient	Limit of detection (ng ml^{-1}) [c]	R.S.D. [d] (%)
SAN	NF	0.1–1.0	$I_F = 20.7c + 0.11$	0.999	30	0.4
SG	NF	0.1–1.0	$I_F = 8.74c + 0.32$	0.995	30	2.6
SAC	NF	0.04–0.2	$I_F = 0.02c + 0.42$	0.999	15	5.0
SMT	PF	0.4–3.0	$I_F = 3.70c - 0.8$	0.999	120	3.4

[a] NF = native fluorescence; PF = photochemically induced fluorescence. [b] I_F = relative fluorescence signal; c = analyte concentration (μg ml^{-1}). [c] $n = 6$. R.S.D. = mid-range relative standard deviation ($n = 4$–6).

TABLE 4

Determination of sulphonamides in pharmaceutical formulations

Sample	Analyte	Recovery [a] (%)
Canidiarix	SG	99–102
Antebor	SAC	100–102
Vitaseptine	SAC	99–101
Sulphadimerazine (33% Noé)	SMT	97–103

[a] Values measured using the standard addition procedure.

Analytical applications

In order to evaluate the analytical usefulness of the method, several sulphonamides were determined in pharmaceutical formulations using the standard addition procedure. Pharmaceutical preparations of SG, SAC and SMT were dissolved in water. Table 4 presents the results. Milk samples were treated with SAN (to give concentrations of 10–50 $\mu g\ ml^{-1}$) and were diluted with water. Satisfactory results were obtained with recoveries ranging from 99 to 103% for SG, SAC and SMT in pharmaceutical formulations and from 100 to 106% for SAN added milk samples.

Conclusion

It has been demonstrated that either photochemically induced fluorescence or native fluorescence detection can be combined with FIA for the determination of sulphonamides. This method was shown to be rapid, simple and sensitive, and it compares favourably with other techniques used for the determination of sulphonamides such as the Bratton–Marshall procedure [1,2] or time-consuming derivatization fluorimetry [28]. Therefore, the use of photochemical reactions in an unsegmented flow system should be valuable from an analytical standpoint for improving the fluorescence detection of analytes.

M.C.M. is grateful to the Spanish Government (Ministerio de Educacion y Ciencia) for financial support. The authors thank Dr. P. Soubiran for assistance with the development of the photoreactor. The gift of pharmaceutical formulations from Thérapeutique Vétérinaire Moderne, Lab. Biologique Ile-de-France, Lab. M. Faure and Lab. Noé-Socopharm is gratefully acknowledged.

REFERENCES

1 A.C. Bratton and E.K. Marshall, J. Biol. Chem., 128 (1939) 537.
2 F. Salinas, A. Espinos Mansilla and B. Nevado, Anal. Chim. Acta, 233 (1990) 289.
3 J. Rieder, Chemotherapy (Basel), 17 (1972) 1.
4 A.G. Xanakis and M.I. Karayannis, Anal. Chim. Acta, 159 (1984) 343.
5 H.B. Falk and R.G. Kelley, Clin. Chem., 11 (1965) 1045.
6 A. Bye and A.F.J. Fox, Clin. Chem., 20 (1974) 288.
7 H.E. Abdellatef, M.N. Elbakiny and A. Aboulkeir, J. Pharm. Biomed. Anal., 7 (1989) 571.
8 V.M. Sadivski, V.V. Petrenko, and B.P. Zorya, Zh. Anal. Khim., 45 (1990) 609.
9 M.Q. Al-Abalhi, E.S. Salih and M.S. Salem, Fresenius' Z. Anal. Chem., 337 (1990) 408.
10 V. Sprinbold and G. Coppi, J. Pharm. Biomed. Anal., 7 (1989) 57.
11 M.E. Sharp, S.M. Wallace, K.W. Hindmarsh and M.A. Brown, Can. J. Pharm. Sci., 15 (1980) 35.
12 S. Horri, K. Jinbo, T. Hashimoto, K. Igusa and T. Maruyama, Kenkyu Nenpo-Tokyo-Toritsu Eisei, Kenkyusho, 40 (1989) 137.
13 M. Horie, K. Saito, Y. Hoshino, N. Nose, N. Hamada and H. Nakazawa, J. Chromatogr., 502 (1990) 371.
14 K. Michels, Landwirtsch. Forsch., 40 (1987) 326.
15 M. Petz, J. Chromatogr., 423 (1987) 217.
16 E.D. McGary, Analyst, 111 (1986) 1341.
17 J. Torel, J. Cillard, P. Cillard and M. Vie, J. Chromatogr., 330 (1985) 425.
18 M.A. Alawi and H.A. Ruessel, Fresenius' Z. Anal. Chem., 307 (1981) 382.
19 R.T. Kon, L. Geissel and R.A. Leavitt, Food Addit. Contam., 1 (1984) 67.
20 M.A.S. Salem, H.N. Alkaysi and A.A. Badwan, Anal. Lett., 23 (1990) 461.
21 L. Hall and V. Chadwick, J. Chromatogr., 478 (1989) 438.
22 A.R. Long, C.R. Short and S.A. Barker, J. Chromatogr., 502 (1990) 87.
23 A.R. Long, L.C. Hsieh, M.S. Malbrough, C.R. Short and S.A. Baker, J. Agric. Food Chem., 38 (1990) 423.
24 M.A. Koupparis and O.I. Anagnostopoulou, Anal. Chim. Acta, 204 (1988) 271.
25 K.K. Verma and K.K. Stewart, Anal. Chim. Acta, 214 (1988) 207.
26 A. Al-Wehaid and A. Townshend, Anal. Chim. Acta, 186 (1986) 289.
27 A.G. Fogg, N.K. Bsebsu and M.A. Abdallah, Analyst, 107 (1982) 1462.
28 J.M. Sterling and W.G. Haney, J. Pharm. Sci., 63 (1974) 1448.

29 M.C. Mahedero and J.J. Aaron, Analusis, 20 (1992) 53.
30 J.W. Birks and R.W. Frei, Trends Anal. Chem., 1 (1982) 361.
31 J.J. Aaron and J. Fidanza, Talanta, 29 (1982) 383.
32 J.J. Aaron and J. Fidanza, Analusis, 16 (1988) 353.
33 R. Fricoteaux, J.J. Aaron and M.G. Quaglia, J. Pharm. Biomed. Anal., 7 (1989) 1585.
34 J. Fidanza and J.J. Aaron, Anal. Chim. Acta, 227 (1989) 325.
35 J.J. Aaron, in S.G. Schulman (Ed.), Molecular Luminescence Spectroscopy, Methods and Applications, Part 3, Wiley, New York, in press.
36 M. Tsuchiya, E. Torres, J.J. Aaron and J.D. Winefordner, Anal. Lett., 18 (1984) 1831.
37 D. Chen, A. Rios, M.D. Luque de Castro and M. Valcarcel, Analyst, 116 (1991) 171.
38 B.M. Patel, H.A. Moye and R. Weinberger, Talanta, 38 (1991) 913; Anal. Lett., 22 (1989) 3057.
39 T. Ahmad, Pharmazie, 37 (1982) 559.
40 S. Tammilehto and M. Lehtonen, Abstract of 2nd International Symposium on Drug Analysis, Brussels, 1986, p. 241.

Analytica Chimica Acta, 269 (1992) 199–203
Elsevier Science Publishers B.V., Amsterdam

Spectrophotometric determination of cardiac glycosides by flow-injection analysis

P. Solich, V. Sedliaková and R. Karlíček

Department of Analytical Chemistry, Faculty of Pharmacy, Charles University, CS-50165 Hradec Králové (Czechoslovakia)

(Received 11th November 1991; revised manuscript received 25th June 1992)

Abstract

An optimized flow-injection method is described for the determination of various cardiac glycosides (lanatoside A, B and C, digoxin, digitoxin, acetyldigitoxin, ouabain) based on their reaction with picric acid in alkaline media using spectrophotometric detection at 486 nm. The calibration graph is linear for 0.025–0.5 g l^{-1} cardiac glycosides (except ouabain) and 0.01–0.2 g l^{-1} ouabain, with R.S.D. between 0.62 and 2.16% ($n = 6$) and a sample throughput of 60 h^{-1}. This method was utilized for the determination of digoxin in tablets and lanatoside C and ouabain in injections.

Keywords: Flow injection; UV–Visible spectrophotometry; Cardiac glycosides; Pharmaceuticals

Cardiac glycosides represent one of the most important groups of therapeutic agents used for the treatment of heart diseases. Their structure is based on the steroid molecule with a lactone ring and various substituents at R_1, R_2 and R_3 (Figs. 1 and 2).

Many methods have been reported for the determination of cardiac glycosides, including liquid chromatography [1–5], thin-layer chromatography, [6,7], UV–visible spectrophotometry [8–12] and enzyme immunoassay [13,14]. There are several reports of the use of an automated system for the determination of cardiac glycosides utilizing the Technicon AutoAnalyzer system, e.g., in combination with 2-thiobarbituric acid for a spectrophotometric method [15] and fluorimetric method [16].

Based on the need for simple, economic and time-saving methods for routine analysis, flow-injection analysis (FIA) has become a widely used tool in many different fields of chemistry [17,18]. Recently increasing attention has been devoted to the area of pharmaceutical analysis [19,20].

Picric acid is a commonly used reagent in analytical chemistry. Several drugs have been determined by FIA using picric acid as an ion-pairing agent followed by extraction into an organic solvent, examples being the analysis of the benzalkonium salts [21] and codeine [22]. For creatinine, direct determination in aqueous media has been reported [23].

So far there has been no attempt to use a picric acid method for the automatic flow determination of cardiac glycosides. In this paper a simple flow-injection method is described for the determination of various cardiac glycosides (lanatoside A, B and C, digoxin, digitoxin, β-acetyldigitoxin and ouabain) based on the spectrophotometric detection of coloured products formed by their reaction with picric acid in alkaline media.

Correspondence to: P. Solich, Department of Analytical Chemistry, Faculty of Pharmacy, Charles University, CS-50165 Hradec Králové (Czechoslovakia).

EXPERIMENTAL

Reagents

Lanatoside A, B and C, digoxin, digitoxin, β-acetyldigitoxin and ouabain were obtained as National Standard (SÚKL, Prague). Stock solutions of these cardiac glycosides were prepared by dissolving 50.0 mg of each in 50 ml of ethanol (Lachema, Brno) and diluting to 100 ml with distilled water. Calibration solutions containing 10–500 mg l^{-1} glycoside were prepared using 50% (v/v) ethanol for dilution.

A carrier was prepared by adding Brij 35 (Sigma, Poole) to 50% (v/v) ethanol to give a total concentration of 0.01% (w/v). Picric acid reagent was prepared by mixing 0.065 M picric acid (Sigma) and 1 M sodium hydroxide (Lachema) and diluting with distilled water to the appropriate concentration as discussed below. When stored in a cool and dark place this solution was stable for 3 days.

Both the carrier and reagent were filtered through a 0.4-μm filter (Synpor, Prague) and degassed under reduced pressure. All chemicals were of analytical-reagent grade and distilled, deionized water was used throughout for the preparation of solutions.

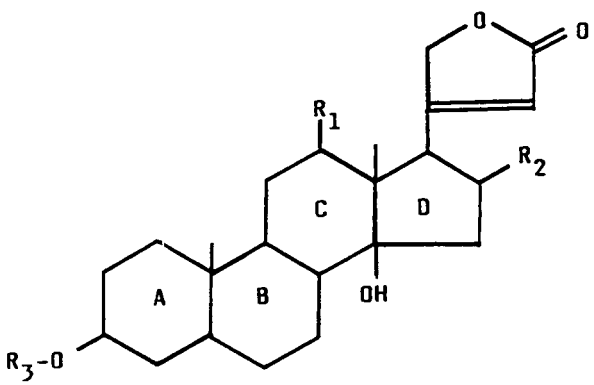

Fig. 1. Structure of cardiac glycosides.

Compound	R_1	R_2	R_3
Lanatoside A	H	H	-d-d-ad-g
Lanatoside B	H	OH	-d-d-ad-g
Lanatoside C	OH	H	-d-d-ad-g
Digitoxin	H	H	-d-d-d
Digoxin	OH	H	-d-d-d
β-Acetyldigitoxin	H	H	-d-d-ad

d = D-digitoxose; ad = acetyldigitoxose; g = D-glucose.

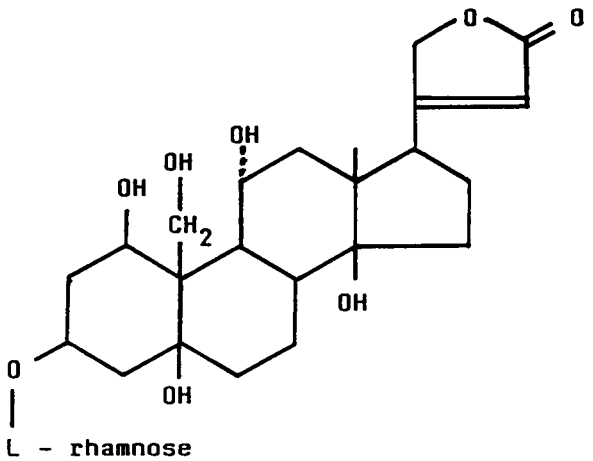

Fig. 2. Structure of ouabain.

Apparatus

The flow-injection manifold is shown in Fig. 3 and consisted of a commercial FIA 20 Analyzer (ZD Pouchov, Piletice, Czechoslovakia) linked to a Spekol 10 single-wavelength photometer (Zeiss, Jena, Germany) equipped with an EKMi accessory (consisting of a flow-through cell of path length 10 mm and volume 18 μl) and a TZ 4200 chart recorder (Laboratorní Přístroje, Prague). All connections and reaction coils were made using 0.5 mm I.D. PTFE tubing.

Procedure

The following parameters of the flow system were optimized with respect to the sensitivity and speed of determination, on the basis of two re-

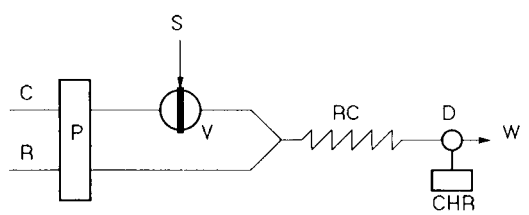

Fig. 3. Flow-injection manifold for determination of cardiac glycosides. C = carrier; R = reagent; P = pump; V = injection valve; S = sample; RC = reaction coil; D = detector; W = waste; CHR = chart recorder.

sponse functions, absorbance at 486 nm and residence time: the flow-rate of the individual streams (in the range 0.5–1.1 ml min^{-1}); the reaction coil length (100–300 cm); the volume of sample injected (40–100 μl); the content of ethanol in the carrier stream (0–50%, v/v); and the concentrations of sodium hydroxide (0.075–0.5 mol l^{-1}) and of picric acid (0.01–0.032 mol l^{-1}) in the reagent stream. All measurements were made at the absorbance maximum of the coloured product, which was confirmed as 486 nm, as previously reported [24].

The digoxin sample was prepared by first grinding and then weighing about 0.7 g of the tablet. After dissolution by stirring for 10 min in 10.0 ml of 50% (v/v) ethanol, the solution was filtered through Whatman No. 4 filter-paper and injected directly into the flow-injection system. The lanatoside C sample was directly injected into the flow system. The ouabain sample was first diluted 1 + 1 with 50% (v/v) ethanol and then injected into the flow-injection system.

RESULTS AND DISCUSSION

The optimized physical parameters of the flow system were found to be flow-rate 0.6 ml min^{-1}, reaction coil length 200 cm and sample volume 100 μl. Under these conditions, various compositions of reagent and carrier were investigated. The most important was found to be the concentration of sodium hydroxide, which must be as high as possible, owing to the mechanism of the reaction between picric acid and the lactone ring in the cardiac glycoside. Under strongly alkaline conditions, the lactone ring is cleaved and the active methylene group formed reacts with picric acid to produce an orange–yellow dye; this is known as the Baljet reaction [9].

The effects of sodium hydroxide and picric acid concentrations are shown in Table 1. A concentration of 0.4 mol l^{-1} sodium hydroxide in the reagent was found to be sufficient. Because of the low solubility of picric acid, the maximum concentration in the reagent investigated was 0.032 mol l^{-1}. Finally, for the flow system, a concentration of 0.02 mol l^{-1} picric acid was adopted to avoid the possible deposition of picrate on the tube walls or inside the cuvette.

TABLE 1

Influence of sodium hydroxide and picric acid concentration on absorbance for lanatoside C (0.2 g l^{-1})

[NaOH] [a] (mol l^{-1})	Absorbance	[PA] [b] (mol l^{-1})	Absorbance
0.075	0.035	0.010	0.143
0.2	0.105	0.016	0.159
0.3	0.137	0.020	0.174
0.4	0.188	0.032	0.188
0.5	0.186		

[a] At constant concentration of picric acid (PA) (0.02 mol l^{-1}).
[b] At constant concentration of sodium hydroxide (0.37 mol l^{-1}).

In earlier work [23], 20% methanol was recommended for the determination of creatinine with picric acid in order to eliminate baseline drift. In this work, the methanol was replaced with ethanol without any adverse effect. Because of the low solubility of cardiac glycosides in water, a concentration of 50% ethanol in the carrier was found to be optimum. The addition of non-ionic Brij 35 at a concentration of 0.01% (v/v) to the carrier stabilized the baseline, probably by preventing the deposition of reagent on the tube walls.

Calibration

For each cardiac glycoside, the linear regression calibration equation was calculated. The results are shown in Table 2. The calibration graph was linear from 0.01 to 0.5 g l^{-1} of cardiac

TABLE 2

Linear regression calibration parameters [a] of cardiac glycosides

Drug	c (g l^{-1})	n	b	a	r
Lanatoside A	0.025–0.5	7	1.58	0.015	0.9999
Lanatoside B	0.05 –0.5	6	1.06	0.004	0.9992
Lanatoside C	0.025–0.5	7	1.66	0.016	0.9999
Digoxin	0.025–0.4	7	2.38	0.019	0.9997
Digitoxin	0.025–0.4	7	2.09	0.015	0.9998
β-Acetyldigitoxin	0.05 –0.5	6	1.66	0.028	0.9995
Ouabain	0.01 –0.2	6	3.45	0.027	0.9996

[a] $A = bc + a$, where A = absorbance, c concentration range, b slope and a intercept; n number of calibration points; r correlation coefficient.

TABLE 3

Reproducibility of determination of cardiac glycosides

Drug	Concentration ($g\ l^{-1}$)	R.S.D. (%) [a]
Lanatoside A	0.2	0.65
Lanatoside B	0.3	1.81
Lanatoside C	0.2	1.69
Digoxin	0.1	1.78
Digitoxin	0.1	2.16
β-Acetyldigitoxin	0.2	0.68
Ouabain	0.1	1.37

[a] $n = 6$.

glycosides, depending on the molecule. The relative standard deviation (R.S.D.) for each analyte is shown in Table 3; the results (R.S.D. = 0.65–2.16%) confirm the good reproducibility of the proposed method. The dispersion coefficient of the system was measured as $D = 6.2$, with a sample throughput of 60 h^{-1}.

Determination in drug formulations

The proposed method was applied to the determination in Digoxin tablets containing 0.25 mg of digoxin (Léčiva, Prague). In contrast to the Pharmacopoeia Bohemoslovaca method [24], where a complicated extraction into an organic solvent is described, in this instance a simple extraction into 50% ethanol and direct injection of the filtrate allow results to be obtained rapidly.

Two other examples investigated were Lanatoside C injections (Léčiva) containing 0.20 mg of active substance in 1 ml and Strophantin G injection (Léčiva) containing 0.25 mg of ouabain in 1 ml. The results are given in Table 4. The effects of lactose, Tween 80, starch, gelatin and calcium stearate used as excipients in tablets and ingredients used in injections were investigated and found to exert no influence on the proposed determinations.

TABLE 4

Determination of cardiac glycosides in commercial drug formulations

Drug formulation	Claimed (mg)	Found (mg) [a]	% of label claim
Digoxin tablets	0.25	0.257 ± 0.006	102.7 ± 2.2
Lanatosid C injection	0.20 [b]	0.194 ± 0.004	97.2 ± 1.9
Strophantin G injection	0.25 [b]	0.252 ± 0.004	101.0 ± 1.6

[a] Mean ± S.D. for five samples, each injected in triplicate.
[b] in 1 ml of sample.

Conclusion

A simple flow-injection method for the determination of various individual cardiac glycosides is proposed based on picric acid under alkaline conditions as a reagent with spectrophotometric detection of the coloured product at 486 nm. The method was utilized for the direct determination of cardiac glycosides in commercial drug formulations.

The authors express their sincere gratitude to Professor Anthony F. Fell (University of Bradford) for his kind interest and valuable advice on the manuscript.

REFERENCES

1 Y. Fujii, Y. Ikeda, I. Okamoto and M. Yamazaki, J. Chromatogr., 508 (1990) 241.
2 Y. Fujii, Y. Ikeda and M. Yamazaki, J. Chromatogr. Sci., 28 (1990) 288.
3 N.A. Kazarinov, M.G. Levin, N.S. Soldin and L.B. Nelzeva, Farm. Zh. (Kiev), 2 (1989) 67.
4 E. Reh, J. Chromatogr., 433 (1988) 119.
5 Y. Fujii, Y. Ikeda and M. Yamazaki, J. Chromatogr., 448 (1988) 157.
6 K.I. Evstratova, V.K. Stashulenok and L.A. Khlebnikova, Khim. Farm. Zh., 22 (1988) 242.
7 Y. Fujii, Y. Ikeda and M. Yamazaki, J. Liq. Chromatogr., 13 (1990) 1909.
8 P. Solich, R. Karlíček and V. Jokl, Cesk. Farm., 37 (1988) 193.
9 G. Baumarten and W. Forster, D. Herzwirksamen Glykoside, Thieme, Stuttgart, 1963.
10 M. Wichtl and K. Drexler, Sci. Pharm., 36 (1968) 257.
11 A.W.M. Indemans, Pharm. Weekbl., 109 (1974) 161.
12 K. Jensen, Arch. Pharm. Chem. Sci. Ed., 1 (1973) 447.
13 K. Yoshimatsu, M. Satake, K. Shimomura, J. Sawada and T. Terao, J. Nat. Prod., 53 (1990) 1498.
14 E.I. Plyugacheva, M.I. Savenkova and D.I. Metelitsa, Khim. Farm. Zh., 22 (1988) 1392.
15 J.W. Myrick, J. Pharm. Sci., 58 (1969) 1018.
16 L.F. Cullen, D.L. Packman and G.J. Papariello, J. Pharm. Sci., 59 (1970) 697.

17 M. Valcarcel and M.D. Luque de Castro, Flow-injection Analysis, Principles and Applications, Wiley, New York, 1987.
18 B. Karlberg and G.I. Pacey, Flow-injection Analysis, a Practical Guide, Elsevier, Amsterdam, 1989.
19 M.D. Luque de Castro and M. Valcarcel, J. Pharm. Biomed. Anal., 7 (1989) 1291.
20 R. Karlíček and P. Solich, Cesk. Farm., 41 (1992) 62.
21 J.J. Halvax, G. Wiese, J.A. Arp, J.M.P. Vermeer, W.P. Van Bennekom and A. Bult, J. Pharm. Biomed. Anal., 8 (1990) 243.
22 B. Karlberg, P.A. Johansson and S. Thelander, Anal. Chim. Acta, 104 (1979) 21.
23 J.V. Van Staden, Fresenius' Z. Anal. Chem., 315 (1983) 141.
24 Pharmacopoeia Bohemoslovaca, Avicenum, Prague, 4th edn., 1987.

Analytica Chimica Acta, 269 (1992) 205–210
Elsevier Science Publishers B.V., Amsterdam

Gas chromatographic method for discriminating between chlorinated pesticides and polychlorobiphenyls in mixtures

Luiz H. Vidal, Wagner R. Trevelin, Maria D. Landgraf and Maria O.O. Rezende

Departamento de Química e Física Molecular, Instituto de Física e Química de São Carlos, Universidade de São Paulo, Cx.P. 369, CEP 13560, São Carlos SP (Brazil)

(Received 5th February 1992; revised manuscript received 25th May 1992)

Abstract

A gas chromatographic method for differentiating between chlorinated pesticides and polychlorobiphenyls (PCBs) in mixtures, based on the effects of temperature on the areas (A) of the peaks obtained with an electron-capture detector, is described. It is shown that plots of peak area vs. temperature for chlorinated pesticides have broad peaks with maxima near 550 K whereas similar plots for PCBs tend to increase continuously with increasing temperature. It is also observed that plots of ln $AT^{3/2}$ vs. $1/T$ are linear with slopes near zero or positive for chlorinated pesticides and negative and large for PCBs. This behaviour is combined with relative retention indices to differentiate between chlorinated pesticides and PCBs in river sediments.

Keywords: Gas chromatography; Organochlorine pesticides, Pesticides, Polychlorobiphenyls, Sediments

Environmental pollution due to chlorinated pesticides and polychlorobiphenyls (PCBs) has aroused significant interest in the determination of these species in the environment. A method commonly used is high-resolution gas chromatography with electron-capture detection (HRGC–ECD) [1–3]. Because ECD shows high sensitivity to many chlorinated pesticides and PCBs and also other pollutants, it is frequently difficult to differentiate among different classes of compounds by using retention times alone [4,5]. This is particularly true for chlorinated pesticides and PCBs, because similar retention times are often obtained for different compounds in these two groups.

In this paper an approach is described that can be used in combination with retention times to differentiate between chlorinated pesticides and PCBs. The method is based on the finding that the effects of detection temperature on peak areas are very different for these two groups of compounds. Whereas plots of peak area (A) vs. temperature for chlorinated pesticides pass through broad maxima, those for PCBs tend to increase monotonically with increasing temperature. Moreover, slopes of plots of ln $AT^{3/2}$ vs. $1/T$ tend to be near zero or positive for chlorinated pesticides but negative and large for PCBs. The shapes of the temperature plots can be explained mechanistically based on the kinetic model of Wentworth [6–9].

Results are reported for prepared mixtures and for extracts of river sediments.

Correspondence to: M.O.O. Rezende, Departamento de Química e Física Molecular, Instituto de Física e Química de São Carlos, Cx.P. 369, CEP 13560, São Carlos SP (Brazil).

EXPERIMENTAL

Samples of sediment from Atibaia River (SP), Brazil, which passes through an industrial district and near an agricultural region were collected.

Reagents and materials

A Model 5890 gas chromatograph (Hewlett-Packard, Palo Alto, CA) with a ^{63}Ni electron-capture detector and a Model 3393 integrator (Hewlett-Packard) were used for the separation of components and integration of peak areas.

All reagents were of analytical reagent grade. Hexane and dichloromethane were purified by distillation.

Certified standards (Supelco, Bellefonte, PA) of both chlorinated pesticides and PCBs were used to prepare all solutions. A standard mixture of the following pesticides (200 $\mu g\ l^{-1}$ each) was prepared in hexane: α-BHC, γ-BHC, β-BHC, heptachlor, δ-BHC, aldrin, heptachlor epoxide, endosulfan I, 4,4′-DDE, dieldrin, endrin, 4,4′-DDD, endosulfan II, 4,4′-DDT, endrin aldehyde and endosulfan sulphate (Supelco).

A standard mixture of PCBs (Aroclor 1254, Supelco) was dissolved in hexane to give a total concentration of all PCBs of 2000 $\mu g\ l^{-1}$.

Gas chromatographic conditions

Hydrogen was used as the carrier gas at a linear velocity of 42 cm s^{-1}. Nitrogen was used as the ECD make-up gas for a flow-rate of 60 ml min^{-1}. The oven temperature was programmed from 160 to 280°C at 4°C min^{-1} and maintained at the final temperature for 5 min.

Two bonded-phase columns were used: a 30 m × 0.25 mm i.d. SBP-35 fused-silica capillary column (Supelco), consisting of 20% diphenyl- and 80% dimethylpolysiloxane with a film thickness of 0.25 μm, and a 25 m × 0.32 mm i.d. Ultra I column (Hewlett-Packard) containing 100% methylpolysiloxane with a film thickness of 0.17 μm.

The volume injected was 1 μl, using a 10-μl Hamilton syringe, and the splitting ratio was 1 : 30. The standard deviation of repeated injections (n = 5) was 0.05 μl.

Relative retention times

The relative retention time for each pesticide was based on the aldrin peak. Average values of absolute and relative retention times were calculated from results for three injections on to each column.

Response vs. detection temperature

The peaks were integrated and the average area of each peak was calculated from three injections at each temperature. Average areas were used to construct plots of response vs. temperature and ln $AT^{3/2}$ vs. $1/T$ [10].

Extraction of pesticides from environmental samples

Sediment (40 g) was extracted with 200 ml of dichloromethane in a Soxhlet apparatus for ten cycles [11], then the solution was concentrated to 10 ml in a rotavapor. This extract was treated with five 1-ml portions of concentrated sulphuric acid. The resulting extract was neutralized with a 5% solution of sodium hydrogencarbonate and then the solvent was evaporated with ultra-pure nitrogen. The residue was dissolved in 1 ml of hexane and 1 μl of this solution was injected into

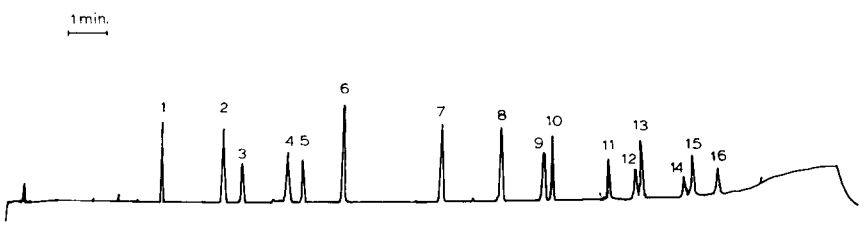

Fig. 1. Chromatogram of a mixture of organochlorine pesticides on the SBP-35 column. Elution order: 1 = α-BHC; 2 = γ-BHC; 3 = β-BHC; 4 = heptachlor; 5 = δ-BHC; 6 = aldrin; 7 = heptachlor epoxide; 8 = endosulfan I; 9 = 4,4′-DDE; 10 = dieldrin; 11 = endrin; 12 = 4,4′-DDD; 13 = endosulfan II; 14 = 4,4′-DDT; 15 = endrin aldehyde; 16 = endosulfan sulphate.

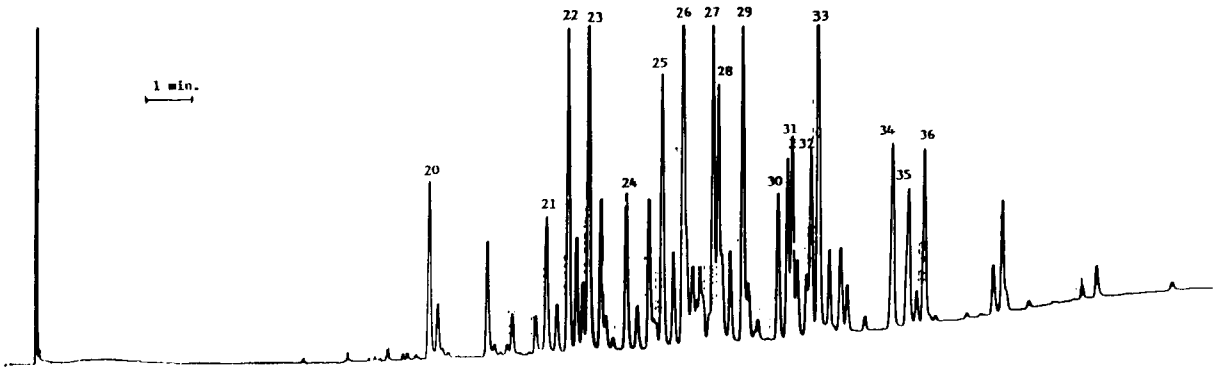

Fig. 2. Chromatogram of mixture of PCBs (Arochlor 1254) on the SBP-35 column.

the gas chromatograph. To obtain relative retention times, the last extract was fortified with aldrin at a concentration of 40 $\mu g\ l^{-1}$.

The temperature response for each peak on each chromatogram of sediment extract was studied by using the SBP-35 column under the same conditions as described above for standard mixtures.

RESULTS AND DISCUSSION

Chromatograms

Figures 1 and 2 show chromatograms for the prepared mixtures of chlorinated pesticides and PCBs, respectively. There are several regions of overlap, e.g., the peaks of endosulphan I and PCB No. 23 and 4,4'-DDT and PCB No. 33. Accordingly, retention times alone cannot be used to differentiate all the chlorinated pesticides from all the PCBs. It is necessary, of course, to identify which peaks represent chlorinated pesticides before one can quantify the pesticides.

Effects of temperatures

Figures 3 and 4 show representative effects of the detector temperature on the peak areas obtained for selected pesticides and PCBs. It is observed that the peak areas for pesticides pass through broad maxima near 550 K (ca. 280°C), whereas the peak areas for PCBs increase with increasing temperature throughout the range examined. This general behaviour is consistent for all the pesticides and PCBs examined. The only significant difference is for endosulfan II, which exhibits a much sharper peak than any of the other pesticides.

Replots of data

It has been shown [10] that plots of ln $AT^{3/2}$ vs. $1/T$ should be linear with different compounds exhibiting different slopes. Figures 5 and 6 show typical examples of such plots for pesticides and PCBs. It is observed that the slopes of the plots for pesticides are all close to zero with

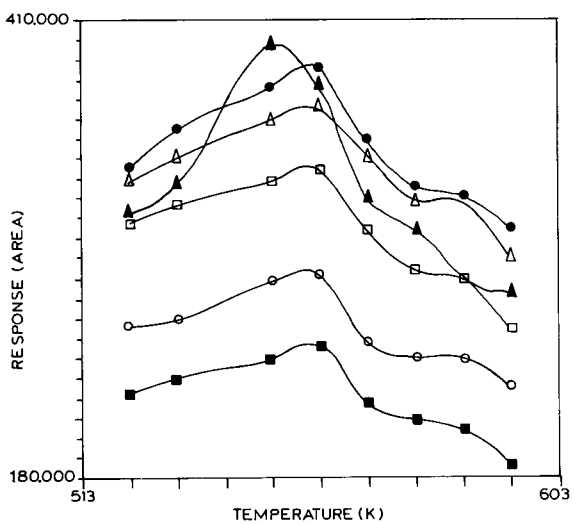

Fig. 3. Response vs. detector temperature for pesticides: △ = Heptachlor epoxide; ▲ = endosulfan II; □ = dieldrin; ■ = endrin aldehyde; ● = endosulfan I; ○ = endosulfan sulphate.

TABLE 1

Least-squares slopes for organochlorine pesticides and PCBs

Pesticide	Peak No.	Slope	PCB Peak No.	Slope α
Endrin aldehyde	15	-0.085 ± 0.004	31	-2.310 ± 0.115
β-BHC	3	-0.645 ± 0.032	27	-2.610 ± 0.130
Endosulfan I	8	-0.375 ± 0.019	36	-2.721 ± 0.136
Heptachlor epoxide	7	-0.326 ± 0.016	30	-3.710 ± 0.185
4,4'-DDD	12	-0.236 ± 0.012	22	-4.032 ± 0.202
Aldrin	6	-0.231 ± 0.012	21	-4.110 ± 0.205
δ-BHC	5	-0.179 ± 0.009	29	-4.143 ± 0.207
4,4'-DDT	14	-0.091 ± 0.005	35	-4.172 ± 0.289
Endrin	11	-0.083 ± 0.004	20	-4.331 ± 0.204
Endosulfan sulphate	16	-0.062 ± 0.003	26	-4.366 ± 0.218
4,4'-DDE	9	-0.052 ± 0.003	34	-4.813 ± 0.206
α-BHC	1	0.037 ± 0.002	28	-4.865 ± 0.243
γ-BHC	2	0.164 ± 0.008	24	-4.884 ± 0.244
Heptachlor	4	0.504 ± 0.025	32	-5.083 ± 0.254
Endosulfan II	13	0.521 ± 0.026	25	-5.342 ± 0.267
Dieldrin	10	1.355 ± 0.067	23	-5.492 ± 0.275
			33	-6.111 ± 0.305

some being slightly positive. On the other hand, the slopes of the plots for all the PCBs have relatively large negative slopes. Least-squares slopes for these and other pesticides and PCBs are summarized in Table 1

Relative retention times for standard compounds are given in Table 2. From the determination of the relative retention times for peaks on the chromatogram of the sediment extract (Fig. 7), four peaks have the same relative retention

TABLE 2

Retention times (t_R) and relative retention times (RRT) for standard pesticides on Ultra I and SBP-35 columns

Ultra I column			SBP-35 column		
Pesticide	t_R (min)	RRT	Pesticide	t_R (min)	RRT
α-BHC	3.219	0.609	α-BHC	5.910	0.649
β-BHC	3.405	0.644	β-BHC	6.950	0.764
γ-BHC	3.676	0.696	γ-BHC	7.175	0.789
δ-BHC	3.756	0.711	Heptachlor	8.066	0.887
Heptachlor	4.774	0.903	δ-BHC	8.235	0.905
Aldrin	5.285	1.000	Aldrin	9.098	1.000
Heptachlor epoxide	6.109	1.156	Heptachlor epoxide	10.909	1.199
Endosulfan I	6.980	1.321	Endosulfan I	12.152	1.336
Dieldrin	7.941	1.503	4,4'-DDE	12.936	1.422
4,4'-DDE	8.663	1.634	Dieldrin	13.213	1.453
Endrin	8.762	1.658	Endrin	14.439	1.587
Endosulfan II	9.170	1.735	4,4'-DDD	14.935	1.641
Endrin aldehyde	9.260	1.752	Endosulfan II	15.129	1.663
4,4'-DDD	9.732	1.841	4,4'-DDT	16.062	1.765
Endosulfan sulphate	9.830	1.860	Endrin aldehyde	16.252	1.786
4,4'-DDT	10.516	1.990	Endosulfan sulphate	16.836	1.851

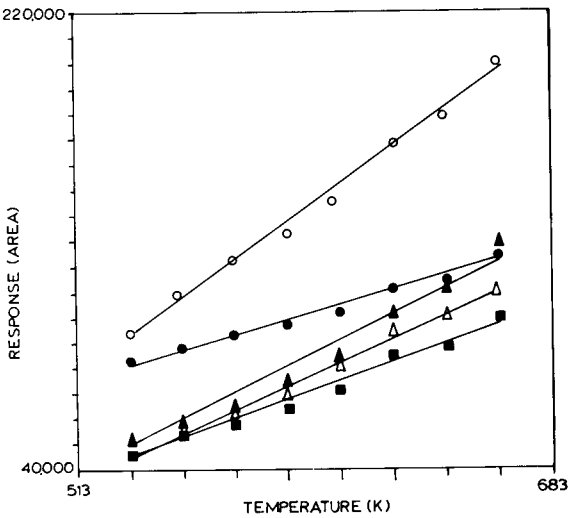

Fig. 4. Response vs. detector temperature for PCBs: △ = No. 21; ○ = No. 34; ▲ = No. 23; ■ = No. 26; ● = No. 25.

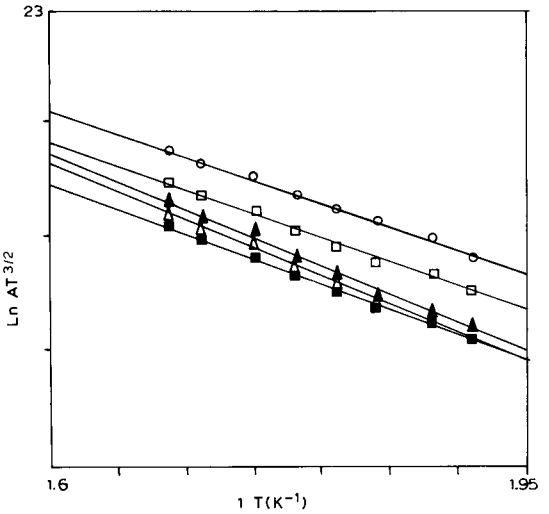

Fig. 6. Plot of ln $AT^{3/2}$ vs. $1/T$ for PCBs. △ = No. 21; □ = No. 25; ○ = No. 34; ▲ = No. 23; ■ = No. 26.

times as standards in both columns (Table 3). For these peaks the relationship between sensitivity and detection temperature was studied and the least-squares slopes of the plot of ln $AT^{3/2}$ vs. $1/T$ for the probable compounds were as follows: α-BHC, 0.076 ± 0.0004; γ-BHC, 0.234 ± 0.012; 4,4′-DDD, -0.008 ± 0.0004; and 4,4′-DDE, 0.078 ± 0.004.

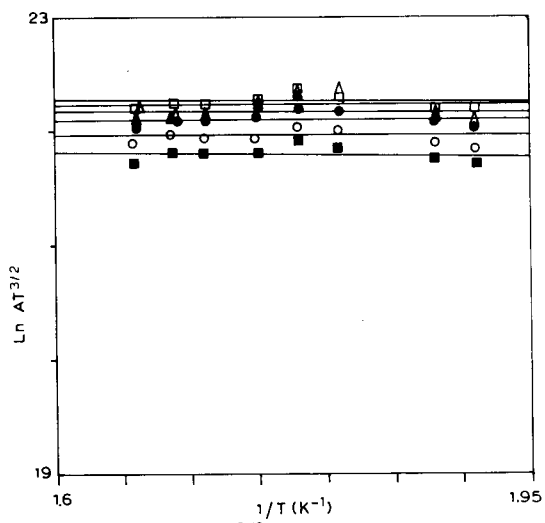

Fig. 5. Plot of ln $AT^{3/2}$ vs. $1/T$ for pesticides. △ = Heptachlor epoxide; □ = endosulfan I; ○ = endosulfan sulphate; ▲ = endosulfan II; ■ = endrin aldehyde; ● = dieldrin.

Conclusion

The results obtained with standard pesticides and PCBs demonstrate that GC–ECD is suitable for the determination of chlorinated pesticides with minimum interference from PCBs. Utilizing the relative retention times and studying the dependence of the response of each peak on the detection temperature, one can identify with good precision an individual peak with the same relative retention index as a standard in both columns and with similar parameters of the plot of ln $AT^{3/2}$ vs. $1/T$. Hence it was possible to iden-

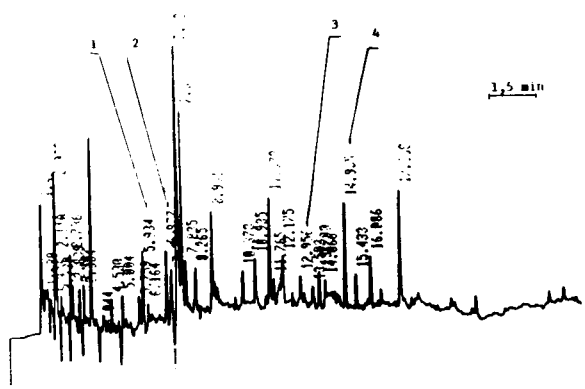

Fig. 7. Chromatogram of sediment extract on the SBP-35 column. Identified pesticides: 1 = α-BHC; 2 = γ-BHC; 3 = 4,4′-DDE; 4 = 4,4′-DDD.

TABLE 3

Retention times (t_R) and relative retention times (RRT) for peaks on chromatograms of sediment extract on SBP-35 and Ultra-I columns

SBP-35 column			Ultra 1 column		
Probable compound	t_R (min)	RRT	Probable compound	t_R (min)	RRT
α-BHC	5.934	0.659	α-BHC	3.258	0.597
γ-BHC	6.977	0.776	γ-BHC	3.789	0.689
δ-BHC	8.265	0.919	4,4′-DDE	8.783	1.629
β-BHC	7.127	0.793	4,4′-DDD	9.725	1.836
Aldrin	8.991	1.000			
Heptachlor epoxide	10.935	1.216			
Endosulfan I	12.175	1.354			
4,4′-DDE	12.956	1.439			
4,4′-DDD	14.955	1.663			
4,4′-DDT	16.086	1.789			

tify in an extract of sediment the presence of four organochlorine pesticides at concentrations less than 50 ng g^{-1}, namely α-BHC, γ-BHC, 4,4′-DDD and 4,4′-DDE.

REFERENCES

1 A.B. Healt and R.R. Black, J. Assoc. Off. Anal. Chem., 11 (1980) 529.
2 L.L. Needhan, A.L. Smrek, S.L. Head, V.W. Burse and J.A. Liddle, Anal. Chem., 52 (1980) 2227.
3 M. Picer and M. Ahel, J. Chromatogr., 150 (1978) 119.
4 C.A. Bache and D.J. Lisk, J. Assoc. Off. Anal. Chem., 43 (1969) 388.
5 S.V. Khan, J. Assoc. Off. Anal. Chem., 58 (1975) 5.
6 A. Zlatkis and C.F. Poole (Eds.), Electron-Capture. Theory and Pratice in Chromatography, Elsevier, Amsterdam, 1981.
7 C.F. Poole, J. Chromatogr., 118 (1976) 280.
8 A. Zlatkis, C.K. Lee, W.E. Wentworth and E.C.M. Chen, Anal. Chem., 55 (1983) 1956.
9 P. Rotocki and B. Drozdowicz, Chromatographia, 27 (1989) 71.
10 W.E. Wentworth and E. Chen, J. Gas Chromatogr., 4 (1967) 170.
11 M. Cooke, K.D. Khallef, G. Nickless and D.R. James, J. Chromatogr., 178 (1979) 183.

Analytica Chimica Acta, 269 (1992) 211–222
Elsevier Science Publishers B.V., Amsterdam

1*H*,5*H*,11*H*-[1]Benzopyrano[6,7,8-*ij*]quinolizine-9-acetic acid 2,3,6,7-tetrahydro-11-oxohydrazide fluorogenic reagent for liquid chromatographic determination of aldehydes and ketones

F. Traoré

Laboratoire de Chimie Analytique II et Service d'Analyse de Médicaments et Métabolites, Faculté de Sciences Pharmaceutiques et Biologiques de l'Université Paris-Sud, 5 rue J.B. Clément, 92290 Chatenay-Malabry (France)

M. Tod

Département de Toxicopharmacologie, Hôpital Avicenne, 125 Route de Stalingrad, 93000 Bobigny (France)

J. Chalom

Eurobio, Z.A. Courtaboeuf, 7 Avenue de Scandinavie, 91953 Les Ulis (France)

R. Farinotti and G. Mahuzier

Laboratoire de Chimie Analytique II et Service d'Analyse de Médicaments et Métabolites, Faculté de Sciences Pharmaceutiques et Biologiques de l'Université Paris-Sud, 5 rue J.B. Clément, 92290 Chatenay-Malabry (France)

(Received 6th March 1992; revised manuscript received 5th June 1992)

Abstract

Carbonyls are widely occurring environmental compounds. Various aldehydes and ketones are major constituents of food aromas, and a large number of pharmaceuticals and biological compounds contain carbonyl groups. Therefore, the determination of traces of carbonyls is of major importance. Methods for the determination of carbonyl compounds by means of liquid chromatography have been improved by the use of fluorescent derivatizing reagents. This paper describes the use of a highly reactive reagent with a 7-aminocoumarin moiety as the fluorophore and carboxylic hydrazide as the group reacting with the carbonyl function. Aliphatic, unsaturated and aromatic carbonyls, dicarbonyls and other difunctional carbonyls react with this reagent and chromatographic separation in both normal- and reversed-phase systems with fluorescence detection can be easily performed. The labelling reaction and the structure of the derivatives are discussed, together with the properties of these derivatives in both normal- and reversed-phase chromatographic systems. UV absorbance, corrected fluorescence spectra data and quantum yields from luminarin 3 and representative luminarin 3 derivatives of carbonyl compounds are presented. The results show that luminarin 3 derivatives of carbonyl compounds give high fluorescence quantum yields ($\phi_f \approx 0.71$) and good intrinsic fluorescence sensitivities (*IFS* ≈ 5.68). Fluorimetric detection limits for most compounds range between 60 and 1950 fmol injected. The method is suitable for quantitative analysis, with a reproducibility of about 1.8% (relative standard deviation) for 100 pmol injected.

Keywords: Fluorimetry; Liquid chromatography; Aldehydes; Carbonyl compounds; Ketones

Correspondence to: G. Mahuzier, Laboratoire de Chimie Analytique II et Service d'Analyse de Médicaments et Métabolites, Faculté de Sciences Pharmaceutiques et Biologiques de l'Université Paris-Sud, 5 rue J.B. Clément, 92290 Chatenay-Malabry (France).

In recent years there has been increasing interest in the development of liquid chromatography (LC) for analyses for biological compounds with a carbonyl moiety in their skeleton (e.g.

sugars and oxosteroids). However, the low molar absorptivities of most of these compounds hinder sensitive detection. Derivatization has therefore been proposed, with various fluorogenic reagents, as follows.

Dansylhydrazine (DNS-H) has been used for both thin-layer chromatographic (TLC) and LC separations of sugars [1–3], ketosteroids [4–8] and various carbonyl compounds [9,10]. This reagent has been reported to give a high fluorescent background, and its degradation products can interfere with the determination of some compounds. During the derivatization reaction between dansylhydrazine and carbonyl compounds, a series of contaminants are also formed [11]. Normally, these contaminants are at such low concentrations that they present no major problems, but a large excess of dansylhydrazine must be added to some materials in order to obtain complete derivatization. Therefore, the sensitivity can be lost if a contaminant peak cannot be separated from the test compounds. High-performance gel-permeation chromatography has been used [12,13] to remove the excess of reagent.

4-Hydrazino-7-nitro-2,1,3-benzoxadiazole (NBD-H), 4-hydrazino-7-nitro-2,1,3-benzoxadiazole hydrazine (NBD-H · NH_2NH_2), 4-aminosulphonyl-7-hydrazino-2,1,3-benzoxadiazole (ABD-H) and 4-(*N*,*N*-dimethylaminosulphonyl)-7-hydrazino-2,1,3-benzoxadiazole (DBD-H) have also been used to good advantage for fluorogenic labelling of aldehydes and ketones [1,3,6,7,12–16]. These reagents are not naturally fluorescent but their reaction products with aldehydes and ketones fluoresce at wavelengths from 548 to 580 nm with excitation from 450 to 470 nm. ABD-H and DBD-H have similar reactivities and are more reactive than NBD-H · NH_2NH_2.

More recently, anthracene-1- and -2-carboxylic acid hydrazides and *O*-(1-, 2- and 9-anthrylmethyl)hydroxylamines have been used as fluorogenic labelling reagents for carbonyl compounds [17].

As the quinolizinocoumarin nucleus is a useful fluorescent and chemiluminescent label [18–20], and taking advantage of the specific reaction between carbonyl compounds and nucleophiles (including hydrazine derivatives), it was considered that substitution of the amino group of luminarin 4 [19] by the hydrazine group would convert the molecule into a good reagent for carbonyl compounds. The appropriate reagent, luminarin 3 (1*H*,5*H*,11*H*-[1]benzopyrano[6,7,8-*ij*]quinolizine-9-acetic acid 2,3,6,7-tetrahydro-11-oxohydrazide), was synthesized and proved to be suitable in practice.

This paper describes the use of luminarin 3 (see Fig. 1) as a fluorescence-based labelling reagent for carbonyl assays. Reactivity towards aldehydes and ketones, UV and fluorescence spectral properties and quantum yields of the reagent and of derivatives in various solvents are reported. A simple LC method (both normal- and reversed-phase) for the separation and determination of a variety of carbonyls, including keto esters, keto acids and aliphatic, aromatic and unsaturated hydroxycarbonyl and dicarbonyl compounds was also developed.

EXPERIMENTAL

Apparatus

Mass spectrometry (MS) was performed with a Nermag R-1010-C instrument. For fluorescence measurements a Perkin-Elmer Model LS 50 luminescence spectrometer was used. A microcomputer coupled to the spectrofluorimeter calculated corrected spectra and quantum yields. A Shimadzu Model UV-2100 UV–visible recording spectrophotometer with a 1-cm quartz cell was used for all absorbance measurements.

LC analyses were performed with a Chromatem 380 pump (Touzart–Matignon, France) equipped with a Model 7125 injector (Rheodyne, Cotati, CA) with a 20-μl sample loop and a Shimadzu RF-530 fluorescence LC monitor (Touzart–Matignon) equipped with a xenon lamp and a micro flow cell. The data were processed with a C-R5A Chromatopac (Shimadzu, Kyoto).

Two LC systems were studied as follows.

System I. Adsorption chromatography was carried out on a 250 × 4.6 mm i.d. 5-μm Nucleosil silica column (Interchim, France) using ethyl acetate–diisopropyl ether (90 + 10, v/v) as the mo-

bile phase at a flow-rate of 1.5 ml min^{-1}. The eluate was monitored at an excitation wavelength of 389 nm and an emission wavelength of 445 nm.

System II. Reversed-phase chromatography was performed on a 250 × 4.6 mm i.d. 5-μm ODS Nucleosil column (Beckman, Les Ulis, France) using acetonitrile–0.01 M imidazole buffer (pH 7.5) (40 + 60, v/v) as the mobile phase at a flow-rate of 1.5 ml min^{-1}. The detector wavelengths were set at 399 and 485 nm for excitation and emission, respectively.

Reagents

All reagents were purchased from Aldrich-Chemie (Steinheim, Germany) or Sigma (St. Louis, MO), except methylmalonaldehyde bisdiethyl acetal and luminarin 3 and its hydrolysis product (luminarin acid), which were manufactured by Eurobio (Les Ulis, France). Stock solutions of luminarin 3 and luminarin acid were prepared in dimethyl sulphoxide and diluted further with the same solvent to the required concentrations. The solvents (LC and fluorimetric grade) were obtained from FSA Laboratory Supplies (UK).

Malonaldehyde (MDA) and methylmalonaldehyde (MeMDA). These were prepared according to Esterbauer and Slater [21]. Stock solutions (10 mM) were prepared by hydrolysis of 1,1,3,3-tetraethoxypropane (0.25 ml) or 2-methyl-1,1,3,3-tetraethoxypropane (0.25 ml), respectively, in 100 ml of 1% sulphuric acid for 2 h at room temperature.

Acetoacetaldehyde. A 10 mM stock solution was prepared by hydrolysis of 1,1-dimethoxybutan-3-one (0.14 ml) in 100 ml of 1% sulphuric acid for 1 h at room temperature.

Succinaldehyde. This was best prepared with an excellent yield during or just before analysis through complete hydrolysis within 30 min of pure 2,5-dimethoxytetrahydrofuran according to the method of Sawicki and Sawicki [22]. A 10 mM stock solution was prepared by hydrolysis of 2,5-dimethoxytetrahydrofuran (0.136 ml) in 100 ml of 1% sulphuric acid for 1 h at room temperature.

Acidified acetylacetone solution. A 1 M solution of acetylacetone in 1% sulphuric acid was prepared and when necessary diluted with the same solvent to the desired concentration.

Acidified acrolein solution. A 0.1 mM solution of acrolein (prop-2-enal) in 1% sulphuric acid was prepared and diluted when necessary with the same solvent to the desired concentration.

Synthesis of luminarin 3 derivatives for the fluorescence study

Luminarin 3 derivatives of malonaldehyde, 2-methylmalonaldehyde and acrolein were prepared as follows. Luminarin 3 (313 mg, 1 mmol) in 10 ml of dimethyl sulphoxide was added to malonaldehyde (72 mg, 1 mmol), 2-methylmalonaldehyde (86 mg, 1 mmol) or acrolein (56 mg, 1 mmol) in 100 ml of 1% sulphuric acid. The reaction was carried out in the dark for 60 min. Sodium hydrogencarbonate (2.5 g) was added to adjust the pH of reaction mixture to 7.0. The required luminarin 3 derivatives were extracted twice with 50 ml of dichloromethane. After separation and drying by the addition of 10 g of anhydrous Mg_2SO_4, the dichloromethane layer was evaporated to dryness under vacuum. The dried extract, dissolved in 5 ml of dichloromethane, was purified by means of column chromatography (25 × 3.5 cm i.d. column) on silica gel 60 (0.04–0.063 mm; Merck, Darmstadt) with a dichloromethane–tetrahydrofuran gradient as eluent to give luminarin 3–malonaldehyde (199 mg, 72.3%), luminarin 3–methylmalonaldehyde (151 mg, 53%) and luminarin 3–acrolein (189 mg, 66%).

The physico-chemical properties of these derivatives were as follows. Luminarin 3–malonaldehyde (yellow powder): EI-MS, *m/z* 367; elemental analysis, calculated for $C_{20}H_{21}N_3O_4$, C 65.40, H 5.72, N 11.44; found, C 65.41, C 5.81, N 11.40%. Luminarin 3–methylmalonaldehyde (yellowish brown needles): EI-MS, *m/z* 381; elemental analysis, calculated for $C_{21}H_{23}N_3O_4$, C 66.14, H. 6.04, N 11.02; found, C 66.06, H 6.18, N 10.97%. Luminarin 3–acrolein (pale yellow powder): EI-MS, *m/z* 351; elemental analysis, calculated for $C_{20}H_{21}N_3O_3$, C 68.38, H 5.98, N 11.97; found, C 68.30, H 6.11, N 11.89%.

Stock solutions (25 mM) in dimethyl sulphoxide were kept frozen at −20°C. The absence of

coumarinic contaminants in the luminarin 3 derivatives was checked by means of LC with fluorescence detection under the conditions described above and by LC–MS with total ionic current monitoring on a Nermag R-1010-L instrument, using positive-ion chemical ionization with ammonia reagent. LC separation was obtained using a 150 × 4.6 mm i.d. 5-μm ODS Nucleosil column (Interchim) and acetonitrile–0.1 M ammonium acetate (30 + 70, v/v) as the mobile phase at a flow-rate of 1.5 ml min^{-1}.

Fluorescence and absorbance measurements

The spectra were fully corrected. Fluorescence quantum yields were determined with reference to quinine hydrogensulphate in 0.05 M sulphuric acid according to Parker and Rees [23]. Measurements of quantum yields were done at room temperature without deoxygenation. The orientational polarizability, a factor used to characterize solvent polarity, was calculated as follows [24]: $\Delta f = (D - 1/2D + 1) - (n^2 - 1/2n^2 + 1)$, where n and D are the refractive index and the dielectric constant of the solvent, respectively. The intrinsic fluorescence sensitivity expressed by the equation $IFS = \phi\epsilon/H$, where H is the half band-width (cm^{-1}) and ϵ is the molar absorptivity (l mol^{-1} cm^{-1}), controls the intensity distribution over the part of the emission spectrum detected and is therefore important for the sensitivity of the detector cell [25].

Derivatization procedure

A 100-μl sample containing 0.5–50 nmol of carbonyl compounds in 0.1 M sulphuric acid was mixed with 100 μl of the latter and 10 μl of 10 mM luminarin 3 solution. The mixture was kept at room temperature for 60 min (aldehydes) or 240 min (ketones) in the dark. A clean control tube was used as a reference system to aid the detection of luminarin 3 and its degradation product. A 100-μl volume of 0.6 M sodium hydrogencarbonate solution was carefully added to adjust the pH to 7.0 and the tube was agitated gently until evolution of gas ceased. Dichloromethane (1 ml) was then added and the mixture was vortex mixed for 2 min. The layers were separated by centrifugation and the upper layer was aspirated and discarded. The remaining dichloromethane layer was evaporated under a stream of nitrogen at room temperature. The resulting residue was dissolved in 100 μl of acetonitrile (system II) or ethyl acetate (system I), and an aliquot was injected into the chromatograph.

RESULTS AND DISCUSSION

Confirmation of reagent structure

The structure of luminarin 3 was confirmed [26] by IR, ^1H NMR, mass spectrometry and elemental analysis. Salient characteristics were as follows: IR (KBr) showed the bands of the quinolizinocoumarin nucleus and the hydrazide function (1100, 1640, 1670, 3060, 3250, 3320 cm^{-1}); ^1H NMR [C_6D_6–CD_3OD (50 + 50, v/v)] gave δ_H 7.10 (1H, s, CH), 6.04 (1H, s, CH), 3.48 (2H, s, CH_2), 2.90 (4H, m, CH_2NCH_2), 2.65 (4H, m, CH_2 and CH_2), 1.70 (4H, m, CH_2 and CH_2); EI-MS showed a fragmentation pattern consistent with the proposed structure, with the molecular ion peak (m/z 313) and fragmentation of the side-chain (m/z 296, 282, 254) and of the lactone ring (m/z 226); elemental analysis, calculated for $C_{17}H_{19}N_3O_3$, C 65.2, H 6.1, N 13.4; found, C 65.1, H 6.1, N 13.4%.

Structure of reaction products

The proposed method for the determination of carbonyls takes advantage of the possible general equation for the labelling reaction of carbonyl compounds with luminarin 3, which proceeds by nucleophilic addition to the carbonyl followed by 1,2-elimination of water and the formation of the luminarin 3 derivatives. Because luminarin 3 is a weak nucleophile, the coupling reaction is carried out in the presence of acid, which promotes protonation of the carbonyl.

The structure of the reaction products of the carbonyl compounds with luminarin 3 was confirmed as luminarin 3 hydrazone by MS. The mass spectra provided particularly convincing data. In all instances, the molecular ion peak was present in the mass spectra of each luminarin 3 derivative. The suggested reaction mechanism is

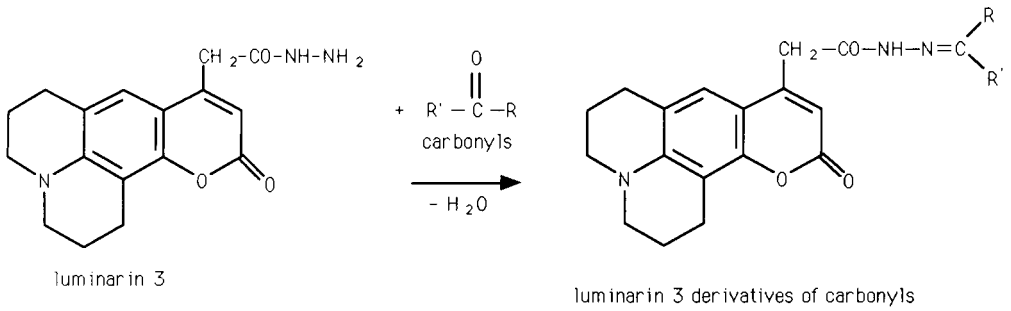

Fig. 1. Reaction of carbonyl compounds with luminarin 3 to give luminarin 3 hydrazone.

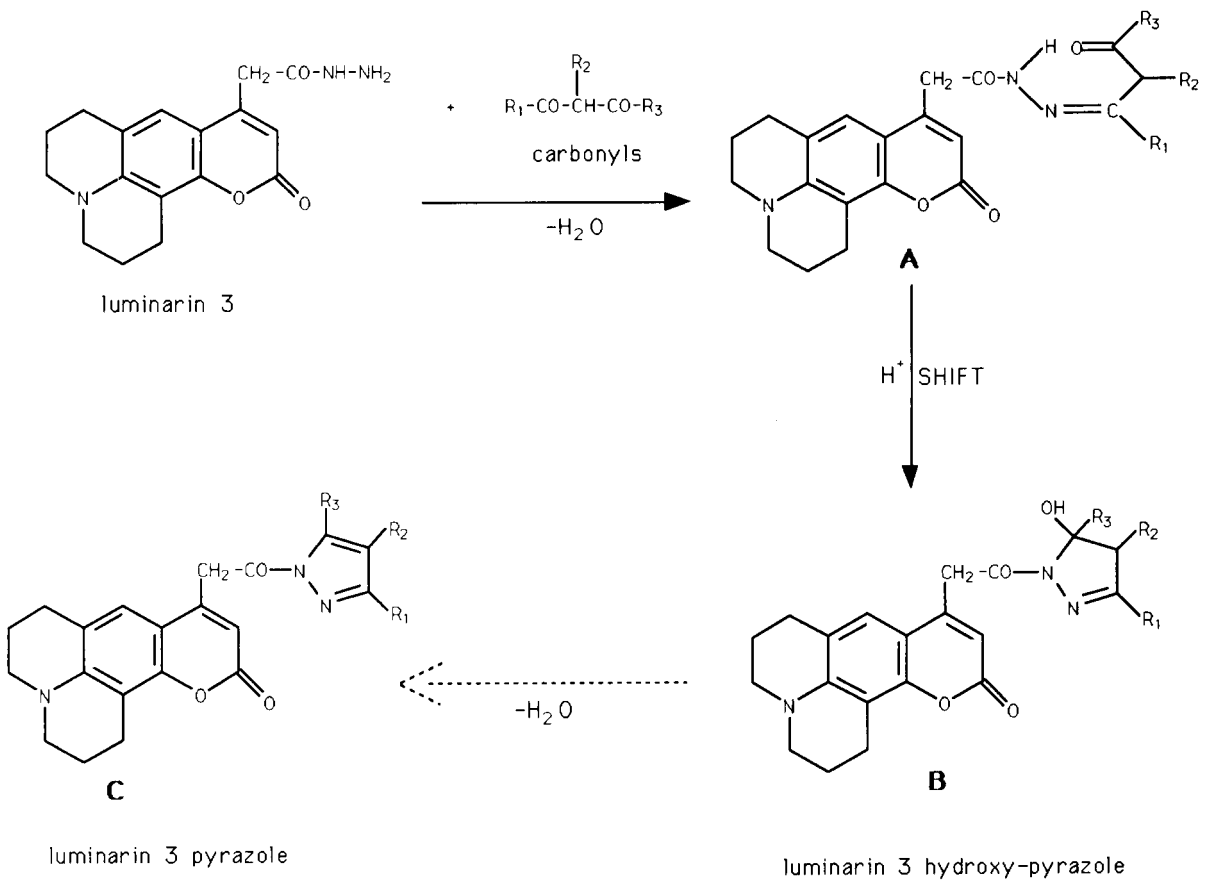

malonaldehyde : $R_1 = R_2 = R_3 = H$

methylmalonaldehyde : $R_1 = R_3 = H$; $R_2 = CH_3$

acetylacetone : $R_1 = R_3 = CH_3$; $R_2 = H$

Fig. 2. Probable mechanism of formation of luminarin 3 derivatives of acetylacetone, malonaldehyde and methylmalonaldehyde.

shown in Fig. 1. Unambiguous evidence for the formation and purity of the luminarin 3 derivatives of malonaldehyde, methylmalonaldehyde and acrolein was provided by LC, spectral data and elemental analysis. Elemental analysis of the luminarin 3 derivatives (malonaldehyde, methylmalonaldehyde and acrolein) conformed with the theoretical values. The luminarin 3 derivative of acrolein showed two peaks in LC (system I), the second (at 4.02 min) being much higher than the first (at 3.57 min). These two peaks were proved to be the *syn* and *anti* isomers of the hydrazone by ^{1}H and ^{13}C NMR (data not shown). The luminarin 3 derivative of methylmalonaldehyde also showed two peaks in LC (System I), the second (at 4.88 min) being much higher than the first (at 4.42 min). These two peaks were proved to be the *threo* and *erythro* isomers. The luminarin 3 derivative of malonaldehyde showed a single peak in both chromatographic systems. LC–MS, EI-MS, ^{1}H NMR and ^{13}C NMR studies proved that the luminarin 3 derivative of malonaldehyde and methylmalonaldehyde had the hydroxypyrazole form (Fig. 2B) (data not shown).

The luminarin 3 derivative of acetylacetone was also analysed with mass spectrometry under chemical ionization and electron impact conditions. The mass spectra clearly showed that the derivative is luminarin 3–pyrazole (molecular mass 377), which is probably obtained by cyclization of the luminarin 3 hydrazone initially formed (molecular mass 395), followed by elimination of water (Fig. 2C).

The occurrence of the hydroxypyrazole and pyrazole structure of β-dicarbonyl compounds has observed with other hydrazine-based reagents, as described by Kost and Grandberg [27].

Reaction conditions

The reaction conditions were investigated with malonaldehyde and acetylacetone, chosen as representative aldehydes and ketones, respectively.

To ensure maximum derivatization of the carbonyl compounds, the reaction between malonaldehyde, acetylacetone and luminarin 3 was studied on a microscale at room temperature. When the reaction is carried out with micromolar amounts, the luminarin 3 derivatives of malonaldehyde and acetylacetone precipitate immediately owing to their low solubility in the aqueous phase. This precipitation shifts the equilibrium toward the almost quantitative formation of the derivative. The insolubility of the luminarin 3 derivatives of malonaldehyde and acetylacetone in water indicates that the reaction can be made quantitative on the microscale.

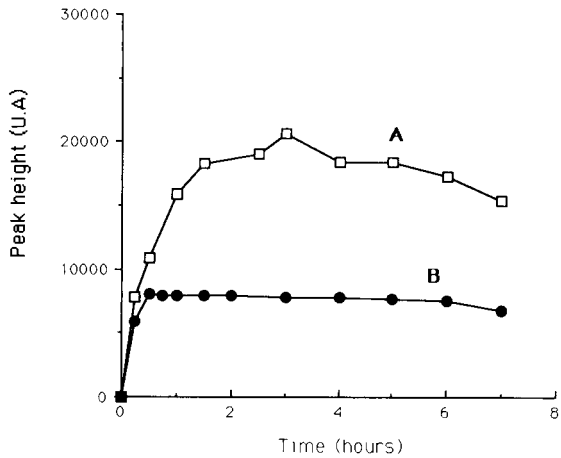

Fig. 3. Effect of reaction time on formation of luminarin 3 derivatives of (A) acetylacetone and (B) malonaldehyde at room temperature.

Malonaldehyde and acetylacetone were added to an excess of the luminarin 3 reagent. Each carbonyl compound (0.02 μmol) was treated in the derivatization procedure for various reaction times. The time-dependent increase in the peak heights of the luminarin 3 derivatives was monitored by LC (Fig. 3).

The peak heights of luminarin 3–malonaldehyde became constant after about 30 min, which suggests that the derivatization yield was maximum within this period. Using an optimum reaction time of 60 min, the other aldehyde compounds were also converted into luminarin 3 derivatives. The reactivities of ketones with this reagent were lower than those of aldehydes, as shown in Fig. 3. Hence, 240 min was necessary for the reaction.

The peak heights of the luminarin 3 derivatives decreased with increased sulphuric acid concentration. Each carbonyl compound (0.02 μmol) was treated in the derivatization procedure using

TABLE 1

UV absorption and fluorescence data for luminarin 3 in various solvents

Solvent	Δf [a]	UV λ_{max} (nm)	ϵ [b]	λ_{ex} (nm)	λ_{em} (nm)	H [c] (cm^{-1})	ϕ [d]	IFS [e]	$\nu_A - \nu_F$ [f] (cm^{-1})
Cyclohexane	0.001	381	1.27	380	423	3129	0.16	0.65	2606
Diisopropyl ether	0.145	376	2.33	376	423	3278	0.36	2.56	2955
Chloroform	0.185	403	2.68	403	455	2722	0.61	6.00	2867
Ethyl acetate	0.199	383	2.57	383	445	2907	0.93	8.23	3638
Tetrahydrofuran	0.209	384	2.66	384	442	2990	0.85	7.56	3451
Dichloromethane	0.218	400	3.09	400	456	2652	0.53	6.18	3101
Dimethyl sulphoxide	0.260	395	2.60	395	463	2843	0.95	8.68	3718
Dimethylformamide	0.276	391	2.50	391	458	2722	0.89	8.17	3741
Acetonitrile	0.304	391	2.55	391	462	2739	0.65	6.05	3963
Methanol	0.308	399	2.58	399	480	2747	0.57	5.35	4261
Water	0.320	408	1.94	408	503	2465	0.42	3.30	4629

[a] Δf = Orientational polarizability. [b] ϵ = Molar absorptivity (10^4 l mol^{-1} cm^{-1}). [c] H = Width at half band-height (cm^{-1}) of the emission band. [d] ϕ = Quantum yield. [e] IFS = Intrinsic fluorescence sensitivity. [f] $\nu_A - \nu_F$ (Absorption maximum − emission maximum), or Stokes shift, expressed in cm^{-1}.

various concentrations of sulphuric acid; 0.1 M H_2SO_4 was preferred for LC analysis because more concentrated acid gave an unknown subpeak on the chromatogram, which was identified by (system II) combined with MS and by comparison with an authentic sample ($M^+ = M - 44 = 255$), as 2,3,6,7-tetrahydro-11-oxo-1*H*,5*H*,11*H*-[1]benzopyrano[6,7,8-*ij*]quinolizine-9-acetic acid (luminarin acid). To avoid the formation of this fluorescent degradation product, the reaction temperature should not exceed 30°C and acid catalysts (H_2SO_4 concentration > 0.1 M) should not be used. Greater peak heights were obtained in the concentration range 0.05–0.1 M H_2SO_4, without affecting the formation of this byproduct.

The influence of the amount of luminarin 3 on the peak heights of the malonaldehyde and acetylacetone derivatives was studied. Each carbonyl compound (0.02 μmol) was treated in the derivatization procedure using various amounts of luminarin 3. The peak heights were almost constant over the range of luminarin 3 concentrations investigated (0.05–0.5 μmol). These experiments indicated that the optimum conditions were

TABLE 2

UV absorption and fluorescence data for luminarin 3–malonaldehyde derivative in various solvents

Solvent	Δf	UV λ_{max} (nm)	ϵ	λ_{ex} (nm)	λ_{em} (nm)	H (cm^{-1})	ϕ	IFS	$\nu_A - \nu_F$ (cm^{-1})
Cyclohexane	0.001	372	2.22	388	438	3501	0.79	5.01	4051
Diisopropyl ether	0.145	373	2.82	379	423	3075	0.67	6.15	3169
Chloroform	0.185	398	3.30	395	449	2370	0.94	13.09	2854
Ethyl acetate	0.199	381	3.19	389	449	2940	0.70	7.59	3975
Tetrahydrofuran	0.209	381	3.25	387	441	2902	0.98	10.99	3571
Dichloromethane	0.218	396	4.19	395	460	2495	0.95	15.94	3513
Dimethyl sulphoxide	0.260	396	2.96	394	464	2763	0.98	10.48	3701
Dimethylformamide	0.276	392	2.96	393	460	2763	0.71	7.60	3771
Acetonitrile	0.304	391	3.21	394	464	2670	0.71	8.55	4024
Methanol	0.308	399	2.93	397	480	2673	0.58	6.36	4229
Water	0.320	406	2.30	401	502	2326	0.39	3.85	4710

TABLE 3

UV absorption and fluorescence data for luminarin 3–methylmalonaldehyde derivative in various solvents

Solvent	Δf	UV λ_{max} (nm)	ϵ	λ_{ex} (nm)	λ_{em} (nm)	H (cm^{-1})	ϕ	IFS	$\nu_A - \nu_F$ (cm^{-1})
Cyclohexane	0.001	388	2.81	386	444	3595	0.43	3.36	3251
Diisopropyl ether	0.145	373	2.53	380	424	2568	0.94	9.27	3225
Chloroform	0.185	399	2.71	394	450	2649	0.97	9.92	2840
Ethyl acetate	0.199	381	2.25	388	443	2933	0.92	7.07	3673
Tetrahydrofuran	0.209	384	2.67	391	449	3009	0.89	7.89	3770
Dichloromethane	0.218	396	3.15	394	453	2835	0.93	10.35	3177
Dimethyl sulphoxide	0.260	396	2.53	393	464	2843	0.91	8.10	3701
Dimethylformamide	0.276	393	2.58	392	458	2786	0.94	8.72	3611
Acetonitrile	0.304	391	2.46	393	462	2629	0.67	6.26	3930
Methanol	0.308	399	2.51	399	480	2506	0.98	9.81	4229
Water	0.320	408	1.87	401	501	2470	0.45	3.41	4550

those used in the derivatization procedure described above.

Fluorescence spectrum

Fluorescence spectra and quantum yields were measured in various solvents. Tables 1, 2, 3 and 4 show the UV–visible absorbance, the corrected fluorescence spectral data and quantum yields for luminarin 3 and its malonaldehyde, methylmalonaldehyde and acrolein derivatives in various solvents.

The wavelength of the fluorescence emission maxima in solvents (polar and apolar) did not vary significantly between the derivatives. However, for cyclohexane and water a red shift of the fluorescence spectrum with increasing polarity of the solvent was observed. The spectral maxima were shifted from 423 nm in cyclohexane to 503 nm in water (Fig. 4). The difference in the Stokes shifts of the fluorescence from cyclohexane and water amounts to 3760 cm^{-1} (Table 1), while the orientational polarizability (Δf) changes by 0.32. Tables 1–4 show that aprotic solvents produce considerably smaller Stokes shifts than those which can form a hydrogen bond by acting as proton donors. Similar effects have been reported for coumarin molecules [28]. The Stokes shift (quoted for some solvents in Tables 1–4) does not follow the solvent polarity defined by orientational polarizability. The quantum yield decreases

TABLE 4

UV absorption and fluorescence data for luminarin 3–acrolein derivative in various solvents

Solvent	Δf	UV λ_{max} (nm)	ϵ	λ_{ex} (nm)	λ_{em} (nm)	H (cm^{-1})	ϕ	IFS	$\nu_A - \nu_F$ (cm^{-1})
Cyclohexane	0.001	389	2.83	381	421	3371	0.20	1.68	1954
Diisopropyl ether	0.145	373	2.74	379	423	3385	0.91	7.38	3169
Chloroform	0.185	399	2.97	398	453	2561	0.98	11.37	2988
Ethyl acetate	0.199	382	2.69	389	444	3248	0.89	7.38	3655
Tetrahydrofuran	0.209	383	2.61	389	444	3177	0.94	7.71	3587
Dichloromethane	0.218	396	3.40	395	454	2769	0.98	12.02	3226
Dimethyl sulphoxide	0.260	397	2.66	394	465	3332	0.96	7.67	3684
Dimethylformamide	0.276	392	2.56	394	461	2722	0.69	6.49	3818
Acetonitrile	0.304	393	2.67	394	466	2767	0.53	5.11	3986
Methanol	0.308	399	2.77	397	480	2736	0.50	5.05	4229
Water	0.320	408	1.98	397	499	3265	0.50	3.03	4470

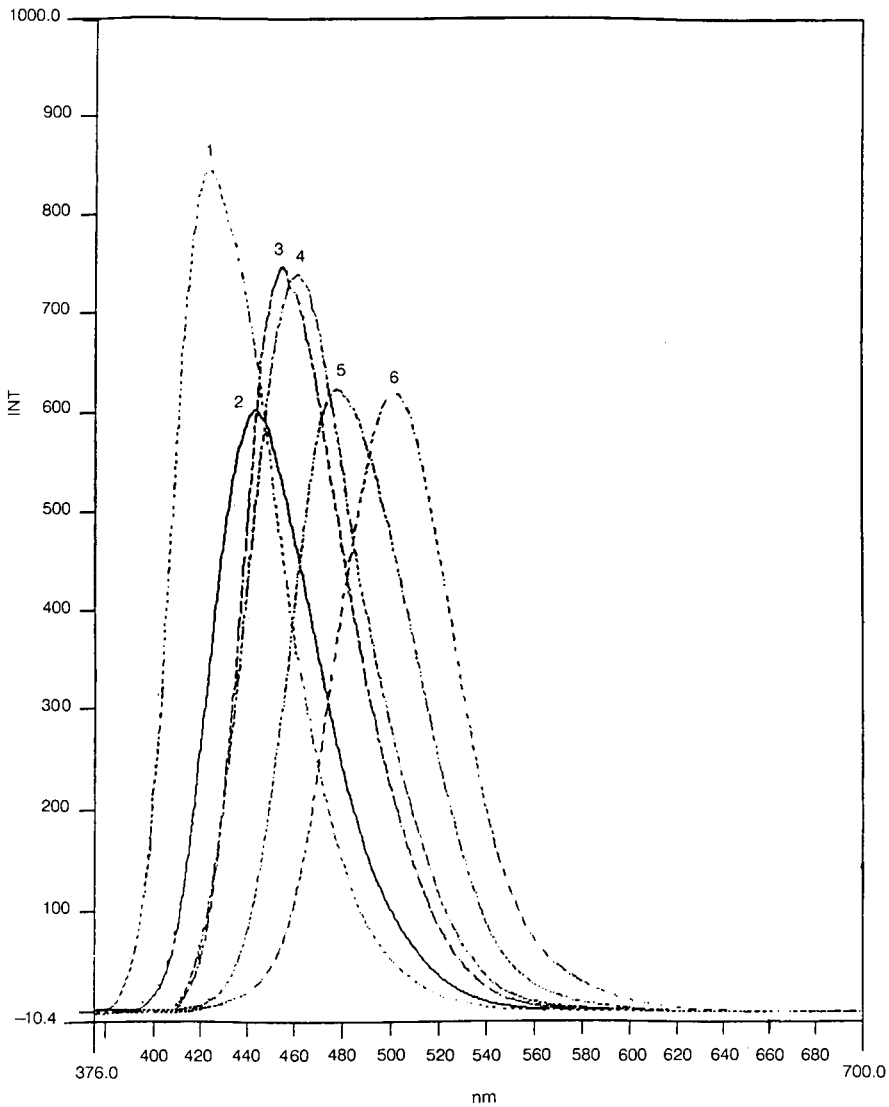

Fig. 4. Fluorescence spectra of luminarin 3 solutions. The successive maxima correspond to (1) cyclohexane, (2) ethyl acetate, (3) dichloromethane, (4) dimethyl sulphoxide, (5) methanol and (6) water. The heights do not reflect relative fluorescence yields.

when the polarity of solvents increases, but is recovered, for example, in viscous solvents. These results are explained by the strong polar character of these molecules in the excited state relative to the ground state when they are dissolved in a polar solvent: the presence of electron-donor (amino) and electron-acceptor (carbonyl) groups leads to a dipolar, planar intramolecular charge-transfer state (ICT), which results in a large increase in dipole moment and a solvatochromic effect; a reduction in the emission spectrum and a bathochromic shift of the fluorescence spectrum are observed in polar solvents.

With luminarins, these phenomena were strongly diminished, because the rigidity of the dye molecule is increased by including the amino nitrogen atom in a planar ring. The mobility of this amino group, whose rotation causes energy dissipation, leads in some instances to the formation of a non-planar twisted intramolecular

charge-transfer state (TICT). When the molecule is rigidized, the rotation of the amino group is hindered and emission is markedly improved. This was demonstrated by the properties of luminarin 3 and its derivatives (Tables 1–4). Similar results have been obtained for coumarin 102 [29–31].

According to these results, a normal-phase system would be more suitable than a reversed-phase system for the trace analysis of luminarin 3 derivatives of carbonyl compounds.

LC separation of hydrazones

Several solvent systems were examined in order to select the most suitable eluent. An organic phase of ethyl acetate–diisopropyl ether (90 + 10, v/v) was found to be suitable when used with a Nucleosil silica column. An excess of reagent and the reaction byproduct (luminarin acid) did not interfere with the LC analysis, because they were eluted after the most of the luminarin 3 derivatives of the carbonyl compounds (Table 5). Separation of the derivatives was obtained in less than 20 min. The separation of diacetyl, acetylacetone, methylmalonaldehyde, malonaldehyde, acrolein, succinaldehyde, acetoacetaldehyde, acetone, ethyl acetoacetate, furfural and hydroxymethyl furfural can be achieved in less than 10 min. The analysis of subsets of the carbonyl compounds listed in Table 5 can be optimized by changing the analytical conditions (e.g., gradient elution, C_{18} instead of silica column for low-molecular-weight carbonyls).

TABLE 5

Capacity factors (k') for luminarin acid, luminarin 3 and individual carbonyl compounds tested as their luminarin 3 derivatives

Compound	k'	
	System I	System II
Luminarin acid	10.61	–
Luminarin 3	5.43	1.49
Acetaldehyde	5.31	3.05
Acetoacetaldehyde	2.13	10.28
Acetoin	5.73	1.53
Acetone	1.89	3.57
Acetoacetic acid	10.86	1.52
Acetylacetone	1.12	10.51
Acrolein	1.71	5.58
	1.38	
Diacetyl	1.17	4.33
Ethyl acetoacetate	2.22	6.51
Formaldehyde	5.70	2.93
Furfural	1.41	7.30
Glyceraldehyde	10.29	0.74
Hydroxymethylfurfural	3.57	2.62
Malonaldehyde	4.26	3.16
Methylmalonaldehyde	2.21	4.72
	1.99	
Succinaldehyde	2.20	5.33

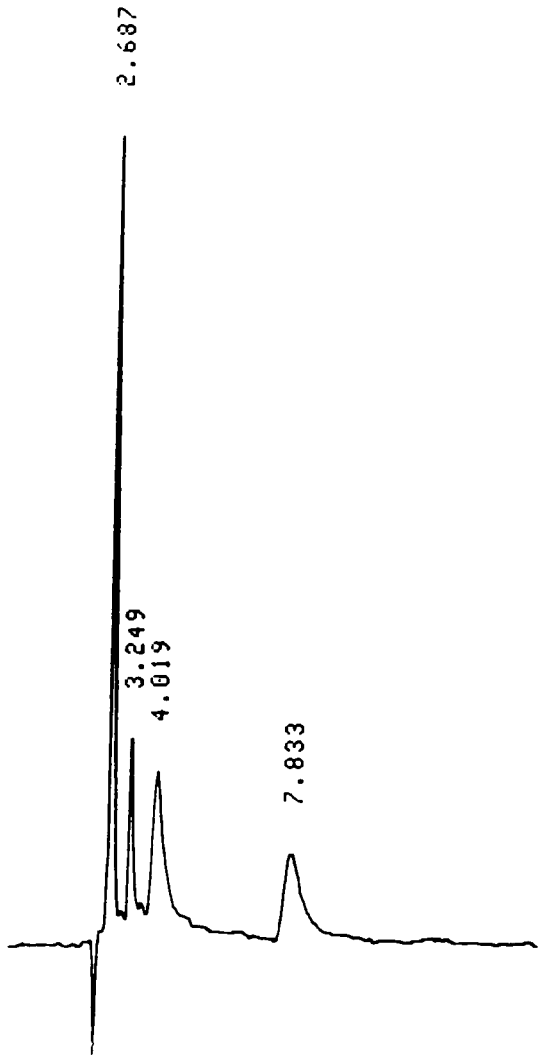

Fig. 5. Separation of luminarin 3 derivatives (system I) with fluorescence detection, 1 mV full-scale. Peaks: diacetyl (3.25 min); acrolein (4.02 min); malonaldehyde (7.83 min). 250 fmol of each derivative were injected on to the column.

TABLE 6

Detection limits of luminarin acid, luminarin 3 and luminarin 3 derivatives of carbonyl compounds in LC with fluorescence detection.

Compound	Detection limit [a] (fmol)	
	System I	System II
Luminarin acid	–	133
Luminarin 3	–	356
Acetaldehyde	–	158
Acetoacetic acid	–	163
Acetoacetaldehyde	175	1950
Acetoin	–	156
Acetone	136	372
Acetylacetone	90	1570
Acrolein	140	650
Diacetyl	83	1950
Ethyl acetoacetate	160	325
Formaldehyde	–	261
Furfural	132	780
Glyceraldehyde	–	473
Hydroxymethylfurfural	294	487
Malonaldehyde	159	163
Methylmalonaldehyde	134	210
Succinaldehyde	65	392

[a] Signal-to-noise ratio = 3.

The effect of carbonyl structure on retention time in normal-phase separation is apparent from the data shown in Table 5. The retention times increased with decreasing chain length for the saturated luminarin 3 derivatives. The retention times fo aromatic aldehydes (e.g., furfural and hydroxymethylfurfural) were consistent with polarity considerations and substituent effects.

Although no attempt is made here to discuss the relationships between retention times and other physico-chemical properties, the data in Table 5 may serve as a guide for optimizing LC conditions for a given mixture of carbonyl compounds.

The octadecyl and silica gel columns were compared for selectivity; although a larger capacity factor ratio was obtained for carbonyl compounds with the octadecyl support, the overall resolution was diminished because of broader peaks.

The octadecyl column with solvents such as methanol, ethanol, propan-2-ol and tetrahydrofuran, either alone or with water, gave lower selectivities than the acetonitrile–water mixture. The mobile phase components (acetonitrile–imidazole buffer) were chosen for their ability to promote peroxyoxalate chemiluminescence (CL) detection, as reported by Tod and co-workers [15,20] for other luminarin derivatives.

The reversed-phase mode was used in this work as it is more popular and easier to use. The reaction byproduct (luminarin acid) peak appeared at the front of the chromatograms. Luminarin 3 derivatives of aliphatic aldehydes (C_3–C_{10} range) and benzaldehyde were separated on the same column using acetonitrile–imidazole buffer (55 + 45, v/v) and with baseline resolution [26]. Luminarin 3 derivatives of even higher aldehydes and ketones should not be difficult to separate but would probably require a higher percentage of acetonitrile. Shorter columns could also be used effectively.

The capacity factors for the carbonyls tested are given in Table 5. Most produced single peaks in the middle of the chromatogram; two peaks for the luminarin 3 derivative of acrolein and methylmalonaldehyde were observed (Table 5, system I), because *anti* and *syn*, *threo* and *erythro* conformers, respectively, were recognized and separated on the silica column, as explained above. How-

TABLE 7

Equations for calibration graphs [defined as $y = ax + b$, where y is the peak area (arbitrary units) and x is the injected amount of sample injected (pmol)] and correlation coefficients (r) for fluorescence detection

Carbonyl compound	Equation [a]	r
Acetoacetaldehyde	$y = 15385x - 1396$	0.993
Acetone	$y = 11741x - 915$	0.999
Acetylacetone	$y = 9979x + 1680$	0.999
Acrolein	$y = 12623x + 1039$	0.996
Diacetyl	$y = 10136x + 1162$	0.991
Ethyl acetoacetate	$y = 8942x + 6104$	0.998
Furfural	$y = 9884x + 2162$	0.999
Hydroxymethylfurfural	$y = 15928x + 7932$	0.998
Malonaldehyde	$y = 28775x - 24650$	0.998
Methylmalonaldehyde	$y = 11462x + 6783$	0.984
Succinaldehyde	$y = 10765x + 176$	0.999

[a] The linear range is 3.125–800 pmol in all instances.

ever, when a reversed-phase system with acetonitrile was used, only a single peak was obtained.

Performance of fluorescence detection

The detection limits of the LC methods are of the order of a few femtomoles. Figure 5 shows the reliability of the detectability of the method. The detection limit (DL) was obtained for 20-μl aliquots of samples using a peak-height integrator signal-to-noise ratio of 3 (Table 6), calculated as $DL = 3\ \sigma b/\bar{a}$, where σb and $\bar{a}$ are respectively the standard deviation of the intercept and the mean of the slope of six calibration graphs determined by linear regression.

To construct calibration graphs for quantification, increasing amounts of carbonyl compounds were derivatized and analysed as described above. From the chromatograms obtained (fluorescence detection) the relationships between peak area and concentration of the carbonyls were calculated using the calibration graph.

Table 7 gives the equations and correlation coefficients obtained with fluorescence detection (system I). The calibration graphs for the carbonyl compounds used were linear over the range 3.125–800 pmol per injection and the relative standard deviations were less than 1.8% ($n = 6$) for 100 pmol per injection.

Conclusion

Derivatization of carbonyl compounds improves the sensitivity of their assay. The luminarin 3 derivatization reagent for carbonyl compounds in LC with fluorescence detection proved satisfactory with respect to reactivity, resolution, analysis time and sensitivity. The method may be of value for carbonyl determinations at trace levels in biological, pharmaceutical and environmental research.

This work was supported in part by a grant-in-aid (Aguire Basualdo) for scientific research from the Chancellery of the University (Paris, France).

REFERENCES

1 G. Avigad, J. Chromatogr., 139 (1977) 347.
2 W.F. Alpenfels, Anal. Biochem., 114 (1981) 153.
3 M. Takeda, M. Maeda and A. Tsuji, J. Chromatogr., 244 (1982) 347.
4 V. Graef, Z. Klin. Chem. Klin. Biochem., 8 (1970) 320.
5 R. Chayen, R. Dvir, S. Gould and A. Harrel, Anal. Biochem., 42 (1971) 283.
6 T. Kawasaki, M. Maeda and A. Tsuji, J. Chromatogr., 232 (1982) 1.
7 T. Kawasaki, M. Maeda and A. Tsuji, J. Chromatogr., 226 (1981) 1.
8 T. Kawasaki, M. Maeda and A. Tsuji, J. Chromatogr., 163 (1979) 143.
9 A.D. Reid and P.R. Barker, J. Chromatogr., 260 (1983) 115.
10 R.W. Frei and J.F. Lawrence, J. Chromatogr., 83 (1973) 321.
11 J.M. Anderson, J. Chromatogr., 330 (1985) 347.
12 K. Imai, S. Higashidate, Y. Tsukamoto, S. Uzu and S. Kanda, Anal. Chim. Acta, 225 (1989) 421.
13 K. Imai, S. Higashidate, A. Nishitani and Y. Tsukamoto, Anal. Chim. Acta, 227 (1989) 21.
14 G. Gübitz, R. Wintersteiger and R.W. Frei, J. Chromatogr., 7 (1984) 839.
15 S. Uzu, S. Kanda, K. Imai, K. Nakashima and S. Akiyama, Analyst, 115 (1990) 1477.
16 R. Weinberger, T. Koziol and G. Millington, Chromatographia, 19 (1984) 452.
17 J. Goto, Y. Saisho and T. Nambara, Anal. Sci., 5 (1989) 399.
18 M. Tod, R. Farinotti, I. Gaury and G. Mahuzier, Anal. Chim. Acta, 217 (1989) 11.
19 M. Tod, M. Prevot, R. Farinotti and G. Mahuzier, J. Chromatogr., 542 (1991) 295.
20 M. Tod, M. Prevot, M. Poulou, R. Farinotti, J. Chalom and G. Mahuzier, Anal. Chim. Acta, 223 (1989) 309.
21 H. Esterbauer and T.F. Slater, IRCS Med. Sci., 9 (1981) 749.
22 E. Sawicki and C.R. Sawicki, Aldehydes: Photometric Analysis, Vol. 2, Academic, London, 1975, p. 264.
23 C.A. Parker and W.T. Rees, Analyst, 85 (1960) 587.
24 G. Weber and F.J. Farris, Biochemistry, 18 (1979) 3075.
25 J.B.F. Lloyd, J. Chromatogr., 178 (1979) 249.
26 M. Tod, PhD Thesis, Université Paris-Sud, 1990, No. 138.
27 A.N. Kost and I.I. Grandberg, Adv. Heterocycl. Chem., 6 (1966) 347.
28 R. Farinotti, Ph. Siard, S. Kirkiacharian, B. Valeur and G. Mahuzier, J. Chromatogr., 269 (1983) 81.
29 G.A. Reynolds and K.H. Drexhage, Opt. Commun., 13 (1975) 222.
30 G. Jones, II, W.R. Jackson and A.M. Halpern, Chem. Phys. Lett., 72 (1980) 391.
31 G. Jones, II, W.R. Jackson, C. Choi and W.R. Bergmark, J. Phys. Chem., 89 (1985) 294.

Analytica Chimica Acta, 269 (1992) 223–228
Elsevier Science Publishers B.V., Amsterdam

Separation and determination of Pt(II), Rh(III), Pd(II), Os(IV), Ni(II) and Co(II) complexes by reversed-phase liquid chromatography

Qiping Liu, Jinchun Liu, Yan Tong and Jieke Cheng

Department of Chemistry, Wuhan University, Wuhan 430072 (China)

(Received 27th March 1992; revised manuscript received 27th May 1992)

Abstract

The use of 2-(6-methyl-2-benzothiazolylazo)-5-diethylaminophenol as a chelating reagent in the reversed-phase liquid chromatographic separation and determination of Pt, Rh, Pd, Os, Ni and Co is reported. A precolumn derivatization method followed by separation on an ODS column with methanol–*n*-butanol–water (70 + 5 + 25) containing 5 mmol l^{-1} tetrabutylammonium bromide, 0.5 mmol l^{-1} ethylenediaminediacetic acid diethyl acetate and 20 mmol l^{-1} acetate buffer (pH 4.5) was used. The detection limits for Pt, Rh, Pd, Os, Ni and Co are 1.5, 0.54, 0.6, 1.0, 0.1 and 0.1 ng ml^{-1}, respectively, with a signal-to-noise ratio of 3. The analyses of a reference sample of noble metals and anode slime are reported. The results corresponded with the certified values, and 94.7–104% recoveries were obtained.

Keywords: Liquid chromatography; Cobalt; Nickel; Osmium; Palladium; Platinum; Rhodium

The separation and determination of noble metals are difficult because of their very similar chemical properties and complicated and variable speciation in solution. Liquid chromatography (LC) is a powerful tool for the determination of traces of noble metals. The method generally used involves complex formation, often using CN^- [1–3], halides [4–6], 1-(2-pyridylazo)-2-naphthol (PAN) [7–9], 2-(5-bromo-2-pyridylazo)-5-(*N*-propyl-*N*-sulfopropylamino)phenol (5-Br-PAPS) [10] and diethyldithiocarbamate (DDTC) [11], etc., as complexing agents.

The use of thiazolylazo reagents in LC analyses for noble metals has been reported but studies on complicated real sample analyses are still very few. Beketova et al. [12] studied the retention of the Pd(II), Pt(II), Rh(II) and Ru(IV) chelates of 1-(2-thiazolylazo)-2-naphthol (TAN), but only separated and determined Pd(II) and Rh(III). Basova et al. [13], using acetonitrile–water, separated Rh(III), Ru(IV), Cu(II) and Co(II) complexes of 4-(2-thiazolylazo)-resorcinol (TAR) on an ODS column. We have also reported the separation and simultaneous determination of Rh(III), Ru(III) and Os(IV) chelates of TAR [14]. In this work more platinum group metals than before were separated and the method was used in real sample analysis.

2-(6-Methyl-2-benzothiazolylazo)-5-diethylaminophenol (MBTAE) has been synthesized as a new thiazolylazo reagent. Using it as a precolumn derivatizing reagent and methanol–*n*-butanol–water (70 + 5 + 25, v/v/v) containing 5 mmol l^{-1} tetrabutylammonium bromide (TBABr), 0.5 mmol l^{-1} ethylenediaminediacetic acid diethyl acetate (EDDD) and 20 mmol l^{-1} acetate buffer (pH 4.5) as the mobile phase, the separation and determi-

Correspondence to: Jinchun Liu, Department of Chemistry, Wuhan University, Wuhan 430072 (China).

nation of Pt, Rh, Pd, Os, Ni and Co on an ODS column were achieved. The detection limits are at the ng ml^{-1} level and the method was applied to analyses of a reference sample of noble metals and anode slime.

EXPERIMENTAL

Apparatus and reagents

A Shimadzu LC-6A LC system with a C-R3A recorder was used. The analytical column was 15 cm × 4.6 mm i.d. and was packed with 5-μm Spherisorb C_{18} (Dalian Institute of Chemistry and Physics). A Shimadzu UV-3000 spectrophotometer, a DF-801 acidimeter (Zhongshan University) and a supersonic degasser were also used.

Ni(II) standard solution was prepared by dissolving the Specpure metal in dilute nitric acid. Stock solutions of Co(II), Rh(III), Pd(II) and Os(IV) in 1 mol l^{-1} hydrochloric acid were prepared from analytical-reagent grade $CoSO_4$, $RhCl_3$, $PdCl_2$ and $(NH_4)_2OsCl_6$. Pt(II) standard solution was prepared from K_2PtCl_6 (analytical-reagent grade) standard solution by reduction with sulphur dioxide gas. All working solutions were diluted to 10.0 μg ml^{-1} with quartz-distilled water before use. Buffer solutions were adjusted to the required pH with 1 mol l^{-1} acetic acid and 1 mol l^{-1} sodium acetate using the acidimeter. EDDD was produced by Wuhan University. A 0.02% solution of MBTAE in absolute ethanol was used. Methanol, *n*-butanol and TBABr were obtained from Shanghai Reagent. All other chemicals were of analytical-reagent grade.

The mobile phase mixture of methanol–*n*-butanol–water (70 + 5 + 5) containing 5 mmol l^{-1} TBABr, 0.5 mmol l^{-1} EDDD and 20 mmol l^{-1} acetate buffer solution (pH 4.5) was filtered through a 0.45-μm Millipore filter and degassed before use.

Procedures

A 5.0-ml volume of 1.0 mol l^{-1} acetate buffer (pH 5.0), 2.0 ml of 0.02% MBTAE solution and 8.0 ml of 95% ethanol were mixed with a known volume of the sample solution, heated in a water-bath at 80°C for 30 min, then cooled to room temperature and diluted to 25.00 ml with water. Volumes of 20 μl of this solution were injected into the chromatographic column for analysis.

For LC analysis, the ODS column was pre-equilibrated with the mobile phase for 30 min. The complexes were eluted at a flow-rate of 1.0 ml min^{-1} and detected at 575 nm. The peak areas were measured for quantitative calculations.

RESULTS AND DISCUSSION

Spectrophotometric properties of MBTAE and its complexes

MBTAE can react with Pt(II), Rh(III), Pd(II), Os(IV), Co(II) and Ni(II) to form stable, coloured complexes. The maximum wavelengths of the complexes and MBTAE were 565–585 nm (Table 1) and 511 nm, respectively. In this work, 575 nm was chosen as the detection wavelength.

Chromatographic conditions

Methanol is a commonly used organic solvent in reversed-phase LC, but the chromatographic plot of each complex was flat and tailing even with the optimum ratio of methanol to water [containing 20 mmol l^{-1} acetate buffer solution (pH 4.0)]. The same experiments were carried out with acetone and acetonitrile instead of methanol, but gave similar results. The experiments showed that adding an auxiliary complexing agent can improve the chromatographic behaviour of the complexes. All the plots were improved and became sharp in the presence of complexon except

TABLE 1

Spectrophotometric properties of MBTAE and its complexes

Complex with MBTAE	λ_{max} (nm)	$\epsilon_{max} \times 10^4$ (l mol^{-1} cm^{-1})	$\epsilon_{575} \times 10^4$ (l mol^{-1} cm^{-1})
Pt(II)	565	3.51	2.73
Rh(III)	575	8.50	8.50
Pd(II)	585	2.66	2.00
Os(IV)	565	1.90	1.36
Ni(II)	577	5.30	5.25
Co(II)	575	7.84	7.84

TABLE 2

Effect of auxiliary complexing agents on the retention time of the complexes [a]

Complexing agent	t_R (min)							
	Pt(II)	Rh(III)	Ni(II)	MBTAE	Pd(II)	Os(IV)	Co(II)	$\overline{\Delta t_R}$
CyDTA [b]	1.83	2.14	6.45	7.70	12.88	13.71	–	2.38
EDTA	–	2.13	6.61	7.69	14.24	13.52	–	3.24
EDDD	1.62	2.01	6.43	7.70	14.10	13.61	–	2.50
NTA [c]	1.92	2.09	6.29	7.60	13.12	13.37	–	2.29
EDDD + TBABr	1.84	2.05	6.24	14.26	12.98	15.50	24.91	3.84

[a] ODS column (5 μm; 150 mm × 4.6 mm i.d.); mobile phase, methanol–water (85 + 15) containing 20 mmol l^{-1} acetate buffer solution (pH 4.0), 3 mmol l^{-1} TBABr, 0.5 mmol l^{-1} auxiliary complexing agent; flow-rate, 1.0 ml min^{-1}; column temperature, 35°C; detection wavelength, 575 nm. [b] CyDTA = cyclohexanediaminetetraacetic acid. [c] NTA = nitrilotriacetic acid.

for Co and Pt (EDTA), whereas the chromatograms of Co and Pt were greatly improved on adding TBABr to the mobile phase. Table 2 shows that not only the separation numbers of the metal ions but also the average retention time difference ($\overline{\Delta t_R}$) of two neighbouring peaks were largest in the EDDD–TBABr system. The sequence of $\overline{\Delta t_R}$ is EDDD + TBABr > EDTA > EDDD > CyDTA > NTA. Therefore, the EDDD–TBABr system was adopted in subsequent work.

Figure 1 shows the ln k' vs. methanol concentration plots. It is clear that ln k' decreased sharply with increasing methanol concentration. When the methanol concentration was > 80% or < 74%, some chromatograms overlapped and the elution order changed. Therefore, 75% methanol was selected.

Figure 2 shows the effect of EDDD concentration on ln k'. Variation of the EDDD concentration in the range of 0.05–1.0 mmol l^{-1} had no effect on the results, and 0.5 mmol l^{-1} EDDD was selected.

The plot of pH vs. ln k' is shown in Fig. 3. The retention values for each complex remained almost constant in the pH range 3.75–6.0, and variation of the buffer solution concentration in the range of 5–30 mmol l^{-1} had no effect on the

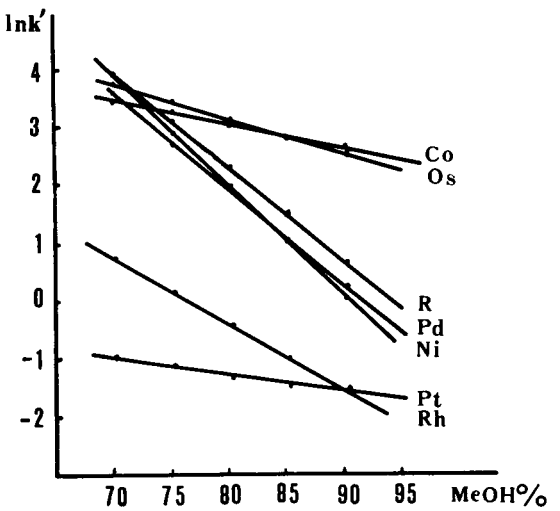

Fig. 1. Plots of ln k' vs. methanol concentration. Mobile phase, 70–90% methanol–5 mmol l^{-1} TBABr–0.5 mmol l^{-1} EDDD; other conditions as in Table 2. R = MBTAE.

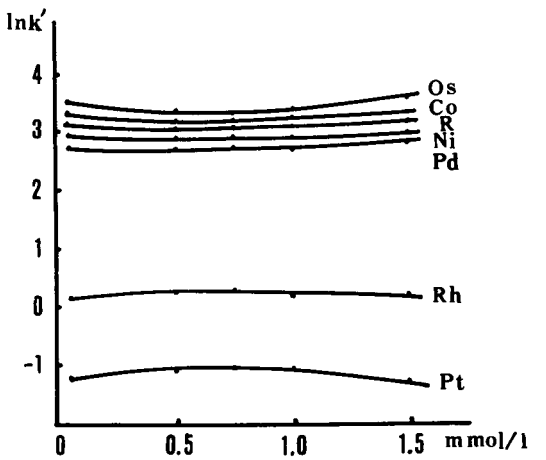

Fig. 2. Effect of EDDD concentration on ln k'. Mobile phase, methanol–water (75+25)–0.05–1.5 mmol l^{-1} EDDD; other conditions as in Fig. 1.

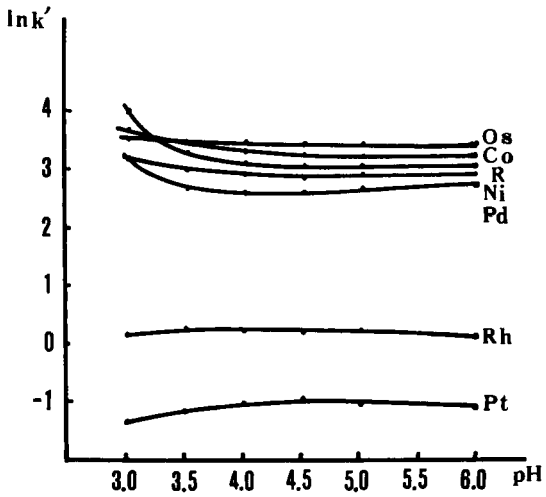

Fig. 3. Effect of pH on ln k'. Mobile phase, pH 3.0–6.0 acetate buffer solution; other conditions as in Fig. 2.

capacity factor of each complex. Therefore, 20 mmol l^{-1} acetate buffer solution (pH 4.5) was selected.

Under the optimum conditions, the chromatograms of the six complexes and MBTAE indicated that the peak widths of the Ni, Pd, Co and Os complexes were still large, the peak valley of some neighbouring peaks overlapped and it

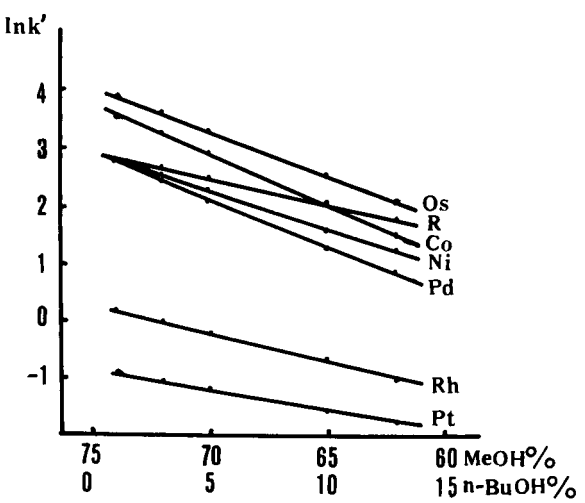

Fig. 4. Effect of organic modifier on ln k'. Mobile phase, (methanol–n-butanol)–water (75+25); other conditions as in Fig. 3.

TABLE 3

Effect of column temperature on ln k' (ln $k' = A + B/T$)

Complexes with MBTAE	A	B	r
Pt(II)	5.1060	−2021.6450	−0.9783
Rh(III)	5.0475	−1717.6880	−0.9832
Pd(II)	−7.2549	2868.7930	0.9996
Os(IV)	−1.8013	1551.2710	0.9920
Ni(II)	−4.5767	2121.5650	0.9849
Co(II)	−1.4869	1317.7680	0.9939

was difficult to obtain quantitative results, which meant that the chromatographic conditions needed to be further optimized. For this reason, some organic modifiers such as ethyl acetate and n-butanol were added to the methanol–water system. The results indicated that n-butanol can effectively improve the resolution of neighbouring peaks, whereas ethyl acetate had no such effect. Typical results are shown in Fig. 4. When the total concentration of organic solvents (methanol + n-butanol) was kept constant at 75%, the ln k' values decreased with increasing concentration of n-butanol. When the concentration of n-butanol was $> 8\%$ or $< 3\%$, the resolution of MBTAE and Co, Ni and Pd decreased. The optimum choice was 70% methanol + 5% n-butanol.

It was found that the ln k' values varied linearly with the reciprocal of temperature in the range 25–55°C, the relationship being ln $k' = A + B/T$, where T is the absolute temperature. The results of linear regression for the experimental data are given in Table 3.

The total flow-rate also affected the separation of the complexes. When the flow-rate was greater than 1.2 ml min^{-1}, MBTAE and Ni overlapped, and the peak widths were enlarged at flow-rates lower than 0.6 ml min^{-1}. Therefore, the flow-rate was kept at 1.0 ml min^{-1}.

Under the optimum conditions, the chromatogram shown in Fig. 5 was obtained for the separation of MBTAE and its complexes. The separation can be completed in 30 min.

Linear response range

The linear response range and detection limits of each metal ion are shown in Table 4.

TABLE 4

Linear response range and detection limit of metal ions

Metal ion	Linear equation [a]	r	Linear range (ng ml^{-1})	Detection limit (signal-to-noise ratio = 3) (ng ml^{-1})
Pt(II)	$y = 1464.277 + 4282.144x$	0.9998	4–640	1.5
Rh(III)	$y = 1966.668 + 10500x$	0.9991	2–400	0.54
Pd(II)	$y = 71.4453 + 9964.283x$	0.9971	2–480	0.6
Os(IV)	$y = 1973.641 + 6657.891x$	0.9928	6–1680	1.0
Ni(II)	$y = 2000.031 + 56285.71x$	0.9997	0.4–280	0.1
Co(II)	$y = 1100.047 + 48128.56x$	0.9895	2–280	0.1

[a] x = Concentration of metal ions (μg ml^{-1}); y = peak areas of complexes (a.u.f.s.).

TABLE 5

Results of analysis of a reference sample of noble metals ($n = 3$)

Element	Certified content (μg g^{-1})	Found (μg g^{-1})	Average (μg g^{-1})	R.S.D. (%)
Pt	5.40	5.29, 5.36, 5.34	5.33	0.68
Rh	0.31	0.29, 0.30, 0.32	0.30	5.10
Pd	7.52	7.54, 7.48, 7.49	7.50	0.43

TABLE 6

Results of analysis of anode slime ($n = 6$)

Element	Average content (μg g^{-1})	R.S.D. (%)	Added (μg g^{-1})	Found (μg g^{-1})	Recovery (%)
Pt	16.0	0.33	30.0	46.0	100.0
			20.0	36.5	102.5
Rh	–	–	15.0	14.2	94.7
			50.0	51.5	103.0
Pd	2.50	1.72	40.0	44.0	103.8
			30.0	32.6	100.3
Os	9.60	0.61	35.0	46.0	104.0
			60.0	69.1	99.2
Ni	17.0	0.30	5.00	21.8	96.0
			10.0	26.8	98.0
Co	4.20	1.12	2.00	6.10	95.0
			5.00	9.30	102.0

Effect of foreign metal ions

Some other metal ions such as Fe(III), Cu(II), Zn(II) and Cd(II) can also react with MBTAE at pH 5.0, but no peaks are observed under the chosen elution conditions. However, they would consume MBTAE. When 2.0 ml of MBTAE was added, the foreign metal ion tolerances were Cu(II) and Fe(III) 20 μg, Zn(II) 100 μg, Cd(II) 80 μg, Ti(IV) 0.5 mg, Au(III) 0.3 mg and Ag(I) 0.2 mg. If the volume of MBTAE were increased to 4.0 ml, the metal ion tolerances would be increased to Cu(II) 80 μg, Fe(III) 60 μg, Zn(II) 200 μg and Cd(II) 200 μg.

Sample analysis

The analysis of a reference sample of noble metals was carried out as follows. A 2.0-g amount of sample was weighed and dissolved in 100 ml of nitric acid–hydrochloric acid (1 + 3), heated until it had all dissolved and evaporated nearly to

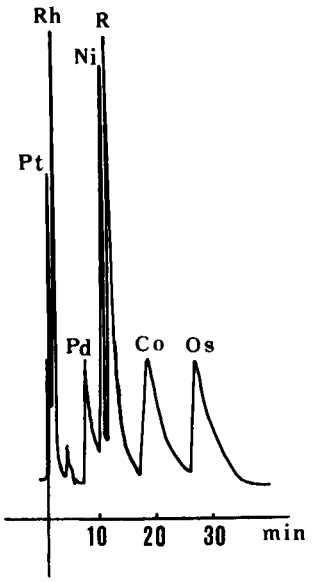

Fig. 5. Separation of MBTAE and its complexes. Column, 5-μm ODS (150 mm×4 mm i.d.); mobile phase, methanol–*n*-butanol–water (70+5+25) containing 20 mmol l^{-1} acetate buffer solution (pH 4.5), 0.5 mmol l^{-1} EDDD, 5 mmol l^{-1} TBABr; flow-rate, 1.0 ml min^{-1}; column temperature, 50°C; detection wavelength 575 nm. R = MBTAE.

dryness. A 10-ml volume of concentrated hydrochloric acid and 0.5 ml of 10% sodium chloride solution were added, the mixture was heated nearly to dryness, cooled to room temperature, dissolved in water and filtered. The residue was washed with 0.5 mol l^{-1} HCl and the solution was transferred into a 50-ml volumetric flask. Concentrated ammonia solution was added dropwise to adjust the acidity and the solution was diluted to the mark with water. A 5.0-ml portion of this solution was analysed as follows. A 0.5-ml volume of 2 mol l^{-1} NaOH solution, 5.0 ml of acetate buffer solution (pH 5.0), 2.0 ml of saturated oxalic acid, 4.0 ml of 0.02% MBTAE and 8.0 ml of 95% ethanol were added in that order and the mixture was heated on a water-bath at 80°C for 30 min, cooled to room temperature and diluted to 25 ml with water in a volumetric flask. The sample was centrifuged and 20 μl of the upper solution was injected on to the ODS column. The results are given in Table 5.

For the analysis of anode slime (the residue on the anode after the electrolysis of copper), the sample was ground, sieved (100 mesh) and dried at 110°C for 2 h. A 5.0-g amount was gently heated with 120 ml of concentrated nitric acid–hydrochloric acid (1 + 3) until it had all dissolved. After cooling the solution, 1 ml of 10% sodium chloride solution was added and the mixture was evaporated nearly to dryness, then transferred into a 100-ml volumetric flask and diluted to the mark with water. A 2.0 ml portion was analysed according to the analytical procedure. The results are given in Table 6.

This project was supported by the National Natural Science Foundation of China.

REFERENCES

1 D.F. Hilton and P.R. Haddad, J. Chromatogr., 361 (1986) 141.
2 P.R. Haddad and N.E. Rochester, Anal. Chem., 60 (1988) 536.
3 P.R. Haddad and N.E. Rochester, J. Chromatogr., 439 (1988) 23.
4 K. Li, B.-S. Xin and X.-G. Cheng, Fenxi Huaxue, 16 (1988) 603.
5 H. Muller and P. Bekk, Fresenius' Z. Anal. Chem., 314 (1983) 758.
6 P. Obergfell and H. Muller, Fresenius' Z. Anal. Chem., 328 (1987) 242.
7 Yu. S. Nikitin, N.B. Morozova, S.N. Lanin, T.A. Bol'shova, V.M. Ivanov and E.M. Basova, Talanta, 34 (1987) 223.
8 T.A. Bol'shova, P.N. Nesterenko, E.M. Basova, V.M. Ivanov and N.B. Morozova, Zh. Anal. Khim., 42 (1987) 1648.
9 E.M. Basova, T.A. Bol'shova, V.M. Ivanov and N.B. Morozova, Zh. Anal. Khim., 44 (1989) 680.
10 N. Uehara, Y. Annoh, T. Shimizu and Y. Shijo, Anal. Sci., 5 (1989) 111.
11 B.J. Mueller and R.J. Lovett, Anal. Chem., 59 (1987) 1405.
12 N.A. Beketova, E.M. Basova, V.M. Ivanov and T.A. Bol'shova, Zh. Anal. Khim., 45 (1990) 2178.
13 E.M. Basova, T.A. Bol'shova, E.N. Shapovalova and V.M. Ivanov, Zh. Anal. Khim., 45 (1990) 1947.
14 Q.-P. Liu, H.-S. Zhang and J.-K. Cheng, Talanta, 38 (1991) 669.

Analytica Chimica Acta, 269 (1992) 229–238
Elsevier Science Publishers B.V., Amsterdam

Mathematical simulation of complex chromatographic systems: a simulation model of reversed-phase liquid chromatography of metal chelates

A.R. Timerbaev, I.G. Tsoi and O.M. Petrukhin

Mendeleev Moscow Institute of Chemical Technology, 125190 Moscow (Russia)

(Received 28th May 1992)

Abstract

An equilibrium model for describing the reversed-phase liquid chromatographic behaviour of metal chelates has been developed. This model takes account of possible chemical reactions accompanying the chromatographic process for metal chelates, i.e., dissociation, hydrolysis, adduct formation, etc. The main experimental parameters affecting on the equilibrium concentration of a metal chelate in a mobile phase (stability and amount of chelate, nature and concentration of an organic modifier, acidity, concentration of a chelating reagent, etc.) were analysed. The basic model conclusions were confirmed experimentally on an example of metal dithiocarbamates and dithiophosphates. Recommendations on selecting the optimum chelates for metal analysis and conditions for chelate stabilization and separation by reversed-phase liquid chromatography were elaborated.

Keywords: Liquid chromatography; Optimization methods; Mathematical simulation; Metal chelates; Simulation

Chromatographic methods for the separation and determination of metal ions as chelate complexes, among which liquid chromatography (LC) is the leading technique, are widely used in trace metal analysis [1,2]. However, in spite of practical achievements [3,4] and the large number of experimental data accumulated over more than 15 years of the development of the LC of metal chelates [5], the problem of describing the chromatographic behaviour of metal chelates on a quantitative basis still remains. This problem is concerned directly with a distinguishing feature of metal chelates (particularly less stable and kinetically labile complexes) as analytes in liquid chromatography, that is, the possibility of chemical reactions in a chromatographic system including dissociation, hydrolysis, ion or ligand exchange, adduct formation, etc. [5]. These processes can make the separation more difficult and worsen the results of metal determinations. Hence one should select metal chelates very carefully or ensure their stabilization in the chromatographic process.

Correlation models of the retention–structure or retention–mobile phase composition type, which are widely used in the LC of organic substances [6,7], are also suitable for predicting and optimizing the separation conditions for metal chelates, but only sufficiently stable ones [8,9]. On the other hand, the description of retention reguliarities with due regard to a variety of chemical processes accompanying the interphase distribution of metal chelates can be made by using a simulation technique. This computer method has proved to be a powerful tool for studing complex chromatographic systems, including thin-layer chromatography [10,11] and normal-phase LC (NP-LC) [12] of metal chelates.

Correspondence to: A.R. Timerbaev, Department of Analytical Chemistry, Johannes Kepler University, Altenbergerstrasse 69, A-4040 Linz (Austria) (present address).

This paper, describes further investigations on the simulation of the chromatographic behaviour of metal chelates and a model for reversed-phase LC (RP-LC) is presented.

EXPERIMENTAL

Materials and apparatus

The synthesis of metal dithiocarbamates and dithiophosphates is described in [13]. A KAX-2 stainless-steel column (64 × 2 mm i.d.) (Russia) packed with Separon C_8 (particle size 5 μm) from Hemapol (Czechoslovakia) and precoated high-performance RP C_8 F_{254} thin-layer chromatographic (TLC) plates (Merck, Darmstadt, Germany) were used for chromatography. The mobile phases were prepared from methanol, acetonitrile, acetone, 1,4-dioxane of chromatography grade, doubly distilled water or 0.1 M acetic acid–ammonia buffer, and organic bases (pyridine, piperidine).

A Milikhrom microcolumn liquid chromatograph (Russia) equipped with a variable-wavelength spectrophotometric detector (190–360 nm) was used. The conditions for the TLC experiments are described in [8].

Calculations

Calculations were carried out on a DVK-2 computer (Russia) with a program in BASIC. A detailed description of the program is presented in [14]. By making initial approximations of the variation of parameters, solutions were obtained for each previous step. This ensured the stability of the algorithm and rapid convergence of results for 5–10 iterations. The corresponding model dependences were obtained by changing the next value of a parameter not more than 100 times. A calculation accuracy of 0.1% was set.

RESULTS AND DISCUSSION

Simulation model

Any mathematical model is effective only if it is sufficiently complete to provide an adequate description of experimental data and simultaneously not so complex that the simulated problem could not be solved in a reasonable computation time. Therefore, one should include in the model only a minimum of the most significant representations, which can describe the main features of the investigated process.

In RP-LC, because of the multi-component composition of both chromatographic phases and the large number of physico-chemical processes, the simulated system has a more complicated description than in NP-LC. Hence the initial equilibria were selected more thoroughly, as the superfluous omission of less valuable equilibria leads to the opposite result, that is, increasing the duration of computation and decreasing the accuracy of the optimized function.

Considering the chromatographic process as an equilibrium one, it is described on a static level and, for simplicity, without taking into consideration the contributions of dynamic and kinetic factors. Such an assumption is stipulated by the equilibrium character and sufficiently high rate of physico-chemical processes occurring in the chromatographic system. The static approach allows one to apply the laws of mass action, conservation of matter and charge for describing the corresponding equilibria, estimating changes in the system composition as a result of chemical reactions and establishing relationships between the amounts of components in the mobile and stationary phases.

The most valuable equilibria were selected on the basis of modern representations of the electronic and geometric structure of metal chelates, the nature of reversed-phase stationary phases, the character of intermolecular interactions and the retention mechanism for metal chelates and the data of theoretical calculations (for details, see [14]). In certain instances a preliminary experiment was done to evaluate the significance of a given equilibrium.

Equilibria in a sorbent–eluent system. In using the binary water–organic mixtures as a mobile phase, the alkyl groups of the stationary phase (SiR) are solvated, partially or completely, by molecules of an organic solvent (E):

$$SiR + E \rightleftharpoons SiR \cdot E \qquad (1)$$

and unmodified (uncapped) silanol groups (SiOH) are hydrated:

$$SiOH + H_2O \rightleftharpoons SiOH \cdot H_2O \quad (2)$$

The specific adsorption of the organic modifier should also be taken into account:

$$SiOH + E \rightleftharpoons SiOH \cdot E \quad (3)$$

By analogy with NP-LC [15], dissociation of residual silanol groups can be assumed. However, in water–organic media this process might be suppressed to a considerable extent by the adsorption effects of strongly polar components of the mobile phase. Therefore, for this reason we neglected the decrease in concentration of SiOH groups and also the participation of SiO^- groups in the overall retention.

Interphase distribution of metal chelate. Addition of metal chelate, ML_n, to the chromatographic system is accompanied by its solvation in the mobile phase followed by the distribution between the volume of mobile phase and a surface layer of the sorbent. These processes can be expressed by the following equations:

$$ML_n + E \overset{K_E^{ML_n}}{\rightleftharpoons} ML_n \cdot E \quad (4)$$

$$ML_n + SiR \rightleftharpoons SiR \cdot ML_n \quad (5)$$

Solvation may take place by different mechanisms (interspheric or intraspheric) and with the participation of both components of the mobile phase depending on the eluent composition and the type of chelate.

It should be borne in mind that from the point of view of solvophobic theory [15], the reason for the retention of metal chelates in RP-LC is the association of molecules of the mobile phase. However, the equations expressing solvophobic interactions do not yield to a description by the law of mass action. Therefore, during simulations, the structural regularity of the mobile phase was taken into account by attaching the corresponding physical meaning to the constant of equilibrium 5.

The equilibria $SiOH + ML_n \rightleftharpoons SiOH \cdot ML_n$ and $mSiOH + ML_n \rightleftharpoons (SiO)_m ML_{n-m} + mHL$ were not included in the model. The contribution of the specific adsorption of metal chelates, which can be followed by their interaction with residual silanol groups, was estimated by using of Nicolov's method [16] based on calculations of the coefficient of accessibility of silanol groups. It has been shown [14] that silanol groups are almost inaccessible for such large molecules as metal dialkyldithiocarbamates and dialkyldithiophosphates taken as model compounds when the common types of alkyl-modified sorbents and RP-LC mobile phases are used.

Reactions of metal chelate in the chromatographic system. Among chemical reactions of metal chelates, which are possible under RP-LC conditions, the following were considered:

dissociation:

$$ML_n \overset{K_1}{\rightleftharpoons} ML_{n-1}^+ + L^- \quad (6)$$

$$\vdots \qquad\qquad \vdots \qquad\qquad \cdots$$

$$ML^{(n-1)+} \overset{K_n}{\rightleftharpoons} M^{n+} + L^- \quad (6a)$$

hydrolysis:

$$ML_n + H_2O \rightleftharpoons M(OH)L_{n-1} + HL \quad (7)$$

$$\vdots \qquad\qquad \vdots \qquad\qquad \cdots$$

$$M(OH)_{n-1}L + H_2O \rightleftharpoons M(OH)_n + HL \quad (7a)$$

interaction with an electron-donor organic base:

$$ML_n + B \overset{K_B}{\rightleftharpoons} ML_n \cdot B \quad (8)$$

In general, the last reaction can occur also by a ligand-exchange mechanism up to the formation of cationic complexes:

$$ML_n + mB \rightleftharpoons MB_m^{n+} + nL^-$$

However, the replacement of chelating ligands from the inner coordination sphere of the metal atom was observed experimentally only at high concentrations of donor-active compounds and hence this reaction was not included in the model.

Other equilibria. Stabilization of metal chelates in the chromatographic process requires special methods [6], among which the addition of the chelating reagent or organic base to the mobile phase and using a buffer as its aqueous component were considered here. With increasing num-

ber of components of the chromatographic system, the number of chemical processes increases:

$$SiR + HL \rightleftharpoons SiR \cdot HL \quad (9)$$

$$HL \overset{K_i^{HL}}{\rightleftharpoons} H^+ + L^- \quad (10)$$

$$SiR + B \rightleftharpoons SiR \cdot B \quad (11)$$

The adducts formed by reaction 8 participate in the interphase distribution as a sorbate with individual chromatographic properties:

$$SiR + ML_nB \rightleftharpoons SiR \cdot ML_nB \quad (12)$$

(the contribution of specific adsorption of HL, B and ML_nB was neglected for the reasons pointed out above.)

The acid–base properties of the mobile phase define the equilibria of reactions 6, 7, and 10. Nevertheless, for simplicity, sorption and solvation interactions of buffer components were not considered in the model, as they do not significally influence the equilibria with the participation of metal chelate.

The material balance and electronegativity equations were written for Eqns. 1–12 considering chelates of doubly charged metals, ML_2 (this limitation does not substantially affect the overall model conclusions). Activities were replaced with concentrations since sufficiently small amounts of metal chelates are applied in LC and changes in concentrations of other components of the chromatographic system can be neglected because of their large excess in comparison with the concentration of metal chelates. All the concentrations in the mobile phase were volume concentrations and those in the stationary phase were surface concentrations. Surface concentrations were expressed as the ratio of the mass of the corresponding component to the area of the sorbent which it occupied. The initial equations were the following:

$$\begin{aligned} n_M = {} & ([ML_2 \cdot E] + [ML_2B] + [M(OH)L] \\ & + [M(OH)_2] + [ML_2] \\ & + [ML^+] + [M^{2+}])V_E \\ & + ([SiR \cdot ML_2] + [SiR \cdot ML_2B])S \end{aligned} \quad (13)$$

$$\begin{aligned} n_L = {} & (2[ML_2 \cdot E] + 2[ML_2B] + [M(OH)L] \\ & + 2[ML_2] + [ML^+] + [HL] + [L^-])V_E \\ & + 2[SiR \cdot ML_2] + [SiR \cdot HL] \\ & + 2[SiR \cdot ML_2B])S \end{aligned} \quad (14)$$

$$\begin{aligned} n_E = {} & ([ML_2 \cdot E] + [E])V_E \\ & + ([SiR \cdot E] + [SiOH \cdot E])S \end{aligned} \quad (15)$$

$$\begin{aligned} n_B = {} & ([ML_2B] + [B])V_E \\ & + ([SiR \cdot B] + [SiR \cdot ML_2B])S \end{aligned} \quad (16)$$

$$\begin{aligned} n_{SiR} = {} & ([SiR] + [SiR \cdot ML_2] + [SiR \cdot HL] \\ & + [SiR \cdot B] + [SiR \cdot E] + [SiR \cdot ML_2B])S \end{aligned} \quad (17)$$

$$\begin{aligned} n_{SiOH} = {} & ([SiOH] + [SiOH \cdot H_2O] \\ & + [SiOH \cdot E])S \end{aligned} \quad (18)$$

$$[ML^+] + [M^{2+}] + [H^+] = [L^-] \quad (19)$$

where n_M, n_L, n_E, n_B, n_{SiR}, and n_{SiOH} are the number of moles of metal, ligand, organic modifier, organic base, alkyl and hydroxyl groups of the stationary phase, respectively, V_E is the volume of mobile phase and S is the total surface area of the stationary phase (the last two values were calculated as described previously [12]).

This set of equations is the basis of the simulation model of the RP-LC of metal chelates at the level of a static description. It was reduced to a set of four non-linear equations with respect to $[ML_2]$, [HL], [SiR] and [SiOH], solved by Newton's method [17]. The equilibrium concentration of metal chelate in the mobile phase was used as an optimized function. $[ML_2]$ is connected with the relative rate of motion of the chromatographic band and if one neglects the diffusive dispersion of the band, retention parameters (k' or R_F) can be easy expressed via $[ML_2]$. In addition, the height (or area) of the chromatographic peak is proportional to the equilibrium concentration. This makes it possible to compare model calculations with experimental data. Characteristics of the chromatographic system, total amounts of the components and equilibrium constants served as variables. Constants were estimated from literature data, by calculations (e.g., proceeding from available thermodynamic data)

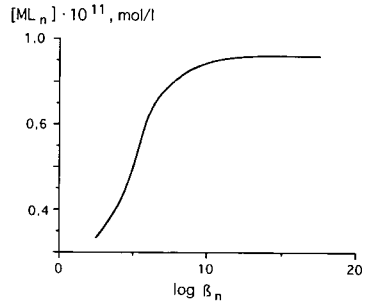

Fig. 1. Dependence of the equilibrium concentration of a metal chelate in mobile phase on its stability constant.

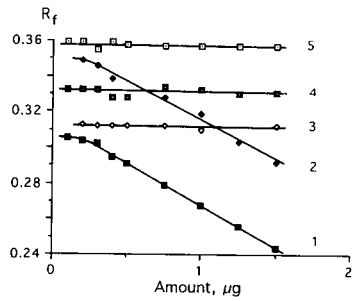

Fig. 2. R_F dependences on sample mass for metal diethyldithiocarbamates. 1 = Cu; 2 = Ni; 3 = Pd; 4 = Cr; 5 = Co. Mobile phase: acetonitrile–water (80 + 20, v/v).

or during the simulation (for more details, see [14]).

Simulation

Metal chelate. The equilibrium concentration of the molecular form of a metal chelate at fixed parameters of the mobile phase is determined by the conditional stability constant $\beta_n = 1/(K_1 \times K_2 \times \ldots \times K_n)$. The dependence of $[ML_n]$ on log β_n presented in Fig. 1 testifies to the existence of a certain critical value of the stability constant (β_n^{crit}), which allows one to judge the possibility of utilizing a given chelate for metal analysis. The absolute value of β_n^{crit} is defined by the mobile phase composition. That this distinguishes RP-LC from NP-LC, where dissociation of metal chelates proceeds in a stationary phase of the hydroxylated sorbent [10]. The polarity (or dielectric permeability) of a surface layer of this stationary phase, and consequently the β_n^{crit} value, is approximately constant. Nevertheless, the calculation of β_n^{crit} values for different mobile phases by means of the developed model offers no difficulty.

Because of instability in the chromatographic system, the mobility of metal chelates shows a strong dependence on their amount. Fig. 2 demonstrates the corresponding experimental data for metal diethyldithiocarbamates obtained by TLC. These dependences confirm that thermodynamically and kinetically stable chelates (palladium, chromium and cobalt complexes) are stable in RP-LC [18].

Thus, dissociation leads to a non-observance of the proportionality between the equilibrium concentration of chelate in the mobile phase and its amount in the chromatographic system. The model dependences of $[ML_n]$ on n_M corresponding to the arbitrarily set stability constants are shown in Fig. 3. Both the absolute deviation of the dependences from linearity in the region of small amounts and the extent of the non-linear interval increase markedly with decreasing stability of the chelate. However, at log $\beta_n > 10$, these non-linear effects can be considered to be negligible. Analogous experimental dependences have an identical character (Fig. 4); this confirms the practical significance of simulation. Such important analytical characteristics as the detection limit and linear concentration range can be directly evaluated on the basis of the data from computational experiments.

Chelating reagent. The model experiment provides the possibility of estimating the influence of the amount of chelating reagent on the equilib-

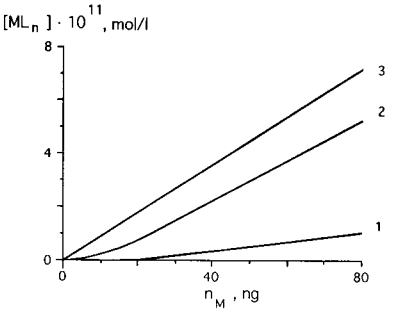

Fig. 3. Dependence of the equilibrium concentration of metal chelates of different stability on their amount. Log β_n: 1 = 6; 2 = 8; 3 = 10.

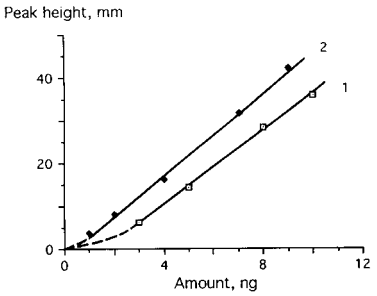

Fig. 4. Dependence of the peak height of (1) copper and (2) nickel diethyldithiocarbamates on the amount injected. Mobile phase: acetonitrile–water–chloroform (70 + 28 + 2, v/v/v).

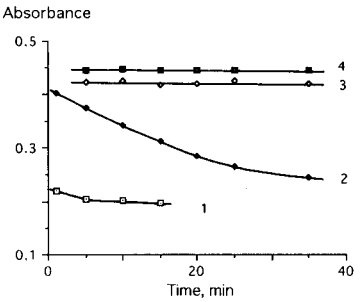

Fig. 6. Effect of reagent concentration on the stability of nickel di-*n*-butyldithiophosphate in dioxane–water (80 + 20, v/v) solutions. Concentration of potassium dibutyldithiophosphate (M): 1 = 0; 2 = 1×10^{-4}; 3 = 1×10^{-3}; 4 = 1×10^{-2}.

rium concentration of metal chelates of different stability. The surface $[ML_n](\log n_L, \log \beta_n)$ relationship depicted in Fig. 5 demonstrates the effect of the dissociation suppression due to a shift of equilibrium 6 to the side of the molecular form of the chelate. As can be seen from Fig. 5, the addition of the reagent to the mobile phase allows the interval of stability constants suitable for metal analysis to be extended to at least four orders of magnitude. According to the simulations, for instance, a metal complex with $\beta_n \approx 10^6$ should display satisfactory chromatographic behaviour in the presence of 10^{-4} mol l^{-1} of the chelating reagent in the mobile phase. Indeed,

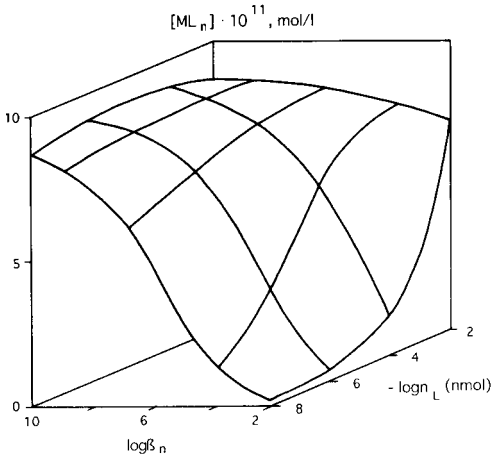

Fig. 5. Effect of the amount of reagent on the equilibrium concentration of metal chelates with different stability contants.

the data on the effect of the reagent concentration on the decomposition of nickel dibutyldithiophosphate ($\log \beta_n = 6.7$) shown in Fig. 6 confirm these simulation results. The upper limit of the permissible concentration of HL in the mobile phase is determined in the general case by the physico-chemical properties of the chelating reagent (solubility, absorbance at the detection wavelength, etc.).

Mobile phase. Nature and concentration of organic modifier. The variation of these parameters of the mobile phase affects the retention of a metal chelate owing to changes in the constants of equilibria 4 and 5 and the ionization constant of the reagent.

The dependences constructed from the data of a model experiment and shown in Fig. 7 characterize changes in the equilibrium concentration of metal chelates of different stability with changing content of the organic modifier and the size of chelate molecule expressed through the number of carbon atoms in the alkyl substituents of the ligand (n_C). As follows from the solvophobic theory [15], the largest response to the change in size (or volume) of a metal chelate was obtained for more associated eluents (i.e., with higher contents of water). However, mobile phases of this type hardly elute large chelate molecules; when the concentration of the organic modifier reaches 40 vol.%, only complexes with methyl and ethyl substituents are chromatographed (surface A). Separation of metal chelates with the same ligand is also impossible under these conditions, as the

contribution of the metal atom to the volume of the molecule is too small in comparison with the increment in methylene groups.

As regards less stable chelates (surface B), the model conclusion is that to attain the highest and steady concentrations of the molecular form, one should use eluents with a high concentration of an organic component (as far as is possible). In that event additional limitations to the water content in the mobile phase are connected with the hydrolysis of the chelates (see below).

The major disadvantage of $[ML_n]$ (C_E, n_C) dependences is a low effectiveness for the optimization of the separation conditions for metals as chelates. The solution of this problem required the simulation of the effect of the value of the solvation constant on the equilibrium concentration of the chelate. For this purpose a number of assumptions were made. First, it was taken into account that for sulphur-containing chelates of "soft" metals [19] used as model compounds, specific interactions in the mobile phase are restricted mainly by hydrogen bonding. Second, $K_E^{ML_n}$ was replaced with Kosover's parameter of proton-donating ability (z) [20], which is characterized by high correlation coefficients with retention parameters of sulphur-containing chelates [9].

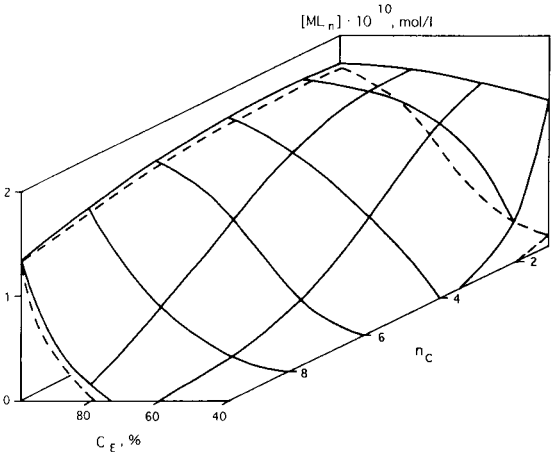

Fig. 7. Dependence of the equilibrium concentration of metal chelates with different alkyl substituents on the organic modifier concentration. Solid lines, surface A; dotted lines, surface B.

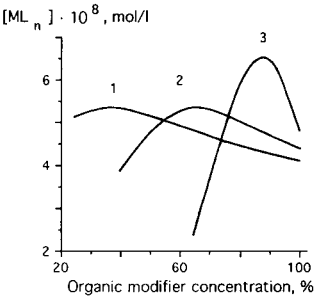

Fig. 8. Dependence of the equilibrium concentration of metal chelate on mobile phase proton-donor ability. 1 = Dioxane–water; 2 = acetonitrile–water; 3 = methanol–water.

The dependences obtained (Fig. 8) confirm that the lower is the concentration of the organic solvent, the stronger are specific interactions of chelates owing to the hydration processes (the proton-donor ability of water is higher than that of organic solvents used in RP-LC). However, on reaching some critical concentration ratio, the influence of proton-donor properties of the mobile phase is compensated for by the cohesion effects. For aprotic solvents, the corresponding maximum is low and shifted to higher water concentrations. This means that in general the selectivity of the separation of metal chelates in RP-LC must be higher when mobile phases modified by proton-donor solvents are used. The best separation should be expected for the eluent composition to which the maximum on the $[ML_n]$–C_E dependence corresponds. The model permits the optimum composition of the mobile phase corresponding to this critical point to be calculated. The chromatograms of synthetic mixtures of metal diethyldithiocarbamates presented in Fig. 9 illustrate this practical value of the model.

Acidity. The model includes the same equilibria with the participation of hydrogen ions which are usually considered in schemes of acid–base equilibria for metal complexes in solutions. Therefore, the dependences of the concentrations of the molecular and ionic forms on the pH of the eluent in general correspond to classical representations.

In the pH range where hydrolysis of metal ions can be negligible (usually pH < 5), the decomposition products are $ML_m^{(n-m)+}$, M^{n+} and L^-. The

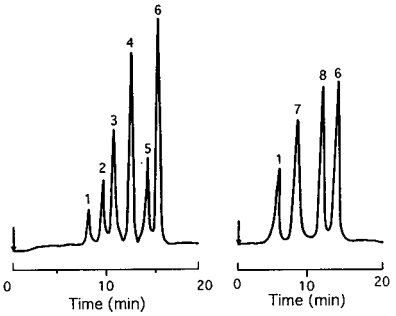

Fig. 9. Separation of metal diethyldithiocarbamates by RP-LC Column, KAX-2; mobile phase, acetonitrile–water (70+30, v/v) containing 2% chloroform; flow-rate, 50 μl min^{-1}; UV detection (280 nm). Peaks: 1 = Cd; 2 = Pb; 3 = Ni; 4 = Co; 5 = Cu; 6 = Hg; 7 = Fe; 8 = Pd.

concentrations of these species depend on the stability constant of the metal chelate and the reagent ionization constant. To shift the equilibrium to the side of the undissociated form, it is neccesary to increase the pH of the mobile phase, and the higher is K_i^{HL}, the more the pH increases. As a result of hydrolytic processes at high pH values, metal complexes of $M(OH)_m$-L_{n-m} type are formed. In this event, the equilibrium concentration of ML_n is determined by its stability constant and the formation constant of hydroxy complexes. One should increase the pH to suppress the formation of these complexes.

Thus, some optimum values of the mobile phase acidity should exist which correspond to the highest possible stability of the chelate. The model experiment shows the range of these optimum pH values (Fig. 10). According to the simulations, reducing the reagent ionization constant increases the shift of this range to acidic media, and the higher the stability constant of the chelate, the wider is the range of optimum pH values. For example, the most suitable pH values for metal dialkyldithiophosphates (the pK_a values of the reagents are ca. 2) are < 4. Concerning metal dialkyldithiocarbamates ($pK_a \approx 4$), the optimum range is extended to basic pH (9–10), i.e. it exceeds the pH values usually recommended in the literature [5].

A verification of the model results for the effect of the mobile phase acidity showed that they correspond well with those found experimentally. Hence sufficient stability of metal dibutyldithiophosphates is provided at pH < 3.

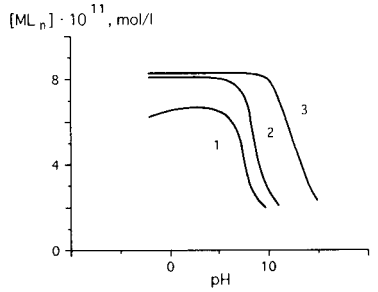

Fig. 10. Dependence of the equilibrium concentration of metal chelates of different stability on the pH of the mobile phase. 1, log $\beta_n = 8$, $pK_a = 2$; 2, log $\beta_n = 10$, $pK_a = 2$; 3, log $\beta_n = 10$, $pK_a = 4$.

Organic base. The equilibrium concentration of a metal chelate in the mobile phase depends on the concentration of the organic base, C_B, and the adduct formation constant, K_B. In accordance with the simulated model dependences which are shown in Fig. 11, an increase in C_B, on reaching some critical value, does not cause any changes in C_{ML_n} (C_{ML_n} is the overall concentration of metal chelate and its adduct with B). The critical concentration is within the limits of 10^{-3}–10^{-4} M for some conditional adduct with $K_B = 100$; for more stable adducts the optimum range of C_B values is shifted to the region of lower concentrations. For the example considered, K_B corresponds approximately to the real values. Therefore, good coincidence of simulated and experimental [21,22] values of C_B was obtained.

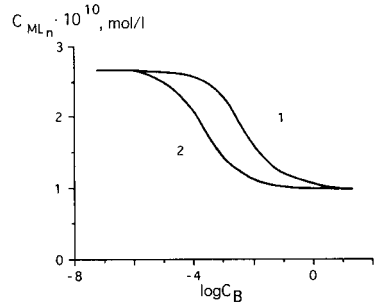

Fig. 11. Effect of the organic base concentration on concentration of metal chelate in mobile phase for an adduct formation constant of (1) 100 and (2) 1000.

TABLE 1

Simulation of the effect of the adduct formation constant and organic base concentration on the equilibrium concentration and distribution coefficient of a metal chelate

K_B	C_B (M)	$[ML_n]\times10^{10}$ (M)	Distribution coefficient
0	0	2.69	401
100	10^{-4}	2.62	415
1000	10^{-4}	2.46	1403

The model experiment clearly demonstates that adduct formation is accompanied by a decrease in the equilibrium concentration of metal chelate in the mobile phase (Table 1). The latter is equivalent to an increase in the retention. The experimentally observed differences in the k' values for metal di-*n*-butyldithiophosphates and diethyldithiocarbamates in the presence and absence of organic base in the mobile phase, as follows from Table 2, are in good accord with this model conclusion.

The permissible concentrations of donor-active compounds in the chromatographic system depend mostly on the stability of the chelates, as the neglect of the ligand-exchange reaction is inadmissible at high concentrations of C_B (decomposition of copper and nickel dibutyldithiophosphates was observed when the concentration of pyridine in the mobile phase was higher than 0.1 M).

Practical recommendations

The practical conclusions obtained during the analysis of the simulation model can be summarized as follows. Only thermodynamically stable metal chelates satisfy the requirements of quantitative analysis for metals by RP-LC. For instance, with water–acetonitrile eluents, the overall stability constants must be not less than 10^{10}. Moreover, when choosing the chelating reagent, one should take into account the kinetic stability of the chelates formed [18]. If the metal chelates are not sufficiently stable, they could be stabilized in several ways: by increasing the organic modifier concentration (taking into consideration the possibility of reducing the separation selectivity with a high concentration of the organic solvent); by using a buffer solution as an aqueous component of the eluent (the optimum range of the pH values can be determined with due regard to the stability constant of the chelate, the formation constant of hydroxy complexes and the reagent ionization constant); by incorporating the chelating reagent in the mobile phase (the necessary concentration is defined by the stability of metal chelates used); or by addition of an organic base (the most suitable concentrations are 10^{-3}–10^{-4} M). To increase the separation selectivity, it is desirable to apply strongly associated eluents with a high proton-donor ability, e.g., eluents modified with methanol or containing not less than 20–30% of an aqueous component.

Conclusions

The equilibrium simulation model not only confirms modern representations of the chemical reactions that accompany the chromatographic process for metal chelates, but also makes it

TABLE 2

Retention of metal chelates and their adducts with donor-active compounds on TLC plates

h3Metal chelate	Capacity factor	
	Dioxane–water (90 : 10) [b]	+1 mM piperidine [b]
Cadmium dibutyldithiophosphate	0.19	0.25
Zinc dibutyldithiophosphate	0.22	0.30
	Acetonitrile–water (90 : 10) [b]	+20 mM pyridine [b]
Zinc diethyldithiocarbamate [a]	0.96	2.79
	Acetonitrile–water (85 : 15) [b]	+20 mM pyridine [b]
Zinc diethyldithiocarbamate [a]	1.13	1.63

[a] Taken from [23]. [b] Mobile phase.

possible to evaluate quantitatively the influence of these reactions on the chromatographic properties of the chelates. The universal character of the model is based on the fact that it can describe the chromatographic behaviour of metal chelates of different types (the differences in the nature of the chelates are simply accounted for by the substitution of corresponding equilibrium constants). A further merit of the simulation is the possibility of analysing the dependences between the retention and individual parameters of the chromatographic system, taking into account the whole complex of their relationships, and of obtaining the neccessary information for the a priori assessment of the applicability of a given chelate in chromatographic metal analysis. The simulation can be considered as a perspective approach for investigating the chromatographic behaviour of metal chelates in LC and other complicated analytical systems.

REFERENCES

1 G.G. Wallace and J.M. Rivello (Eds.), Complexation Chromatography, Royal Society of Chemistry, Cambridge, 1990.
2 K. Robards, P. Starr and E. Patsalides, Analyst, 116 (1991) 1247.
3 I.S. Krull (Ed.), Trace Metal Analysis and Speciation (Journal of Chromatographic Library, Vol. 47), Elsevier, Amsterdam, 1991.
4 A.R. Timerbaev, O.M. Petrukhin, I.P. Alimarin and T.A. Bol'shova, Talanta, 38 (1991) 467.
5 A.R. Timerbaev and O.M. Petrukhin, Liquid Adsorption Chromatography of Metal Chelates, Nauka, Moscow, 1989 (in Russian).
6 R. Kaliszan, Quantitative Structure–Chromatographic Retention Relationships, Wiley, New York, 1987.
7 V.D. Shatz and O.V. Sakhartova, High Performance Liquid Chromatography. Theoretical Principles. Methodology. Application in Drug Chemistry, Zinatne, Riga, 1988 (in Russian).
8 A.R. Timerbaev, I.G. Tsoi and O.M. Petrukhin, J. Chromatogr., 498 (1990) 337.
9 A.R. Timerbaev, I.G. Tsoi and O.M. Petrukhin, J. Chromatogr., 555 (1991) 163.
10 A.R. Timerbaev, V.V. Salov, O.M. Petrukhin and Yu. A. Zolotov, Dokl. Akad. Nauk SSSR, 292 (1987) 926.
11 V.V. Salov, A.R. Timerbaev and O.M. Petrukhin, J. Planar Chromatogr., 3 (1990) 73.
12 A.R. Timerbaev, A.Yu. Malykhin, T.A. Bol'shova and O.M. Petrukhin, Zh. Anal. Khim., 45 (1990) 1113.
13 A.R. Timerbaev and O.M. Petrukhin, Anal. Chim. Acta, 159 (1984) 229.
14 I.G. Tsoi, PhD Thesis, Mendeleev Moscow Institute of Chemical Technology, Moscow, 1990.
15 W. Melander and Cs. Horváth, in Cs. Horváth (Ed.), High Performance Liquid Chromatography – Advances and Perspectives, Vol. 2, Academic Press, New York, London, 1980, pp. 113–319.
16 R.N. Nicolov, J. Chromatogr., 286 (1984) 147.
17 G.A. Korn and T.M. Korn, Mathematical Handbook for Scientists and Engineers, McGraw-Hill, New York, 1968.
18 A.R. Timerbaev and O.M. Petrukhin, Zh. Anal. Khim., 44 (1989) 1424.
19 R.G. Pearson, J. Am. Chem. Soc., 85 (1963) 3533.
20 B.P. Johnson, M.C. Khaledi and J.C. Dorsey, Anal. Chem., 58 (1986) 2354.
21 G.G. Wallace and G. Heneghan, Chromatographia, 22 (1986) 275.
22 G. Heneghan and G.G. Wallace, Anal. Proc., 23 (1986) 29.
23 W. Schunk and G. Schwedt, Fresenius' Z. Anal. Chem., 318 (1984) 47.

Analytica Chimica Acta, 269 (1992) 239–247
Elsevier Science Publishers B.V., Amsterdam

Liquid chromatographic study of the interaction between aflatoxins and β-cyclodextrin

M.L. Vazquez

Facultad de Farmacia, Departamento de Quimica Analitica, Nutricion y Bromatologia, 15706 Santiago de Compostela (Spain)

C.M. Franco and A. Cepeda

Facultad de Veterinaria, Departamento de Quimica Analitica, Nutricion y Bromatologia, Aguas Ferreas s.n., 27002 Lugo (Spain)

P. Prognon and G. Mahuzier

Faculté de Pharmacie, Laboratoire de Chimie Analytique II, Rue J.B. Clément, 92290 Châtenay-Malabry (France)

(Received 28th April 1992; revised manuscript received 15th June 1992)

Abstract

The interaction between the four main aflatoxins (G_2, G_1, B_2 and B_1) and β-cyclodextrin (β-cyd) was studied using reversed-phase liquid chromatography (RP-LC). These aflatoxins are structurally very similar compounds that exhibit in RP-LC, and with methanol–water as eluent, a characteristic elution profile, i.e., $k'_{G_2} < k'_{G_1} < k'_{B_2} < k'_{B_1}$. In the presence of β-cyd in the eluent, this elution order remains constant and the decrease in all the capacity factors (k') is used to calculate the respective complex formation constant (K_f) of each compound with β-cyd, which are 263, 327, 215 and 258 l mol^{-1} for aflatoxins G_2, G_1, B_2 and B_1, respectively. The enthalpy (ΔH_β) and entropy (ΔS_β) changes associated with the interaction of the C_{18} support with the complexed solutes were extracted from the temperature dependance of k'. All the established thermodynamic data strongly suggest the occurrence of a 1:1 stoichiometry inclusion process between the aflatoxins and the introduced β-cyd. On the other hand, the discrepancy between some of the thermodynamic parameters (ΔS) and some of the chromatographic parameters (k') suggests that the driving forces involved in the chromatographic partition process and in the inclusion in the β-cyd cavity may be due to different parts of the aflatoxin molecule. Finally, the results obtained with the proposed method indicate that RP-LC can be successfully used to calculate complex formation constants and to contribute to a better insight into the β-cyd–aflatoxin interaction.

Keywords: Liquid chromatography; Aflatoxins; Cyclodextrin; Inclusion compounds

Aflatoxins B_1, B_2, G_1 and G_2 are the four main *Aspergillus flavus* sp. toxins. Because of the well established carginogenic and mutagenic potentiality of these toxins, their determination at low levels (nM range), e.g., in various foodstuffs, is of major interest [1,2]. Among the numerous published methods for their determination (especially chromatographic and immunological), reversed-phase liquid chromatography (RP-LC) coupled with fluorimetric detection occupies an important position because of the natural fluorescence emission of the aflatoxin moiety [3,4].

The pentaheterocyclic structure of these coumarin derivatives (Fig. 1) involves different

Correspondence to: P. Prognon, Faculté de Pharmacie, Laboratoire de Chimie Analytique II, Rue J.B. Clément, 92290 Châtenay-Malabry (France).

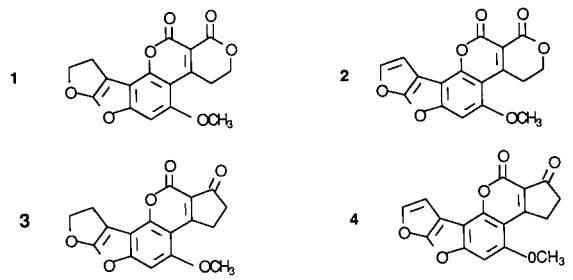

Fig. 1. Formulae of the four aflatoxins studied: **1** = aflatoxin G_2; **2** = aflatoxin G_1; **3** = aflatoxin B_2; **4** = aflatoxin B_1.

luminescence characteristics in solution [5], creating a clear distinction between furano-saturated derivatives (B_2 and G_2) and furano-unsaturated derivatives (B_1 and G_1). The saturated aflatoxins B_2 and G_2 exhibit, in a given solvent, a fluorescence quantum yield much higher (about ten-fold) than those of the unsaturated B_1 and G_1. Unfortunately, the latter are the more carcinogenic toxins. As a consequence, many attempts have been made to improve the detection limits of aflatoxins B_1 and G_1 in LC, among which postcolumn halogenation (especially iodination) is the most popular [6–10].

To overcome some specific drawbacks of such a procedure (e.g., instability of iodine in solution), attempts have been made to explore the possibility of using β-cyclodextrin (β-cyd) as a more convenient fluorescence enhancer with the aim of including the aflatoxins in the hydrophobic internal cavity of β-cyd. β-Cyd is able to include a wide variety of organic and inorganic species [11], which promises an enormous field of chemical applications of the use of β-cyd [12,13].

In the analytical field, there is interest in studying the interactions of coumarins and furocoumarins with β-cyd and their possible chromatographic use in fluorescence detection [14,15]. Among these kinds of compounds, aflatoxins have attracted attention because preliminary experiments had shown an interesting fluorescence increase on addition of β-cyd after an LC procedure [16]. Therefore, before making a detailed analytical evaluation of β-cyd on the limit of detection of aflatoxins in LC, and because its use should be based on an inclusion process taking place directly in the mobile phase, in this work attempts were made to study, from a mechanistic point of view, the aflatoxin–β-cyd interaction directly in a selected eluent.

Thus, under dynamic flow conditions, the complex formation constant (K_f) and the enthalpy and entropy changes of the solutes associated with their transfer between the mobile phase and stationary phase, in the absence and in presence of β-cyd, were established for each aflatoxin. In addition, some attempts were made to link the thermodynamic data with the structures of the aflatoxins and with the chromatographic parameters.

EXPERIMENTAL

Chemicals

β-Cyclodextrin (β-cyd) was purchased from Roquette (Lestrem, France) and recrystallized once from hot water before use. Aflatoxins G_2, G_1, B_2 and B_1 from *Aspergillus flavus* were obtained from Sigma (St. Louis, MO). All solvents used were of LC grade (Merck, Darmstadt) and water was triply distilled before use.

Apparatus

All LC measurements were made using a Shimadzu LC 9A metering pump equipped with a Rheodyne Model 7185 5-μl loop injector and the mobile phase flow-rate was 1 ml min^{-1}. The analytical column was a 5-μm reversed-phase C_{18} μBondapak (15 × 4.6 mm i.d.) from SFCC (France). A Shimadzu CTO 6A oven was used to keep the column temperature constant with an accuracy of ±0.1°C. For temperature effect studies (enthalpy and entropy calculations), nine temperatures from 26.5 to 47°C were investigated. A Kratos FS 970 fluorimetric detector was used with an excitation wavelength set at 360 nm and a 417 nm cut-off emission filter. The chromatograms were recorded on a Shimadzu LC 5A integrator.

Solutions

Stock solutions of aflatoxins were prepared by dissolving 1 mg of each compound in 5 ml of chloroform–methanol (1:3, v/v). Each solution,

protected from light, was kept at 4°C for no more than 3 days.

Successive dilutions were made with methanol and then with the mobile phase in order to give working concentrations of 1×10^{-7} M for aflatoxins B_2 and G_2 and 1×10^{-6} M for aflatoxins B_1 and G_1.

Stock aqueous solutions (1×10^{-2} M) of β-cyd were kept at room temperature for 2 days.

Chromatography

Throughout this study a basic methanol–water (40 + 60) eluent was used after careful degassing [helium, Ultrapur (Air Liquide, France)] and filtering (Waters–Millipore 0.45-μm filter).

With each change in the composition of the mobile phase or in temperature, the void volume (as t_{R_0}) was verified by injection of a methanol solution of sodium nitrite (UV detection at 220 nm with a Shimadzu SPD 6A UV detector), and the mean of three measurements of t_{R_0} was used in subsequent calculations of the capacity factors.

When β-cyd was added to the eluent the appropriate amount of β-cyd was dissolved in water and then methanol was added to give the final desired concentration (from 10^{-3} to 10^{-2} M).

The poor water solubility of aflatoxins (10^{-5} M at 26°C, depending of the compound) and the low concentrations to be used in the study led to the adoption of fluorimetric detection according to the conditions described above.

For the determination of the complex formation constant (K_f), different eluents characterized by an increasing concentration of β-cyd (in the range 10^{-3}–10^{-2} M) were used. In order to study the influence of methanol on the complex formation, five eluents were tested with methanol contents ranging from 40 to 65% (v/v). Higher concentrations were not tested in order to avoid the risk of precipitation of the fixed β-cyd concentration (3.6×10^{-3} M) in the eluent.

All capacity factor (k') measurements were made systematically in triplicate. All the experimental data reported here refer to the average of these three measurements, with an estimated error never higher than 0.5%.

Enthalpy and entropy changes in the absence and presence of β-cyd (ΔH, ΔS and ΔH_β, ΔS_β, respectively) were calculated according to Van't Hoff equations and using a R value of 1.99 cal K^{-1} mol^{-1} (8.314 J K^{-1} mol^{-1}).

RESULTS AND DISCUSSION

In this work, methanol was used as the organic modifier because of its wide use in LC determinations of aflatoxins and because it interacts less than acetonitrile with β-cyd [17]. Nevertheless, in the presence of β-cyd in the eluent, methanol acts as a non-negligible competitor of the aflatoxins towards the inclusion process. According to [17], the association constant of methanol with β-cyd ($K_M = 0.32$ l mol^{-1}) must be taken into account, not because of its low value, but because of its high molar concentration in the eluent.

Experimentally, the methanol content of the eluent was chosen to be as low as possible (i.e., 40%), compatible with an acceptable analysis time (< 25 min) and a correct selectivity, $\alpha_{SG_2/G_1} = 1.30$, $\alpha_{SG_1/B_2} = 1.25$, $\alpha_{SB_2/B_1} = 1.31$, as shown in Fig. 2.

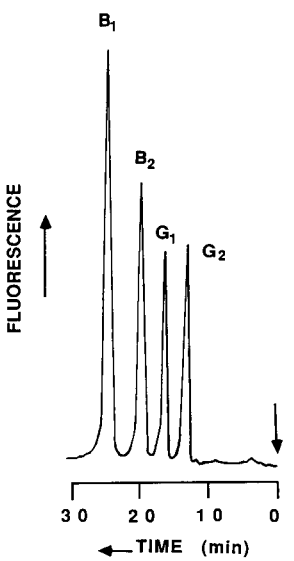

Fig. 2. Typical chromatogram of the mixture of the four aflatoxins. Mobile phase, methanol–water (40 + 60, v/v); β-cyd added, 3.6×10^{-3} M. For detailed chromatographic conditions, see text.

If the interaction between β-cyd and the apolar stationary phase is neglected, owing to the polarity of the outer hydroxyl groups of β-cyd [18], the total concentration of the β-cyd added to the system ($[CD_T]$) can be expressed by

$$[CD_T] = [CD_m] + [CD \cdot M]_m \quad (1)$$

where $[CD_m]$ is the available cyclodextrin concentration in the mobile phase (available for the inclusion process) and $[CD \cdot M]_m$ is the methanol-complexed cyclodextrin in the mobile phase. From the equilibrium constant K_m of the equilibrium

$$[CD_m] + [M] \rightleftharpoons [CD \cdot M]_m$$

and from Eqn. 1, $[CD_m]$ can be calculated [19]:

$$[CD_m] = [CD_T]\left(\frac{1}{K_m[M] + 1}\right)$$

As a consequence, in RP-LC when a concentration $[CD_T]$ of β-cyd is introduced into the eluent, only $[CD_m]$ of β-cyd can interact with the injected solute (S) and must be taken into account. Moreover, because of the very low concentration of the solute with respect to $[CD]_m$ and [M], we can consider that the fraction of β-cyd complexed with S (i.e., $[CD \cdot S]$) is negligible [18]. Therefore, using an eluent spiked with β-cyd, and after injection of a solute (S), the complexation involves a decrease in the measured capacity factor owing to the modification of the mass transfer process in comparison with the same eluent without cyclodextrin [20]. Therefore, it can be shown that the formation constant of the complex (K_f) can be obtained from the following equation [21,22]:

$$1/k' = 1/k'_0(1 + K_f[CD_m]) \quad (2)$$

where k' is the capacity factor of the solute in the presence of a concentration $[CD_m]$ of β-cyd, k'_0 is the capacity factor in the same eluent in the absence of β-cyd and $K_f = [CD \cdot S]_m / \{[CD]_m \times [S]_m\}$, $[CD \cdot S]_m$ being the concentration of solute complexed in the eluent and $[S]_m$ the concentration of the free solute. Thus, Eqn. 2 assumes a 1:1 stoichiometry in complex formation between the solute and β-cyd [23].

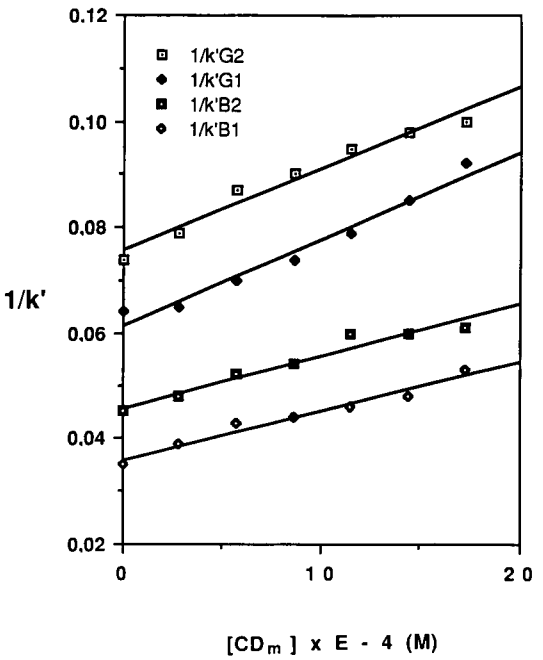

Fig. 3. Plots of $1/k'$ versus equilibrium available concentration of β-cyd $[CD_m]$ with methanol–water (40+60) eluent. For detailed chromatographic conditions, see text. G_2: $1/k' = 0.076 + 0.002\ [CD_m]$ ($r = 0.982$). G_1: $1/k' = 0.061 + 0.002\ [CD_m]$ ($r = 0.984$). B_2: $1/k' = 0.046 + 0.000991\ [CD_m]$ ($r = 0.971$). B_1: $1/k' = 0.036 + 0.000930\ [CD_m]$ ($r = 0.986$).

Variation of capacity factors in the presence of various concentrations of β-cyclodextrin

Figure 3 shows the evolution of $1/k'$ versus $[CD_m]$ for the four aflatoxins at 26.5°C with a concentration of added β-cyd ranging from 1.2×10^{-3} to 7.2×10^{-3} M (i.e. from 2.88×10^{-4} to 17.3×10^{-4} M available β-cyd). Experimentally, the elution order $G_2 < G_1 < B_2 < B_1$ remains unchanged on increasing the concentration of β-cyd and the linear plot of $1/k'$ fits well with Eqn. 2, with good values of r (> 0.97 in all instances).

This satisfactory linear relationship between β-cyd and $1/k'$ confirms a 1:1 complexation ratio between the studied compounds and β-cyd. Indeed, if two or more cyclodextrins bind to one molecule of aflatoxin, a curvature in the plot according to Eqn. 2 should be observed rather than a straight line. Hence the assumption of a 1:1 stoichiometry seems reasonable.

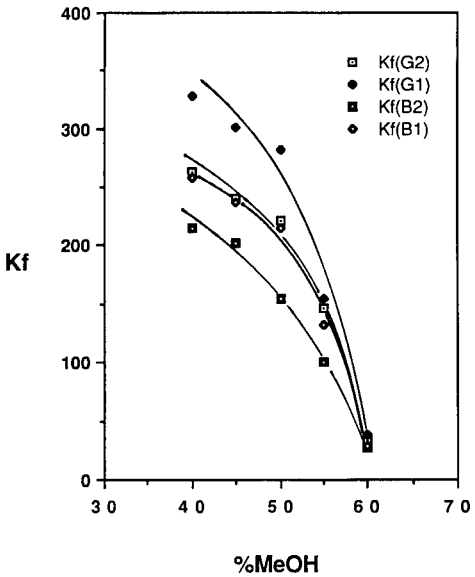

Fig. 4. Plots of K_f (l mol^{-1}) versus methanol content (%, v/v) of the eluent established at 26.5°C for the four aflatoxins. β-Cyd introduced = 3.6×10^{-3} M.

From a structural point of view, the elution order appears to be due to small structural differences in the aflatoxin molecules. Hence the presence of the pyrone ring attached to the coumarin nucleus of aflatoxins G_2 and G_1 rather than to a cyclopentanone nucleus for aflatoxins B_2 and B_1 appears to rule the elution order. At the opposite side of the aflatoxin molecule, the saturation of the furan ring seems to have a less important effect with regard to the interaction with the stationary phase.

Effect of methanol content

Figure 4 shows the complex formation constants (K_f) at 26.5°C for aflatoxins G_2, G_1, B_2 and B_1 for a methanol content ranging from 40 to 65% (v/v). An increase in methanol content dramatically decreases K_f, clearly emphasizing the importance of the role played by methanol as a competitor regarding inclusion in the internal cavity of β-cyd. Moreover, as seen in Fig. 4, the plot of K_f versus methanol content is non-linear owing to methanol competition, which perhaps suggests a progressive change in the strict 1:1 stoichiometry.

It should be pointed out that K_f becomes nearly identical (30 l mol^{-1}) for all the compounds at methanol contents higher than 55%; this indirectly shows that the methanol content must be as low as possible to allow the correct determination of K_f.

Results of this kind are now well documented for different organic species, e.g., phenols [24], and polycyclic aromatic hydrocarbons [25]. Under the described standard conditions [CH_3OH–H_2O (40 + 60) + β-cyd = 3.6×10^{-3} M, column temperature 26.5°C], the K_f values for complex formation are fairly close to each other (263, 328, 215 and 258 l mol^{-1} for G_2, G_1, B_2 and B_1 respectively). Moreover, it should be noted that the K_f values are not correlated with the elution order, but seem to be linked to the saturation of the furan moiety, saturated aflatoxin B_2 exhibiting a lower K_f than the unsaturated corresponding B_1, and in the same way for G_2 with respect to G_1.

Effect of temperature

In the absence of cyclodextrin. Table 1 shows the decrease in the capacity factors of the four aflatoxins with increase in temperature. In RP-LC, when the temperature increases the partition coefficient (K) decreases according to [26]

$$\ln K = -\Delta G/RT \quad (3)$$

TABLE 1

Variation of k' [measured in triplicate, as $(t_R - t_{R_0})/t_{R_0}$] of the four aflatoxins as a function of temperature and in the absence of β-cyd [a]

T(°C)	k'			
	G_2	G_1	B_2	B_1
26.5	9.693	12.607	15.804	20.757
30	9.133	11.804	14.767	19.288
32	8.864	11.420	14.284	18.604
35	8.343	10.648	13.590	17.199
37	7.709	9.707	12.169	15.512
40	7.261	9.066	11.344	14.269
42	7.083	8.801	11.002	13.797
45	6.712	8.285	10.326	12.905
47	6.477	7.952	9.888	12.307

[a] For chromatographic conditions, see the text.

so

$$\ln K = -\Delta H/RT + \Delta S/R \quad (4)$$

where ΔG is the Gibbs free energy for solute–stationary phase interaction, R is the gas constant, T is temperature (K) and ΔH and ΔS are the enthalpy and entropy changes, respectively, associated with the transfer of a solute from the mobile to the stationary phase [26].

As the capacity factor (k') of the solute is related to K by $k' = \phi K$, where ϕ is the phase ratio of the stationary to the mobile phase ($\phi = V_s/V_m$), the Van't Hoff equation describes the relationship between the capacity factor and the temperature of the chromatographic system:

$$\ln k' = -\Delta H/RT + \Delta S/R + \ln \phi \quad (5)$$

According to [27,28], and with the assumption that V_m can be obtained from a non-retained solute, e.g., sodium nitrite (see Experimental), $\ln \phi$ can be calculated to be equal to -0.853. Figure 5 shows the plot of Eqn. 5. From this plot, the enthalpy changes associated with the chromatographic partition process can be obtained from the slope ($-\Delta H/R$) and the entropy change from the intercept ($\ln \phi + \Delta S/R$).

Concerning the enthalpy change, it can be said that the more negative the value of ΔH, the longer is the retention time, so the more efficient is the transfer of the solute to the stationary phase. As shown here, the data agree satisfactorily with the model for all the aflatoxins, and show a larger affinity of the aflatoxin B compounds to the C_{18} stationary phase in comparison with the more polar aflatoxin G compounds. Thus, as stated above, from a chromatographic point of view, the polarity of the aflatoxin G compounds

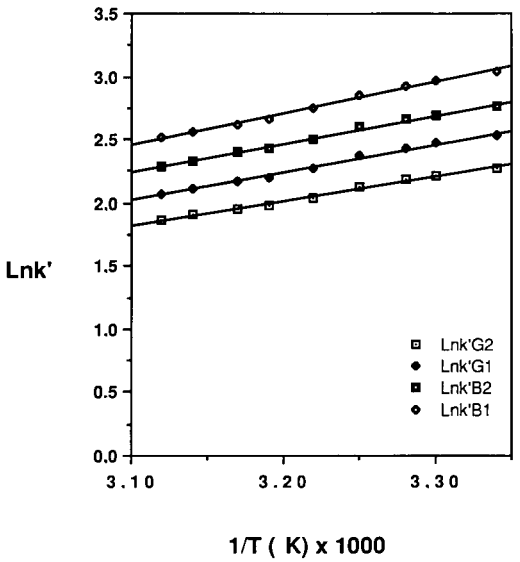

Fig. 5. Plots of $\ln k'$ versus $1/T$ in the absence of β-cyd in the eluent for the four aflatoxins. G_2: $\ln k' = -4.080 + 1.095\ (1/T)$ ($r = 0.9997$). G_1: $\ln k' = -4.758 + 2.188\ (1/T)$ ($r = 0.998$). B_2: $\ln k' = -4.653 + 2.250\ (1/T)$ ($r = 0.997$). B_2: $\ln k' = -5.245 + 2.484\ (1/T)$ ($r = 0.999$).

TABLE 2

ΔH, ΔH_β, ΔS and ΔS_β of the four aflatoxins in methanol–water (40 + 60) and methanol–water (40 + 60) + 3.6×10^{-3} M added β-cyclodextrin on an RP C_{18} column

Aflatoxin	Without β-cyd		With β-cyd	
	ΔH (kcal mol^{-1}) (kJ mol^{-1}) [a]	ΔS (cal mol^{-1} K^{-1}) (J mol^{-1} K^{-1}) [a]	ΔH_β (kcal mol^{-1}) (kJ mol^{-1}) [a]	ΔS_β (cal mol^{-1} K^{-1}) (J mol^{-1} K^{-1}) [a]
G_2	−3.79 (−15.86)	−7.27 (−30.42)	−0.124 (−0.519)	+11.496 (+48.1)
G_1	−4.35 (−18.20)	−8.61 (−36.02)	−0.173 (−0.724)	+10.49 (+43.90)
B_2	−4.47 (−18.70)	−8.41 (−35.19)	−0.237 (−0.992)	+11.45 (+47.91)
B_1	−4.94 (−20.67)	−9.585 (−40.10)	−0.22 (−0.920)	+10.41 (+43.55)

[a] Values in parentheses.

favours more rapid elution than the aflatoxin B compounds.

Conversely, the k' and the entropy changes (ΔS) are apparently not correlated, as shown in Table 2. According to the literature [23], ΔS can be associated with the change in ordering of the solute during its transfer between the mobile phase and the stationary phase. From Table 2, it seems that the structures of the studied compounds play a crucial role in the organization of the molecules in both phases, as suggested by the lower ΔS values of unsaturated aflatoxins (B_1 and G_1) relative to those of aflatoxins B_2 and G_2.

In the presence of cyclodextrin. In order to evaluate the effect of β-cyd on k' with varying temperature at a fixed percentage of methanol, a concentration of 3.6×10^{-3} M β-cyd was chosen (i.e. 8.6×10^{-4} M available β-cyd, $[CD_m]$). This concentration corresponds to the middle of the range of the above studied variation of k' versus $[CD_m]$.

In the presence of β-cyd, the aflatoxin–β-cyd complex formation constant, K_f, must be taken into account. Taking logarithms of Eqn. 2 gives

$$\ln k'_\beta = \ln k' - \ln K_f - \ln[1/(K_f + [CD_m])] \quad (6)$$

where k'_β is the capacity factor of the solute in the presence of β-cyd. Combining Eqns. 6 and 5, the variation of the capacity factor in the presence of β-cyd can be evaluated by

$$\ln k'_\beta = (\Delta H_\beta - \Delta H)/RT + (\Delta S - \Delta S_\beta)/R + \ln \phi - \ln\{1/(K_f + [CD_m])\} \quad (7)$$

where ΔH_β and ΔS_β are the standard enthalpy and entropy changes of the solute associated with its transfer from the mobile to the stationary phase on addition of β-cyd to the eluent.

Table 3 shows the decrease in the capacity factors with temperature in the presence of β-cyd.

Figure 6 shows the plot of $\ln k'_\beta$ versus $1/T$ according to Eqn. 7, with the corresponding equations. The data clearly show that the linear relationship between $\ln k'$ and $1/T$ remains valid on addition of β-cyd.

On the other hand, Table 2 summarizes the influence of the added β-cyd on ΔH and ΔS. As

TABLE 3

Variation of k' of the four aflatoxins as a function of temperature and in presence of 3.6×10^{-3} M β-cyd [a]

T(°C)	k'			
	G_2	G_1	B_2	B_1
26.5	9.411	12.240	15.344	20.152
30	8.867	11.460	14.337	18.727
32	8.606	11.087	13.868	18.063
35	8.100	10.338	12.941	16.698
37	7.595	9.586	11.967	15.290
40	7.290	9.088	11.326	14.428
42	7.039	8.759	10.932	13.817
45	6.573	8.130	10.101	12.661
47	6.269	7.778	9.710	12.104

[a] For chromatographic conditions, see text.

can be seen, the introduction of β-cyd into the eluent for all compounds led to a significant increase in their enthalpies which become nearly positive. This can be interpreted as a decrease in the interaction between the solute and the stationary phase, probably because of the competition of the dissolved cyclodextrin molecules in the mobile phase. Nevertheless, it should be pointed

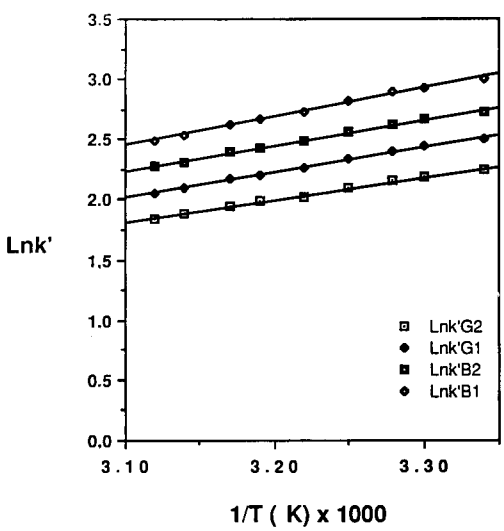

Fig. 6. Plots of $\ln k'$ versus $1/T$ in the presence of 3.6×10^{-3} M β-cyd in the eluent for the four aflatoxins. G_2: $\ln k' = -3.899 + 1.842\ (1/T)$ ($r = 0.999$). G_1: $\ln k' = -4.490 + 2.099\ (1/T)$ ($r = 0.990$). B_2: $(\ln k' = -4.359 + 2.127\ (1/T)$ ($r = 0.997$). B_2: $(\ln k' = -4.894 + 2.370\ (1/T)$ ($r = 0.999$).

out that ΔH_β is not so well correlated with k' as ΔH was, especially for the most retained compounds (aflatoxins B_2 and B_1); this may be due to the same perturbing effect of β-cyd on the transfer process.

On the other hand, the introduction of β-cyd has a pronounced influence on the entropy changes (ΔS_β), which in all instances become highly positive. It should be noted that the calculated values of ΔS_β are in good agreement with some reported data on the interaction with hydroxyaromatic compounds and β-cyd [23]. This strongly emphasizes the increasing perturbation generated by β-cyd, involving, as a consequence, greater disorder in the transfer process. Moreover, as noted in the absence of β-cyd, the entropy changes (ΔS_β) do not follow the elution order, but seem to be strictly associated with the structures of the aflatoxins. As seen in Table 2, unsaturated derivatives (aflatoxins B_1 and G_1) exhibit a significantly lower ΔS_β than the aflatoxins B_2 and G_2. This appears to be extremely important with regard to the mechanism of the retention of aflatoxins in RP-LC and also to the inclusion process with β-cyd. To some extent, the correlation between ΔS (in the presence and absence of β-cyd) with the structures of the aflatoxins suggests that the part of the aflatoxin skeleton mainly involved in the chromatographic process cannot be similar. More precisely, the 1,11- or 1,12-dione (β-diketone) part of the aflatoxin molecule seems to be mainly involved in the partition phenomena, as shown by the more rapid elution of the relatively polar pyrone (1,12-dione) aflatoxin G derivatives.

On the other hand, the driving forces of the process of inclusion in β-cyd could essentially involve the furan side of the aflatoxin nucleus, as suggested by the ΔS and ΔS_β values which are significantly different between furano-saturated and furano-unsaturated derivatives. In a certain way, the interpretation of the thermodynamic data can partially answer the questions arising in some previous spectroscopic studies on aflatoxins and β-cyd complexation. Indeed, it has recently been shown that on addition of β-cyd a specific and large fluorescence emission enhancement occurs only with aflatoxins B_1 and G_1, the furano-saturated aflatoxins B_2 and G_2 being unaffected [29]. This appears to favour of a specific inclusion of the unsaturated derivatives and, indirectly, emphasizes the importance of the furanic part of aflatoxin nucleus with regard to the inclusion process.

This last point seems to be closely linked with the measurements of entropy changes in the present study. Strictly, ΔS_β should be associated, in the presence of β-cyd in the eluent, with the transfer process of the solute between the two phases. Nevertheless, if we assume that β-cyd is negligibly adsorbed on the C_{18} support (see earlier), the transfer process is mainly altered by the β-cyd present in the eluent. Therefore, ΔS_β can also conveniently represent the degree of disorder in the whole mobile phase.

On the other hand, low values of ΔS_β seem to be associated with high K_f and vice versa, but only in the same group of aflatoxins (i.e., G derivatives), as reported in Table 2. From the structural point of view, the furan double bond in aflatoxins B_1 and G_1 seems to favour a good fit into the cavity, as shown by the high values of K_f. As a consequence, this furan unsaturation involves a better ordering of the aflatoxin B_1 and G_1 microenvironment in comparison with that for aflatoxins B_2 and G_2. Hence ΔS_β can finally be considered, after careful interpretation, as a satisfactory measure of the fitting of a guest molecule into the cyclodextrin cavity.

Inclusion thus appears to be common to all the compounds studied, certainly by moving the aflatoxin molecule furan-side first into the internal cavity of β-cyd. In this case, the mentioned difference in the fluorescence properties might be attributed to the different nature of the interaction between host and saturated or unsaturated guest compounds and not, as suggested previously [29], to a selective inclusion of unsaturated aflatoxins. In any case, the furan double bond in unsaturated derivatives seems to be directly involved in the driving forces of the interaction with the internal cavity of β-cyd. Nevertheless, a detailed study of this interaction would be beyond the scope of the present chromatographic approach. Hence, this example again emphasizes the need for associated techniques in studying the

association phenomena between host and guest compounds in solution.

These experiments have demonstrated the use of LC for the determination of complex formation constants between cyclodextrin derivatives and various organic species, especially highly toxic compounds such as aflatoxins. More detailed analytical studies are in progress in order to evaluate the use of cyclodextrin derivatives as versatile fluorogenic postcolumn reagents in LC for the determination of aflatoxins.

REFERENCES

1 W.F. Busby, Jr., and G.N. Wogan, Chemical Carcinogens, American Chemical Society, Washington, DC, 2nd edn., 1984, p. 945.
2 H.P. van Egmond, Food Addit. Contam., 6 (1989) 139.
3 B.L. van Duuren, T.-L. Chan and F.M. Irani, Anal. Chem., 40 (1968) 2024.
4 M.W. Dirr, Int. J. Biochem., 19 (1987) 1137.
5 M.J. Sherperd and J. Gilbert, Food Addit. Contam., 1 (1984) 325.
6 L.G.M.T. Tuinstra and W. Haasnoot, J. Chromatogr., 282 (1983) 457.
7 P.G. Thiel, S. Stockenstrom and P.S. Gathercole, J. Liq. Chromatogr., 9 (1986) 103.
8 R.W. Beaver, Arch. Environ. Contam. Toxicol., 18 (1989) 315.
9 M. Holcomb and H.C. Thompson, Jr., J. Agric. Food Chem., 39 (1991) 137.
10 H. Jansen, R. Jansen, U.A.Th. Brinkman and R.W. Frei, Chromatographia, 24 (1987) 555.
11 J. Slejtli, Cyclodextrin Technology, Kluwer, Dordrecht, 1988.
12 J. Slejtli, Cyclodextrins and Their Inclusion Complexes, Akadémiai Kiadó Budapest, 1982.
13 D. Duchene, Cyclodextrins and Their Industrial Uses, Santé, Paris, 1987.
14 J. Blais, P. Prognon, G. Mahuzier and P. Vigny, J. Photochem. Photobiol. B, 2 (1988) 455.
15 A. Cepeda, P. Prognon, G. Mahuzier and J. Blais, Anal. Chim. Acta, 211 (1988) 333.
16 O.J. Francis, Jr., G.P. Kirschenheuter, G.M. Ware, A.S. Carman and S.S. Kuan, J. Assoc. Off. Anal. Chem., 71 (1988) 725.
17 Y. Matsui and K. Mochida, Bull. Chem. Soc. Jpn., 52 (1979) 2808.
18 K. Fujimura, T. Ueda, M. Kitagana, H. Takayagani and M. Ando, Anal. Chem., 58 (1986) 2668.
19 J. Zukowski, D. Sybilska and J. Jurczak, Anal. Chem., 57 (1985) 2215.
20 H. Seno, M. Lin and K. Iwamoto, J. Chromatogr., 523 (1990) 293.
21 D.W. Armstrong, F. Nome, A. Spinol and T.D. Golden, J. Am. Chem. Soc., 108 (1986) 1418.
22 R.M. Mohseni and R.J. Hurtubise, J. Chromatogr., 499 (1990) 395.
23 R.M. Mohseni and R.J. Hurtubise, J. Chromatogr., 537 (1991) 61.
24 R.M. Mohseni and R.J. Hurtubise, J. Chromatogr., 514 (1990) 19.
25 L.A. Blyshak, K.Y. Dodson, I.M. Patonay Warner and W.E. May, Anal. Chem., 61 (1989) 955.
26 W.R. Melander, D.E. Campbell and Cs. Horváth, J. Chromatogr., 158 (1978) 215.
27 K.B. Sentell and J.G. Dorsey, J. Liq. Chromatogr., 11 (1988) 1875.
28 W. Cheng, Anal. Chem., 57 (1985) 2409.
29 M.L. Vazquez, A. Cepeda, P. Prognon, G. Mahuzier and J. Blais, Anal. Chim. Acta, 255 (1991) 343.

Analytica Chimica Acta, 269 (1992) 249–255
Elsevier Science Publishers B.V., Amsterdam

Evaluation of a strontium-specific extraction chromatographic method for isotopic analysis in geological materials

Christian Pin and Chantal Bassin

Département de Géologie, URA 10 CNRS, Université Blaise Pascal, 5 rue Kessler, 63038 Clermont-Ferrand Cedex (France)

(Received 25th March 1992; revised manuscript received 9th June 1992)

Abstract

The suitability of a recently published extraction chromatographic method to isolate strontium from geological samples for isotopic analyses by thermal ionization mass spectrometry was evaluated. This method has several significant advantages over conventional ion-exchange techniques: high selectivity combined with high recoveries, overall simplicity and the use of very small reagent volumes of a single acid (HNO_3). Satisfactory blank levels were obtained on new columns, but memory effects could not be totally eliminated from already used extraction chromatographic material. Determinations of $^{87}Sr/^{86}Sr$ ratios and Sr concentration by isotope dilution following the proposed method are reported for thirteen international rock standards.

Keywords: Isotope dilution methods; Liquid chromatography; Mass spectrometry; Extraction; Geological materials; Isotope ratios; Strontium

By virtue of the radioactive decay of ^{87}Rb into ^{87}Sr (half-life = 48.8×10^9 years), the isotope composition of strontium is variable in nature, and its determination is of great interest for the earth and planetary sciences. First, the ^{87}Rb–^{87}Sr system can be used as a chronometer. By measuring the Rb/Sr and $^{87}Sr/^{86}Sr$ ratios in a suite of cogenetic samples (e.g., minerals, rocks, meteorites), the age of the last isotopic equilibration in a geological or extra-terrestrial system can be determined [1]. Second, when corrected for in situ radioactive decay, the $^{87}Sr/^{86}Sr$ ratio can be used as a natural tracer, reflecting the time-integrated Rb/Sr ratio of the reservoir from which the analysed sample was extracted [2]. This is useful in provenance studies and in modelling any mixing process between contrasted end-members. For example, materials from the upper continental crust typically have high $^{87}Sr/^{86}Sr$ values, indicative of ancient enrichment in Rb relative to Sr in the outer shell of the solid earth. In contrast, rocks from the oceanic crust and most of the terrestrial upper mantle are characterized by low $^{87}Sr/^{86}Sr$ ratios (less than 0.704), reflecting a long residence time in reservoirs with low Rb/Sr ratios. Third, the measurement of Sr isotope ratios is necessary for the determination of strontium contents by isotope dilution, a definitive method for quantitative elemental analysis [3].

In every instance, thermal ionization mass spectrometry (TIMS) is used for isotope ratio determinations, and a very clean separation of strontium from major and other trace elements is a prerequisite. The most commonly used separation technique involves cation-exchange chromatography [4–7] in HCl medium. For example,

Correspondence to: C. Pin, Département de Géologie, URA 10 CNRS, Université Blaise Pascal, 5 rue Kessler, 63038 Clermont-Ferrand Cedex (France).

in 2 M HCl, Sr is more retained than the major elements on the strongly acidic cation-exchange resin AG 50W-X8 [8]. However, the separation factors between Sr^{2+} (distribution coefficient $D = 17.8$) and other elements present in much larger higher concentrations such as Ca^{2+} ($D = 12.2$) and Al^{3+} ($D = 12.5$) are limited, and long columns or further clean-up are required for adequate purification of strontium. More complicated methods to improve the separation of Sr from Ca have been published [9], but they involve the use of several organic solvents or complexing agents. Recently, Horwitz et al. [10] described a new method, based on extraction chromatography of Sr from nitric acid media. Using a solution of a crown ether in octanol sorbed on an inert substrate, they obtained an efficient separation of strontium from the other elements in nuclear waste solutions and bioassay samples. This method is attractive in its selectivity and simplicity, and shows great promise for other applications. In this work, its suitability for the isolation of strontium for isotopic analyses in geological samples was evaluated.

EXPERIMENTAL

Reagents and instrumentation

Nitric and hydrochloric acids distilled in sub-boiling silica glass stills (Quartex, Paris), water purified through a Milli-Q system (Millipore) and Suprapur oxalic acid (Merck) were used throughout.

The crown ether-loaded resin described by Horwitz et al. [10] consists of bis-*tert*-butyl-*cis*-dicyclohexano-18-crown-6 (DtBuCH18C6) in octan-1-ol sorbed on Amberchrom CG-71ms, and was obtained in a ready-to-use form from EIChroM Industries (Darien, IL) as Sr.Spec sps (particle size 50–100 μm) extraction chromatographic material. Small polypropylene columns (5 cm × 5 mm i.d.) with a 30-μm polyethylene frit in the bottom (Touzart et Matignon, Paris) were used for separation work.

The behaviour of Sr and other elements of interest during column loading and further elution was investigated by inductively coupled plasma atomic emission spectrometry (ICP-AES) using a Jobin-Yvon JY 70 II spectrometer. Isotopic analyses were performed on a Vacuum Generators 54 E thermal ionization mass spectrometer. Amounts of 1–3 μg of Sr were loaded with a drop of 1 M H_3PO_4 on to flat tantalum filaments and analysed in the double collection mode, with total ionic currents of 20–40 pA.

Column experiments and initial set-up

Distribution coefficient data for Sr [10,11] indicate that Sr breakthrough from Sr.Spec sps does not occur before ca. 30 free column volumes of 3 M HNO_3, and that 0.05 M HNO_3 would provide a suitable eluent for Sr. In a preliminary test, 50 μg of pure Sr were loaded on to a 1-ml column (free column volume ca. 0.65 ml). No Sr could be detected by ICP-AES in the next 20 ml of 3 M HNO_3, and 98% of the 50 μg loaded were found in the first 2 ml of 0.05 M HNO_3.

As a first step in studying the behaviour of Sr and other rock-forming elements on Sr.Spec sps columns, a sample having an intermediate bulk composition and a comparatively elevated Sr concentration is useful. For that purpose, an in-house standard was selected, namely Volvic trachyandesite lava (57 wt.% SiO_2, 18 wt.% Al_2O_3, 6.7 wt.% Fe_2O_3, 5.6 wt.% Na_2O, 4.5 wt.% CaO, 3.4 wt.% K_2O, 2 wt.% MgO, 1.1 wt.% TiO_2, 0.2 wt.% MnO, 757 $\mu g\ g^{-1}$ Sr, 1000 $\mu g\ g^{-1}$ Ba). A solution obtained by dissolving 100 mg of this rock was loaded on to the 1-ml column in 3 ml of 3 M nitric acid–0.05 M oxalic acid ($H_2C_2O_4$). After rinsing the column reservoir twice with 1 ml of the loading medium, three portions of 5 ml of 3 M HNO_3 were passed through the column and analysed by ICP-AES. Sr was below the detection limit in these fractions and Ca was absent in the second and third 5-ml portions. Barium eluted mainly in the second portion but was still present at a high level (ca. 20 μg, i.e. about 20% of the amount initially loaded on the column) in third portion. This indicated that, despite a more favourable concentration ratio, the separation of Sr from Ba would be more difficult than that of the Ca–Sr pair.

All further experiments with the same rock were conducted on smaller, 0.5-ml columns, with

sample loading in 3 ml and rinsing twice with 1 ml of 3 M HNO_3–0.05 M $H_2C_2O_4$ or just 1 ml of 3 M HNO_3, followed by elution with 3 M HNO_3. ICP-AES analyses of the column effluents (Fig. 1) showed that Al, Fe, Mg, Ca, Ti, Mn and Na decrease to background levels as soon as the second 1-ml rinse. Clearly, these elements are not extracted to any significant extent from 3 M HNO_3 solutions. Among the major elements, only potassium is slightly retained on the column, but it is removed rapidly during column rinsing. Most of the barium, in contrast, is retained by the column during the loading and initial rinses, and elutes as a broad peak in the subsequent 3 M HNO_3 fractions.

The tail of the barium peak and the initial breakthrough of Sr were then studied. A 5-ml volume of pure 3 M HNO_3 was passed after column loading and rinsing, followed by five 1-ml portions of the same acid. Finally, Sr was eluted with 4 ml of 0.05 M HNO_3. The Ba and Sr concentrations found in each fraction by ICP-AES are given in Table 1. These results showed that good separations of Sr could be obtained on very small columns using limited reagent volumes, with high chemical yields. For further analyses, the elution of any residual major elements (mostly K) and barium was made with two successive fractions of 5 ml and 3.5 ml of 3 M HNO_3.

TABLE 1

Behaviour of Ba and Sr on a 0.5-ml column of Sr.Spec sps extraction chromatographic material (analyses by ICP-AES)

Fraction	Ba (μg)	Sr (μg)
0 (5 ml of 3 M HNO_3)	80	0.35
1 (1 ml of 3 M HNO_3)	9	0.10
2 (1 ml of 3 M HNO_3)	4.4	0.15
3 (1 ml of 3 M HNO_3)	2.1	0.25
4 (1 ml of 3 M HNO_3)	0.9	0.50
5 (1 ml of 3 M HNO_3)	0.4	0.90
6 (4 ml of 0.05 M HNO_3)	0.6	72 (95% of Sr loaded)

Sample decomposition

About 100-mg aliquots of powdered rock were dissolved on a hot-plate in closed 15-ml PFA vessels (Savillex, Minnetonka, USA) with 1 ml of

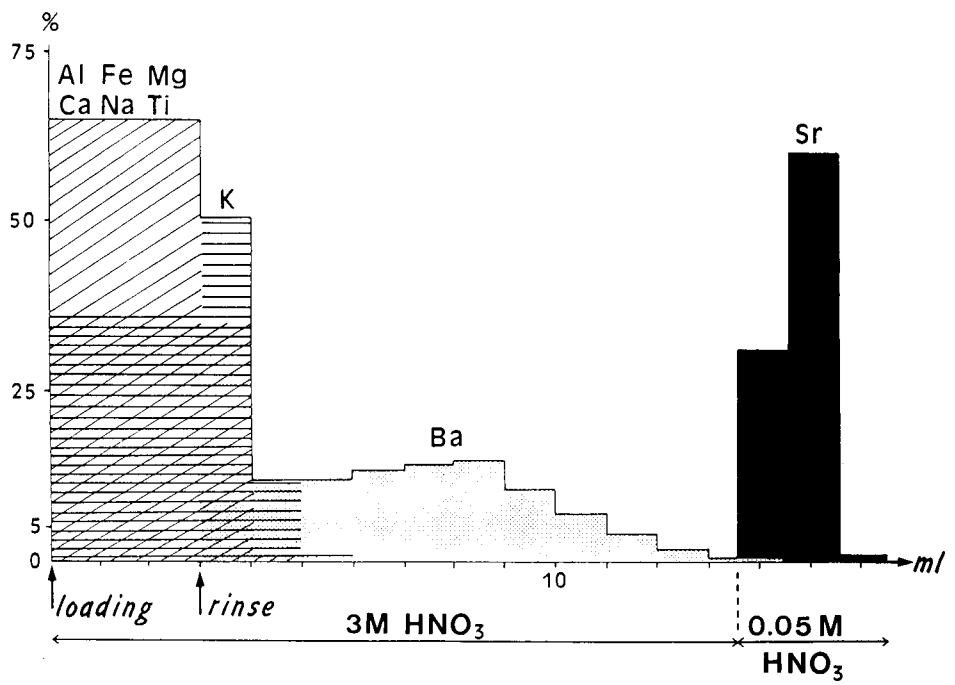

Fig. 1. Typical elution curves for the major elements, barium and strontium on a 0.5-ml column of Sr.Spec sps extraction chromatographic material.

29 M HF + 0.5 ml of 14 M HNO_3. After evaporation of volatile silicon fluoride and excess of HF, the residue was digested in 5 ml of 6 M HCl overnight and evaporated to dryness. The residue was taken up in 1 ml of 14 M HNO_3, dried again and the final residue dissolved in 3 ml of 3 M HNO_3–0.05 M $H_2C_2O_4$ or just 3 ml of 3 M HNO_3 and centrifuged before loading on the column. Titanium and zirconium tend to form sparingly soluble hydrated oxydes in nitric acid [12]. During the early stages of this study, oxalic acid was added to the 3 M HNO_3 loading medium to overcome this problem [12]. However, oxalic acid was subsequently found to contribute considerably to the Sr blank. As similar elution curves were obtained with and without oxalic acid, and as Ti hydroxides caused no apparent problems in pure 3 M HNO_3, this medium is preferable.

Column preparation and Sr separation

A 165 ± 1 mg amount of Sr.Spec sps material was slurried in a few ml of 3 M HNO_3 and transferred to a column, resulting in a ca. 0.5 ml bed. The "resin" was resettled to eliminate any bubbles and preconditioned with 2 ml of 3 M HNO_3 with or without 0.05 M $H_2C_2O_4$. The sample solution was loaded on to the column in 3 ml of 3 M HNO_3 with or without 0.05 M $H_2C_2O_4$, then rinsed twice with 1 ml of the same solution. A 5-ml then a 3.5-ml volume of 3 M HNO_3 were passed through the column to remove major elements and barium, before elution of Sr with 4 ml of 0.05 M HNO_3. The whole column separation was completed in about 3 h.

RESULTS AND DISCUSSION

Matrix effects, behaviour of critical element pairs

In order to check that no first-order chemical interference occurred during the separation, and to verify that the purity of Sr was adequate for TIMS measurements, a set of in-house standards covering a wide range of major element compositions (namely a peridotite, a basalt, a trachyandesite, a diorite and a granite) were analysed in duplicate.

Chemicals yields, determined by ICP-AES (Table 2), were 96–98% for all but the peridotite sample (70%), demonstrating that nearly quantitative separations are possible for most common silicate rock types. It should be noted that 200 mg of powder (instead of ca. 100 mg) were dissolved for the peridotite, suggesting that the column might have been overloaded to some extent in that case.

TABLE 2

Results of analyses of in-house standards representative of common silicate rock types

Sample	Rock-type [a]	Sr present ($\mu g\ g^{-1}$) [b]	Sr found ($\mu g\ g^{-1}$) [c]	Yield (%) [d]	$^{87}Sr/^{86}Sr$ [e]
BRIAN	Peridotite	8.43	5.8	69	0.70315 (2)
			6.0	71	0.70317 (4)
LAG	Basalt	776	745	96	0.70361 (2)
			744	96	0.70358 (2)
VOLV	Trachy-andes.	757	742	98	0.70418 (1)
			743	98	0.70415 (2)
LOT	Diorite	165	160	97	0.72213 (1)
			161	98	0.72212 (2)
FAY	Granite	205	201	98	0.72355 (2)
			200	98	0.72342 (2) [f]

[a] The data are for two different dissolutions of each sample. [b] Independently determined by isotope dilution TIMS. [c] As calculated from ICP-AES analyses after isolation of Sr on Sr.Spec sps columns; uncertainties arising from weighing, aliquoting and ICP calibration are estimated to be ≤ 5%. [d] Total chemical yield, including dissolution and separation on Sr.Spec sps. [e] TIMS results; standard error at the 95% confidence level is on the last digit; [f] The poor agreement between duplicate results is believed to reflect heterogeneity of the rock powder at the 100-mg level, specifically a heterogeneous distribution of biotite flakes (with elevated $^{87}Sr/^{86}Sr$).

For each of these analyses of in-house standards, an aliquot of Sr purified on Sr.Spec sps columns was analysed by TIMS for the $^{87}Sr/^{86}Sr$ ratio. In all instances these gave satisfactory mass spectrometric runs, with good internal precision and reproducibility (Table 2).

These preliminary results suggest that the extraction chromatographic method proposed by Horwitz et al. [10] for nuclear waste solutions and biological samples can be extended to the isolation of Sr from common geological samples for isotopic analysis. This is highlighted by the very sharp separation of critical elements, which are often difficult to achieve by standard cation-exchange methods, namely Ca and Rb. Ca has close chemical similarities with Sr, and elutes just before it from conventional AG 50W-X8 columns. As the Ca/Sr ratio ranges from 100 to 1000 in most geological samples [9], significant amounts of Ca are still present in the Sr fraction, unless special methods are used [9]. Residual calcium decreases the ionization efficiency of Sr and the stability of the ion beam during mass spectrometric analyses. In contrast, an excellent separation of the Ca–Sr pair is easily obtained on Sr.Spec sps columns. Perfect isolation of Sr from Rb is necessary for accurate determinations of $^{87}Sr/^{86}Sr$ ratios because of the isobaric interference at $m/z = 87$. The separation factor between Rb and Sr on cation-exchange columns in 2 M HCl is high. However, the ionization of Rb by TIMS is highly effective, and even minor tailing of the Rb elution peak may result in intense m/z 85 and 87 ion beams at the beginning of Sr analyses. This is of special concern when samples with high Rb/Sr ratios are analysed. No Rb, as monitored at $m/z = 85$, was ever detected during mass spectrometric runs with Sr separated on Sr.Spec sps columns, even from rocks with very high Rb concentrations (e.g. the MA-N reference material, with 3600 $\mu g\ g^{-1}$ Rb). In fact, Sr is very selectively isolated from all major and minor elements present in silicate rocks, with the exception of barium. This element ionizes readily, and decreases the electron work function of the filament material [13], and could thereby suppress Sr ionization. It seems, however, that the separation obtained in this work is adequate for common silicate rocks. If required, a better resolution of the Ba–Sr pair could be achieved using longer columns. Alternatively, work in progress suggests that a better separation can be obtained by using ca. 7 M instead of 3 M HNO_3 for eluting barium.

TABLE 3

Tailing of Sr peaks on two Sr.Spec sps columns

Fraction	Sr (μg)	
	Col. A	Col. B
1	0.65	0.54
2	0.55	0.52
3	0.30	0.32
4	0.25	0.24
5	0.29	0.14
6	0.11	0.17

Memory effects, column blanks

Although sharp peaks and high Sr recoveries are obtained with 0.05 M HNO_3 as eluent, the shape of the peak tail and the behaviour of residual Sr need to be investigated before deciding whether Sr.Spec sps columns may be used several times. In a first experiment, two columns were loaded with 50 μg of Sr and processed as described previously. Amounts of 47.3 and 47.8 μg, i.e. 95 and 96%, respectively, were found in the Sr elution fraction (4 ml of 0.05 M HNO_3). Six additional fractions of 1 ml each of 0.05 M HNO_3 were collected and analysed by ICP-AES.

The data (Table 3) show a slow decrease, indicating that a totally quantitative elution of Sr is not easily obtained. The "resin" was then resettled in 5 ml of 0.05 M HNO_3, which was collected and analysed by ICP-AES, giving 1.1 and 1.0 μg of Sr on the two columns. The next 5 ml still contained detectable amounts.

In another experiment, two columns previously used for the isolation of large (ca. 70 μg) amounts of Sr from geological samples were washed with 5 ml of 0.05 M HNO_3, resettled in 5 ml of the same medium, then used for blank runs with determination of Sr by isotope dilution TIMS (Table 4). These gave consistent results of 57 and 58 ng on the two columns. Three newly prepared, virgin columns processed at the same time gave much lower values of 2.9 ng (loading medium 3 M

TABLE 4

Blank data obtained on five Sr.Spec sps columns

Blank [a]	Column [b]				
	A	B	C	D	E
1	57 ng	58 ng	2.9 ng	140 pg	30 pg
2	12 ng	13 ng			
3	6.9 ng	7.2 ng			

[a] 1 = First column blank, after washing the columns with 5 ml of 0.05 M HNO_3 and resettling Sr.Spec in 5 ml of 0.05 M HNO_3. 2 = Second blank determination, after washing the columns four times with 8 ml of 0.05 M HNO_3, with intervening resettlings in 5 ml of 0.05 M HNO_3. 3 = Third blank determination, after eight further resettling–washing cycles. [b] A and B = columns previously used for the extraction of about 70 μg of Sr. C, D and E = newly prepared columns. Loading medium: (C) 3 M HNO_3–0.05 M $H_2C_2O_4$; (D, E) 3 M HNO_3.

HNO_3–0.05 M $H_2C_2O_4$) and 140 and 30 pg (loading medium pure 3 M HNO_3). Two reagent blanks (13.5 ml of 3 M HNO_3 without $H_2C_2O_4$ and 4 ml of 0.05 M HNO_3) of 20 and 26 pg were determined.

From these results, it is concluded that negligible column blanks can be obtained when new extraction chromatographic material is used and oxalic acid is avoided. In marked contrast, drastic memory effects plague already used Sr.Spec sps columns.

In an attempt to achieve better decontamination, the two columns having given ca. 60-ng "first-stage" blanks were further studied (Table 4). After three cycles of "resin" resettling in 5 ml of 0.05 M HNO_3 followed by rinsing four times with 8 ml of 0.05 M HNO_3, "second-stage" blanks of 12 and 13 ng, respectively, were measured. A third blank run was performed on the same two columns after eight additional resettling–washing cycles, giving only marginally better results (6.9 and 7.2 ng). Finally, two other already used columns were washed with warm (ca. 45°C) 0.05 M HNO_3. First-stage blanks of 14 and 50 ng were measured, suggesting that improved kinetics do not overcome this problem.

Summarizing, although ca. 95% of the Sr extracted on Sr.Spec sps columns is back-extracted as a sharp peak with 0.05 M HNO_3, a small but significant portion appears to be very strongly held on the column. This is released in an exceedingly slow manner, and the resulting memory effect generates blank levels that are not adequate for isotopic work, in which samples with contrasted Sr concentrations (1–1000 $\mu g\ g^{-1}$) and $^{87}Sr/^{86}Sr$ ratios are analysed. Therefore, until more efficient decontamination procedures are proposed, it is advisable to discard the Sr.Spec material after every sample.

TABLE 5

Concentration and isotopic composition data for a set of international reference rock samples [a]

Reference material	Sr ($\mu g\ g^{-1}$)		$^{87}Sr/^{86}Sr$ [b]	
	Found	Certified		
BE-N (basalt)	1383	1370	0.70380	(4) [c]
			0.70374	(2) [d]
W-2 (diabase)	195	194	0.70692	(4) [c]
			0.70696	(2) [d]
BIR-1 (basalt)	109	108	0.70304	(3) [c]
			0.70313	(2) [d]
BHVO-1 (basalt)	390	403	0.70344	(3) [c]
			0.70339	(2) [d]
AGV-1 (andesite)	664	662	0.70391	(6) [c]
			0.70395	(2) [d]
G-2 (granite)	479	478	0.70971	(4) [c]
			0.70964	(2) [d]
RG-M (rhyolite)	100.3	108	0.70420	(6) [c]
	103.4		0.70413	(3) [c]
	101.3		0.70412	(4) [c]
			0.70415	(3) [d]
ST-M (syenite)	658	700	0.70375	(3) [c]
	691		0.70371	(4) [c]
	767		0.70372	(3) [c]
			0.70367	(3) [d]
DR-N (diorite)	410	400	0.70793	(4) [c]
			0.70789	(2) [d]
AN-G (anorthosite)	76.0	76	0.70243	(4) [c]
			0.70244	(2) [d]
DNC-1 (dolerite)	141	145	0.70582	(4) [c]
			0.70579	(2) [d]
MA-N (granite)	86.6	84	1.2782	(2) [c]
			1.27366	(3) [d]
NIST SRM 607	64.7	65.5 ± 0.3	1.20130	(10) [c]
(K-feldspar)	65.5		1.20064	(4) [c]

[a] Seventeen mass spectrometric analyses of NIST SRM 987 (strontium carbonate isotopic standard) during the period of these analyses gave a mean $^{87}Sr/^{86}Sr = 0.710211$ (one standard deviation = 0.000017). [b] Corrected for mass-dependent fractionation by normalizing to $^{86}Sr/^{88}Sr = 0.1194$. [c] Isotope dilution (spiked with ^{84}Sr tracer) run. [d] Isotope composition (unspiked) run.

Analysis of standard reference materials

The proposed procedure was used to analyse a set of international silicate rock standards for Sr concentration, using isotope dilution, and $^{87}Sr/^{86}Sr$ ratios. The results are given in Table 5, together with recommended values [14]. For isotope dilution analyses, a 98%-enriched ^{84}Sr tracer was used, permitting the $^{87}Sr/^{86}Sr$ ratio to be measured concomitantly.

In general, the concentration data found are in reasonably good agreement with the recommended values. Three replicate measurements of the USGS syenite standard ST-M show large discrepancies. The mean of three determinations (705 $\mu g\ g^{-1}$) compares well with the generally accepted value (700 $\mu g\ g^{-1}$), and the observed scatter might reflect powder heterogeneity at the 100-mg level. There are very few published data for $^{87}Sr/^{86}Sr$ ratios in geological standards, and it is therefore difficult to assess the accuracy of the results. NIST (formerly NBS) SRM 607 Potassium Feldspar has a recommended $^{87}Sr/^{86}Sr = 1.20039 \pm 20$. The two determinations here differ significantly from each other and from the NIST value. However, the results are consistent with the range of values reported by Foland and Allen [15], and provide further evidence for sample heterogeneity of this standard on ca. 100-mg powder aliquots. Likewise, the two determinations of the $^{87}Sr/^{86}Sr$ ratio in the MA-N standard do not overlap within mass spectrometric error. Small-scale isotopic heterogeneity is likely to occur in ancient rocks containing minerals with very high Rb/Sr ratios (lepidolite in MA-N). In this instance, $^{87}Sr/^{86}Sr$ should be correlated with Rb/Sr. Further analyses of both Sr isotope composition and Sr and Rb concentrations in MA-N are required to clarify this point.

Conclusions

The extraction chromatographic method proposed by Horwitz et al. [10] provides an attractive technique for the isolation of Sr from geological samples for isotopic analyses. Distinct advantages over conventional cation-exchange methods include simplicity, efficiency and very good selectivity, as exemplified by the excellent separation of critical elements such as Ca and Rb. In addition, this method requires very small reagent volumes of a single mineral acid and Sr is eluted with very dilute HNO_3. The only major shortcoming recognized in this exploratory study arises from memory effects. Until better decontamination of the extraction chromatographic material becomes possible, repeated use of the columns is precluded for isotopic work. However, the possibility of achieving good separations on very small columns makes this method relatively inexpensive.

The authors thank S. Rajkovich (EIChroM Industries) for cooperation and advice and D. Briot, J.L. Duthou and F. Poitrasson for useful suggestions on the manuscript.

REFERENCES

1 L.O. Nicolaysen, Ann. N.Y. Acad. Sci., 91 (1961) 198.
2 G. Faure and J.L. Powell, Strontium Isotope Geology. Springer, Berlin, 1972.
3 K.G. Heumann, in F. Adams, R. Gijbels and R. van Grieken (Eds.), Inorganic Mass Spectrometry (Chemical Analysis Series, No. 95), Wiley, New York, 1988, p. 301.
4 L.T. Aldrich, G.L. Davis, G.R. Tilton and G.W. Wetherill, J. Geophys. Res., 61 (1956) 215.
5 D.A. Papanastassiou and G.J. Wasserburg, Earth Planet. Sci. Lett., 11 (1971) 37.
6 R.J. Pankhurst and R.K. O'Nions, Chem. Geol., 12 (1973) 127.
7 S.R. Hart and C. Brooks, Geochim. Cosmochim. Acta, 38 (1974) 1799.
8 F.W.E. Strelow, Anal. Chem., 32 (1960) 1186.
9 J.L. Birck, Chem. Geol., 56 (1986) 73; and references cited therein.
10 E.P. Horwitz, M.L. Dietz and D.E. Fischer, Anal. Chem., 63 (1991) 522.
11 E.P. Horwitz, R. Chiarizia and M.L. Dietz, Solvent Extr. Ion Exch., 10 (1992) 313.
12 J. Korkisch, I. Steffan, G. Arrhenius, M. Fisk and J. Frazer, Anal. Chim. Acta, 90 (1977) 151.
13 M. Wachsmann and K.G. Heumann, Int. J. Mass Spectrom. Ion Processes, 108 (1991) 75.
14 K. Govindaraju (Ed.), Geostand. Newsl., Spec. Issue, 13 (1989).
15 K.A. Foland and J.C. Allen, Contrib. Mineral. Petrol., 109 (1991) 195.

Analytica Chimica Acta, 269 (1992) 257–261
Elsevier Science Publishers B.V., Amsterdam

Fluorimetric determination of operational pH in 1,4-dioxane–water solutions

Robert W. Townsend and Stephen G. Schulman

College of Pharmacy, University of Florida, Gainesville, FL 32610 (USA)

(Received 16th March 1992; revised manuscript received 1st July 1992)

Abstract

2-Hydroxybiphenyl demonstrates proton transfer in the lowest excited singlet state in 1,4-dioxane–water mixtures. The dissociation reaction of the directly excited neutral molecule is strongly solvent dependent and independent of solution acidity. The reprotonation of the conjugate base, however, depends predominantly on the acidity of the solution and on the bulk dielectric constant of the solvent. A linear relationship between the ratio of the relative fluorescence efficiencies of 2-hydroxybiphenyl and its conjugate base, and the hydrogen ion concentration is obtained only if proper Brønsted activity factors are included in the relationship. These factors can be calculated from electrostatics and are simple powers of the activity coefficients which would be derived from Debye–Hückel theory and which are necessary to convert the formal hydrogen ion concentration to hydrogen ion activity. Using this approach it is possible to calculate pH from hydrogen ion concentration in dioxane–water solutions, containing mole fractions of up to 0.1 of the organic component.

Keywords: Fluorimetry; Brønsted activity factors; Debye–Hückel theory; Dioxane–water mixtures; pH determination

Dioxane–water solutions are widely used as solvents for the synthesis, dissolution and chromatographic analysis of drugs and other molecules. As in aqueous solutions control of the acidity of the solvent will often be necessary to obtain the desired synthetic and analytical results. It is generally recognized that the more accurately and thermodynamically acidity can be described, the more control the scientist has in effecting an outcome favorable to his studies. In pure aqueous solutions the pH concept has been applied with great success to the quantitative description of solution acidity. But in mixed organic–aqueous solvents and in pure organic solvents such a thermodynamically significant concept as pH is not yet accepted [1].

Correspondence to: S.G. Schulman, College of Pharmacy, University of Florida, Gainesville, FL 32610 (USA).

Current theories of pH suggest that the activity of the solvated proton cannot be determined in solutions other than pure water containing very low electrolyte concentrations [1]. Recent work in this laboratory, however, has shown that this conclusion is not necessarily correct and that subject to the universal limitation of not being able to determine single ion activities rigorously [1], a very good approximation to a thermodynamic pH in mixed solvent systems can be made [2].

Studies of the dependence of the relative quantum yields of fluorescence of hydroxyaromatics, particularly the phenolic compound 2-hydroxybiphenyl, in aqueous acetonitrile [2] upon hydrogen ion concentration, show that activity coefficients calculated from the classical Debye–Hückel type electrostatic treatment and the continuum dielectric properties of the solvent are sufficient to calculate proton activities from concentrations.

The acid dissociation rate of 2-hydroxybiphenyl in the lowest excited singlet state, as reflected in the acidity dependence of the fluorescence spectrum, decreases exponentially with increase of the mole fraction of the organic cosolvent. However the reprotonation rate of the excited conjugate base shows a different kind of solvent dependence [2]. This complex dependence of acid–base behavior on the organic cosolvent renders it nearly impossible to deduce the solvent dependence of the hydrogen ion activity from equilibrium measurements. However, from the fluorescence of 2-hydroxybiphenyl, the strongly solvent dependent, pH independent dissociation reaction can be evaluated independently of the minimally solvent dependent, pH dependent reprotonation reaction. This allows the effect of the solvent on the reprotonation reaction to be independently evaluated. Brønsted kinetic activity factors required to linearize the relationship between the relative quantum yield of fluorescence of 2-hydroxybiphenyl and the hydrogen ion concentration are related to the protonic activity coefficients by a simple quadratic expression. The protonic activity coefficients are functions of the bulk dielectric constant and the temperature of the solvent.

The approach will be applied here to solutions of 2-hydroxybiphenyl in several binary mixtures of water with 1,4-dioxane and pH scales in each solvent mixture will be calculated.

EXPERIMENTAL

Materials

2-Hydroxybiphenyl (99$^+$%) was purchased from Aldrich (Milwaukee, WI) and used as supplied. 1,4-Dioxane was stored over Davison 4Å molecular sieves. 5.0 M sodium hydroxide and perchloric acid (analytical grade) were purchased from Fisher (Fairlawn, NJ). A Fisher Accumet 950 pH meter employing a Fisher pencil, gel-filled silver/silver chloride combination electrode was used for the standardization of perchloric acid and for pH measurements.

Absorption measurements were made on a Cary Model 219 spectrophotometer. Steady-state fluorescence measurements were made on a Perkin-Elmer LS-5 fluorescence spectrophotometer whose monochromators were calibrated against the xenon line emission spectrum. An isosbestic point in the absorption spectrum at 290 nm, which was the same in all solvent combinations, was used to excite the hydroxybiphenyl and its emission spectrum was monitored from 320 to 520 nm. A Gilmont Pipetman was employed to deliver volumetric amounts of water and cosolvent mixtures.

Methods

A 10^{-2} F ethanolic stock solution of 2-hydroxybiphenyl was prepared prior to experimentation. A known volume of the stock solution was then micropipetted into a series of 10 ml volumetric flasks and the solvent was evaporated under a stream of nitrogen gas. The residue was brought to volume by addition of a known concentration of acid or base along with a specific volume of organic cosolvent to give the designed mole fraction of the latter. The final concentration of 2-hydroxybiphenyl in each test solution was 2×10^{-5} F. The probe concentration was chosen to keep the absorbance at the excitation wavelengths below 0.02, thereby ensuring the simple proportionality between fluorescence intensity and concentration.

Titrations were performed as follows: 2 ml of test solution of known mole fraction of organic cosolvent were pipetted into a 1 cm^2 cuvette having a 3 ml capacity and the emission spectrum was obtained. The above solution was titrated with a solution 1.17 F in perchloric acid and 2×10^{-5} F in 2-hydroxybiphenyl, so that the concentration of the latter remained constant throughout the titration. Fluorescence spectra were scanned after each increment of titrant had been added and the titration was carried out until the fluorescence of the 2-hydroxybiphenylate anion could no longer be observed and the fluorescence of the 2-hydroxybiphenyl was maximal and constant. Calculation of the ionic strength at each point in the titration was carried out using the formal concentration of the perchloric acid.

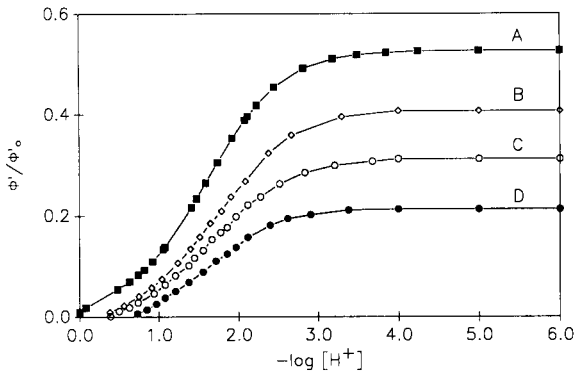

Fig. 1. Variation of the relative quantum yield of fluorescence (ϕ'/ϕ'_0) of 2-hydroxybiphenyl with the logarithm of the hydrogen ion concentration ([H^+]) at various mole fractions of dioxane (X_d) in aqueous dioxane: A ($X_d = 0$), B ($X_d = 0.023$), C ($X_d = 0.050$), and D ($X_d = 0.083$).

RESULTS AND DISCUSSION

The dependences of the relative quantum yields of fluorescence (the ratios of the fluorescence efficiencies at any pH to those at the extremes of pH where the acid and conjugate base emissions are isolated) of 2-hydroxybiphenyl, in solvents containing varying mole fractions of dioxane and water, on the molar hydrogen ion concentration [H^+] are shown in Fig. 1. At hydroxide ion concentrations greater than 1×10^{-2} M, the organic anion is the sole absorbing and emitting species. In the intervals 1×10^{-3} M > [H^+] > 1×10^{-7} M and 1×10^{-6} M > [OH^-] > 1×10^{-8} M, the neutral molecule is the sole absorber. However fluorescence is observed from the anion as well as from the neutral molecule. This results from the dissociation, in the lowest excited singlet state, of the phenol group of the directly excited neutral molecule [3]. In this region of acidity or alkalinity, the relative quantum yields of fluorescence of the neutral molecule, ϕ/ϕ_0 and of the anion, ϕ'/ϕ'_0, are invariant with respect to [H^+] and [OH^-] and are related to the kinetics of dissociation in the excited state, in mixed aqueous organic solvents as well as in water, by [3–5]:

$$\frac{\phi'/\phi'_0}{\phi/\phi_0} = k_a\tau_0 \qquad (1)$$

where k_a is the rate constant for prototropic dissociation of 2-hydroxybiphenyl in, and τ_0 the lifetime of, the excited state. It was previously shown for some hydroxyaromatics, in other organic solvents mixed with water, that $(\phi'/\phi'_0)/(\phi/\phi_0)$ and therefore, $k_a\tau_0$ varies exponentially with the mole fraction of organic cosolvent [4–7] and that the slope of the plot of log $k_a\tau_0$ against X_c, the mole fraction of cosolvent, is a function of the activity of water and the distance separating the fully hydrated hydrogen ion and the fully hydrated conjugate base in the encounter complex (or solvent separated ion-pair) [5].

In the acidity region where ϕ/ϕ_0 and ϕ'/ϕ'_0 vary with [H^+], the relationship between them is given by [3,4]:

$$\frac{\phi/\phi_0}{\phi'/\phi'_0} = \frac{1}{k_a\tau_0} + \frac{k_b\tau'_0}{k_a\tau_0}F[H^+] \qquad (2)$$

where k_b is the rate constant for reprotonation of 2-hydroxybiphenylate (ArO^-) in the excited state and F is the Brønsted kinetic activity factor [8,9] which corrects each experimental value of k_b to zero ionic strength in the solvent mixture chosen. F is derived along the same lines as the extended Debye–Hückel equation [10] for the reaction

$$ArO^- + H^+ \rightleftharpoons X$$

where X is the transition state (or activated complex) preceding the formation of ArOH, and is given, for a uni-univalent ionic reaction such as the hydrogen ion-hydroxybiphenylate reaction, by

$$-\log F = \frac{2A\sqrt{\mu}}{1 + aB\sqrt{\mu}} \qquad (3)$$

where μ is the ionic strength. A is related to the dielectric constant ϵ [11] and the absolute temperature T by [12,13]

$$A = 1.826 \times 10^6(\epsilon T)^{-3/2} \qquad (4)$$

B is related to ϵ and T by

$$B = 5.031 \times 10^9(\epsilon T)^{-1/2} \qquad (5)$$

and a is the mean distance of closest approach of the fully solvated proton and the 2-hydroxybiphenylate ion, calculated for present purposes to be 11.1 Å [5].

TABLE 1

Debye–Hückel terms (A and B) calculated from Eqns. 4 and 5 at 25°C and used in the calculation of the Brønsted activity factor (F) at various 1,4-dioxane mole fractions (X_d) having different dielectric strengths (ϵ) in dioxane–water solutions
(Also presented are the products of the rate constants and corresponding fluorescence decay times $k_a\tau_0$, calculated from Eqn. 1 and $k_a\tau_0$ and $k_b\tau_0'$, determined from the intercept and slope of Fig. 2 with its resulting correlation coefficient, r^2)

Volume percent dioxane	X_d	ϵ	A	$B \times 10^{-7}$	$k_a\tau_0$ (Eqn. 1)	$k_a\tau_0$ (Fig. 2)	$k_b\tau_0'$	r^2
0	0	78.54	0.509	3.29	1.11	1.13	121	0.994
10	0.023	69.87	0.608	3.48	0.686	0.671	117	0.998
20	0.050	60.62	0.752	3.74	0.451	0.458	105	0.998
30	0.083	51.74	0.954	4.05	0.271	0.290	114	0.996

Values of ϵ, A and B for various alcohol water mixtures at 25°C, in which fluorimetric titrations were carried out, are listed in Table 1. As seen in Fig. 2, plots of $(\phi/\phi_0)/(\phi'/\phi_0')$ vs. $F[H^+]$ are linear for $[H^+] = 0.04$–0.1 M. Moreover, the ordinate intercepts of these lines which, according to Eqn. 2 should correspond to $(k_a\tau_0)^{-1}$, agree well with the corresponding terms calculated from Eqn. 1 even though the former depend on the activity correction while the latter do not. Although $k_a\tau_0$ is extremely solvent dependent, $k_b\tau_0'$ (Table 1) is nearly independent of the mole fraction of dioxane in the solvent. These observations lead to the conclusion that the form of the Brønsted kinetic activity factor chosen here is a reasonably accurate means of correcting the parameters of the chosen reaction for non-ideal behavior. Each fluorescence measurement has about two percent uncertainty so that each value of $(\phi/\phi_0)/(\phi'/\phi_0')$ has about four percent uncertainty. Since this is the principal source of error in all measurements, each value of $F[H^+]$ calculated can be assumed to be about five percent uncertain. While the solvent influence on

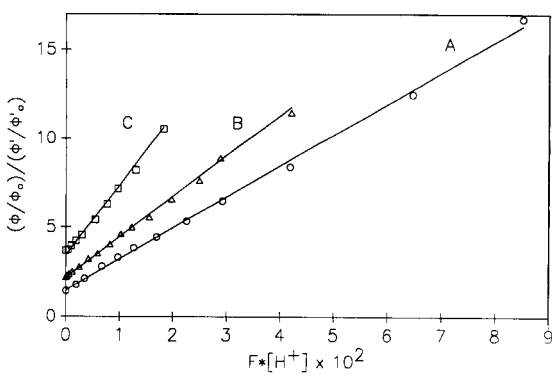

Fig. 2. Plots of $(\phi/\phi_0)/(\phi'/\phi_0')$ vs. $F[H^+]$ for 2-hydroxybiphenyl in aqueous dioxane: A ($X_d = 0.023$), B ($X_d = 0.050$), and C ($X_d = 0.083$).

TABLE 2

pH of dilute perchloric acid solutions in aqueous 1,4-dioxane as a function of the logarithm of the reciprocal hydrogen ion formal concentration ($-\log[H^+]$) and the mole fraction of dioxane (X_d)

log $[H^+]$	pH ($X_d = 0$)	pH ($X_d = 0.023$)	pH ($X_d = 0.050$)	pH ($X_d = 0.083$)
3.40	3.41	3.41	3.41	3.42
3.20	3.21	3.21	3.22	3.22
3.00	3.02	3.02	3.02	3.03
2.90	2.92	2.92	2.92	2.93
2.80	2.82	2.82	2.83	2.83
2.70	2.72	2.72	2.73	2.74
2.60	2.62	2.63	2.63	2.64
2.50	2.53	2.53	2.53	2.54
2.40	2.43	2.43	2.44	2.45
2.30	2.33	2.33	2.34	2.35
2.20	2.24	2.24	2.24	2.26
2.10	2.14	2.14	2.15	2.16
2.00	2.04	2.04	2.05	2.07
1.90	1.95	1.95	1.96	1.97
1.80	1.85	1.85	1.86	1.88
1.70	1.76	1.76	1.77	1.78
1.60	1.66	1.66	1.67	1.69
1.50	1.57	1.56	1.58	1.59
1.40	1.48	1.47	1.48	1.50
1.30	1.38	1.37	1.39	
1.20	1.29	1.28	1.29	
1.10	1.20	1.18	1.20	
1.00	1.11	1.09		

the dissociation reaction cannot be described by continuum electrostatics [4] the influence of the solvent on the reprotonation reaction can. Accordingly, since F is a good activity factor for the overall reprotonation reaction, $f_{H^+} = \sqrt{F}$ should be a good activity coefficient for the solvated proton. In any of the dioxane–water mixtures, then, the activity of the hydrogen ion is

$$a_{H^+} = f_{H^+}[H^+] \quad (6)$$

and the pH is

$$pH = -\log a_{H^+}$$

$$= \frac{1.826 \times 10^6 (\epsilon T)^{-3/2} \sqrt{\mu}}{1 + 558\sqrt{\frac{\mu}{\epsilon T}}} - \log[H^+] \quad (7)$$

Tabulations of pH corresponding to $[H^+]$ for several dioxane–water mixtures at 25°C are given in Table 2. According to Table 2, the influence of the cosolvent of the pH is remarkably small, suggesting that H^+ is solvated almost exclusively by water.

REFERENCES

1 R.G. Bates, Determination of pH: Theory and Practice, 2nd edn., Wiley, New York 1973, Ch. 2.
2 S.G. Schulman, R.W. Townsend and Y. Zhang, Anal. Chim. Acta, 255 (1991) 329.
3 A. Weller, Z. Elektrochem., 56 (1952) 662.
4 S.G. Schulman, R.N. Kelly and N.J. Gonzalez, Pure Appl. Chem., 59 (1987) 665.
5 S.G. Schulman, R.N. Kelly and S. Chen, Chimica Oggi, 8 (1990) 13.
6 D. Huppert and E. Kolodney, Chem. Phys., 63 (1981) 401.
7 D. Huppert, E. Kolodney, M. Gutman and E. Nachliel, J. Am. Chem. Soc., 104 (1982) 6949.
8 J.N. Brønsted, Z. Phys. Chem., 102 (1922) 169.
9 J.N. Brønsted, Z. Phys. Chem., 115 (1925) 337.
10 P. Debye and E. Hückel, Phys. Z., 24 (1923) 185.
11 G. Akerlof, J. Am. Chem. Soc., 54 (1932) 4123.
12 D.A. MacInnes, The Principles of Electrochemistry, Reinhold, New York, 1939, Ch. 7.
13 R.A. Robinson and R.H. Stokes, Electrolyte Solutions, 2nd edn., Academic Press, New York, 1959, Ch. 4.

Analytica Chimica Acta, 269 (1992) 263–268
Elsevier Science Publishers B.V., Amsterdam

Microprobe analysis of geological materials by laser ablation inductively coupled plasma mass spectrometry

Noboru Imai

Geological Survey of Japan, 1-1-3 Higashi, Tsukuba, Ibaraki 305 (Japan)

(Received 12th March 1992; revised manuscript received 9th July 1992)

Abstract

The distribution of 25 elements from Mg to U in the geological materials, stalactite and fossil shell were obtained by laser ablation inductively coupled plasma mass spectrometry (LA-ICP-MS). The laser pulses in the free-running mode were fired several times at the same position while the samples were fixed in each measurement. The variation of the signal intensity was normalized using the ^{43}Ca signal as the internal standard, assuming that the $CaCO_3$ content is 100% in every position. The standards were made from part of the samples themselves, whose elemental concentrations were determined separately by solution method. The analytical results by laser method for the inhomogeneous geological samples were assessed with those obtained by solution analysis.

Keywords: Inductively coupled plasma mass spectrometry; Geological materials; Laser ablation; Microprobe analysis

Recently, direct introduction of solids by laser ablation to the ICP for qualitative and quantitative analysis has been investigated as a method of sample introduction for ICP-MS [1–7]. The laser method requires almost no sample preparation and has low levels of polyatomic ion interferences which are normally derived from water and acid. However, there is a problem with the large variation of analytical results which depends on the quality of the material and surface state. This variation may be corrected for by using the signal of one of the elements analysed as the internal standard [2,3,5], or by evaluating the evaporated volume via measurement of the size of the laser shot crater [8]. Hager showed that the relative sensitivity of the elements can be used for the semi-quantitative analysis [4] and Pang et al. demonstrated that a 100-Hz laser improved the reproducibility of the data [9].

Correspondence to: N. Imai, Geological Survey of Japan, 1-1-3 Higashi, Tsukuba, Ibaraki, 305 (Japan).

However, all these studies have been mainly concentrated on bulk analysis of the sample. In this work, some non-homogeneous geological samples were studied using a focused laser to obtain the spatially resolved distribution of the elements.

The samples in this experiment were stalactite and fossil shell. It is reported that the concentrations of minor elements in stalactite increased from the edge to the center, and accumulated in the center during its growth [10]. On the other hand, in the mollusc shell the minor elements are usually incorporated from environmental water, which is often used as a marker of pollution. As for the fossil shell, it is important to determine the concentrations of the minor elements, especially U and Th, in the shell accurately, because they could cause serious errors in dating the shell [11].

In previous work [5] mineral inclusions of biotite in granite were analysed, correcting for the variation of the evaporated volume by measuring

the weight loss after each laser shot. In this work, however, the variation of the signal intensity was corrected using the ^{43}Ca signal, assuming that the content of $CaCO_3$ is 100% in every position. The accuracy of the laser analysis was assessed by comparison with solution analysis.

This normalization technique can be used similarly for any of the other carbonate materials or other samples and minerals which have a single chemical composition or for samples in which one of the elements is distributed uniformly.

EXPERIMENTAL

Samples

The stalactite used in this experiment (Akiyoshidai, Japan) is shown in Fig. 1A. The stalactites were formed in limestone caves and they are composed of calcium carbonate which grows in the form of an "icicle" during geologic time. The specimen was cut horizontally into 1-cm thick slices and then cut in half. The diameter was about 85 mm and the cross section shows concentric structures. The inner part was dark brown and non-crystalline while the outer part was transparent, light brown and crystalline.

The fossil shell (*Mya oonogai*) is shown in Fig. 2A. The shell was about 80×120 mm. It was collected from the Shimosueyoshi Formation, Yokohama, Japan. The formation was 100–150 thousand years old, by electron spin resonance dating [11].

Sample preparations for laser analysis

The stalactite was cut again into two smaller pieces so that it could be placed in a cylindrical sample cell (diameter 42 mm, height 31 mm). The fossil shell was washed well in deionized water and cut into 36 square pieces of about 1.5×1.5 cm each, then placed in a sample cell for the analysis, although the pieces from the edge were not exactly square. For the powdered sample, the pressed discs were prepared in the same manner as in previous work [5].

Standards

The selection of standards is of primary importance for the analysis by LA-ICP-MS. The matrixes of limestone, stalactite and shell are all composed of calcium carbonate, however the concentrations of several elements vary greatly from one sample to another, which sometimes causes serious errors. In this work part of the sample itself was powdered and pelletted for use as a standard for the laser ablation analysis to minimize errors. The concentrations of the elements in the standard were determined separately by the solution method of ICP and ICP-MS as described before [12,13]. The calibration line for each element was made by two points between the blank and standard values.

ICP-MS analysis

All the acids used were of atomic absorption analysis grade (Cica-Merck) and purified water was produced by deionizing and then distilling; this was further purified with Millipore system (Milli-Q SP reagent water system).

The Nd–YAG laser (1.06 μm) was a NEC SL136B free-running laser (half-width 130 μs), SL231H Q-switched laser (half-width 17 ns) and SL213 optics. Details of the laser instruments have been described [5]. In this work the optics were changed so that the crater size was about 0.5 mm for the stalactite and about 0.1 mm for the fossil shell.

The ICP-MS instrument used was a Yokogawa Electrics PMS-200. The operating conditions for the ICP-MS are given in Table 1. The 25 elements and isotopes chosen for analysis were

TABLE 1

Operating conditions of ICP-MS

RF power	1.2 kW
Argon gas flow-rate	
Outer gas	14 l min^{-1}
Auxiliary gas	0.8 l min^{-1}
Carrier gas	0.6 l min^{-1}
Load coil sampling aperture distance	4.0 mm
Sampling aperture diameter	0.5 mm
Skimmer aperture diameter	1 mm
Data acquisition	
Dwell time for each element	20 ms
Scan period	0.553 s
Number of scans	180 sweeps
Measuring time	99.57 s

Mg(24), Al(27), Si(29), P(31), Ca(43), Ti(49), V(51), Cr(52), Mn(55), Fe(57), Co(59), Ni(60), Cu(63), Zn(66), Rb(85), Sr(86), Y(89), Ba(138), La(139), Ce(140), Pr(141), Nd(143), Pb(208), Th(232) and U(238).

RESULTS AND DISCUSSION

Laser ablation

The ICP-MS spectra for the stalactite and the fossil shell show a very large signal from Ca and smaller signals from Al, Si, Fe, Sr and Ba and much smaller signals from La, Ce, U and other elements. In this work the signal from ^{43}Ca whose isotope ratio is much smaller than the ^{44}Ca was used as an internal standard, because the ^{44}Ca signal is too strong to be measured for this analysis.

In this work a free-running laser was used for the analysis, although the technique of successive pulses in the Q-switched mode is usually used for the bulk analysis with LA-ICP-MS while the sample is constantly moved [4,6,9]. It is suggested that the pulse in the Q-switched mode has a more uniform response function for the elements, and is more suitable for semi-quantitative analysis than in the free-running mode [4]. However, the pulse in the free-running mode makes a narrower and deeper crater than in the Q-switched mode and is more advantageous for microprobe analysis [14]. Therefore, since in this work the higher spatial resolution is of primary importance for the microprobe analysis, the sample was fixed at each measuring point and the laser pulse was fired several times at the same position. Moreover, the signal intensity measured in the free-running mode is much more stable than that in the Q-switched mode [5].

Stalactite analysis

Figure 1 shows the analysis of stalactite. A cross section of the stalactite sample, shown in Fig. 1A, was analysed by firing 10 pulses of 0.95 J in the free-running mode in a straight line from the edge to the center in 0.5 mm steps. The standard used was a powdered disc which was made from the center of the same stalactite. The variation of the ablated amount was normalized

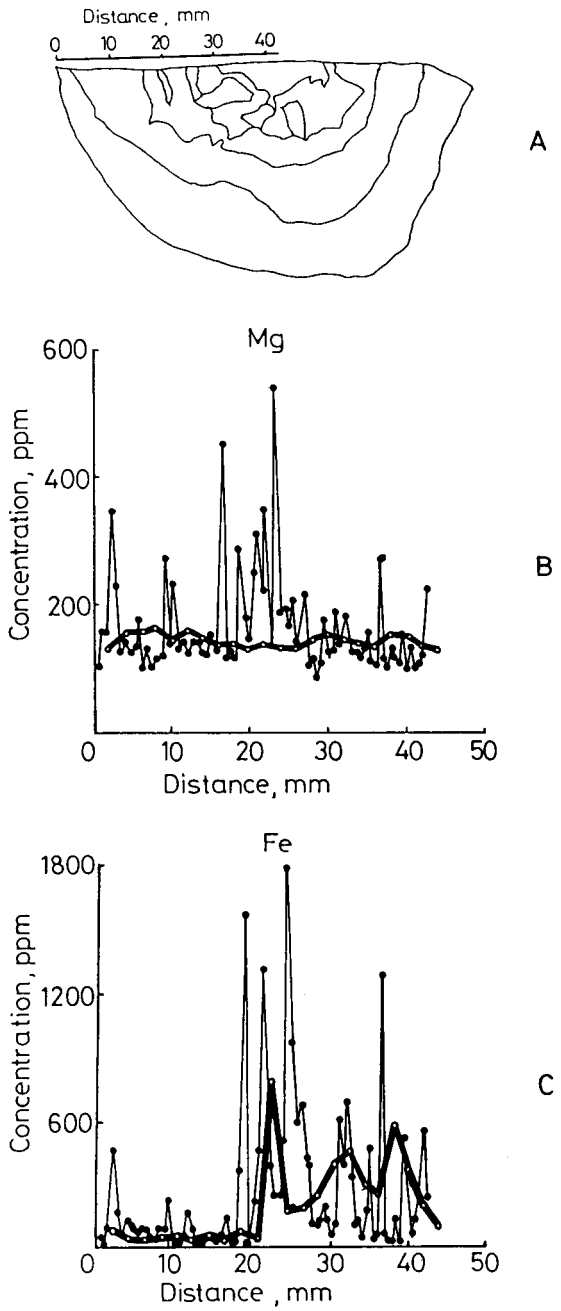

Fig. 1. (A) Cross section of the stalactite (Akiyoshidai, Japan); the lines in the figure are the dark brown physical marks on the cross section, representing the structural concentric circles. The concentrations of Mg (B) and Fe (C) along a straight line of the cross section of the stalactite. Solid circles show the laser values and open circles show the solution values.

by the ^{43}Ca signal, assuming that the content of $CaCO_3$ is 100% in each position. In fact in this experiment the measured $CaCO_3$ content in different parts for the stalactite by the solution method was $101.1 \pm 2.66\%$ (the number of samples $N = 22$) and $99.51 \pm 1.30\%$ ($N = 36$) for the fossil shell. Figure 1B and 1C show the results of the analysis of Mg and Fe across the cross section. In Fig. 1B, most of the Mg concentrations by laser method represented by the solid circles are in the range of 150–200 $\mu g\ g^{-1}$ from the edge to the center, and there are several sharp peaks which correspond to the dark brown concentric circles of the sample. The accuracy of the results

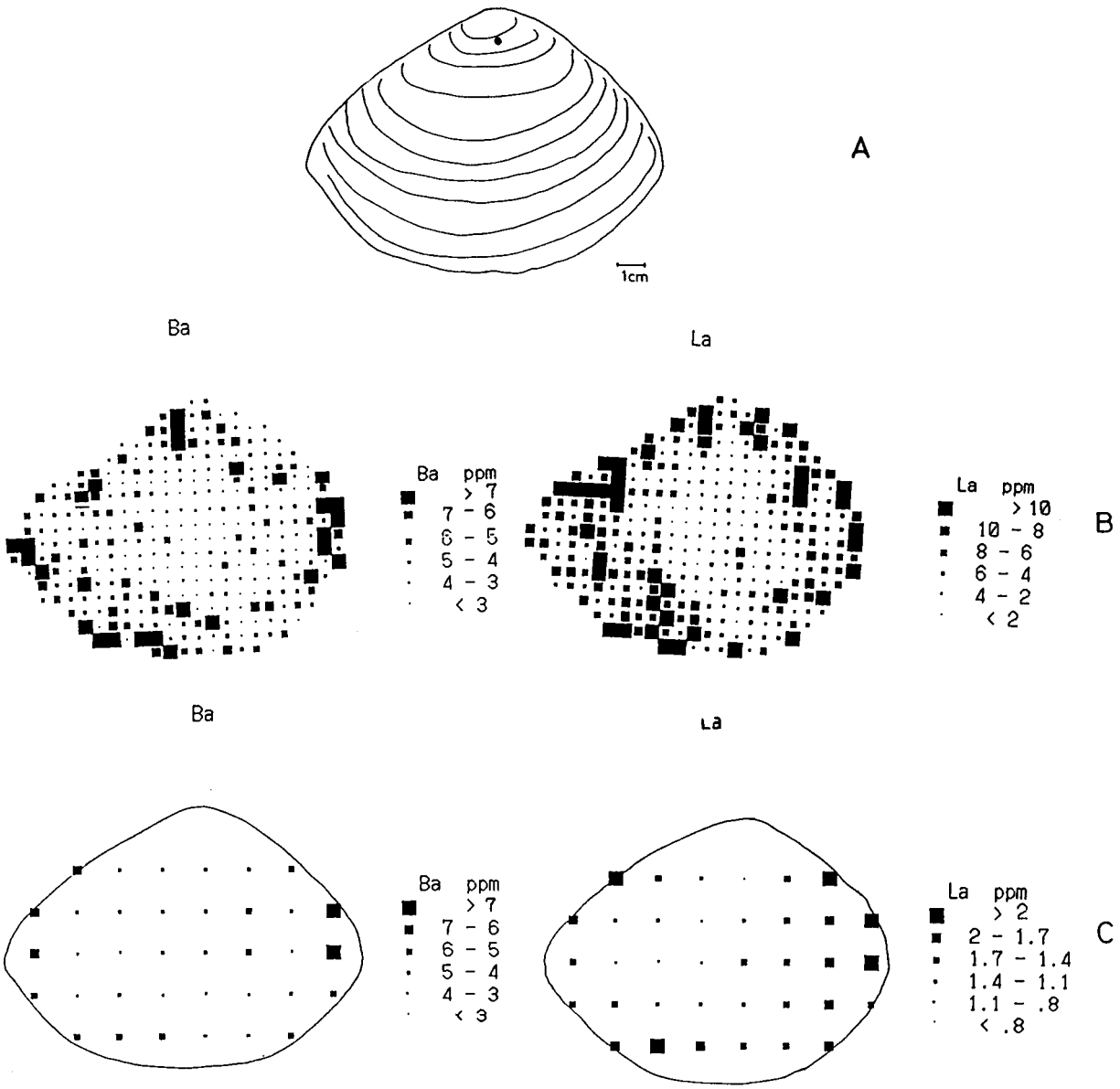

Fig. 2. (A) Fossil shell (*Mya oonogai*, Ohiso hills, Japan). (B) The distributions, determined by laser method, of Ba and La in a fossil shell. (C) The distributions, obtained by solution method, of Ba and La in a fossil shell.

by the laser method was assessed by the solution method. The measured part of the stalactite by the laser method was cut in every 2 mm, then crushed and powdered. These samples were digested by mixed acids and analysed by the solution method [12,13]. The open circles are the values obtained by the solution method, which are almost constant from the edge to the center and have no major sharp peak. The concentration range of the values by the solution method is similar to that by the laser method except for several sharp peaks. As shown in the figure, the values obtained by the laser methods are not always exactly the same as those by the solution method, probably because the sampling positions and the depth for the two analyses are different for the laser method (every 0.5-mm step in the surface part of the sample) and the solution method (every 2-mm step for the bulk samples from the surface to the centre). However, the comparison is still useful as one way of validating the results obtained using the laser method.

Figure 1C shows the analysis of Fe. The values by the laser method (solid circles) are low (less than 100 $\mu g\ g^{-1}$) in transparent outer ring, and have several very large sharp peaks (200–1800 $\mu g\ g^{-1}$) in the dark brown center. The values by the solution method (open circle) also give low values (less than 100 $\mu g\ g^{-1}$) in the outer part and high values (200–600 $\mu g\ g^{-1}$) in the center. The results show that both values by the laser and solution methods show the similar tendency of elemental distribution, although they do not agree exactly with each other.

Fossil shell analysis

Figure 2 shows the analysis of fossil shell. In this work, the shell (*Mya oonogai*, Fig. 2A) was analysed for each of 36 pieces of 1.5×1.5 cm fragment which was prepared by cutting the shell to be placed in the sample cell. The analysis was made in 5 mm steps by firing a 0.62 J laser in the free-running mode. Figure 2B shows the Ba and La distributions as determined by the laser method. In both elements the concentrations in the center are apparently lower than those near the edges, and the concentration range in both cases was about 0 to 10 $\mu g\ g^{-1}$. For comparison, the solution values were obtained for each of 36 pieces of the shell, after they had been crushed, powdered and then analysed by the solution method. The results of the solution method are shown in Fig. 2C. The concentrations of Ba and La by the solution method in the center were also lower than those near the edge. For Ba, the concentration ranges for both methods were similar (1–10 $\mu g\ g^{-1}$), however the solution values of La (0–2 $\mu g\ g^{-1}$) were much lower than the laser values. To explain this concentration difference, the Ba and La concentrations along the direction of thickness of the shell were analysed. The thickness of this shell was about 4 mm, and the laser was fired in 0.1-mm steps on the cross section, starting from the outer layer through to the inner

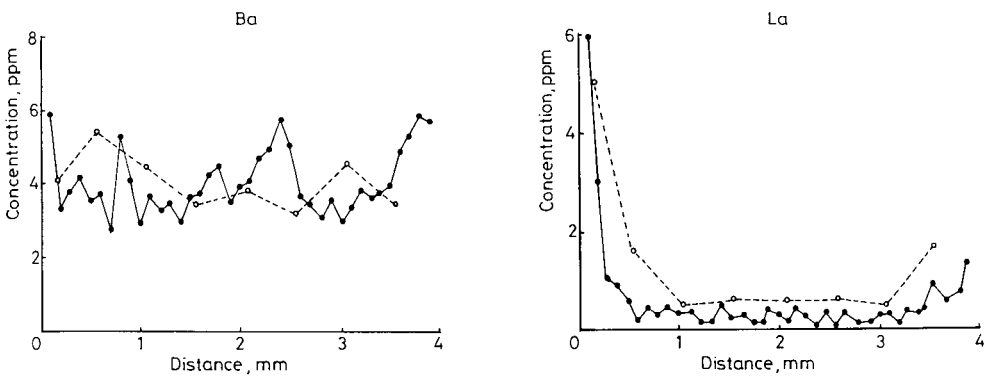

Fig. 3. The concentrations of Ba and La through the fossil shell. Solid circles (solid line) represent the laser values and open circles (dotted line) show the solution values. The analysed position was the hinge region marked as a dot on the shell in Fig. 2A.

layer. The results by the laser method are the solid circles (and solid line) in Fig. 3. The concentrations of Ba were in the range of 3–6 $\mu g\ g^{-1}$ from outside to inside, in spite of some fluctuations. In contrast, the concentration of La decreased rapidly from 6 $\mu g\ g^{-1}$ to less than 1 $\mu g\ g^{-1}$ within 0.3–0.5 mm from the outer surface. For comparison, the solution values were also obtained for the samples which were prepared by cutting the measured part of the shell by the laser method in 0.5-mm steps very carefully, then powdered and analysed by the solution method. Open circles (dotted line) show the solution values. The solution values of Ba were in the same range, 3–6 $\mu g\ g^{-1}$ as the laser values and that of La decreased from 5 $\mu g\ g^{-1}$ to less than 1 $\mu g\ g^{-1}$ from the surface to the inside. The elemental distribution as determined by the solution method is very similar to that obtained by the laser method. This suggests that La is concentrated only in the outer surface of the shell, since it was adsorbed from the outside while underground during geologic time. The laser method analysed only the outer surface part of the shell, therefore the laser values are much higher than the solution values. The same patterns were also clearly observed for Fe, Al, and the rare earth elements.

REFERENCES

1 A.R. Gray, Analyst (London), 110 (1985) 551.
2 P. Arrowsmith, Anal. Chem., 59 (1987) 1437.
3 T. Mochizuki, A. Sakashita, H. Iwata, T. Kagaya, T. Shimamura and P. Blair, Anal. Sci., 4 (1988) 403.
4 J.W. Hager, Anal. Chem., 61 (1989) 1243.
5 N. Imai, Anal. Chim. Acta, 235 (1990) 381.
6 M. Broadhead, R. Broadhead and J.W. Hager, At. Spectrosc., 11 (1990) 205.
7 J. Marshall, J. Franks, I. Abell and C. Tye, Anal. At. Spectrom., 6 (1991) 145.
8 G. Remond, A. Batel, C. Roques-Carmes, D. Wehbi, I. Abell, and G. Seroussi, Scanning Microsc., 4 (1990) 249.
9 H. Pang, D.R. Wiederin, R.S. Houk, and E.S. Yeung, Anal. Chem., 63 (1991) 390.
10 M. Ikeya, Nature, 255 (1975) 48.
11 K. Shimokawa, N. Imai, H. Nakazato, and K. Mizuno, Quat. Sci. Rev., 11 (1992) 219.
12 N. Imai, Bunseki Kagaku, 36 (1987) T41.
13 N. Imai, Anal. Sci., 6 (1990) 389.
14 E.R. Denoyer, K.J. Fredeen and J.W. Hager, Anal. Chem., 63 (1991) 445A.

Analytica Chimica Acta, 269 (1992) 269–272
Elsevier Science Publishers B.V., Amsterdam

Stability of dithizone in chloroform–acetic acid solvent system

N. Thiagarajan and M. Subbaiyan

Department of Analytical Chemistry, University of Madras, Guindy Campus, Madras 600 025 (India)

(Received 11th July 1991; revised manuscript received 7th June 1992)

Abstract

Dithizone is very unstable in solution when exposed to direct sunlight and more so when kept at high room temperature. An efficient method for preparing the reagent solution and using it under the above-mentioned conditions was developed. The simple protocol involves equilibrating the reagent solution in chloroform with 6 M acetic acid. This mixture can be stored for a reasonable length of time ($\geqslant 3$ weeks) without any deterioration and consequent decrease in activity.

Keywords: UV–Visible spectrophotometry; Dithizone; Stabilization

The deterioration of stock solutions of dithizone in organic solvents when exposed to sunlight and at high room temperatures is well established. Other prominent factors contributing to its instability include the presence of traces of heavy metals and oxidants [1,2]. Its unstable nature therefore makes it more difficult to use as careful measures have to be undertaken during its preparation and storage.

Irving and co-workers investigated dithizone extensively and reported the causes of its deterioration in chloroform under light and temperature conditions [3], and also identified the oxidation products in the presence of different oxidizing agents and in different media [4–6].

In this laboratory it was found that when the ambient temperature reached 35°C and above in summer and in bright light (under laboratory conditions) a 0.001% dithizone solution diluted immediately from a freshly prepared stock solution of 0.01% in chloroform deteriorated rapidly. Attempts to preserve this solution immediately after preparation by refrigerating it at 10°C under diffuse light conditions also failed. This may possibly be because the time lag of 5–10 min that is required for the preparation of the reagent solution under the above-mentioned conditions can have an adverse effect on its stability and once the deterioration has commenced it presumably cannot be controlled or reversed merely by refrigeration. The stock solution was also found to be similarly affected, although to a lesser extent, and was not fit for continuous use.

To obtain a stable dithizone solution, many workers have suggested the use of the pure reagent [7] and/or the solvent [8]. Some have attempted to give a standardization procedure for the reagent [9] prior to use. The use of sulphurous acid or other holding reductants such as hydroxylamine or sodium thiosulphate for this purpose proved to be less effective. All these approaches, although aiding the potential use of the reagent, are laborious.

Correspondence to: N. Thiagarajan, Department of Analytical Chemistry, University of Madras, Guindy Campus, Madras 600 025 (India).

From previous work [10] it is evident that the photochromic deterioration of metal dithizonates is not favoured in polar media, and this is especially so in acetic acid. Also, it has been emphasized that photochromism is probably an inherent property of the ligand and it is the central metal atom that determines the photochemical stability and the rate of the return reaction. Hence it can be deduced that if the ligand solution in chloroform is kept in the same polar medium (acetic acid), the ligand and the metal complex should be stabilized against photochemical conversion.

Based on these facts, in this investigation chloroform–dithizone solution mixed with acetic acid by suitable means was tested for its stability under various conditions. The effect of acetic acid association on the solubility of the ligand in the aqueous phase and thereby its influence on the complexation and extractability of the metal complex were also established and are discussed. The results are compared with those obtained for a simple dithizone–chloroform solution.

EXPERIMENTAL

Dithizone was obtained from E. Merck (India) and assayed for a minimum of 99% purity by chelatometry [11]. Chloroform, acetic acid and mercury(II) chloride were of AnalaR grade (BDH). Doubly distilled water was used for cleaning the glassware and preparing the required solutions.

Glassware was washed with chromic–sulphuric acid cleaning solution, followed by hot (1 + 1) nitric acid, and copiously rinsed with water.

Procedure

Initially, 25 ml of 6 M acetic acid in a separating funnel were equilibrated with 5 ml of chloroform by vigorous mixing and the organic phase was discarded. Then 100 ml of 0.01% dithizone solution in chloroform were transferred immediately into the above acetic acid solution, shaken well for 3–4 min to ensure complete equilibration, removed from the aqueous phase and stored.

A 10-ml volume of the above stock solution was diluted to 100 ml with chloroform to give a solution of concentration 0.001% and when further dilution was required the 100 ml of this mixture was again equilibrated with 25 ml of 6 M acetic acid that had been thoroughly mixed with 5 ml of chloroform beforehand as mentioned earlier, removed from the aqueous phase and stored. The entire procedure was carried out at room temperature ($\geqslant$ 35°C) and in daylight. The reagents were protected from direct exposure to sunlight only on storage. One-day-old reagent solution stored at 10°C and under diffuse light conditions was used for the analysis.

The simple dithizone–chloroform solution was prepared at 20°C and in diffuse light.

The amount of acetic acid transferred into the organic phase was determined titrimetrically [12] using sodium hydroxide and phenolphthalein as indicator, in the aqueous phase before and after equilibration of the dithizone solution with the above aqueous acetic acid solution.

Beer's law

From a stock solution of mercury(II) chloride in 0.5 M sulphuric acid with a metal ion concentration of 5 μg ml^{-1}, aliquots containing 5–25 μg of metal ion were placed in a separating funnel in a total volume of 20 ml. To this, 7 ml of 0.001% reagent solution were added and shaken well for 1–2 min and the absorbance was read at 495 nm, at which the complex exhibits the absorption maxima. Beer's law was found to be obeyed up to 22.5 μg for the acetic acid–dithizone–chloroform system and for the simple dithizone–chloroform solution. The amount of acetic acid (sp.gr. 1.05) transferred was found to be 3.9 g.

RESULTS AND DISCUSSION

The absorption spectrum of the reagent exhibited two maxima, one corresponding to 600 nm and the other to 450 nm, as reported earlier [1].

The freshly prepared acetic acid–dithizone–chloroform solution was found to have a greater absorbance (absorbance at 600 nm = 2.32 and at 450 nm = 1.40) than the simple dithizone–chloroform solution (absorbance at 600 nm = 1.55 and at 450 nm = 0.58) with the same dithizone con-

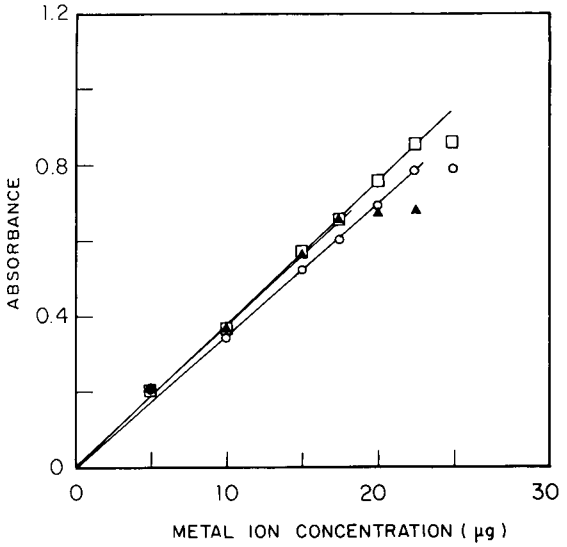

Fig. 1. Adherence to Beer's law. ○ = Dithizone–chloroform solution; □ = fresh acetic acid–dithizone–chloroform solution; ▲ = 1-day-old acetic acid–dithizone–chloroform solution kept at 10°C and in diffuse light.

centration (3.9×10^{-5} M). Further, Beer's law was obeyed up to 22.5 μg of the metal ion in 7 ml of extract, in both instances. However, slightly higher absorbance values were obtained for the metal dithizonate complex at higher metal ion concentrations in the working range (Fig. 1) with the former system.

For the reagent solution after storage for 1 day at 10°C in diffuse light, the absorbance values were comparable to that of the dithizone–chloroform reagent (absorbance at 600 nm = 1.67 and at 450 nm = 0.65) and, as possible stabilization of the medium was attained, it remained almost unaltered for the minimum period of 3 weeks tested. However, for this 1-day-old solution the Beer's law upper limit was found to decrease from 22.5 to 17.5 μg and the absorbance values for the metal dithizonate complex remained almost constant thereafter. However, below 17.5 μg of the metal ion, the absorbance values are comparable with that of the fresh solution (Fig. 1) and also no further change in this trend was observed for the same minimum period mentioned with this solution. This discrepancy was also observed to the same extent when 5 ml of the reagent solution were employed and the Beer's law upper limit was found to be 12.5 μg for the 1-day-old solution compared with 17.5 μg for the fresh acetic acid–dithizone–chloroform solution. An experiment carried out at either 20 or ca. 35°C in diffuse light gave the same trend.

This increased absorbance in acetic acid medium is possibly due to its stronger association with the ligand, thereby decreasing the solubility of the ligand in the aqueous phase and keeping the concentration of the ligand in the organic phase high. This in turn would aid extractability, resulting in higher absorbance values. The decreased Beer's law limit for 1-day old solution is probably due to the more stronger association which may lead to insufficient ligand concentration in the aqueous phase resulting in earlier saturation.

The trend observed with the absorbance values clearly indicates the continued association of acetic acid with the ligand both during and after extraction in the organic phase, although some might have been back-extracted. This is an added advantage for the stabilization of the metal dithizonate complex against light conditions as reported earlier [13], which involves the use of acetic acid in the aqueous phase for this purpose during extraction. Supporting this, the metal–ligand complex was found to be stable for a minimum of 2 days in daylight and at high room temperature (ca. 35°C) under laboratory conditions.

The reagent stored at room temperature (maximum $\geqslant$ 35°C, minimum 26°C) and in diffuse light can be used effectively for 3 days without any change in the Beer's law limit or in the absorbance values. Subsequently a decreasing trend was observed as mentioned earlier, which starts slowly and saturates within 3–4 days. This trend shows that a longer time is required for the enhanced association of acetic acid with the ligand kept at higher room temperatures.

The original stock solution (0.01%) stored at 10°C in diffuse light gave identical 0.001% solutions for at least 1 month. It can also be stored without any deterioration at 18–20°C, and exposed to the maximum daylight possible under laboratory conditions in a mildly air-conditioned

room for the same minimum duration. It could also be stored at room temperature (ca. 35°C) in diffuse light for a minimum of 20 days tested.

The development of a new absorption peak at 312.5 nm by suppressing the characteristic peak for dithizone was not observed with these solutions, i.e. one stored at 10°C (tested for 3 weeks) and the other at room temperature (ca. 35°C, tested for 10 days) under diffuse light conditions. This is in accordance with an earlier report [5] in which the absorption peak (at 312.5 nm) started to appear notably after a period of 4 days due to the photochemical formation of thiadiazoline products. However, this is for a simple dithizone solution containing a higher concentration of acetic acid (ca. 10-fold excess) in the absence of chloroform under unspecified storing conditions.

Mode of stabilization

The primary cause of the deterioration of dithizone in chloroform medium was reported to be due to abstraction of hydrogen from dithizone by phosgene [3] originating from the photochemical degradation of chloroform. The use of acetic acid with this solution may hinder this process by protecting the reagent through hydrogen bonding. In a similar way, condensation of the aldehydic and ketonic impurities with the ligand by hydrogen abstraction, thus leading to its deterioration [5], is possibly also prevented. Moreover, as the reagent is taken in chloroform medium and acetic acid is not added directly but by an equilibration (phase-transfer) process, the possibility of incipient rapid association of these impurities with the reagent is minimized to a great extent as their effective concentration is very low under this condition whereas the well distributed acetic acid associates and protects the reagent favourably through hydrogen bonding. These factors permit the solution to be prepared in daylight and at a high room temperature without any damage to the reagent and to be stored for a reasonable period of time.

Conclusion

Dithizone solution equilibrated with 6 M acetic acid is more suitable for routine determination of metal ions as no stringent care needs to be taken with respect to light and high temperature either during preparation of the reagent or in its use. As the stock solution is stable for a reasonable length of time, the reagent is also fit for infrequent use. This eliminates the need for standardization of the stock solution before each set of experiments and the purification of the reagent and/or the solvent before use.

One of the authors (N.T.) thanks UGC, India, for financial assistance.

REFERENCES

1 H.M.N.H. Irving, Dithizone (Analytical Sciences Monograph No. 5), Chemical Society, London, 1977.
2 G. Iwantsheff, Das Dithizon und seine Anwendung in der Mikro- und Spurenanalyse, Verlag Chemie, Weinheim, 1958.
3 H.M.N.H. Irving and D.C. Rupainwar, Anal. Chim. Acta, 48 (1969) 187.
4 H.M.N.H. Irving, A.M. Kiwan, D.C. Rupainwar and S.S. Shota, Anal. Chim. Acta, 56 (1971) 205.
5 H.M.N.H. Irving and U.S. Mahnot, Talanta, 15 (1968) 811.
6 H.M.N.H. Irving and U.S. Mahnot and D.C. Rupainwar, Anal. Chim. Acta, 49 (1970) 261.
7 I. Natama and D. Matukawa, J. Biochem. (Tokyo), 30 (1939) 395.
8 D.A. Biddle, Ind. Eng. Chem., Anal. Ed., 8 (1936) 99.
9 S. Alegret, M. Blanco and J.M. Paul, Anal. Chim. Acta, 177 (1985) 285.
10 L.S. Meriwether, E.C. Breitner and C.L. Sloan, J. Am. Chem. Soc., 87 (1965) 4441.
11 P. Grey and G.C.B. Cave, Can. J. Chem., 47 (1969) 4543.
12 A.I. Vogel, Text Book of Quantitative Inorganic Analysis, Longman, 4th edn., 1985, p. 308.
13 J.F. Peith and K.W. Gerritsma, Recl. Trav. Chim. Pays-Bas, 64 (1945) 4.

Analytica Chimica Acta, 269 (1992) 273–279
Elsevier Science Publishers B.V., Amsterdam

Automatic kinetic method for the determination of reduced glutathione in blood

Rafael Jiménez-Prieto, Antonio Velasco, Manuel Silva and Dolores Pérez-Bendito

Department of Analytical Chemistry, Faculty of Sciences, University of Córdoba, E-14004 Córdoba (Spain)

(Received 21st February 1992; revised manuscript received 5th June 1992)

Abstract

A simple kinetic method is reported for the determination of reduced glutathione (GSH) by the continuous addition of reagent technique that is suitable for routine analyses in blood samples. The method is based on the oxidation reaction between GSH and copper(II) in a weakly acidic medium in the presence of neocuproin to form the coloured copper(I)–neocuproin complex, the rate of formation of which is monitored spectrophotometrically. Two kinetic methodologies were tested for the determination of GSH. The calibration graph was linear over a wide range, 1.6×10^{-6}–1.6×10^{-4} M (R.S.D. $\approx 2\%$), and the method is fairly selective and offers several advantanges over the classical 5,5′-dithiobis(2-nitrobenzoic acid) method for the routine determination of GSH in blood samples, namely ease of automation, faster sample throughout and no need for a blank.

Keywords: Kinetic methods; UV–Visible spectrophotometry; Blood; Reduced glutathione

The tripeptide glutathione (γ-L-glutamyl-L-cysteinylglycine, GSH) is the major intracellular thiol and occurs in many physiological fluids and animal, plant and microbial cells and has a number of biologically significant functions [1]. A variety of methods have been developed for its determination. Among these, liquid chromatographic methods are among the more frequently used in conjunction with pre- or postcolumn derivatization procedures for the separation and determination of this tripeptide by using various detection systems (e.g., spectrophotometric [2,3], spectrofluorimetric [4–10] and electrochemical [11–16]). However, these determinations may occasionally involve side-reactions. Other alternatives recently reported for the determination of GSH include titrimetric [17–20], spectrophotometric [21,22], spectrofluorimetric [23,24]), and enzymatic [25–29] methods. The non-enzymatic methods are generally less selective, because other reductants present in the sample may also be detected. The non-chromatographic method most commonly used for determining GSH is based on its reaction with 5,5′-dithiobis(2-nitrobenzoic acid) (DTNB) to form a highly coloured anion with maximum absorption at 412 nm [30]. This method is the standard for the determination of GSH in biological fluids such as blood samples [31] and has also been used for the determination of GSH in mixtures with cysteine by the stopped-flow technique [32] and for the simultaneous determination of oxidized and reduced glutathione [33].

This paper reports a very simple method for the determination of GSH by the continuous addition of reagent (CAR) technique using spectrophotometric detection. The method is based on the reducing action of GSH on copper(II) in the presence of neocuproin to form the copper

Correspondence to: D. Pérez-Bendito, Department of Analytical Chemistry, Faculty of Sciences, University of Córdoba, E-14004 Córdoba (Spain).

(I)–neocuproin complex. The method was applied to blood samples and the results were compared with those provided by the classical DTNB method.

EXPERIMENTAL

Reagents

All reagents were of analytical-reagent grade. A 3.25×10^{-3} M stock solution of reduced glutathione was prepared daily by dissolving 100.0 mg of GSH (Sigma) in 100 ml of doubly distilled water. A 8.65×10^{-3} M stock solution of neocuproin (2,9-dimethyl-1,10-phenanthroline) was made by dissolving 180 mg of reagent in 100 ml of ethanol. A 3.15×10^{-2} M copper(II) stock solution was prepared by dissolving 2.000 g of pure electrolytic copper in the minimum volume of 1 + 1 nitric acid and diluting to 1 l with 1% (v/v) nitric acid. A sodium acetate–acetic acid buffer was made by mixing 4.12 g of the salt and 54.3 ml of concentrated acid in 500 ml of distilled water. Under these conditions, the solution was 0.1 M in sodium acetate and 1.9 M in acetic acid and the final pH was 3.5. The following solutions were used for the determination of GSH by the DTNB method: a stock DTNB solution prepared by dissolving 40.0 mg of reagent (Sigma) in 100 ml of 0.1% sodium citrate; and a phosphate solution made by dissolving 42.59 g of Na_2HPO_4 in 1 l of distilled water. Blood samples required a precipitating solution containing 4.014 g of trichloroacetic acid and 30.0 g of sodium chloride in 100 ml of distilled water.

Apparatus

All kinetic measurements were made on a CAR system described previously [34] and were acquired and processed by a microcomputer. A Hanna HI 8418 pH meter was also used.

Kinetic determination of reduced glutathione

The reaction vessel of the CAR system was filled with a solution containing between 30 and 3000 μg of reduced glutathione, 5.0 ml of 8.65×10^{-3} M ethanolic neocuproin and 6.0 ml of sodium acetate–acetic acid buffer (pH 3.5) in 60 ml of distilled water. The reaction was started by adding 3.15×10^{-2} M copper(II) solution from the autoburette at a rate of 1.0 ml min^{-1} while stirring at 200 rpm. The absorbance was monitored at 455 nm and a data acquisition rate of 250 ms per point. The initial and maximum reaction methods recently developed on the basis of the CAR technique [35] were applied to the kinetic curve and the concentration of GSH in the sample was determined from a calibration graph.

Determination of GSH in blood samples

In a 50-ml beaker were mixed 0.8 ml of whole blood and 7.2 ml of distilled water for a haemolysation and then 12.0 ml of precipitating solution. The mixture was allowed to stand for 5 min at room temperature and subsequently filtered through coarse-grade filter-paper. Then 10.0- and 2.0-ml aliquots were processed as described above for the GSH determination by the CAR and DTNB methods, respectively.

RESULTS AND DISCUSSION

Many of methods available for the determination of GSH by redox reactions are subject to a large number of interferences. In this work, a new chemical system was chosen for the determination of this tripeptide in order to improve the selectivity, namely the rapid oxidation of GSH by copper(II) in the presence of neocuproin to form the copper(I)–neocuproin complex. The reaction was monitored through kinetic measurements which surpass equilibrium measurements in selectivity [36]. This copper(II)/copper(I)–neocuproin chemical system had not been used previously in kinetic-based analytical methods. A similar chemical system, viz., the reversible transformation of ferroin–ferriin complexes, was used recently for indication purposes with good results [37–41].

Figure 1 shows a typical kinetic curve provided by the CAR technique on addition of copper(II) at a constant rate to a much more dilute GSH solution containing neocuproin and the buffer, and monitoring of the reaction spectrophotometrically at 455 nm [the wavelength of maximum absorbance of the copper(I)–neocuproin com-

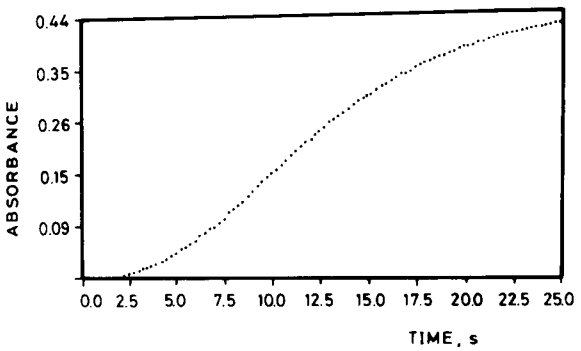

Fig. 1. Absorbance vs. time plot obtained in the determination of 10 μg ml^{-1} of reduced glutathione by the CAR technique. For experimental conditions, see text.

plex]. From the integral form of the overall reaction-rate equation, which includes the reaction and dilution rates, two kinetic methods were used: the initial reaction method, on account of the linear dependence of the analytical signal on t^2 (t = time) in the early stages of the reaction (the slope of the signal vs. t^2 plot is proportional to the analyte concentration); and the maximum reaction method, which relies on the linear relationship between the slope of the straight portion of the kinetic curve and the analyte concentration. Both methods were recently developed [35].

Effect of variables

The kinetic determination of GSH is influenced by several variables, both instrumental and chemical, which must be studied and optimized in order to obtain as accurate and reproducible results as possible. All concentrations quoted here are referred to the volume in the reaction vessel or the autoburette.

The effect of the rate of addition of the copper(II) solution (500 μg ml^{-1}) was studied over a broad range, viz., between 0.05 and 8.0 ml min^{-1}. The results found by using the maximum reaction method are shown in Fig. 2a, which is a plot of this kinetic parameter against the square root of addition rate, in accordance with the theoretical basis for the CAR technique [35]. The two parameters were found to be almost linearly related, as in the initial reaction method, where the reaction rate is plotted against the rate of addition. An addition rate of 1.0 ml min^{-1}, which lay within the straight portion of the plot, was selected for further experiments. Higher addition rates could be used with the only advantage of a shorter reaction time (e.g., the reaction took ca. 25 s to develop for 1.0 ml min^{-1} compared with ca. 10 s for 5.0 ml min^{-1}). This made virtually no difference to the sample throughput, but resulted in increased irreproducibility in the reaction rate

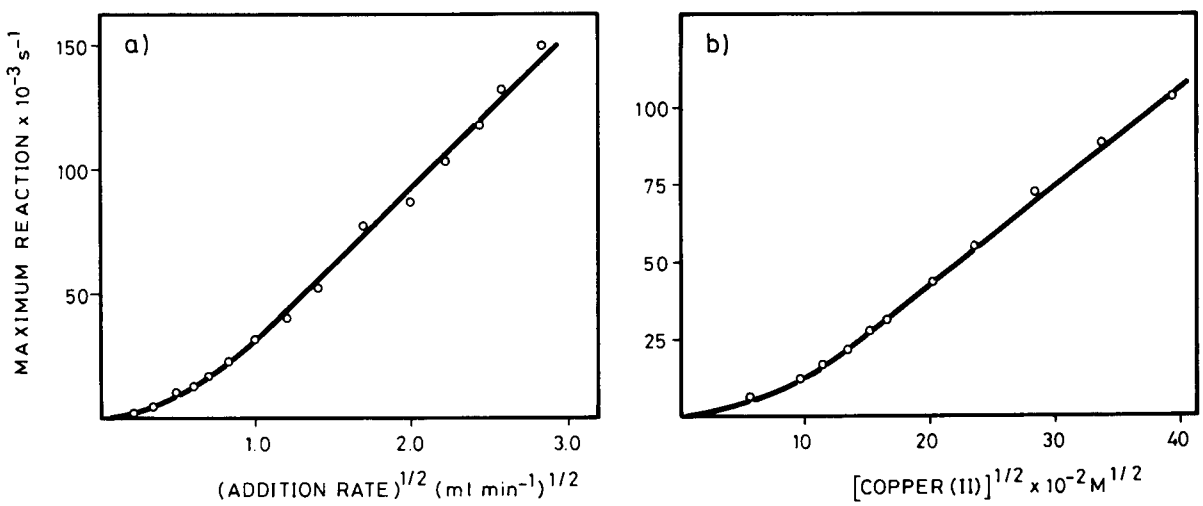

Fig. 2. Effect of (a) rate of addition and (b) copper(II) concentration on the maximum reaction of 10 μg ml^{-1} of reduced glutathione. For details, see text.

measurements, especially with the initial reaction method. The stirring speed and the initial sample volume were fixed at 200 rpm and 60 ml, respectively, which were the optimum values found in previous determinations by the CAR technique [42].

The influence of the copper(II) concentration was also assessed over a wide range (4.72×10^{-3}–1.57×10^{-1} M). The absorbance vs. time curves obtained showed that both reaction rates increased with increase in copper(II) concentration (Fig. 2b shows the dependence in relation to the maximum reaction). The relationships were similar to that of the addition rate, and the following regression equations were obtained for their straight portions:

$$\text{maximum reaction} = -2.27 \times 10^{-2} + 0.338[\text{copper(II)}]^{1/2}$$
$$r = 0.997,\ n = 8$$
$$\text{initial reaction} = -3.09 \times 10^{-4} + 9.57 \times 10^{-2}[\text{copper(II)}]$$
$$r = 0.997,\ n = 8$$

where the copper(II) concentration is expressed in mol l^{-1}. The relatively large intercepts obtained result from the deviations of the linear regression equations at low concentrations of copper(II). A 3.15×10^{-2} M copper(II) concentration was chosen for subsequent experiments.

The influence of the neocuproin concentration on the reaction rates was studied over the range 2.84×10^{-4}–3.22×10^{-3} M. The plot of the maximum reaction vs. neocuproin concentration shows an inverse, non-linear relationship (Fig. 3), similar to that obtained in the application of the initial reaction method. A 7.26×10^{-4} M neocuproin concentration was consequently selected for use. One other variable that is closely related to the neocuproin solution is the amount of ethanol used to dissolve this reagent. An increase in ethanol content from 8.3 to 90% increased the irreproducibility of the results. The final solution adopted was 5.0 ml of 8.65×10^{-3} M ethanolic neocuproin in a final volume of 60 ml in the reaction vessel.

The effect of pH on the reaction rates was studied over the range 3.5–5.5. A pseudo-zero-order dependence was found throughout this interval for both for maximum and the initial reaction methods, and a pH of 4.7 was adopted for subsequent experiments, being adjusted and maintained by using 2.0 M acetic acid–sodium acetate buffer. This pH was similar to that used in the spectrophotometric determination of copper with neocuproin [43].

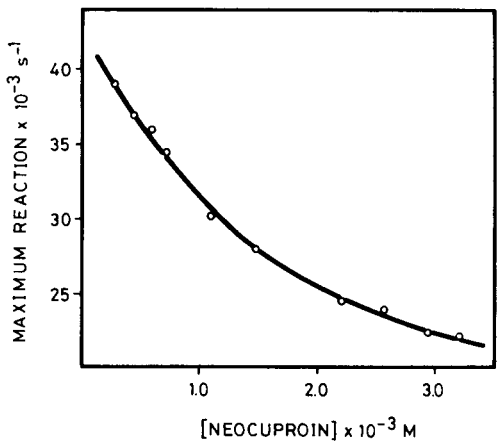

Fig. 3. Effect of neocuproin concentration on the maximum reaction. Reduced glutathione concentration = 10 μg ml^{-1}. For other experimental conditions, see text.

From the above results, the kinetic determination of GSH by the CAR technique can be assumed to rely on the following reaction scheme:

$$2\ \text{GSH} + 2\ \text{Cu(II)} \rightarrow \text{GS–SG} + 2\ \text{Cu(I)} + 2\ \text{H}^+ \quad (1)$$

$$\text{Cu(I)} + 2\ \text{neocuproin} \rightarrow \text{Cu(neocuproin)}_2^+$$
$$2\ \text{neocuproin} + \text{Cu(II)} \rightarrow \text{Cu(neocuproin)}_2^{2+} \quad (2)$$

where GS–SG is oxidized glutathione.

Copper(II) can react competitively with GSH (Eqn. 1) or neocuproin (Eqn. 2) to a greater or lesser extent depending on the ratio between their concentrations and the rate of each process. Increased neocuproin concentrations favour the formation of the copper(II)–neocuproin complex (Eqn. 2), thereby decreasing the actual copper(I) concentration in the reaction medium, and hence diminishing the reaction rate (see Fig. 3). This

TABLE 1

Comparison of the features of the maximum and initial reaction rate methods in the determination of GSH with the copper–neocuproin system by the CAR technique

Figure of merit	Maximum reaction method	Initial reaction method
Dynamic linear range (M)	1.63×10^{-6}–7.82×10^{-5}	4.89×10^{-6}–1.63×10^{-4}
Detection limit (M)	5.0×10^{-7}	8.7×10^{-7}
Precision (R.S.D.) (%) [a]	1.35	3.87
Sample throughput (h^{-1})	35	40

[a] Eleven determinations of 5.0×10^{-6} M GSH.

seemingly indicates that the reaction between copper(II) and GSH is slower than the formation of the copper(II)–neocuproin complex. This complex, which has not been used for analytical purposes, is relatively stable, showing maximum absorption in the UV region (297 nm). On the other hand, the above reaction scheme also accounts for influence of the addition rate and copper(II) concentration. These variables are closely related to each other, as both directly affect the actual concentration of copper(II) that has been added to the reaction vessel at any time. In fact, a low addition rate or copper(II) concentration (see Fig. 2) results in a large excess of neocuproin and hence in a decreased reaction rate. A pseudo-induction period is also apparent from the above relationships. There is no possibility of the copper(I)–neocuproin complex being formed through the reaction

$$2\ \mathrm{Cu(neocuproin)_2^{2+}} + 2\ \mathrm{GSH} \rightarrow \mathrm{GS{-}SG} + 2\ \mathrm{Cu(neocuproin)_2^{+}} + 2\ \mathrm{H^+}$$

because an increase in the neocuproin concentration would also increase the overall reaction rate, which is inconsistent with the experimental results.

Kinetic determination of traces of GSH

Solutions containing different amounts of reduced glutathione were analysed under the optimum conditions by the maximum and initial reaction methods, the performances of which are compared in Table 1. The detection limits given

TABLE 2

Effect of different concentrations of potential interferents on the determination of 10 μg ml^{-1} (3.2×10^{-5} M) reduced glutathione

Foreign species	Concentration [a] (μg ml^{-1})	Reduced glutathione found (μg ml^{-1})			
		Maximum reaction method	Error (%)	Initial reaction method	Error (%)
Glucose [b]	400	9.95	−0.5	10.15	+1.5
Fructose	200	9.88	−1.2	10.31	+3.1
Uric acid [b]	10	10.34	+3.4	12.38	+23.8
Urea	250	9.98	−0.2	9.85	−1.5
Thiourea	0.75	10.38	+3.8	11.35	+13.5
Ascorbic acid	1.5	11.08	+10.8	54.31	+443
Cysteine	1.0	9.12	−8.84	29.74	+197
N-Acetylcysteine	1.0	11.00	+10.0	21.44	+114
Cystine	125	9.62	−3.8	10.98	+9.8
Methionine	350	9.65	−3.5	9.06	−9.4
Alanine	200	9.93	−0.7	9.61	−3.9
Glycine	100	9.69	−3.1	9.91	−0.9

[a] Maximum concentration tested. [b] The determination was carried out at pH 3.5.

were calculated according to the IUPAC recommended procedure [44]; the sample throughput was calculated from the time taken to perform three replicate analyses including sample changeover in the CAR system (ca. 30 s). As can be seen, both methods can be used for the kinetic determination of GSH; however, the maximum reaction method performs especially well, particularly in terms of precision and detection limit.

Some substances chemically related to GSH such as sulphur-containing amino acids or common concomitants in real samples, such as blood (e.g., glucose, urea, uric acid) were tested for potential interferences. Solution of GSH and each tested compound were mixed to obtain samples containing 10 μg ml^{-1} of GSH and up to 400 μg ml^{-1} of interferent. Table 2 lists the GSH concentrations obtained in the presence of different concentrations of these species by using the maximum and initial reaction methods. As can be seen, the highest selectivity was provided by the maximum reaction method because some of the assayed substances are more powerful reductants than GSH, and react faster, and hence only interfere at the beginning of the reaction. In general, the tested substances are well tolerated, although in some instances (e.g., glucose and uric acid) the assays were carried out at pH 3.5 rather than the selected pH 4.7 in order to raise the tolerance to these compounds, which permitted the application of the proposed method to the determination of GSH in blood samples. The selectivity factors for these substances were 4.0 and 10.0 for glucose and uric acid, respectively. A pH of 3.5 was accordingly chosen for further experiments, namely the determination of GSH in blood samples. The effects of thiourea, ascorbic acid, cysteine and *N*-acetylcysteine were more troublesome because they were tolerated in an interferent to GSH ratio of only ca. 1:10, but this is of little concern as they rarely occur at higher levels in blood samples.

Determination of GSH in blood samples

The determination of reduced glutathione is essential to many clinical diagnoses. Thus, increased GSH levels are typical of myeloproliferative disorders, whereas markedly decreased levels are associated with malnutrition, renal and hepatic failure, diabetes, mental diseases and deficiencies in glucose-6-phosphate dehydrogenase, 6-phosphogluconate dehydrogenase and vitamin B_2 [45]. In this context, and in order to validate the proposed kinetic method, the maximum reaction method was applied to the determination of natural GSH in blood samples.

TABLE 3

Determination of reduced glutathione in blood samples

Sample No.	Reduced glutathione found [a] (μg ml^{-1})	
	CAR method	DTNB method
1	176.4 ± 2.6	184.8
2	165.6 ± 2.8	158.4
3	223.2 ± 3.2	207.9
4	175.4 ± 2.4	178.4

[a] Average of three determinations ± S.D.

The samples were processed as described under Experimental and the DTNB method was applied (2.0 ml of sample containing between 10 and 50 μg of GSH were mixed with 8.0 ml of phosphate solution and 1.0 ml of DTNB). The absorbance measured against a reagent blank at 412 nm after 4 min was used to compare the results yielded by the proposed kinetic method on the basis of the maximum reaction method. The results obtained are given in Table 3. As can be seen, both methods provided consistent results, which indicates that the proposed method is suitable for the determination of reduced glutathione in this type of sample. In addition, the proposed method is better suited to routine analyses for GSH than is the batch DTNB method on account of its higher sample throughput (35 h^{-1} vs. 5 h^{-1} for three replicate analyses) and the lack of a need for a blank solution.

The authors are grateful to the DIGICyT for financial support.

REFERENCES

1 O.W. Griffith, in J. Bergmeyer and M. Grassl (Eds.), Methods of Enzymatic Analysis, Vol. 8, VCH, Weinheim, 3rd edn., 1981, p. 521.

2 D. Beales, R. Finck, A.E.M. McLean, M. Smith and I.D. Wilson, J. Chromatogr., 226 (1981) 498.
3 A.J. Alpert and H.F. Gilbert, Anal. Biochem., 144 (1985) 553.
4 H. Nakamura and Z. Tamura, Anal. Chem., 53 (1981) 2190.
5 H. Nakamura and Z. Tamura, Bunseki Kagaku, 37 (1988) 35.
6 D.A. Keller and D.B. Menzel, Anal. Biochem., 151 (1985) 418.
7 G. Morineau, M. Azoulay and F. Frappier, J. Chromatogr., 467 (1989) 209.
8 A.I. Minchinton, Int. J. Radiat. Oncol., Biol. Phys., 10 (1984) 1503.
9 N.K. Burton and G.W. Aherne, J. Chromatogr., 55 (1986) 253.
10 S. Velury and S.B. Howell, J. Chromatogr., 68 (1988) 141.
11 T. Iwamoto, M. Yoshiura, K. Iriyama, N. Tomizawa, S. Kurihara, T. Lee and N. Suzuki, Jikeikai Med. J., 32 (1985) 245.
12 A.F. Stein, R.L. Dills and C.D. Klaassen, J. Chromatogr., 54 (1986) 259.
13 D. Dupuy and S. Szabo, J Liq. Chromatogr., 10 (1987) 107.
14 W. Buchberger and K. Winsauer, Anal. Chim. Acta, 196 (1987) 251.
15 K. Irayama, T. Iwamoto and M. Yoshiura, J. Liq. Chromatogr., 9 (1986) 955.
16 G. Carro-Ciampi, P.G. Hunt, C.J. Turner and P.G. Wells, J. Pharmacol. Methods, 19 (1988) 75.
17 K.K. Verma, Talanta, 29 (1982) 41.
18 K.K. Verma and A.K. Gupta, Talanta, 29 (1982) 779.
19 K.K. Tiwari and R.M. Verma, Talanta, 30 (1983) 440.
20 B.N. Usha and H.S. Yathirajan, Indian. J. Chem., Sect. A, 23 (1984) 685.
21 C.S.P. Sastry, P. Satyanarayana and M.K. Tummuru, Analyst, 110 (1985) 189.
22 M.K. Tumuru, B.S. Reddy and C.S.P. Sastry, Microchem. J., 36 (1987) 159.
23 K. Imai, T. Toyota and Y. Watanabe, Anal. Biochem., 128 (1983) 471.
24 K. Nakashima, H. Akimoto, K. Nishida, S. Nakatsuji and S. Akiyama, Talanta, 32 (1985) 167.
25 W.O. Griffith, Anal. Biochem., 106 (1980) 207.
26 U. Forsman, Anal. Chim. Acta, 166 (1984) 141.
27 I. Satoh, S. Arakawa and A. Okamoto, Anal. Chim. Acta, 214 (1988) 415.
28 L.R. Kankaanpaa, J. Photochem. Photobiol., B, 2 (1988) 406.
29 C. Hua, M.R. Smyth and C. O'Fagain, Analyst, 116 (1991) 929.
30 F. Tietze, Anal. Biochem., 27 (1969) 502.
31 V.F. Fairbanks and G.G. Klee, in N.W. Tietz (Ed.), Fundamental of Clinical Chemistry, Saunders, Philadelphia, PA, 1987.
32 K. Inouye and M. Matsumoto, Toyo Soda Kenkyu Hokoku, 25 (1981) 13.
33 D. Mergel, G. Andermann and C. Andermann, Methods Findings Exp. Clin. Pharmacol., 1 (1979) 277.
34 M. Márquez, M. Silva and D. Pérez-Bendito, Analyst, 113 (1988) 1733.
35 A. Velasco, M. Silva and D. Pérez-Bendito, Anal. Chem., in press.
36 D. Pérez-Bendito and M. Silva, Kinetic Methods in Analytical Chemistry, Horwood, Chichester, 1988, Chap. 8.
37 E. Pelizzetti and E. Mentasti, Anal. Chim. Acta, 108 (1979) 441.
38 A. Garrido, M. Silva and D. Pérez-Bendito, Anal. Chim. Acta, 184 (1986) 227.
39 M. Carmona, M. Silva and D. Pérez-Bendito, Anal. Chim. Acta, 218 (1989) 313.
40 M. Carmona, M. Silva and D. Pérez-Bendito, Fresenius' Z. Anal. Chem., 334 (1989) 261.
41 M. Carmona, M. Silva and D. Pérez-Bendito, Analyst, 116 (1991) 1075.
42 D. Pérez-Bendito, M. Silva and A. Gómez-Hens, Trends Anal. Chem., 8 (1989) 302.
43 Z. Marczenko, Spectrophotometric Determination of Elements, Horwood, Chichester, 1976, p. 243.
44 G.L. Long and J.D. Winefordner, Anal. Chem., 55 (1983) 712A.
45 J.A. Demetriou, P.A. Drewes and J.B. Gin, in R. Henry, D.C. Cannon and J.W. Winkelman (Eds.), Clinical Chemistry, Harper and Row, Hagerstown, MD, 1974, Chap. 21.

Analytica Chimica Acta, 269 (1992) 281–287
Elsevier Science Publishers B.V., Amsterdam

Detection of organophosphate and carbamate pesticides using disposable biosensors based on chemically modified electrodes and immobilized cholinesterase

Petr Skládal

Department of Biochemistry, Masaryk University, Kotlářská 2, 611 37 Brno (Czechoslovakia)

(Received 7th April 1992; revised manuscript received 23rd June 1992)

Abstract

An amperometric biosensor for the detection of organophosphate and carbamate pesticides was constructed as a disposable strip containing a cobalt phthalocyanine-modified carbon composite electrode and a cross-linked cholinesterase layer. With butyrylthiocholine as substrate, enzymatically produced thiocholine was oxidized at +250 mV. The steady-state current, I_{ss}, was used as a measure of the enzyme activity. In the presence of pesticides, an irreversible inhibition of cholinesterase occurred, resulting in a decrease in the rate of current change, dI/dt. The ratio $(dI/dt)/I_{ss}$ was used for evaluations. The influence of the cholinesterase loading and the cholinesterase to glutaraldehyde ratio on the biosensor response was studied and the measuring conditions (pH, temperature, substrate concentration) were optimized. Detection limits of 0.30, 1.2 and 11 nmol l^{-1} for paraoxon, dichlorvos and carbaryl, respectively, were achieved. The time of inhibition varied from a few seconds (high pesticide concentrations) to 6 min required for reliable measurements at levels close to the detection limit. When the analysis was performed by 10 min preincubation of the biosensor or free cholinesterase with sample, paraoxon concentrations above 3.0 nmol l^{-1} could be detected.

Keywords: Amperometry; Biosensors; Carbamate pesticides; Organophosphorus pesticides; Pesticides

Monitoring of organophosphate and carbamate pesticides is of considerable importance. These pesticides are preferred in agriculture for their relatively low persistence in the environment, but some of them exhibit fairly high acute toxicity [1]. Consequently, detection systems are required for the protection of living organisms and for the identification of pesticide residues in food products.

Biosensors for the detection of these substances are mostly based on acetylcholinesterase (AChE) (E.C. 3.1.1.7) or cholinesterase (ChE) (E.C. 3.1.1.8). In the reaction of cholinesterases with inhibitors, first an enzyme–inhibitor complex is formed, which is subsequently converted into an inactive phosphorylated (or carbamylated) form of enzyme [2]. This mechanism explains the inhibitory action of pesticides and it can also be used as a basis for biochemical analysis. Cholinesterases as molecular recognition elements can be combined with a variety of transducers. Thus, pH electrodes [3–7] and pH-sensitive ISFETs [8,9] are very popular, various optical spectrophotometric [10–12] and fluorimetric [13] flow-through systems have been utilized and conductimetric [14], voltammetric [15] and piezoelectric [16] systems have been investigated. When ChE or AChE is used together with choline oxi-

Correspondence to: P. Skládal, Department of Biochemistry, Masaryk University, Kotlářská 2, 611 37 Brno (Czechoslovakia).

dase, the resulting enzyme system can be linked with O_2 or H_2O_2 probes, thus providing amperometric sensors suitable for analyses for pesticides [17–19]. When acetyl- or butyrylthiocholine (BTCh) is chosen as a substrate, thiocholine produced in the enzymatic reaction can be anodically oxidized on platinum [20,21] or mercury [15] electrodes, but a chemically modified carbon electrode (CME) is better suited for this purpose [22–24]. So far, tetracyanoquinodimethane [22] and cobalt phthalocyanine (CoPC) [23,24] have been tested as possible modifiers; both of these mediators permitted the oxidation of thiocholine at potentials substantially lower in comparison with metallic electrodes.

The previous versions of CoPC composite electrodes were linked with a separate enzyme membrane. In this work, a compact disposable enzyme electrode based on CoPC–CME with increased sensitivity was developed and various approaches to the determination of pesticides were investigated.

EXPERIMENTAL

Chemicals

Cholinesterase from horse serum (specific activity 147 nkat mg^{-1} protein) was obtained from USOL (Prague), paraoxon from Sigma (St. Louis, MO) and dichlorvos and carbaryl were kindly provided by Dr. B. Šafář (Institute of Analytical Chemistry, Brno). Cobalt phthalocyanine was supplied by Aldrich (Milwaukee, WI), glutaraldehyde by Reanal (Budapest) and graphite powder (particle size < 50 μm) by Merck (Darmstadt, Germany). All other reagents were supplied by Lachema (Brno).

Construction of biosensors

Plastic sheets ($10 \times 35 \times 0.8$ mm) covered with copper foil (commonly used for electronic links) were used as a support for the biosensors. The copper foil was partially etched away in order to obtain the desired conductive pattern, i.e., a 5-mm diameter disc at one end joined with a 1-mm wide conducting line with the opposite end of the strip. The line was isolated with a layer of epoxy glue, leaving free only a small end part for contact. The remaining free surface of disc was then completely covered with an electrode layer, which was prepared by depositing 10 μl of a suspension obtained by mixing 5 mg of CoPC, 100 mg of graphite powder and 300 μl of 1.5% acetylcellulose solution in acetone–cyclohexanone (1 + 1), similarly to [25]. The resulting electrode had a diameter of 8 mm. The enzyme layer was made by spreading on the dried electrode surface 20 μl of 50 mmol l^{-1} phosphate buffer solution (pH 7.3) containing 125 μg of ChE and 25 μg of glutaraldehyde (the optimized composition, see below). Complete biosensors were ready for use the next day, and were stored dry at 4°C.

Instrumentation and procedures

A three-electrode system, consisting of an Ag/AgCl/saturated KCl reference electrode, platinum counter electrode and the biosensor as working electrode, was used for amperometric measurements. The potential of the working electrode was set at 250 mV using an ADLC 2 detector (Laboratory Instruments, Prague) as a potentiostat. The detector was connected through a 12-bit A/D converter to a PC/AT compatible computer, which was equipped with its own software for data acquisition and evaluation of results. The experiments were done in a thermostated vessel containing 3.5 ml of 50 mmol l^{-1} phosphate (pH 7.3), stirred at 300 rpm.

The activity of free cholinesterase was determined amperometrically with 2 mmol l^{-1} butyrylthiocholine, the bare CoPC modified electrode served for the detection of thiocholine.

Two methods were utilized for the determination of pesticides using biosensors. The previously described [23,24] inhibition in the presence of substrate (0.50 mmol l^{-1} butyrylthiocholine) provided the relative inhibition parameter *RI*, which was calculated as

$$RI = (dI/dt)/I_{ss} \quad (1)$$

where I_{ss} is the biosensor steady-state current with substrate and dI/dt is the rate of decrease of the current observed after the addition of a sample containing pesticide (an inhibitor). The other method was based on a 10-min preincuba-

tion of the biosensor or free cholinesterase in the presence of inhibitor. The percentage inhibition was calculated according to

$$I(\%) = 100(I_{ss1} - I_{ss2})/I_{ss1} = 100(a_1 - a_2)/a_1 \quad (2)$$

Steady-state currents or enzyme activities (a) were determined with 2 mmol l^{-1} butyrylthiocholine; the subscripts 1 and 2 correspond to measurements performed before and after incubation, respectively.

RESULTS AND DISCUSSION

Development of the enzyme layer

For substrate biosensors, diffusion control of the response is preferred, because it provides a wider linear working range. Diffusional limitation is usually achieved for enzyme layers containing high loadings of activity; it can also be realized with the help of an additional control membrane [26]. With biosensors for inhibitors, kinetic control of the response is desired and the signal of the biosensor should be proportional to the content of activity in the enzyme layer. Generally, the lower the enzyme loading, the greater is the sensitivity to inhibitors observed [6,17–19,24].

Here, enzyme layers were prepared by cross-linking of ChE by glutaraldehyde. This method is simple and is widely used in various modifications [3,6,22,23]. However, it has to be used carefully, otherwise layers containing high portions of latent activity could be obtained. During the immobilization, the absolute ChE loading on the sensor (Fig. 1) and the ChE (protein) to glutaraldehyde ratio (Fig. 2) were optimized. The influence on substrate reaction (Fig. 1, inset) was evaluated as the slope of the calibration graph, dI/dc, for BTCh. It increased up to 40 nkat cm^{-2}, then a sharp decrease occurred, which was probably due to the unfavourable thickness of the layer. For low concentrations of inhibitor (paraoxon, 9 nmol l^{-1}, 2.5 $\mu g\ l^{-1}$), maximum inhibition was achieved for sensors containing 37 nkat cm^{-2} ChE (Fig. 1). The fact that maximum sensitivity to inhibition was not achieved for the lowest loading tested

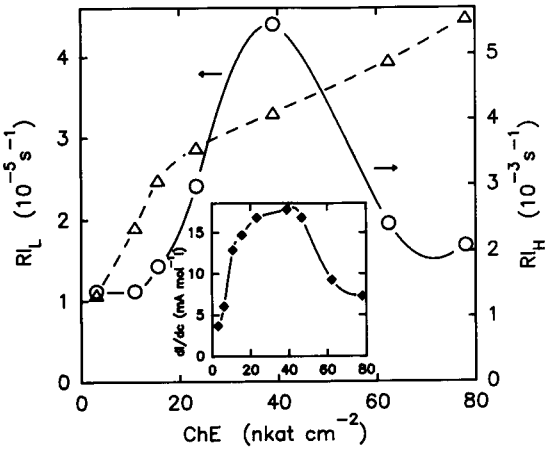

Fig. 1. Effect of ChE content in the enzyme layer on sensor responses to substrate (inset, slope of calibration graph dI/dc, ♦) and inhibitor [inhibitions obtained for 9.0 nmol l^{-1} (○), RI_L, or 3.6 μmol l^{-1} (△), RI_H, paraoxon]. The ChE to glutaraldehyde weight ratio of 1:1 was constant for all enzyme layers being prepared.

corresponds with the previous results with ChE cross-linked on nylon nets [23]. For 3.6 μmol l^{-1} (1 mg l^{-1}) paraoxon, RI increased throughout the whole investigated interval of ChE loadings.

The influence of the ChE to glutaraldehyde ratio on the sensitivity for the substrate is shown in Fig. 2. A maximum is found for the ratio 3:2.

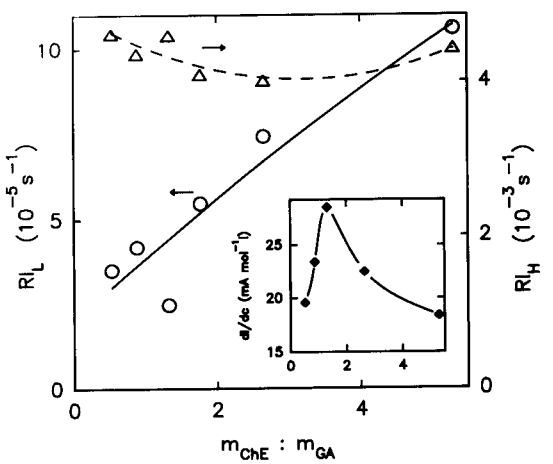

Fig. 2. Effect of ChE to glutaraldehyde ratio on responses to substrate (inset graph) and inhibitor. Symbols as in Fig. 1. 18 nkat of ChE were used for all biosensors.

However, for low pesticide concentrations, the highest *RI* was determined for layers with the lowest glutaraldehyde content (5 : 1 ratio). Inhibitions by higher paraoxon concentrations were not affected. For further measurements, the enzyme layers were prepared from 125 μg of ChE (maximum of RI_L, Fig. 1) and 25 μg of glutaraldehyde. A significant saving of cholinesterase was achieved in comparison with the previously used cross-linking on nylon nets [24]. For the resulting biosensor, the apparent K_m was 4.08 ± 0.63 mmol l^{-1} and I_{max} 51.1 ± 3.2 μA (calculated using non-linear regression, $n = 15$). For soluble ChE, the K_m value was 0.199 ± 0.024 mmol l^{-1} ($n = 7$), which indicates the existence of a diffusional barrier of the sensor even after the optimization with respect to inhibition.

Optimization of the operating conditions

Working potentials from 0 to 500 mV (vs. Ag/AgCl) were tested. The useful signal resulting from thiocholine oxidation increased up to 300 mV; for further measurements, a smaller value of 250 mV was selected because it ensured a lower background current (0.63 μA). Iodide ions did not interfere at this low potential. The optimum pH region from 7.2 to 8.0 was similar to that with previous versions of this sensor [23,24] and with the soluble enzyme [2]. pH 7.3 was selected, which minimizes spontaneous hydrolysis of butyrylthiocholine. Phosphate and borate buffers were studied as working solutions. The sensor current decreased with increasing buffer concentration; a 1.5 times higher response to substrate could be obtained in 5 mmol l^{-1} than 50 mmol l^{-1} phosphate. However, when using the lower concentration, the steady-state current was unstable; similar behaviour was also observed when working in borate buffers. Consequently, 50 mmol l^{-1} phosphate (pH 7.3) was selected as a suitable compromise.

An interesting temperature dependence of biosensor responses to substrate and inhibitor was observed (Fig. 3). Different temperature optima were found for the reaction with substrate and for inhibition, the former being about 30–40°C and the latter reaching its maximum at 50°C. At this temperature, ChE became thermally denatured. Subsequent analyses were performed at 30°C. From Fig. 3 it follows that a constant temperature is very important for precise measurements, because the possible temperature fluctuations could be misinterpreted as false inhibitions.

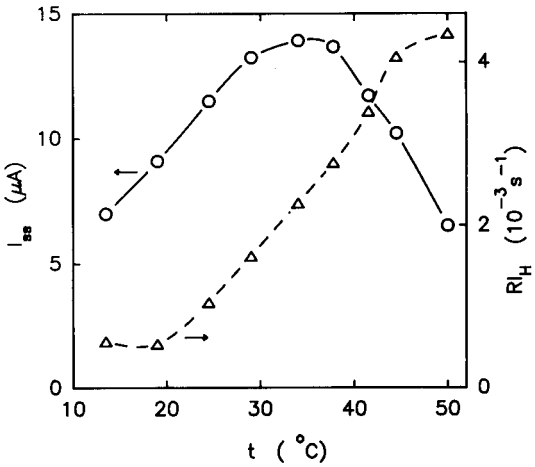

Fig. 3. Temperature dependences of substrate (○) (0.5 mmol l^{-1} butyrylthiocholine) and inhibitor (△) (3.6 μmol l^{-1} paraoxon) reactions of biosensor.

For the determination of inhibitors, the substrate concentration is an important factor. Substrates and inhibitors (organophosphates and carbamates) bind to the same active site of cholinesterase, so that competition exists between them [2]. In the case of soluble enzyme, the rate of ChE inhibition in the presence of substrate could be expressed as [27]

$$d[EP]/dt = k_2 K_m[I]([E]_0 - [EP]) / (K_m[I] + K_m K_d + K_d[S]) \quad (3)$$

where K_d is the dissociation constant of the enzyme–inhibitor complex EI, k_2 is the rate constant of transformation of EI to the phosphorylated enzyme EP, K_m is the Michaelis constant for ChE, [I] and [S] are concentrations of inhibitor and substrate, respectively, and $[E]_0$ is the initial ChE concentration.

For kinetically controlled operation of biosensors, dI/dt is proportional to $d[EP]/dt$ and I_{ss} to $[E]_0 - [EP]$; even if the constants of proportionality are unknown, they could be assumed to

be equal. Then, for the proposed measurement of pesticides, the Eqn. 3 may be rearranged to

$$RI = k_2 K_m[I]/(K_m[I] + K_m K_d + K_d[S]) \quad (4)$$

This could be used for the interpretation of the results in Fig. 4, where dependences of *RI* and the absolute rate of current decrease, dI/dt on the substrate concentration are presented. The observed hyperbolic dependence of *RI* on [S] is in good agreement with Eqn. 4; a more detailed study of this problem will be published elsewhere. From the practical point of view, the lowest substrate concentrations are not useful because the signal is small in comparison with the background current. For analysis, 0.5 mmol l^{-1} butyrylthiocholine was chosen as a reasonable compromise.

Various methods for pesticide determination

Three approaches to the analysis were compared, preincubation of the biosensor or free ChE with inhibitor and the proposed inhibition in the presence of substrate. The incubation approach is based on the widely used equation of Aldridge [28]:

$$\Delta \ln a = k_i[I]t \quad (5)$$

where k_i is the inhibition bimolecular rate constant ($k_i = k_2/K_d$) and $\Delta \ln a$ is the difference in the logarithms of ChE enzyme activities (in chosen units) measured before and after the incubation with inhibitor for time t. It is evident that the extent of inhibition is directly proportional to the time of incubation and this fact is often used to make detection more sensitive. Thus, analyses are performed for 30–60-min incubation [5,17]. The incubation methods have recently been automated by using stopped flow techniques [7,11,12]. Here, 10-min incubations with samples were performed. Calibration graphs for the biosensor and for an equal amount of free ChE are shown in Fig. 5. Both methods exhibit comparable detection limits (defined as the concentration required for 5% inhibition) equal to 3.0 nmol l^{-1} paraoxon. The advantage of immobilized ChE is the much wider working range. For free ChE, 0.6 μmol l^{-1} paraoxon represents the upper limit for measurements, whereas up to 0.12 mmol l^{-1} could be determined with the biosensor, which could even be used for several analyses provided that zero or very low concentrations of inhibitors had been detected during previous measurements.

The experimental traces obtained with the other method are shown in Fig. 6. As can be seen, the steady state after the addition of substrate is established quickly (95% of steady state

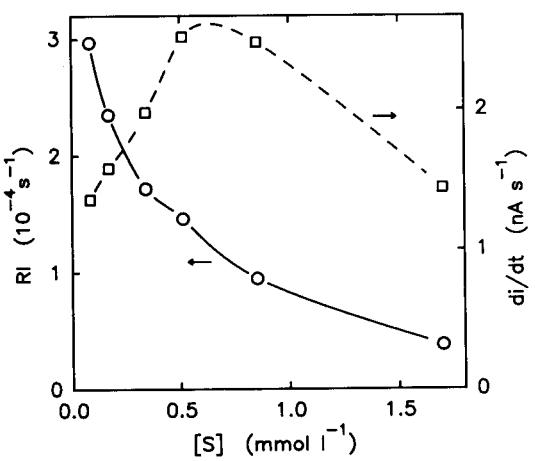

Fig. 4. Influence of substrate concentration on the inhibition by paraoxon (9.0 nmol l^{-1}). The effects on the absolute rate of current decrease, dI/dt (□), or *RI* (○) are demonstrated.

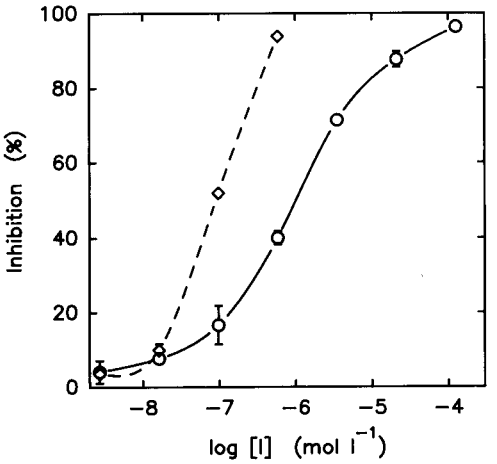

Fig. 5. Calibration graphs for determinations of paraoxon using 10-min preincubation with sample. The measurements with the biosensor (○) or with an equal amount (18 nkat) of free ChE (◇) are compared. Inhibitions were calculated according to Eqn. 2. Experimental points represent averages of three measurements; standard deviations are shown as error bars.

after 45 s). The total time required for a complete analysis depends also on the washing time (less than 3 min) and especially on the period required for reliable determination of dI/dt. This can range from several seconds for high pesticide concentrations up to ca. 6 min necessary for the lowest nanomolar levels, when the influence of noise has to be considered. A limiting value of *RI* is ca. 5×10^{-5} s, it is also used for the definition of the limit of detection. For measurements of low concentrations, when the current decrease is very small compared with the initial I_{ss}, the approach has to be slightly different than in Fig. 6; the relatively high I_{ss} is almost completely compensated for and a greater sensitivity of the detector is utilized.

Calibration graphs for selected pesticides are shown in Fig. 7. The shape of these graphs corresponds with Eqn. 4 only for higher inhibitor concentrations; below micromolar levels, higher *RI*s were obtained than expected, probably owing to the adsorption of pesticides in the more hydrophobic environment of the enzyme layer. Based on the above-stated *RI* limit, 0.30, 1.2 and 11 nmol l^{-1} concentrations of paraoxon, dichlorvos and carbaryl could be detected. This method therefore exhibits better sensitivity than the incubation approach. The detection limit is significantly improved by 1000 and 18 times in comparison with the carbon paste and cross-linked enzyme membrane [23] and with the sensor based on ChE covalently bound to nylon net [24], respectively. The practical use of a strip sensor is also easier than working with separate electrodes and enzyme membranes. The proposed method achieves the published detection limits for paraoxon obtained by incubation approaches, for which concentrations from 0.1 nmol l^{-1} to micromolar levels have been reported [5–7,10–12,17,18].

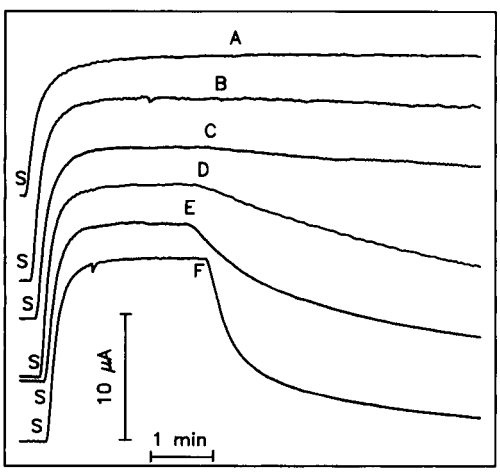

Fig. 6. Examples of experimental traces obtained during determinations of pesticides. S indicates addition of substrate and A–F show additions of paraoxon to final concentrations of 32, 160 and 800 nmol l^{-1} and 4, 20 and 100 μmol l^{-1}, respectively.

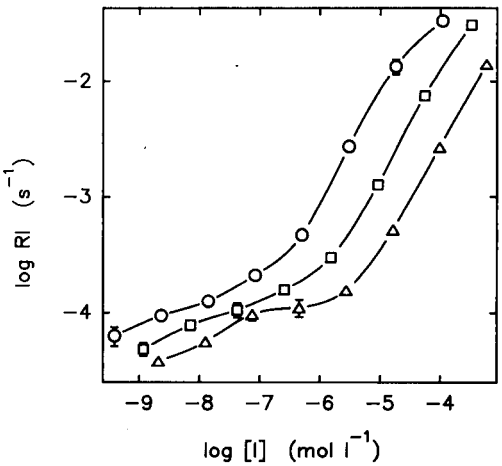

Fig. 7. Calibration graphs for (○) paraoxon, (□) dichlorvos and (△) carbaryl determined by measuring the inhibition in the presence of substrate. Experimental points represent averages of three measurements, standard deviations are shown as error bars.

This biosensor can be used as a basis for the construction of continuously working monitoring systems for pesticides and for measurements of separate samples. The most important advantages are the short time of analysis and possible application in various analytical arrangements.

REFERENCES

1 R. Cremlyn, Pesticides – Preparation and Mode of Action, Wiley, Chichester, 1978, p. 213.
2 M. Eto, Organophosphorus Pesticides: Organic and Biological Chemistry, CRC, Boca Raton, FL, 1974, p. 123.
3 P. Durand, J. Mallevialle and J.M. Nicaud, J. Anal. Toxicol., 8 (1984) 112.

4 C. Tran-Minh, Ion-Sel. Electrodes Rev., 7 (1985) 41.
5 C. Tran-Minh, P.C. Pandey and S. Kumaran, Biosensors Bioelectron., 5 (1990) 461.
6 S. Kumaran, H. Meier, A.M. Danna and C. Tran-Minh, Anal. Chem., 63 (1991) 1914.
7 S. Kumaran S. and C. Tran-Minh, Anal. Biochem., 200 (1992) 187.
8 J. Janata, R.J. Huber, R. Cohen and E.S. Kolesar, Aviat. Space Environ. Med., 52 (1981) 666.
9 K.R. Rogers, M. Foley, S. Alter, P. Koga and M. Eldefrawi, Anal. Lett., 24 (1991) 191.
10 O. Wolfbeis and E. Koller, in R.D. Schmid and F. Scheller (Eds.), GBF Biosensor Workshop, GBF Monographs, Vol. 13, VCH, New York, 1989, p. 221.
11 R. Kindervater, W. Kunnecke and R.D. Schmid, Anal. Chim. Acta, 234 (1990) 113.
12 M.F. Leon-Gonzales and A. Townshend, Anal. Chim. Acta, 236 (1991) 267.
13 K.R. Rogers, C.J. Cao, J.J. Valdes, A.T. Eldefrawi and M. Eldefrawi, Fundam. Appl. Toxicol., 16 (1991) 810.
14 J.M. Wallach, Gov. Rep. Announce. Index (U.S.), 90 (1990) Abstr. 039 166.
15 E.P. Medyantseva, G.K. Budnikov and S.S. Babkina, Zh. Anal. Khim., 45 (1990) 1386.
16 G.G. Guilbault and J. Ngeh-Ngwainbi, in G.G. Guilbault and M. Mascini (Eds.), NATO ASI Ser. C: Mathematical and Physical Sciences, Vol. 226, Reidel, Dordrecht, 1989, p. 187.
17 M. Bernabei, C. Cremisini, M. Mascini and G. Palleschi, Anal. Lett., 24 (1991) 1317.
18 L. Campanella, M. Achilli, M.P. Sammartino and M. Tomassetti, Bioelectrochem. Bioenerg., 26 (1991) 237.
19 U. Wollenberger, K. Setz, F. Scheller, U. Loffler and W. Gopel, Sensors Actuators B, 4 (1991) 257.
20 L.H. Goodson and W.B. Jacobs, Methods Enzymol., 44 (1976) 647.
21 R. Gruss, F. Scheller, M.J. Shao and C.C. Liu, Anal. Lett., 22 (1989) 1159.
22 J. Kulys and E.J. D'Costa, Biosensors Bioelectron., 6 (1991) 109.
23 P. Skládal, Anal. Chim. Acta, 252 (1991) 11.
24 P. Skládal and M. Mascini, Biosensors Bioelectron., 7 (1992) 335.
25 S.A. Wring, J.P. Hart and J.B. Birch, Analyst, 116 (1991) 123.
26 L.X. Tang and P.M. Vadgama, in D.L. Wise (Ed.), Bioinstrumentation, Research, Development and Applications, Dekker, New York, 1991, p. 211.
27 I.M. Kovach, J. Enzyme Inhib., 4 (1991) 201.
28 W.N. Aldridge, Biochem. J., 46 (1950) 451.

Analytica Chimica Acta, 269 (1992) 289–300
Elsevier Science Publishers B.V., Amsterdam

Evaluation of coating materials used on piezoelectric sensors for the detection of organophosphorus compounds in the vapour phase

Olga S. Milanko and Stevan A. Milinković

Institute for Technical and Medical Protection (ITMP), Katanićeva 15, 11000 Belgrade (Yugoslavia)

Ljubinka V. Rajaković

Department of Analytical Chemistry, Faculty of Technology and Metallurgy, University of Belgrade, Karnegijeva 4, 11000 Belgrade (Yugoslavia)

(Received 13th April 1992; revised manuscript received 12th June 1992)

Abstract

Several materials were evaluated as possible coatings for a sensitive, reversible and reproducible piezoelectric sensor for organophosphorus compounds (diisopropylmethyl phosphonate and *O,O*-dimethyl-2,2-dichlorovinyl phosphate). A few experiments were also done with malathion. The effects of coating material, concentration and type of compound on sensitivity, reversibility and reproducibility were investigated. Mechanisms for the interaction between target vapour and coatings are proposed and briefly discussed.

Keywords: Piezoelectric sensors; Coatings; Organophosphorus compounds;

The use of piezoelectric crystals as chemical sensors depends, almost entirely, on the availability of appropriate coatings. Since the introduction of this technique, dozens of substrates have been tried as possible coatings for the detection of organophosphorus compounds, e.g., pesticides, chemical warfare agents and their simulants. Most papers dealing with the use of bulk-wave piezoelectric sensors for organophosphorus compounds in the vapour phase are by Guilbault and co-workers [1–9]. Most of the work was aimed at finding a selective coating, as it is well known that a lack of selectivity is the principal drawback of the technique. However, there are applications in which the absolute selectivity is not an essential feature. Sometimes, only group selectivity is required or even none at all, because the task is to determine the concentration of a known agent in the absence of interfering substances (a common situation in laboratory conditions). Under these circumstances, sensitivity, reversibility and reproducibility become the predominant requirements.

Sensor sensitivity is determined by the efficiency with which the coating sorbs the target vapour. Reversibility depends mainly on the nature of the interaction between coating and vapour, whereas sensor reproducibility is affected by various factors, mostly related to the methodology of coating application and frequency measurement technique.

Previous work [10] resulted in the development of a dynamic apparatus for generating precise

Correspondence to: Lj.V. Rajaković, Department of Analytical Chemistry, Faculty of Technology and Metallurgy, University of Belgrade, Karnegijeva 4, 11000 Belgrade (Yugoslavia).

concentrations of selected chemical vapours and a method for the automatic and continuous determination of crystal resonance frequency in the flow-through system.

In this work, several materials were evaluated as possible coatings for a sensitive, reversible and reproducible piezoelectric sensor for organophosphorus compounds. Two compounds, diisopropylmethyl phosphonate (DIMP) and *O,O*-dimethyl-2,2-dichlorovinyl phosphate (DDVP), were chosen because they represent two different types of organophosphorus compounds and because they are volatile enough to permit the generation of desired vapour concentrations without excessive heating.

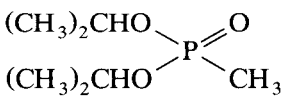

DIMP

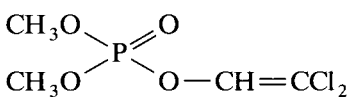

DDVP

EXPERIMENTAL

Reagents

Triton X-100 [polyethylene glycol *p*-(1,1,3,3-tetramethylbutyl)phenyl ether] and L-histidine monohydrochloride were obtained from Merck. Bovine serum albumin (BSA) (lyophilized, > 92%) and Aerosol-OT (sodium dioctylsulphosuccinate) were purchased from Serva and dibutyl phthalate (DBP) from Fluka. Carbowax 20M was obtained from Supelco. Collodion was supplied by Jugolek (Belgrade). The three oximes HI-6 [1-({[4-(aminocarbonyl)pyridinio]methoxy}methyl)-2-[(hydroxyimino)methyl]pyridinium dichloride], 2-PAM (2-pyridylaldoxime methiodide) and Toxogonin {1,1′-[oxybis(methylene)]bis[4-(hydroxyimino)methyl]pyridinium dichloride} were supplied by Bosnalijek (Sarajevo). Trinitrobenzene (TNB) and Barsil were obtained from Prva Iskra (Barič). Liquid crystal 4-cyano-4′-*n*-pentyldiphenyl (CPD) was a gift from the Institute Jožef Štefan (Ljubljana). Cholinesterase (ChE) from horse serum, lyophilized, was produced at the ITMP (Belgrade). Diisopropylmethyl phosphonate (DIMP) was synthesized at the ITMP and *O,O*-dimethyl-2,2-dichlorovinyl phosphate (DDVP) was obtained from INEP (Belgrade). All solvents used for preparation of coating solutions were of analytical-reagent grade (Merck).

Apparatus

The experimental set-up for the evaluation of piezoelectric sensors has been described elsewhere [10]. As explained previously [10], special care was taken to prevent any changes in crystal resonance frequency that could be caused by factors other than the presence of chemical stimulus.

All experiments were done with bulk acoustic wave sensors operating in the thickness shear mode (BAW/TSM). The piezoelectric crystals used were 9 MHz AT-cut quartz, with 6-mm aluminium, silver or gold electrodes plated on both sides and mounted in an HC-6/U holder. Several preliminary tests were made with 5-MHz crystals with 8-mm aluminium electrodes. All crystals were obtained from the Institute Mihajlo Pupin, Crystal Department (Belgrade).

A low-frequency oscillator powered by a regulated power supply set at 5 V was used. The output from the oscillator was monitored with an HP 5328A frequency counter. By means of a Keithley 263 programmable voltage source and an HP 86B computer, the experimental data were collected automatically and, simultaneously, stored in a computed memory and sent to an HP 7004B recorder.

Procedures

Free and coated piezoelectric crystals were exposed in sequence to pure carrier gas, carrier gas saturated with sample vapour and pure carrier gas again, at room temperature ($t_s = 20°C$). The flow-rate through the sensor cell, Q_s, was 100 ml min^{-1}. Most of the experiments were done with purified laboratory air as carrier gas, although a few tests were conducted in nitrogen and argon. Laboratory air was purified by passing it through a particulate filter, charcoal scrubber

and drying column packed with molecular sieve and anhydrous calcium sulphate [10]. Nitrogen and argon were used from pressurized gas cylinders and treated in the same way.

Crystals were coated by dropping 0.5 or 1 μl of the appropriate solution on the centre of each electrode and allowed to dry in a desiccator for at least 30 min before use. For preparing the coating solutions, several solvents were used: distilled water for ChE, BSA, oximes and Aerosol-OT, ethanol for Triton X-100, DBP and TNB, acetic acid for Barsil, diethyl ether–ethanol (3 + 1, v/v) for collodion, chloroform for Carbowax 20M and *n*-hexane for CPD.

Two standard analytical methods were customized and used for vapour concentration measurements: gas chromatography–mass spectrometry (GC–MS) and a spectrophotometric method based on enzyme inhibition [16].

RESULTS AND DISCUSSION

The resonance frequency (f_0) and dynamic resistance (R) of each 9-MHz piezoelectric crystal that was used in the experimental work were determined. Mean values of the measured characteristics, with the standard deviations (s), are given in Table 1.

TABLE 1

Characteristics of 9-MHz crystals used

Parameter [a]	Electrode		
	Au	Ag	Al
No. of crystals	60	20	20
$\bar{f}$ (Hz)	8994012	9022980	8994744
s (Hz)	±1307	±1032	±2317
$\bar{R}$ (Ω)	7.1	5.7	7.6
s (Ω)	±0.5	±0.8	±1.0

[a] $\bar{f}$ = resonance frequency; $\bar{R}$ = dynamic resistance; s = standard deviation.

The mass sensitivity of a crystal (Δf_c), in terms of frequency change per unit mass, was determined by measuring its resonance frequency before and after successive adding of 1 μg of cholinesterase (ChE), up to a total of 10 μg. Two 5-MHz crystals with aluminium electrodes and two 9-MHz crystals with gold electrodes were used in these measurements. Results are given in

TABLE 2

Mass sensitivity of the crystals with cholinesterase coating

Mass of coating (μg)	Δf_c (Hz μg^{-1})			
	f_0 = 5 MHz		f_0 = 9 MHz	
	1	2	1	2
1	162	149	935	1024
2	190	201	990	780
3	142	138	1000	903
4	186	118	912	895
5	151	132	1033	732
6	121	132	1416	1015
7	101	140	517	835
8	150	124	900	1315
9	183	90	1063	933
10	172	216	585	605
$\Delta\bar{f}_c \pm s$ (Hz μg^{-1}) [a]	156 ± 29	144 ± 38	935 ± 250	904 ± 193
	150 ± 33		920 ± 218	
d(mm) [a]	8		6	
A(cm^2) [a]	1		0.565	
Δf_{cf} (Hz μg^{-1}) [a]	57.5		329.2	

[a] s = Standard deviation; d = electrode diameter; A = area of the electrode; Δf_{ct} = mass sensitivity calculated from the Sauerbrey equation.

Table 2. Experimentally determined values (Δf_c) were compared with theoretical values (Δf_{ct}) derived from the Sauerbrey equation.

It was found that the mass sensitivity of a crystal depends largely on the type of coating. From the results presented in Table 2 it can be seen that for ChE the experimentally determined mass sensitivity is about 2.7 times greater than that predicted theoretically for both crystal frequencies. This can be attributed to the nature of the enzyme, which probably precludes the formation of uniform, monolayer coatings to which the Sauerbrey equation applies. For a solid coating that is not of a macromolecular or polymeric nature, e.g., 1,3,5-trinitrobenzene, carefully weighed and applied from ethanol, the experimentally obtained mass sensitivity was identical with the theoretical value, i.e., 329 Hz μg^{-1} for a 9-MHz crystal. For liquid polymers such as Triton-X100, Barsil and collodion, the mass sensitivity was about 700 Hz μg^{-1}. Therefore, when presenting results for piezoelectric sensor sensitivity, it is much better to state the frequency shift due to the coating than to calculate the coating mass from the Sauerbrey equation. An exception can be made only if the mass sensitivity is experimentally determined for a specific coating material.

The effect of carrier gas on sensor response was studied using laboratory air, nitrogen and argon, all purified in the same way. Table 3 shows the responses to DDVP (6.5 $\mu g\ l^{-1}$) obtained with three different sensors. As can be seen, the influence of the carrier gas on the sensor response is negligible.

For the purpose of comparison, several already tested coatings [2,3,9,11–14] were investigated, together with some new ones. Table 4 lists the coatings used. For materials that had been used previously by other workers the appropriate references are given.

Tables 5 and 6 give the results obtained with DIMP and DDVP, respectively. The frequency shift due to coating (Δf_c) was always measured and is stated together with the frequency response obtained. Sensor responses to target vapours (Δf) were read after 10-min exposures. The sensor responses presented here are the mean values of 3–10 measurements. All crystals reported in Tables 5 and 6 were with gold electrodes, unless stated otherwise.

TABLE 3

Influence of carrier gas on sensor response ($Q_s = 100$ ml min^{-1}, $t_s = 20°C$, $c_{DDVP} = 6.5\ \mu g\ l^{-1}$)

Coating	Δf_c (Hz)	Response (Hz)		
		Air [a]	Nitrogen [a]	Argon [a]
Au	–	13	13	13
Carbowax 20M	17025	218	225	226
CPD	5200	56	56	54

[a] Carrier gas.

The results in Table 5 show that for DIMP, the greatest sensitivity is obtained with collodion, TNB, Triton X-100 and DBP. A crystal coated with ca. 3 μg of collodion exhibited a frequency response of 1266 Hz for DIMP in the gas phase, at a concentration of 1.1 $\mu g\ l^{-1}$. Lowering the mass of the coating decreases the response, but the sensor still retains very good sensitivity (480 Hz for less than 2 μg of coating). A crystal coated with ca. 3 μg of Triton X-100 gave half the response obtained with the same amount of collodion. TNB gave a very large response (1068 Hz for 2.7 $\mu g\ l^{-1}$ DIMP). However, this was obtained with a crystal coated with 10 μg of TNB. DBP gave the same response as Triton X-100, but with approximately double the amount of coating. Aerosol OT and Barsil are also promising because the responses, although significantly lower, were obtained with a very small amount of coating. For instance, less than 1 μg of Barsil gave a response of 141 Hz for 2.7 $\mu g\ l^{-1}$ DIMP. For practical application of piezoelectric gas sensors, it is very important to keep the ratio of the frequency response to the mass of coating high. In other words, the aim is to achieve the greatest possible sensitivity with as little coating as possible, because lowering the mass loading increases the stability and reproducibility of the crystal.

Other coatings investigated, which can be roughly classified as metals (Au, Ag, Al), proteins (ChE, BSA), oximes (His, HI-6, 2-PAM, Toxogonin) and a liquid crystal (CPD), gave poor responses.

TABLE 4

Coating materials used

Abbreviation	Coating material	Structural formula	Type
ChE [9,11]	Butyrylcholinesterase	–	Enzyme
BSA [11,12]	Bovine serum albumin	–	Protein
His [3]	L-Histidine monohydrochloride	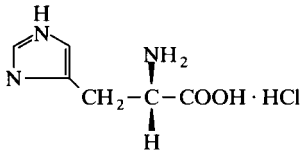	Amino acid
HI-6	1-({[4-(Amino-carbonyl) pyridinio]methoxy}methyl)-2-[(hydroxyimino)methyl]-pyridinium dichloride	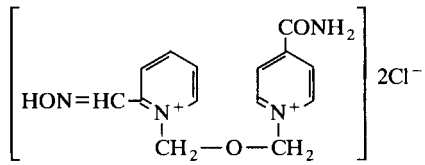	Oxime
2-PAM [2]	2-Pyridylaldoxime methiodide	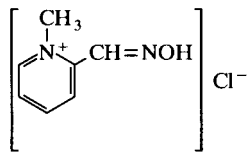	Oxime
Toxogonin	1,1′-[Oxybis(methylene)] bis[4-(hydroxyimino) methyl]pyridinium dichloride	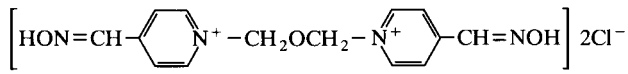	Oxime
Triton X-100 [3,13]	Polyethylene glycol *p*-(1,1,3,3-tetramethylbutyl)-phenyl ether	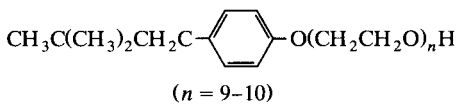 (n = 9–10)	Non-ionic detergent
Aerosol OT	Sodium dioctylsulphosuccinate	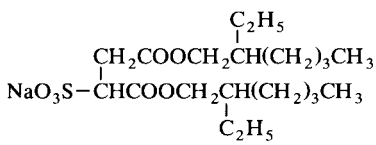	Wetting agent
DBP	Dibutyl phthalate	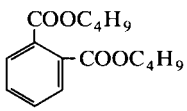	Polar solvent
TNB	1,3,5-Trinitrobenzene	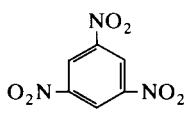	Explosive
Barsil	Dimethylsilicone	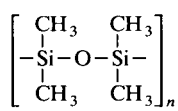	Rubber membrane
Collodion [13]	Nitrocellulose	–	Membrane
Carbowax 20M	Polyethylene glycol	$CH_2OH[CH_2CH_2]_nCH_2OH$ (n = 455)	GC liquid stationary phase
CPD [14]	4-Cyano-4′-*n*-pentyl-diphenyl	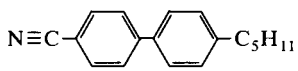	Liquid crystal

As can be seen from Table 6, the most sensitive coatings for DDVP were the same as those for DIMP. The greatest response was obtained with Triton X-100 (120 Hz for 1 $\mu g\ l^{-1}$ with only 3 μg of coating). Carbowax 20M, which is basically a polyethylene glycol (like Triton X-100), gave a similar response as Triton to DDVP, but with about 20 times more coating.

Of the coatings that gave the best results, only dibutyl phthalate was not suitable for the intended purpose, because it evaporated from the surface and reproducibility could not be preserved for more than 1 week. The other five selected coatings proved to be stable and reproducible for more than 3 months. The day-to-day variations of sensor response (signal amplitude) were less than 10%. They are probably caused by inhomogeneity of the coatings.

Figures 1 and 2 illustrate the effect of coating on response amplitude and rate for DIMP and DDVP, respectively. Each response curve was obtained in a 30-min recording, using the previously developed methodology [10].

According to Fig. 1, the largest responses for DIMP were obtained with TNB and DBP. However, taking into account the mass of coating, collodion is the most sensitive coating for DIMP (ca. 55 Hz per μg of coating and nmol of DIMP). For DDVP (Fig. 2), Triton X-100 was both absolutely and relatively the most sensitive coating (9 Hz per μg of coating and nmol DDVP). It can be seen that, with DIMP, the response and recovery rates are almost insensitive to the type of coating (Fig. 1). For DDVP, this dependence exists and the curves have a distinctly different shape since they are far from saturation point after a 10-min exposure (Fig. 2). However, the responses are relatively symmetrical, i.e., the initial response and recovery rates are approximately the same. In Fig. 3 the original DDVP absorption and desorption curves for a Triton X-100 coating are presented. It can be seen that the response and

TABLE 5

Sensitivity (response, Hz) of coatings listed in Table 4 to diisopropylmethyl phosphonate (DIMP)

Coating	Δf_c (Hz)	DIMP concentration			
		6 nmol l^{-1} (1.1 $\mu g\ l^{-1}$)	15 nmol l^{-1} (2.7 $\mu g\ l^{-1}$)	23 nmol l^{-1} (4.2 $\mu g\ l^{-1}$)	205 nmol l^{-1} (37 $\mu g\ l^{-1}$)
Au	0	21	–	24	48
Ag	0	18	–	–	–
Al	0	15	–	–	30
ChE	7752	–	–	52	–
ChE + buffer	18722	107	–	214	–
BSA	6919	–	–	28	–
His	5210	–	–	36	–
HI-6	15510	–	–	0	–
2-PAM	8863	–	–	19	–
Toxogonin	8230	10	–	76	–
Triton X-100	2481	666	964	–	–
Aerosol OT	963	121	182	278	–
	5087	–	–	–	2303
DBP	4353	663	965	–	–
TNB	3294	–	1068	–	–
Barsil	638	–	141	–	–
	1389	–	–	–	354
Collodion	2167	1266	–	–	–
	1438	534	633	–	–
	1269	480	–	–	–
Carbowax 20M	8640	–	–	–	297
CPD	2419	–	–	–	95

recovery rates are virtually identical, indicating that both processes are governed by diffusion. Because of the concentration gradient, the vapour dissolves in the coating. When the direction of the gradient changes, as no firm bonds are created, the vapour molecules diffuse back and the frequency of the crystal is increased at the same as it decreased during absorption.

Figure 4 shows the response curves for two concentrations of DIMP and two similar concentrations of DDVP, obtained with the same sensor, coated with ca. 3 μg of Triton X-100. As can be seen, Triton X-100 is more sensitive to DIMP than to DDVP. The same is true for all the coatings investigated and also for crystals without a coating.

Most of the sensors tested showed a linear response for the concentration range investigated. In Fig. 5, excellent and reproducible calibration graphs for three DDVP sensors with three different coatings are presented. Sensors were exposed to various concentrations of DDVP, produced with a dilution method described previously [10]. Each point in Fig. 5 is the mean value of five measurements. The results in Fig. 5 indicate that the limit of detection, even for one of the poorest sensors (CPD), is ca. 5 nmol l^{-1}. The coated sensors possess a high reproducibility of response.

It should be noted that unlike DIMP, the DDVP response rates depend largely on the concentration of the reagent [10]. Hence the concentration of DDVP can be determined by measuring the initial response rate, without waiting for saturation.

The exact mechanism of the interaction between vapour and coating is usually unknown. Nieuwenhuizen and Barendsz [15] made the first, and almost only, attempt to classify and explain the processes in sensor coating. Their work provides the basis for a better understanding of the relationships between performance characteristics of a chemical sensor and interactions in the coating.

TABLE 6

Sensitivity (response, Hz) of coatings listed in Table 4 to *O,O*-dimethyl-2,2-dichlorovinyl phosphate (DDVP)

Coating	Δf_c (Hz)	DDVP concentration				
		5 nmol l^{-1} (1 μg l^{-1})	16 nmol l^{-1} (3.5 μg l^{-1})	23 nmol l^{-1} (5 μg l^{-1})	29 nmol l^{-1} (6.5 μg l^{-1})	36 nmol l^{-1} (8 μg l^{-1})
Au	0	–	–	10	–	–
Ag	0	–	–	20	–	–
Al	0	–	–	14	–	–
ChE	7827	32	–	–	–	–
ChE + Triton	4989	–	490	–	1084	–
Triton X-100	845	–	159	–	341	–
	2525	120	390	541	755	–
	6867	–	622	1034	–	–
Aerosol OT	5087	–	197	368	490	–
DBP	5325	61	–	271	–	–
	6360	–	356	683	–	801
Barsil	768	22	–	62	98	–
	1389	–	88	124	151	167
Collodion	1588	31	–	341	805	–
Carbowax 20M	8640	–	93	121	141	150
	17025	65	157	244	320	–
CPD:						
Au	372	–	14	–	28	–
	2419	–	30	75	–	81
	2511	–	43	84	95	114
	5200	–	60	103	115	162
Ag	2412	–	47	74	93	125
Al	2407	–	39	82	–	95

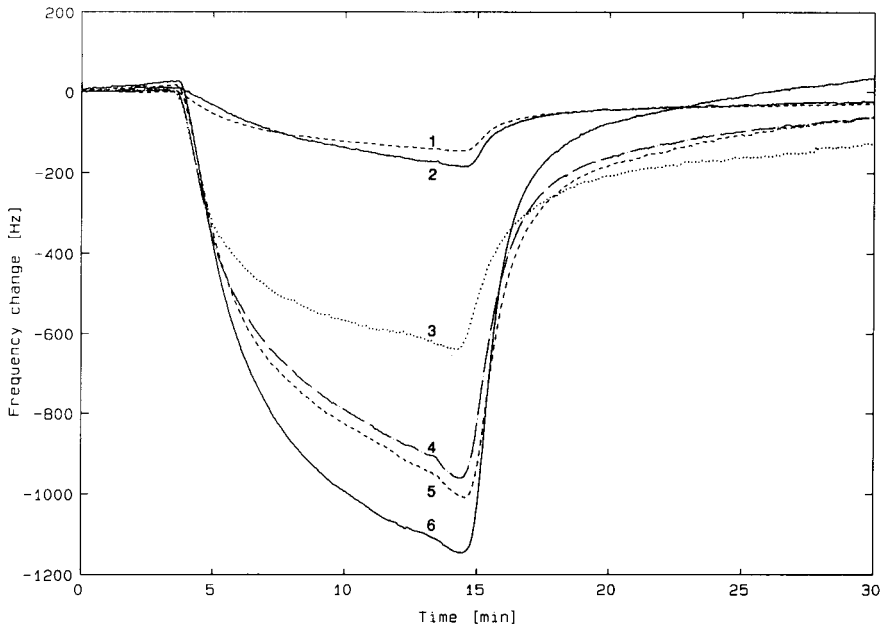

Fig. 1. Sensor responses to DIMP as a function of crystal coating. Coating: 1 Barsil, $\Delta f_c = 638$ Hz; 2 Aerosol-OT, $\Delta f_c = 963$ Hz; 3 Collodion, $\Delta f_c = 1438$ Hz; 4 Triton X-100, $\Delta f_c = 2481$ Hz; 5 dibutyl phthalate, $\Delta f_c = 4353$ Hz; 6 trinitrobenzene, $\Delta f_c = 3294$ Hz. $c_{DIMP} = 15$ nmol l^{-1}.

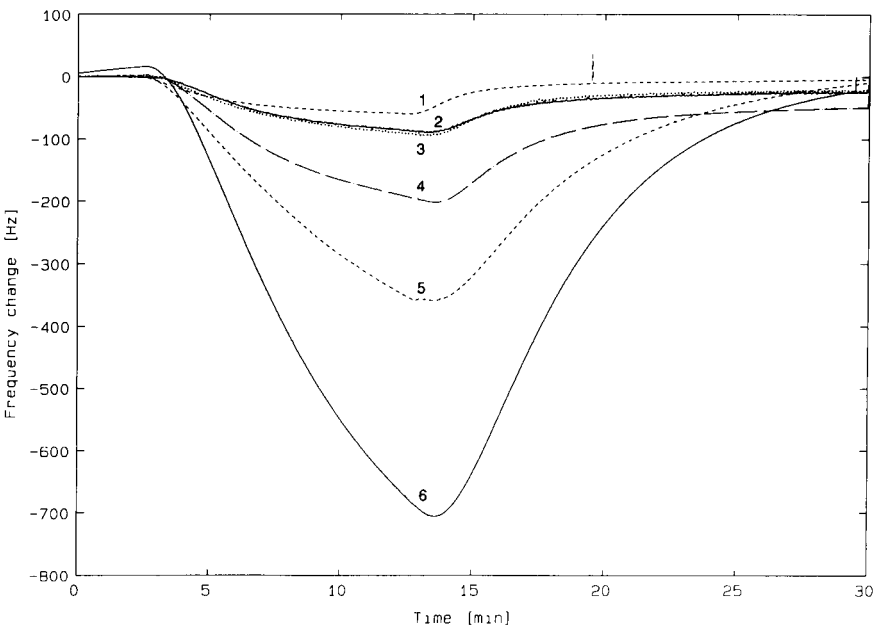

Fig. 2. Sensor responses to DDVP as a function of crystal coating. Coating: 1 liquid crystal (CPD), $\Delta f_c = 5200$ Hz; 2 Barsil, $\Delta f_c = 1389$ Hz; 3 Carbowax 20M, $\Delta f_c = 8640$ Hz; 4 Aerosol-OT, $\Delta f_c = 5087$ Hz; 5 dibutyl phthalate, $\Delta f_c = 6360$ Hz; 6 Triton X-100, $\Delta f_c = 6867$ Hz. $c_{DDVP} = 16$ nmol l^{-1}.

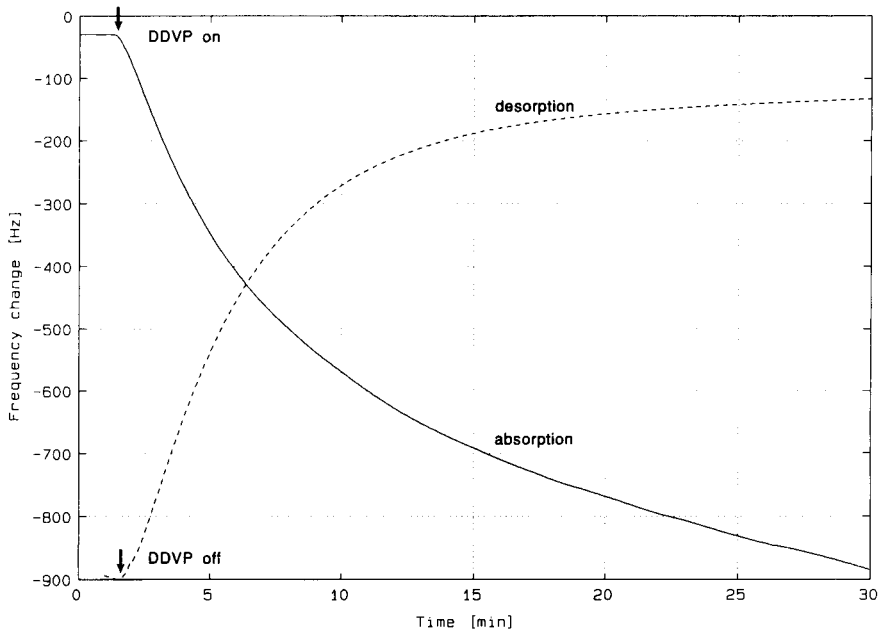

Fig. 3. Sensor response and recovery rate. Conditions: coating = Triton X-100; $\Delta f_c = 2525$ Hz; $c_{DDVP} = 23$ nmol l^{-1}.

All reactions presented in this paper are reversible, which indicates that no chemisorption occurs. As most of the coatings that gave good responses are polymers and the response increases with increasing mass (Fig. 6) and not area of the coating, the dominant interaction is un-

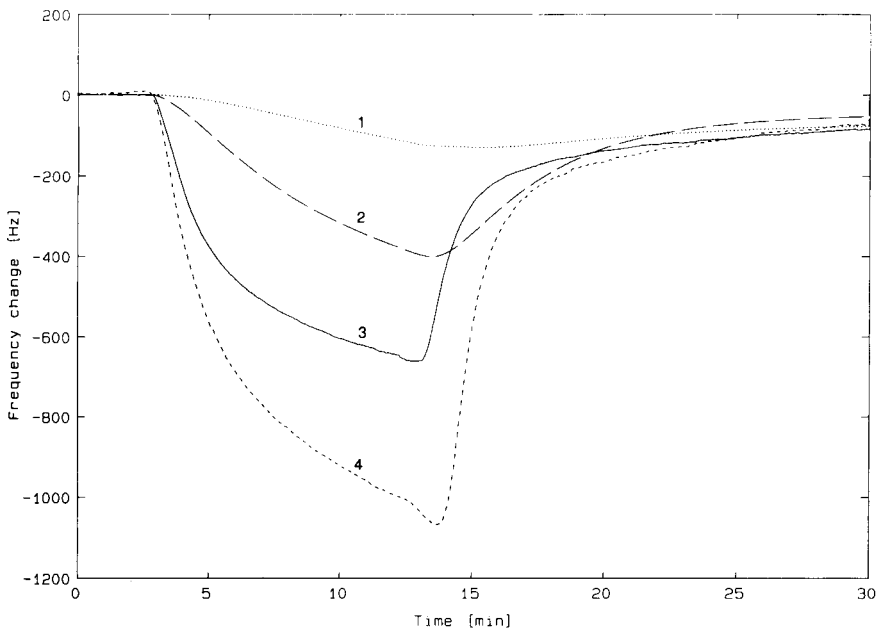

Fig. 4. Sensor responses to various concentrations of DIMP and DDVP. Coating: Triton X-100. 1 $c_{DDVP} = 5$ nmol l^{-1}; 2 $c_{DDVP} = 16$ nmol l^{-1}; 3 $c_{DIMP} = 6$ nmol l^{-1}; 4 $c_{DIMP} = 15$ nmol l^{-1}.

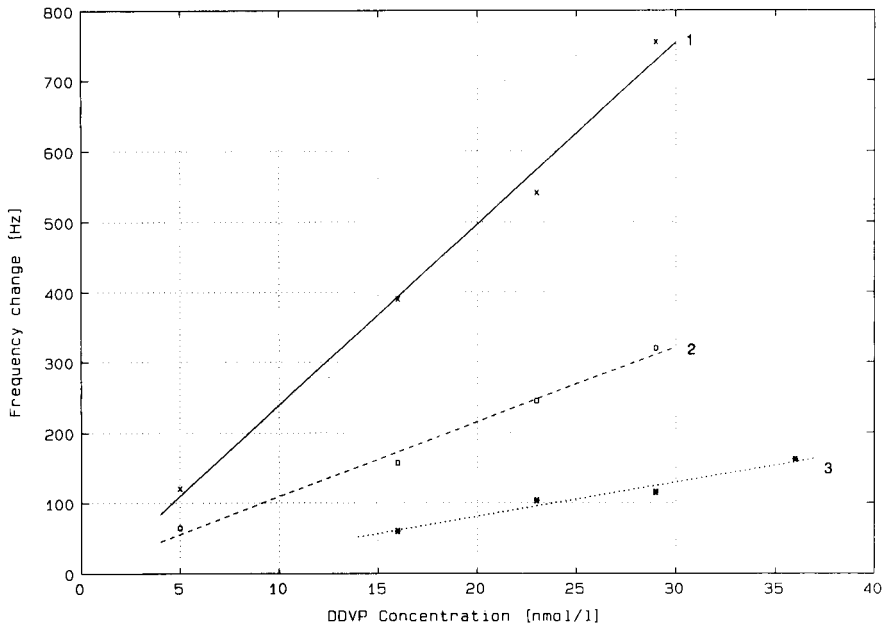

Fig. 5. Calibration graphs for DDVP. Coating: 1 Triton X-100, $\Delta f_c = 2525$ Hz; 2 Carbowax 20M, $\Delta f_c = 17025$ Hz; 3 liquid crystal (CPD), $\Delta f_c = 5200$ Hz.

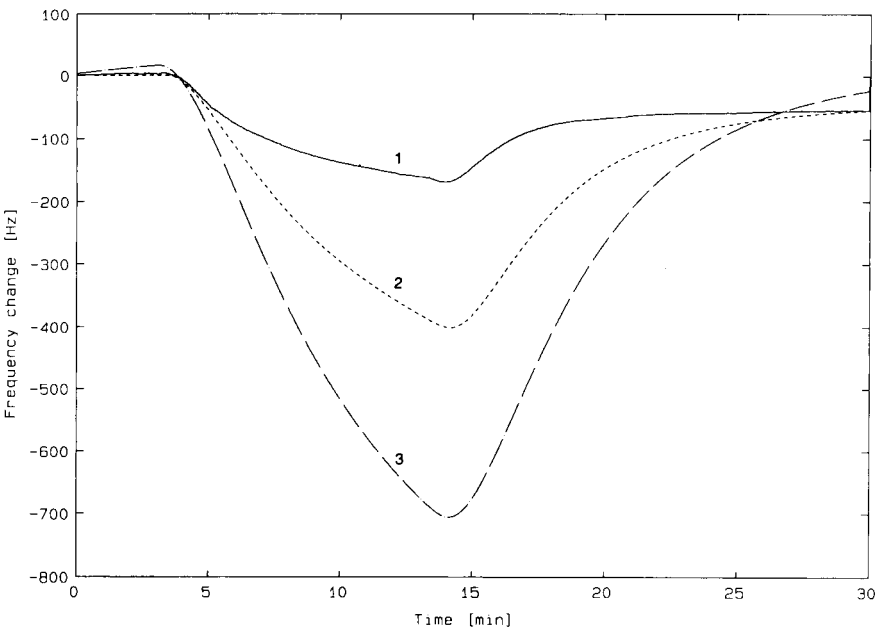

Fig. 6. Sensor responses to DDVP as a function of coating mass. Coating: Triton X-100. 1 $\Delta f_c = 845$ Hz; 2 $\Delta f_c = 2525$ Hz; 3 $\Delta f_c = 6867$ Hz.

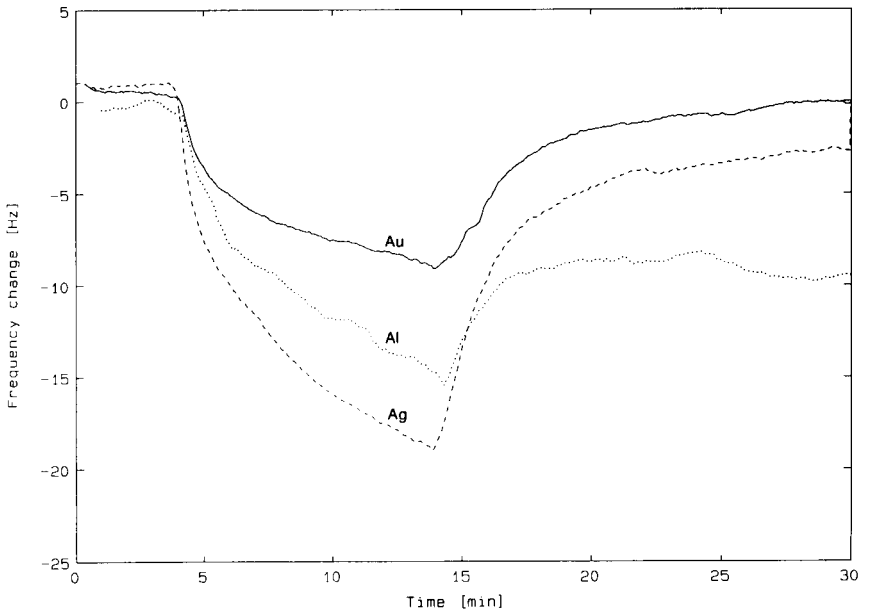

Fig. 7. Sensor responses to DDVP as a function of electrode material. $c_{DDVP} = 23$ nmol l^{-1}.

doubtedly absorption. All kinds of intermolecular reactions that can occur during a dissolution process are possible: formation of Van der Waals bonds (dipole–dipole, dipole–induced dipole, dispersion forces, repulsive forces) and hydrogen bonds. The different shapes of the curves for DIMP and DDVP are attributed to a difference in diffusion rates as a consequence of different molecular structures. With DDVP, even exposure for 30 min is insufficient for a response to reach the saturation level (Fig. 3).

Adsorption is possible but has only a marginal significance because of the negligible surface area of polymer coatings. However, for crystals without a coating (bare metal electrodes), adsorption is the only possible mechanism of interaction. As shown in Fig. 7, only gold electrodes provide a completely reversible response to DDVP. It is assumed that aluminium and silver surfaces are irreversibly modified by reaction with some air constituent or DDVP itself. Hence in this instance, the response could be attributed to a chemisorption process. The greatest response was obtained with silver electrodes, probably because DDVP reacts with a "coating" that spontaneously forms on the metal surface.

TABLE 7

Effect of cholinesterase coating mass (m_c) on sensor response to 2.1 nmol l^{-1} (0.7 μg l^{-1}) malathion ($Q_s = 100$ ml min^{-1}, $t_s = 20$°C)

m_c (μg)	$f_0 = 5$ MHz		$f_0 = 9$ MHz	
	Δf_c (Hz)	Δf (Hz per 5 min)	Δf_c (Hz)	Δf (Hz per 5 min)
10	1260	7	7050	57
20	2619	12	13888	66
30	–	–	22248	121
40	5106	17	39470	151
50	–	–	40722	153
100	–	–	97980	304

The question of reversibility is especially interesting with enzyme-coated sensors. It is well known that cholinesterase is irreversibly inhibited by organophosphorus compounds in aqueous media. However, it has been reported that a gas-phase inhibition reaction was observed [9]. Results for malathion were given and reversible and reproducible responses ranging from 403 to 454 Hz were obtained. The frequency shift due to coating and the concentration of malathion were not noted.

In the present experiments, several tests were made with crystals coated with various amounts of cholinesterase. Table 7 gives the results obtained for 2.1 nmol l^{-1} (0.7 μg l^{-1}) malathion. The responses pertain to 5-min exposures.

The responses were completely reversible and increased as the mass of coating increased, as with the other sensors investigated. The responses further increased after prolonged exposure to malathion and also after the enzyme had been denaturated by high temperature in an oven. It was concluded that the reaction between cholinesterase and malathion was definitely not inhibition, but non-specific absorption, which is in accordance with the results reported previously [12].

Conclusions

Sensitive, reversible and reproducible piezoelectric sensors that permit the detection and/or determination of organophosphorus compounds in the vapour phase in the μg l^{-1} range and in up to 10 min are described. With regard to sensitivity, reproducibility, reversibility, stability and short response and recovery times, polymers proved to be the best coatings for both DIMP and DDVP. Collodion is the most efficient coating for DIMP (55 Hz per μg of coating and nmol of DIMP) and Triton X-100 for DDVP (9 Hz per μg of coating and nmol of DDVP). It is believed that non-specific absorption is the dominant reaction and cannot be avoided, especially when the coating, or at least one of its components, is of a polymeric nature.

Ljubinka Rajaković gratefully acknowledges the support given by the Serbian Research Council.

REFERENCES

1 E.P. Scheide and G.G. Guilbault, Anal. Chem., 44 (1972) 1764.
2 W.M. Shackelford and G.G. Guilbault, Anal. Chim. Acta, 73 (1974) 383.
3 Y. Tomita and G.G. Guilbault, Anal. Chem., 52 (1980) 1484.
4 G.G. Guilbault, J. Affolter, Y. Tomita and E.S. Kolesar, Anal. Chem., 53 (1981) 2057.
5 G.G. Guilbault and Y. Tomita, Sensors Actuators, 2 (1981/82) 43.
6 J. Kristoff and G.G. Guilbault, Anal. Chim. Acta, 149 (1983) 337.
7 G.G. Guilbault, J. Kristoff and D. Owen, Anal. Chem., 57 (1985) 1754.
8 J. Ngeh-Ngwainbi, P.H. Foley, S.S. Kuan and G.G. Guilbault, J. Am. Chem. Soc., 108 (1986) 5444.
9 G.G. Guilbault and J. Ngeh-Ngwainbi, in R.D. Schmid (Ed.), Biosensors International Workshop 1987, GBF Monographs, Vol. 10, GBF Braunschweig–Stöckheim, 1987, p. 187.
10 O.S. Milanko, S.A. Milinković and Lj.V. Rajaković, Anal. Chim. Acta, 264 (1992) 43.
11 G.G. Guilbault and J.M. Jordan, CRC Crit. Rev. Anal. Chem., 1 (1988) 1.
12 Lj. Rajaković, V. Ghaemmaghami and M. Thompson, Anal. Chim. Acta, 217 (1989) 111.
13 D.M. Davis and R.E. Miller, Microsensor Data Base Search MSRCH User's Guide, AD-A 202 479, U.S. Army Armament Munitions Chemical Command, Aberdeen Proving Ground, MD, 1988.
14 A. Mierzwinski and Z. Witkiewicz, Talanta, 34 (1987) 865.
15 M.S. Nieuwenhuizen and A.W. Barendsz, Sensors Actuators, 11 (1987) 45.
16 O. Milanko, ITMP Technical Report No. 6349 595, ITMP, Belgrado, 1991.

Analytica Chimica Acta, 269 (1992) 301–306
Elsevier Science Publishers B.V., Amsterdam

Microtitre plate enzyme amplified immunoassay for thyroid stimulating hormone

Robert Wilson

Research Centre for Advanced Science and Technology, University of Tokyo, Tokyo (Japan)

(Received 7th April 1992)

Abstract

Methods for removing contaminating FAD and alkaline phosphatase from apo-aminoacid oxidase are described. A method for phosphorylating flavin adenine dinucleotide is also described. Its hydrolysis to flavin adenine dinucleotide catalysed by alkaline phosphatase is demonstrated by liquid chromatography. Flavin adenine dinucleotide can reactivate apo-aminoacid oxidase and result in the formation of hydrogen peroxide. The hydrogen peroxide can be detected colorimetrically. These reactions are used in an enzyme amplified immunoassay for thyroid stimulating hormone in which alkaline phosphatase is the enzyme label. A limit of detection of 0.03 μIU ml^{-1} for thyroid stimulating hormone makes the assay suitable for diagnosing hyperthyroidism.

Keywords: Immunoassay; Enzyme amplified immunoassay; Flavin adenine dinucleotide phosphate; Microtitre plate; Nitroethane; Suicide substrate; Thyroid stimulating hormone

Enzyme amplification can be used to increase the speed and sensitivity of an immunoassay [1–4]. In order to realize the full potential of this technique it is necessary to remove all sources of interference from the reagents. The assay described here (Fig. 1) is designed for use with immunoassays in which the reporter enzyme is alkaline phosphatase. It is essential, therefore, to remove all traces of alkaline phosphatase from other reagents used in the assay. This is done using affinity chromatography in which contaminating phosphatase is bound to L-histidyldiazobenzylphosphonic acid. The substrate for the reporter enzyme is flavin adenine dinucleotide phosphate (FADP). On reaction it is converted to flavin adenine dinucleotide (FAD). Contaminating FAD is removed from FADP by ion exchange chromatography and from apo-aminoacid oxidase (apo-AOD) with the suicide substrate nitroethane. Using this system it is possible to detect thyroid stimulating hormone (TSH) with a lower limit of detection of 0.03 μIU ml^{-1}. This compares with a lower limit of detection of 0.32 μIU ml^{-1} for an otherwise identical immunoassay in which nitrophenylphosphate was the chromogen.

Correspondence to: R. Wilson, Research Centre for Advanced Science and Technology, University of Tokyo, Tokyo (Japan).

EXPERIMENTAL

Materials

D-Aminoacid oxidase (AOD, EC 1.4.3.3) Type I from porcine kidney, alkaline phosphatase (AP) (EC 3.1.3.1), 4000 DEA units mg^{-1} enzyme protein from bovine intestinal mucosa, peroxidase (POD) (EC 1.11.1.7) Type II from horseradish, an enzyme immunoasay kit for thyroid stimulating hormone, L-histidyldiazobenzylphosphonic acid attached to agarose, 4-aminoantipyrine, dihydrox-

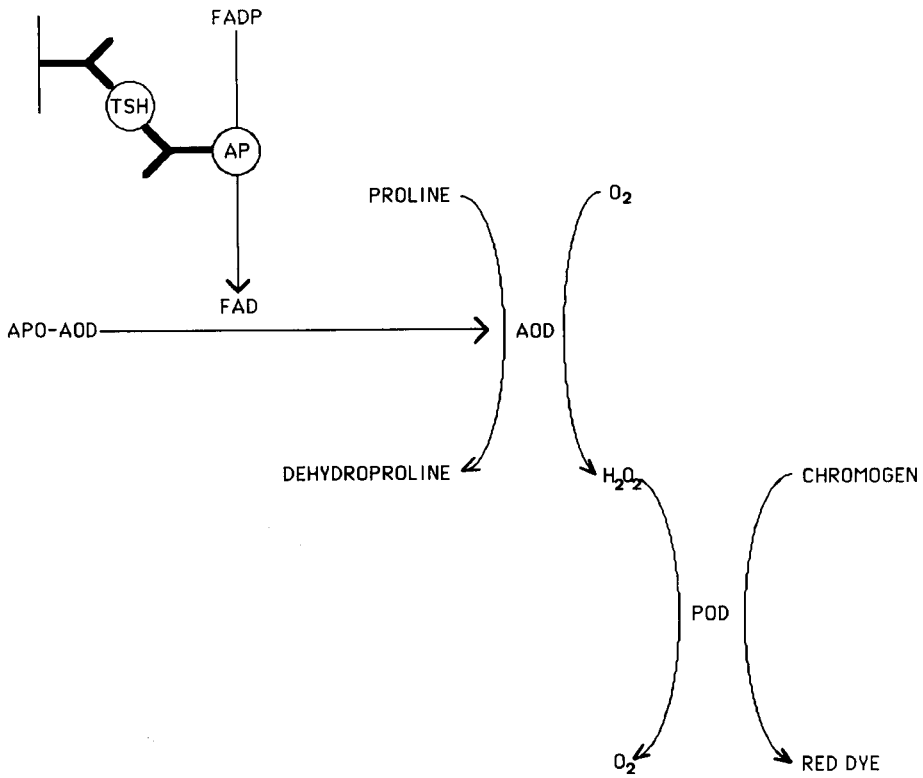

Fig. 1. Schematic representation of enzyme amplified immunoassay for TSH.

ybenzenesulfonic acid (DHBS) and eight channel multiple pipettes were from Sigma. Thyroid stimulating hormone (TSH) solutions were made up by diluting a stock solution (12 μIU ml^{-1}) that had been standardized against a World Health Organization reference preparation. Nitroethane solutions were prepared by dissolving nitroethane in 10 mM potassium hydroxide to a final concentration of 10 mM; they were allowed to stand for 1 h prior to use and then used within 24 h of preparation. Alkaline phosphatase-free peroxidase was prepared by adapting the method of Landt et al. for phosphatase removal rather than purification [5]. All other reagents were of the highest grade commercially available. All buffer solutions were adjusted to the correct pH at 25°C. Liquid chromatography was carried out using a Varian LC 5000 High Performance Liquid Chromatograph (Varian, Walton on Thames). The chromatographic system consisted of two pumps that were used to deliver eluant to a Waters μ-Bondpak C-18 reversed-phase column (150 mm $\times$ 39 mm i.d.) (Waters Chromatography Division, Millipore Bedford, UK). The column was fitted with a Waters Guard Pak that had a μ-Bondpak C-18 insert. Sample injection was by a Varian fixed loop injector (100 μl). Eluate was monitored at 254 nm with a fixed wavelength photometric detector. Data was fed into a Varian 401 Data system that produced a plot of absorbance against time. The plate reader was from Tosoh, Tokyo. The plate shaker was from Scientific Industries, Bohemia, NY.

Preparation of FADP

The preparation of FADP has been described previously [4]. Briefly, FAD (50 mg) was added to 2 ml of dry dimethylsulfoxide, sonicated, and dried under vacuum at 30–40°C. Orthophosphoric acid (1 M) in dimethylsulfoxide (100 μl) and *N*,*N*-diisopropylethylamine (200 μl) were added to this solution, and it was resonicated. Next 100

μl of trichloroacetonitrile was added to the solution followed by further sonication. After 20 min the reaction was terminated with anhydrous acetic acid added to a final concentration of 50% (v/v). The product was loaded onto a DEAE cellulose column equilibriated with 50% aqueous acetic acid (v/v). Monophosphate derivatives of FAD were eluted with a gradient of 100 to 400 mM ammonia in 50% aqueous acetic acid. The eluate was dried by rotary evaporation from water at 30°C and stored at −20°C.

Liquid chromatographic analysis of FADP hydrolysis

FAD, FADP, and FADP, after treatment with alkaline phosphatase, were investigated by liquid chromatography (LC). FAD and FADP were dissolved to a final concentration of 10 μM in 0.1 M Tris buffer, pH 9.0, that contained magnesium nitrate (1 mM) and zinc nitrate (0.1 mM). The FADP solution was divided into two aliquots. To one of these was added alkaline phosphatase to a final concentration of 0.1 IU ml^{-1}. These solutions were allowed to stand in darkness for 1 h at room temperature and then analyzed.

Eluant was pumped into the LC column from two reservoirs. One contained ammonium acetate (5 mM), pH 7.2, and the other 25% methanol (v/v) in ammonium acetate solution (5 mM) pH 7.2. Both solutions were passed through a 0.2-μm cellulose acetate filter and degassed before use. The column was equilibriated overnight with 5% methanol. Samples were analyzed by introducing them into a 10-μl injection loop from which they were loaded onto the column at time zero. They were eluted as follows:

1. For the first 15 min 5% methanol (v/v) was pumped through the column.
2. From 15 to 30 min a linear gradient was run from 5 to 20% methanol (v/v).
3. From 30 to 50 min the methanol concentration was maintained at 20% (v/v).
4. From 50 to 60 min a linear gradient was run from 20 to 5% methanol (v/v).

The absorbance of the eluate at 254 nm as it emerged from the column was plotted against time.

Preparation of apo-aminoacid oxidase

Full details of this method have been described elsewhere [4]. Briefly, AOD (10 mg) in 5 ml of 0.1 M Tris buffer, pH 8.5, containing potassium bromide (1 M) and EDTA (5 mM) was dialyzed against 3 × 250 ml of the same buffer for a total of 36 h in darkness at 4°C, and then against 3 × 250 ml of 0.1 M Tris buffer pH 8.5 for 36 h in darkness at 4°C.

Removal of contaminants from apo-AOD

Apo-AOD prepared as described above is contaminated with 1% FAD as a percentage of the binding molarity [4]. This can be removed by modifying the preparation procedure. After dialyzing against 3 × 250 ml of Tris buffer that contained potassium bromide and 1 × 250 ml of Tris buffer, potassium cyanide and nitroethane were added to the solution to a final concentration of 0.1 M and 100 μM, respectively. This solution was allowed to stand for 1 h at 4°C and then it was dialyzed against a further 2 × 250 ml of Tris buffer.

Alkaline phosphatase was removed from the apo-AOD by affinity chromatography on L-histidyldiazobenzylphosphonic acid–Sepharose. Initially 10 ml of 0.1 M Tris buffer, pH 8.0, containing sodium orthophosphate (10 mM) was run through the column (1 ml gel in 8 mm i.d. column). This was followed by 20 ml of 0.1 M Tris buffer, pH 8.5. In order to avoid diluting the apo-AOD, this buffer was expelled from the column under pressure. Then 5 ml of apo-AOD was loaded dropwise onto the column. It was necessary to pass the apo-AOD through the column more than once to ensure thorough removal of the contaminating phosphatase. To the final eluate was added 4-aminoantipyrine to a concentration of 1 mM.

Immunoassay for thyroid stimulating hormone (TSH) with one step colour development

TSH solutions (100 μl) in the range 0–2 μIU ml^{-1} were added to the wells of a microtitre plate coated with antibodies to TSH. The plate was covered with plastic cling-film and gently shaken at room temperature for 1 h. At the end of this time the wells were washed five times with

a buffered surfactant solution. After each wash the plate was inverted and vigorously blotted against a clean paper towel. After washing, an alkaline phosphatase-labelled antibody solution was added to the wells of the plate. The plate was incubated for 1h, and washed as described previously. After washing, FADP solution (100 μl) and apo-AOD solution (100 μl) were added to the wells of the microtitre plate. The FADP solution (50 μM) was made up in 0.1 M Tris buffer, pH 9.5, that contained POD (0.1 mg ml^{-1}), D-proline (50 mM), DHBS (5 mM), magnesium nitrate (1 mM), and zinc nitrate (0.1 mM). The absorbance at 492 nm relative to a reagent blank was read at zero time and at 10-min intervals thereafter for a total of fifty minutes. Except when the absorbance was being measured the plate was covered with aluminium foil and gently shaken.

Immunoassay for TSH with two step colour development

In the two step immunoassay FADP solution was added a zero time but the addition of apo-AOD solution was delayed for 30 min. The change in absorbance was read after a further 20 min. An immunoassay in which nitrophenyl phosphate (10 mM) in 0.1 M diethanolamine buffer, pH 9.8, was the chromogen was also carried out.

RESULTS

Liquid chromatographic analysis of FADP hydrolysis

Full details of the yield, purity and stability of the FADP have been described previously [4]. Plots of absorbance vs. time for the elution of FAD and FADP from the LC column are shown in Fig. 2. FADP eluted at around 27 min, but when FADP was treated with alkaline phosphatase the 27-min peak was replaced by a peak at around 36 min after injection. FAD also eluted at this time. This demonstrates that alkaline phosphatase can be used to convert FADP to FAD.

Removal of contaminating FAD and alkaline phosphatase from apo-AOD

Apo-AOD free of contaminating FAD has been prepared by affinity chromatography on Cibacron blue Sepharose [6] but the method is complicated and it is difficult to achieve the desired result. Treatment with the suicide substrate nitroethane and cyanide converts contaminating FAD to an inactive cyanoethyl derivative [7]. A similar method in which holo-AOD was inactivated with nitropropane and cyanide has been described previously [8]. For the assay described here it was necessary to remove the cyanide because even at a very low concentration it inhibits POD [9]. One way to do this is to add an excess of an aldose sugar like D-mannose. This converts the cyanide to a cyanohydrin which does not inhibit any of the enzymes used in the assay. In the colorimetric assay described here, however, this is not possible because high concentrations of aldose sugars interfere with colour development by converting the red chromophore to a colourless product. In the enzyme amplified immunoassay described in this paper removal of contaminating FAD from the apo-enzyme does not markedly improve the limit of detection. For practical purposes it can be omitted. In more sensitive assays based on luminol, however, it is important to remove the FAD.

It is important to remove all the alkaline phosphatase from the reagents. For this work, apo-AOD was passed through the affinity column until the increase in background absorbance was around 0.25 after 20 min of colour development relative to a reagent blank that contained no

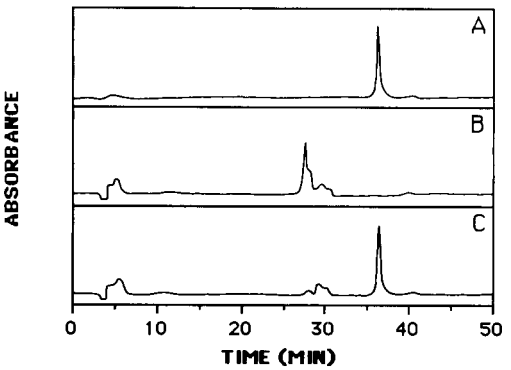

Fig. 2. Plot of absorbance vs. time for LC analysis of FAD (A), FADP (B), and FADP after treatment with alkaline phosphatase (C).

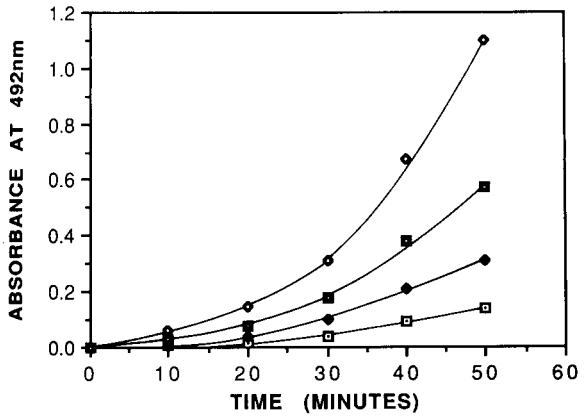

Fig. 3. Increase in absorbance with time for the enzyme amplified immunoassay with different concentrations of TSH. (μIU TSH ml^{-1}): □ = 0.25; ◆ = 0.5; □ = 1.0; ◇ = 2.0.

apo-AOD. Typically this meant passing the apo-AOD through the column five times. The column used in this work had a gel volume of 1 ml. If a larger column were used it would probably be uneccessary to pass the apo-AOD through the column more than once. Bound alkaline phosphate can be eluted from the column with 0.1 M Tris buffer pH 8.0, containing sodium orthophosphate (10 mM). The ligand (histidyldiazobenzylphosphonic acid that is used to bind contaminating phosphatase is a potential inhibitor of this enzyme. Investigation of the eluate, however, indicated that it did not leak from the column at a rate sufficient to inhibit it.

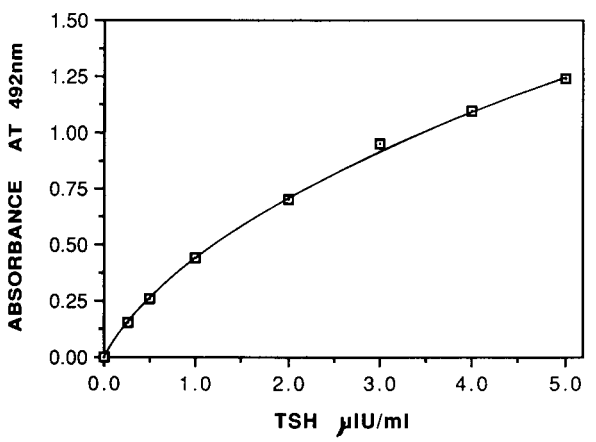

Fig. 4. Enzyme amplified TSH immunoassay with two step colour development.

Immunoassays for TSH

The resolving power of the amplifier increases with time as shown in Fig. 3. It is advantageous, therefore, to delay colour development until a large difference in FAD concentration between blank and samples has built up. This helps to distinguish between alkaline phosphatase non-specifically adsorbed to the microtitre plate and wells that contain bound TSH. A plot of colour development vs. TSH concentration for the two step enzyme amplified immunoassay is shown in Fig. 4. The limit of detection (2 × S.D. of eight zero calibrators) for low concentrations of TSH was 0.03 μIU ml^{-1}. This compares with 0.32 μIU ml^{-1} for the assay in which nitrophenylphosphate was the substrate.

DISCUSSION

In order to achieve a low limit of detection in the enzyme amplified immunoassay described here it is necessary to remove contaminants that contribute to background absorbance. Chief amongst these are FAD and alkaline phosphatase. It was also necessary to limit the effect that alkaline phosphatase-labelled antibodies nonspecifically adsorbed to the microtitre plate had on the assay. After removal of the contaminants and the introduction of a protocol that curtailed the effects of adsorbed alkaline phosphatase, TSH was detected with a lower limit of detection of 0.03 μIU ml^{-1}. This compares well with other sensitive assays for TSH [10–12] and represents a tenfold improvement on an identical assay in which nitrophenylphosphate was the substrate. Figure 4 indicates that TSH concentrations of less than 0.7 μIU ml^{-1}, which are encountered in the blood of subjects suffering from hyperthyroidism [10–12], can readily be distinguished with this assay.

FADP is not limited to use with apo-AOD. It can also be used for enzyme amplification with apo-glucose oxidase [13,14] and, in all likelihood, most other flavoenzymes as well. It is not known to occur naturally. FAD-3-pyrophosphate (FAD-PP), however, has been synthesized enzymatically and shown to be inactive as a coenzyme with

apo-AOD [15]. The authors of that paper have speculated that phosphorylation of the coenzyme could function as a means of controlling the activity of flavoenzymes in microorganisms. A large number of FAD analogues has been produced enzymatically using *Brevibacterium amoniagenes* [16]. These analogues usually contain modifications to the isoalloxazine moiety of FAD, but it would be worth investigating if FADP could be produced in this way. The transphosphorylating system of *Proteus mirabilis* which has already been used to produce phosphoylated forms of NAD is also worthy of investigation in this respect [17]. If either of these systems is capable of producing FADP then speculation about a biochemical role for it would be warranted.

Financial support for this work was from the Japan Society for the Promotion of Science. This support is gratefully acknowledged.

REFERENCES

1 A. Johannsson, D.H. Ellis, D.L. Bates, A.M. Plumb and C.J. Stanley, J. Immunol. Meth., 87 (1985) 7.
2 R.I. Carr, M. Mansour, H. Sadi, H. James and J. Verrier-Jones, J. Immunol. Meth., 98 (1989) 201.
3 T.K. Christopoulos and E.P. Diamandis, Anal. Chem., 64 (1992) 342.
4 R. Wilson, Analyst, 117 (1992) 1547.
5 M. Landt, S.C. Boltz and L.G. Butler, Biochemistry, 17 (1978) 915.
6 J. Leonil, S. Langrene, S. Silsic and F. Le Goffic, J. Chromatogr., 347 (1985) 316.
7 T.A. Alston, D.J.T. Porter and H.J. Bright, J. Biol. Chem., 258 (1983) 1136.
8 J.W. Kitzler and I. Fridovich, Anal. Biochem., 174 (1988) 613.
9 J. Keesey, Biochemica Information, Boehringer Mannheim Biochemicals, Indianapolis, IN, (1987) 56.
10 W.E. Cobb, R. Preston Lamberton and I.M. Jackson, Clin. Chem., 30 (1984) 1558.
11 J. Seth, H.A. Kellet, G. Caldwell, V.M. Sweetin, G.J. Beckett, S.M. Gow and A.D. Toft, Br. Med. J., 289 (1984) 1334.
12 M.J. Roddis, J.M. Burrin, A. Johannsson, D.H. Ellis and C.H. Self, Lancet, i (1985) 277.
13 R. Wilson, Ph.D. Thesis, Cranfield Institute of Technology, Bedford, (1990).
14 R. Wilson and A.P.F. Turner, Biosensors, 7 (1992) 165.
15 A. Raazzaque, Y. Hanada, J.-I. Mukai, S. Murao and T. Nishino, FEBS Lett., 93 (1978) 335.
16 S. Ghisla and V. Massey, Biochem. J., 239 (1986) 1.
17 M. Kuwahara, T. Tachiki, T. Tochikura and K. Ogata, Agric. Biol. Chem., 35 (1971) 177.

Analytica Chimica Acta, 269 (1992) 307–316
Elsevier Science Publishers B.V., Amsterdam

Robust Kalman filter as a chemometric method for analytical data processing

Yu-Long Xie, Ji-Hong Wang, Yi-Zeng Liang and Ru-Qin Yu

Department of Chemistry and Chemical Engineering, Hunan University, Changsha 410082 (China)

(Received 26th March 1992; revised manuscript received 25th June 1992)

Abstract

The Kalman filter has been made robust by altering the scheme of the information feedback in the recursive algorithm of the ordinary Kalman filter. A limiting transformation which operates on the innovation term has been defined to eliminate or reduce the influence of outliers on the performance of the Kalman filter. The behaviour of the proposed robust Kalman filter was studied by computer simulation and the robustness to outliers was demonstrated.

Keywords: Signal processing methods; UV–Visible spectrophotometry; Kalman filter; Robust statistics

Chemometric data processing methods have become routine procedures in analytical practice [1]. The effect of outliers in a chemical measurement process is one of important aspects to be considered. In analytical chemistry measurements, unexpected outliers in experimental data are common, because of the drift of instruments, artificial errors during the measuring process or a departure between the true underlying distribution of data and the assumed mathematical model used for the data interpretation. Incorrect analytical results would be obtained if one attempted to treat data containing outliers by using ordinary statistical methods based on the assumption of some idealized data distribution. Robust statistical methods are very useful for handling this kind of problem.

The characteristic features of a robust method can be summarized as follows: the performance of the method should be optimum or quasi-optimum when there is no departure from the statistical assumption concerning the data distribution; it should be robust in the sense that small deviations from the model assumptions should impair the performance only slightly; and the deterioration of the method's performance should not be catastrophic when the data under treatment depart substantially from the assumed theoretical model.

The Kalman filter has been used extensively in chemistry because of familiarity and computational simplicity, but the ordinary Kalman filter is non-robust. Making the Kalman filter robust was discussed by Masreliez and Martin [2]. Based on a limiting transformation operating on the innovation term of the ordinary Kalman filter, in this paper a simpler approach for making the Kalman filter robust is proposed with the aim of solving the multivariate analytical calibration problem. The performance of the proposed robust Kalman filter as a chemometric data processing method was evaluated by using computer simulation.

Correspondence to: Ru-Qin Yu, Department of Chemistry and Chemical Engineering, Hunan University, Changsha 410082 (China).

THEORY

The Kalman filter algorithm is based on two equations. One is the system dynamic equation:

$$\mathbf{x}(k) = \mathbf{F}(k,k-1)\mathbf{x}(k-1) + \mathbf{w}(k) \quad (1)$$

and the other is the measurement model equation:

$$z(k) = \mathbf{h}(k)^{\mathrm{T}}\mathbf{x}(k) + v(k) \quad (2)$$

where k identifies the measurement number, in spectrophotometry corresponding to a wavelength. The vector $\mathbf{x}(k)$ is the system state vector referring to the kth measurement, which consists of the parameters to be estimated, e.g., the component concentration vector in multivariate calibration or a set of dynamic parameters in dynamic monitoring. The state transition matrix $\mathbf{F}(k,k-1)$ describes how the states change from $k-1$ to k and it is actually an identity matrix in calibration. The state error vector $\mathbf{w}(k)$ consists of the noise contribution to each of the system states and the vector $\mathbf{h}(k)$ is the measurement function vector. The scalar $z(k)$ represents the response of the kth measurement and $v(k)$ the corresponding measurement noise. Both the system and measurement noise process are assumed to be zero-mean and uncorrelated (i.e white noise).

The recursive algorithm of the Kalman filter as applied, for instance, to multi-component spectrophotometry consists of a series of equations listed below:

State-estimate extrapolation:

$$\mathbf{x}(k \mid k-1) = \mathbf{x}(k-1 \mid k-1) \quad (3)$$

Error covariance extrapolation:

$$\mathbf{P}(k \mid k-1) = \mathbf{P}(k-1 \mid k-1) \quad (4)$$

State-estimate update:

$$\mathbf{x}(k \mid k) = \mathbf{x}(k \mid k-1) + \mathbf{k}(k)\mathrm{INV}(k) \quad (5)$$

Error covariance update:

$$\mathbf{P}(k \mid k) = \left(\mathbf{I} - \mathbf{k}(k)\mathbf{h}(k)^{\mathrm{T}}\right)\mathbf{P}(k \mid k-1) \quad (6)$$

Kalman gain:

$$\mathbf{k}(k) = \mathbf{P}(k \mid k-1)\mathbf{h}(k) \times \left[\mathbf{h}(k)^{\mathrm{T}}\mathbf{P}(k \mid k-1)\mathbf{h}(k) + R(k)\right]^{-1} \quad (7)$$

Innovation:

$$\mathrm{INV}(k) = z(k) - \mathbf{h}(k)^{\mathrm{T}}\mathbf{x}(k \mid k-1) \quad (8)$$

In Eqns. 3–8, the error covariance matrix $\mathbf{P}$ describes the errors in the state estimates and the Kalman gain $\mathbf{k}$ is analogous to the weighting factor. The innovation INV is a scalar which is the difference between the latest measurement and the current prediction for that measurement and actually is the prediction residual. This series of values INV(k) is called innovation sequence. The scalar $R(k)$ is the measurement noise variance.

The series of equations of the Kalman filter were derived when the Gaussian distribution for both $\mathbf{w}$ and v was specified. If the assumption was satisfied, the linear filter estimation would be optimum in the sense of minimum mean-squared error and the innovation sequence should be a zero-mean white noise sequence. On the other hand, when some outliers are present, the distributions would deviate from the Gaussian distributions in a heavy-tailed manner; this would affect the performance of the Kalman filter and the innovation sequence would become abnormal. The use of the innovation sequence in checking the reliability of analytical results has been discussed elsewhere [3]. As the algorithm is recursive and the innovation affects the filter estimation in a linear fashion, the performance of the Kalman filter will be seriously degraded even if one outlier exists. Therefore, in this sense, the ordinary Kalman filter is non-robust.

In order to obtain a robust Kalman filter, one can execute some non-linear transformation on the innovation of the ordinary Kalman filter:

$$\mathrm{INV}(k)' = \mathrm{Lt}[\mathrm{INV}(k)] = \mathrm{Lt}\left[z(k) - \mathbf{h}(k)^{\mathrm{T}}\mathbf{x}(k \mid k-1)\right] \quad (9)$$

where Lt represents a limiting transformation or an analogous non-linear transformation of this sort. The transformation of the innovation can reduce the influence of outliers on the performance of the filter, and therefore the algorithm with the transformed innovation INV(k)′ will possess some robustness.

In this paper, a limiting transformation, Lt, is used as the basis of the robust Kalman filter, which is defined as

$$\begin{aligned} &\mathrm{Lt}[\mathrm{INV}(k)] \\ &\quad = \mathrm{INV}(k) \\ &\qquad \text{for } |\mathrm{INV}(k)| \leqslant C \cdot \mathrm{Max}\,|\mathrm{INV}(k)| \qquad (10) \\ &\quad = C \cdot \mathrm{Max}\,|\mathrm{INV}(k)| \\ &\qquad \text{for } |\mathrm{INV}(k)| > C \cdot \mathrm{Max}\,|\mathrm{INV}(k)| \end{aligned}$$

where C is an adjustable limiting factor which is a constant between 0 and 1 and INV(k) is the innovation of the ordinary Kalman filter.

If some outliers indeed exist, the corresponding innovation sequence of the ordinary Kalman filter would contain some abnormal points (usually points with abnormally large amplitudes). When an appropriate limiting factor C is adopted, several terms with large amplitude in the innovation sequence of the ordinary Kalman filter will be replaced by a fixed value of $C \cdot \mathrm{Max}\,|\mathrm{INV}(k)|$, where $\mathrm{Max}\,|\mathrm{INV}(k)|$ is the absolute value of the largest term in the innovation sequence, and other terms of the innovation sequence remain unchanged. The Kalman filter is then invoked again by using the transformed innovation in the recursive calculation. In this way, the influence of outliers is eliminated or reduced and the Kalman filter becomes robust.

A selection principle for C can be formulated from the following reasoning. If no outlier exists and the Gaussian assumption is satisfied, the innovation sequence should be characterized as a random noise sequence. In the presence of outliers, however, the innovation sequence would show more or less non-random character, which is a sign of correlation. Hence if the influence of outliers is removed or reduced by the action of a limiting factor C, the innovation sequence of the robust Kalman filter should possess random noise character. Therefore, the appropriate limiting factor C will be the one that results in a random innovation sequence, which can be determined by inspecting the innovation plots of the robust Kalman filter obtained for various C in an interactive fashion. This is actually a procedure similar to checking the reliability of analytical results by inspection of the behaviour of the innovation sequence [3].

EXPERIMENTAL

Phenol, resorcinol and other chemicals were of analytical-reagent grade. Absorbance was recorded on a Beckman Du-7 UV–visible spectrophotometer and all calculations were done on a Macintosh II microcomputer.

RESULTS AND DISCUSSION

Selection of the limiting factor

The selection of appropriate value of C which produces a random innovation sequence involves the following steps. First, a mixture is treated by the ordinary Kalman filter and the innovation sequence of the ordinary Kalman filter is recorded. The largest amplitude of the innovation, $\mathrm{Max}\,|\mathrm{INV}(k)|$, is thus obtained. An arbitrary value of C in the range 0–1 is taken as an initial guess and the transformed innovation sequence is calculated according to Eqn. 10. The innovation sequence displayed on the screen is examined; if it contains some obvious spikes, a smaller value of C should be used in the next trial; if it shows some platforms, a larger value of C should be used. The process is repeated until the new innovation sequence shows a random noise feature. As soon as the appropriate C is determined, the filter estimate of the robust Kalman filter is obtained simultaneously.

In order to elucidate the influence of the value of C on the innovation sequence and the obvious range of an appropriate C, a simulated example was analyzed in detail. In the simulation, two Gaussian bands $\boldsymbol{a}'$ and $\boldsymbol{b}'$ were generated and each consisted of 100 points with unit peak height. The peak width was fixed at 40, which was the number of points between the peak centre and the location with 2% of the peak height. The locations of the centres of the bands were fixed at the 40th and 75th points. Two component spectra were obtained from $\boldsymbol{a}'$ and $\boldsymbol{b}'$, i.e., $\boldsymbol{a} = 0.8\boldsymbol{a}' + 0.3\boldsymbol{b}'$ and $\boldsymbol{b} = \boldsymbol{b}'$. A mixture spectrum, $\boldsymbol{m} = 0.5(\boldsymbol{a}$

TABLE 1

Influence of limiting factor C on filtering results

C [a]	Predictive results	
	a (0.5000)	*b* (0.5000)
1	0.8108	0.7014
0.5	0.6718	0.6402
0.1	0.5341	0.5281
0.05	0.5168	0.5140
0.01	0.5030	0.5028
0.005	0.5013	0.5014
0.003	0.5007	0.5009
0.002	0.5007	0.5004
0.001	0.4999	0.5004
0.00095	0.4998	0.5004
0.0009	0.4994	0.5006
0.0008	0.5525	1.6284
0.0005	0.4851	70.3458
0.0001	0.1039	121.2193

[a] Referring to Fig. 1.

$+ \boldsymbol{b}$), was constructed by linear combination of $\boldsymbol{a}$ and $\boldsymbol{b}$ and random numbers of normal distribution with zero-mean and a standard deviation of 0.004 were added to simulate the measurement error. Four stochastic points of the mixture spectrum were altered by adding sufficient large random numbers to simulate outliers.

The contributions (concentrations) of components $\boldsymbol{a}$ and $\boldsymbol{b}$ to the mixture spectrum $\boldsymbol{m}$ were estimated by both the ordinary and the robust Kalman filter algorithms with various values of C. Figure 1 presents the innovation sequence of the robust Kalman filter under different values of the limiting factor C and Table 1 shows the corresponding results of filter estimation. The case with $C = 1$, referring to Fig. 1a, is equivalent to the ordinary Kalman filter. It can be seen that the existence of outliers produced a non-random innovation sequence for the ordinary Kalman filter, and the filter estimate was erroneous as expected. From Fig. 1b to 1i the limiting effect increased as C decreased and the influence of outliers was gradually reduced. The corresponding innovation sequence tended to be more and more a random one and the precision of the filter estimate gradually improved. The best result was obtained with a limiting factor of 0.001 (Fig. 1i), when the innovation sequence was almost a white noise sequence. With further decrease in C, some platforms began to appear in the innovation sequence plots and the width of these platforms tended to broaden (see Fig. 1j–n); the innovation sequence did not converge for these cases. The reason for this was that if the limiting action was too strong, the information of many normal measurement points was also decreased and the robust Kalman filter could not acquire enough information for processing. Inspecting the plots of the innovation sequence of the robust Kalman filter with various values of C, one finds sharp peaks in the innovation sequence when too large a value of C is adopted, there are cases when the limiting action is not strong enough to eliminate the effect of outliers and the innovation sequence is still correlated. On the other hand, platforms appear in the resultant innovation sequence when C is too small, and here much useful information contained in the normal measurements was also decreased with the excessive action of limiting. In both situations, the filter estimates were poor; the appropriate limiting factor C should lie between the two extremes and be characterized by a random innovation sequence, which can be determined by several trials with different values of C.

Influence of random error

Several mixtures with different concentration (contribution) ratios of components were constructed based on the same two components $\boldsymbol{a}$ and $\boldsymbol{b}$ as used above, and normal random numbers with zero-mean and three different standard deviations, $s = 0.001$, 0.004 and 0.009, were added to the mixture spectra to simulate the experimental error. In each mixture spectrum four outliers were embedded in the same manner as discussed above. The data were treated with the proposed method together with the ordinary Kalman filter. For each mixture the simulation was repeated ten times for each noise level and the results obtained are given in Table 2. It can be seen that the existence of outliers considerably decreased the performance of the ordinary Kalman filter, but did not have much influence on the robust Kalman filter. As expected, the errors of the filter estimates increased with increase in noise level,

TABLE 2

Results of simulation of two-component systems with three different noise levels

σ	$m = 0.5a + 0.5b$				$m = 1a + 0.1b$				$m = 0.1a + 1b$			
	OKF [a]		RKF [a]		OKF		RKF		OKF		RKF	
	a	b	a	b	a	b	a	b	a	b	a	b
0.001	0.5384	0.5543	0.5005	0.4998	0.9967	0.3935	0.9999	0.1004	−0.6787	1.1114	0.0999	0.9999
	1.3618	0.1261	0.5005	0.4994	0.9150	−0.2885	1.0008	0.0989	−0.2278	1.1645	0.0995	1.0005
	0.6308	0.3440	0.4997	0.4997	1.3114	0.3012	1.0002	0.1003	−0.3715	1.1927	0.0995	1.0001
	1.5194	0.3083	0.5019	0.4500	0.7525	−0.2136	0.9996	0.0995	−1.0507	1.1944	0.0996	0.9999
	0.0173	1.4310	0.4981	0.5018	1.7490	−0.1815	0.9998	0.0996	0.2163	0.6967	0.0999	1.0001
	−0.3917	0.5426	0.4997	0.4997	−1.0966	1.5307	0.4967	0.5020	0.0096	0.8645	0.1002	0.9995
	−0.7201	0.9461	0.4984	0.5004	−0.2407	0.9689	0.9984	0.1017	0.5174	0.9633	0.1000	1.0006
	0.3920	0.4323	0.4980	0.5010	2.4335	−0.9637	1.0010	0.0992	0.0852	0.8915	0.1008	1.0005
	0.3159	0.4899	0.4988	0.5001	0.7479	0.0040	0.9989	0.0990	0.4417	1.1792	0.1001	0.9999
	0.3678	−0.3716	0.4989	0.4990	0.5763	−0.0671	0.9994	0.1000	1.2218	1.6912	0.0999	1.0005
0.004	−0.7424	1.3706	0.4961	0.5035	1.4930	−0.1754	0.9997	0.1005	0.7752	1.2222	0.0993	0.9998
	1.9341	−0.5642	0.5012	0.4990	1.0679	0.1048	1.0004	0.1000	−0.5115	1.2731	0.0991	1.0013
	0.2478	0.4038	0.5000	0.4956	1.4412	−0.1792	1.0014	0.1001	0.3217	0.7942	0.0997	1.0013
	0.4152	0.1108	0.5006	0.4983	0.6727	0.0934	1.0009	0.0996	0.2138	0.9626	0.1004	1.0018
	0.1021	0.7936	0.5003	0.5008	1.4441	0.0328	0.9972	0.1016	−0.2470	1.1437	0.0995	1.0009
	0.8108	0.7014	0.4999	0.5004	0.6257	0.3720	0.9997	0.0994	0.3689	1.1262	0.1005	0.9990
	0.2522	0.1865	0.4992	0.4992	0.5281	0.1335	0.9998	0.1008	−0.3087	1.1799	0.1027	0.9984
	1.2482	0.2186	0.4998	0.4999	0.2838	−0.5275	0.9983	0.0998	−0.2615	1.1488	0.0997	1.0003
	0.0771	0.3328	0.4993	0.5000	−0.5305	0.7784	0.9967	0.1010	−0.5039	1.2567	0.0979	1.0004
	−0.1021	0.7936	0.5003	0.5008	0.9927	0.0776	0.9999	0.0983	0.7335	1.8389	0.1020	1.0003
0.009	0.8190	0.4233	0.4997	0.5018	0.3921	0.3668	0.9997	0.0998	0.6275	−0.1992	0.0979	0.9981
	−0.7323	1.1572	0.4984	0.5002	1.1899	−0.0142	0.9988	0.0995	0.2156	2.5290	0.1044	0.9984
	2.3937	0.0500	0.5034	0.4980	1.4150	−0.0969	1.0007	0.0991	0.2385	0.4744	0.0980	0.9950
	0.8990	0.6684	0.4985	0.5006	1.2747	−1.1340	1.0018	0.0995	0.0857	1.6154	0.1024	1.0002
	1.2027	0.5149	0.4998	0.5009	0.5920	0.8116	0.9958	0.1067	−0.4999	1.2937	0.1006	1.0017
	−1.0966	1.5307	0.4967	0.5020	1.6783	−0.5400	1.0043	0.0980	0.0156	0.6096	0.1010	0.9964
	0.4055	0.5177	0.5026	0.4989	1.0876	−0.2524	0.9980	0.0992	0.4098	1.2018	0.1020	1.0000
	1.1242	0.4909	0.5018	0.5003	1.7038	0.1286	0.9944	0.1054	−0.1484	0.6866	0.0979	0.9981
	1.2215	0.6898	0.5018	0.4990	1.1708	−0.0077	1.0015	0.0983	0.8468	0.7189	0.0973	0.9999
	0.7169	0.4721	0.4998	0.5010	0.2991	0.4445	0.9972	0.1002	−1.1453	1.8735	0.0922	1.0070

[a] OKF = ordinary Kalman filter; RKF = robust Kalman filter.

TABLE 3

Results of simulation of two-component systems at the same noise level

σ	$m = 0.01a + 1b$				$m = 0.005a + 1b$				$m = 0.001a + 1b$			
	OKF		RKF		OKF		RKF		OKF		RKF	
	a	*b*	*a*	*b*	*a*	*b*	*a*	*b*	*a*	*b*	*a*	*b*
0.004	0.3208	1.2014	0.0099	1.0004	−0.5971	1.2936	0.0053	1.0008	1.4351	−0.0642	0.0022	0.9991
	−0.2378	0.6865	0.0092	0.9992	−0.0798	0.6108	0.0061	0.9980	−0.2512	0.9038	0.0010	0.9955
	0.7582	0.7186	0.0088	0.9998	0.3158	1.2014	0.0049	1.0004	−0.4219	0.8328	0.0003	1.0000
	−1.2324	1.8706	0.0061	1.0037	−0.2428	0.6865	0.0042	0.0992	−0.4958	1.3982	0.0006	1.0018

TABLE 4

Influence of spectral overlap (σ = 0.004; total number of points = 100; peak width = 30; number of outliers = 4)

Distance between peaks	OKF						RKF					
	$m = 0.5a + 0.5b + 0.5c$											
	a	*b*	*c*				*a*	*b*	*c*			
20	0.6741	−0.2092	0.7268				0.4897	0.4713	0.5084			
	0.6932	0.3954	0.4648				0.5255	0.5161	0.4806			
	0.3908	0.9236	0.5392				0.4991	0.5011	0.4990			
15	0.3672	0.4664	1.4855				0.5002	0.4986	0.5009			
	1.0749	−0.4005	1.1878				0.5003	0.4957	0.5011			
	0.9177	0.3886	0.4897				0.5083	0.5044	0.4928			
10	−1.1349	1.0122	0.5967				0.4646	0.5162	0.4994			
	1.6372	0.3406	0.1501				0.5054	0.5135	0.4844			
	0.8224	−0.2630	0.2749				0.5010	0.4980	0.5012			
5	1.8138	−1.3278	1.1112				0.5035	0.4987	0.4959			
	−5.1108	9.4324	−2.5523				0.4921	0.5150	0.4943			
	1.1363	−2.0106	2.5136				0.4982	0.5023	0.5030			
	$m = 0.5a + 0.5b + 0.5c + 0.5d$											
	a	*b*	*c*	*d*			*a*	*b*	*c*	*d*		
25	0.4731	0.6003	0.5068	0.8941			0.4877	0.5060	0.4997	0.5106		
	0.9075	0.1782	0.1622	0.3550			0.4964	0.4980	0.5105	0.4987		
	1.5787	0.2003	0.4318	0.5170			0.5122	0.4851	0.4937	0.5003		
	$m = 0.5a + 0.5b + 0.5c + 0.5d + 0.5e$											
	a	*b*	*c*	*d*	*e*		*a*	*b*	*c*	*d*	*e*	
20	0.3033	0.9458	0.6855	0.2119	0.6208		0.4877	0.5165	0.4987	0.4902	0.5057	
	1.0664	0.4082	−0.2858	0.8724	0.7701		0.4944	0.5056	0.4880	0.4979	0.5088	
	0.5254	0.4824	0.9236	0.1461	0.6168		0.4850	0.5114	0.5123	0.4906	0.5042	
	$m = 0.5a + 0.5b + 0.5c + 0.5d + 0.5e + 0.5f$											
	a	*b*	*c*	*d*	*e*	*f*	*a*	*b*	*c*	*d*	*e*	*f*
15	0.6674	0.1751	0.8097	1.3007	0.1606	0.6895	0.4851	0.5100	0.4928	0.5106	0.5084	0.4973
	0.3151	1.0068	−0.5109	0.4158	0.5839	0.4512	0.4771	0.5310	0.4792	0.4829	0.5136	0.4995
	−0.0385	1.6250	−0.5173	0.0855	0.8692	0.2947	0.4569	0.5630	0.4536	0.4748	0.5240	0.4873

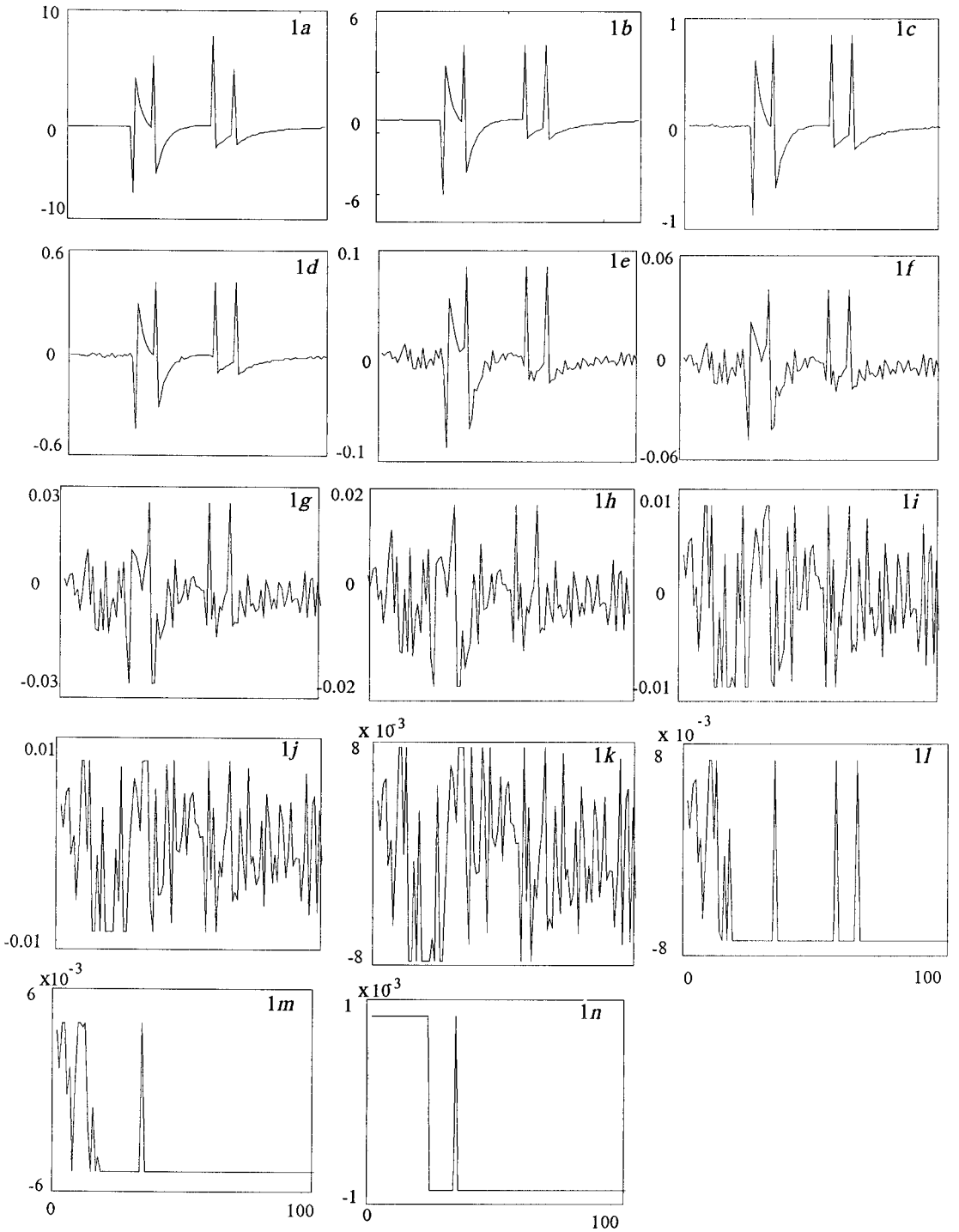

Fig. 1. Innovation sequence obtained with different values of the limiting factor C: (a) 1.0; (b) 0.5; (c) 0.1; (d) 0.05; (e) 0.01; (f) 0.005; (g) 0.003; (h) 0.002; (i) 0.001; (j) 0.00095; (k) 0.0009; (l) 0.0008; (m) 0.0005; (n) 0.0001. Abscissas: measurement numbers, k. Ordinates: innovation, INV (k).

especially for the components with lower concentrations. Table 3 shows the results obtained for various component concentration ratios at the same noise level. The lower the concentration, the worse are the estimated results, but it seems that those components with lower concentrations did not substantially influence the analytical results for the components with higher concentrations.

Influence of spectral overlap

The influence of spectral overlap was studied with some three- to six-component systems. Different spectral overlapping was simulated by changing the distance among peaks (i.e., the centre of the bands) of the components in the system. All components were generated by using pure Gaussian bands and the parameters are given in Table 4. It can be seen that the robust Kalman filter can provide satisfactory results for mixtures with considerable spectral overlap.

Influence of total number of outliers

The influence of the total number of outliers was studied by simulation using mixtures of a three-component system and the locations of outliers were determined by using random numbers. The results are given in Table 5 and show that more than ten outliers did not have a significant influence on the filtering results of the robust Kalman filter.

Interpretation of real analytical systems

Spectrophotometric data for phenol–resorcinol mixtures were treated with both the ordinary and the robust Kalman filter. This data set does not contain any outliers, and the filtering results

TABLE 5

Effect of number of outliers (σ = 0.004; peak width = 30; total number of points = 100)

Number of outliers	$m = 0.5a + 0.5b + 0.5c$					
	OKF			RKF		
	a	*b*	*c*	*a*	*b*	*c*
4	0.2042	0.7001	0.09554	0.5007	0.5009	0.5015
	0.3244	0.3694	0.4994	0.5011	0.5017	0.5005
	0.6027	0.1970	−0.0271	0.5037	0.4989	0.4964
5	0.6803	0.6401	0.7988	0.5057	0.4960	0.5070
	0.7372	−1.4336	1.0590	0.5012	0.4930	0.5000
	1.3202	−0.6704	0.6424	0.5089	0.4895	0.5018
6	0.3003	0.3974	1.5554	0.4976	0.4993	0.5057
	−0.9947	1.2753	1.0443	0.4966	0.5057	0.5046
	0.6640	−0.8951	0.5403	0.5026	0.4875	0.5002
7	0.0654	−0.1655	0.8815	0.4972	0.4784	0.5069
	0.1259	0.3323	0.7500	0.4996	0.4970	0.5013
	0.5131	0.7571	0.8599	0.5000	0.5035	0.5060
8	0.7851	1.1050	0.6354	0.4978	0.5262	0.5033
	0.8054	−0.2874	0.0885	0.5036	0.4990	0.4936
	0.8338	0.0142	0.2740	0.5006	0.4996	0.4937
9	1.3563	−1.4300	0.3306	0.5036	0.4954	0.4989
	1.4752	−0.5412	1.4632	0.5014	0.4971	0.5030
	0.5399	2.1251	0.1194	0.4989	0.5038	0.4983
10	0.5317	0.9182	0.6962	0.5028	0.5012	0.4977
	0.2782	0.8169	0.3766	0.4979	0.5061	0.4963
	−0.1176	1.5222	0.1057	0.4967	0.5027	0.4999
11	0.4604	3.0980	−0.0728	0.4884	0.6127	0.4832
	0.5826	2.6083	0.4587	0.4975	0.5055	0.5013
	−0.8032	0.3380	0.9612	0.4976	0.5107	0.5081
12	1.4229	−0.2701	0.6789	0.5131	0.5047	0.5034

TABLE 6

Comparison of results with the ordinary and robust Kalman filters for spectrophotometric analysis of phenol (P) and resorcinol (R) mixtures

No.	Species	True value (mg ml^{-1})	found by OKF (mg ml^{-1})	Recovery (%)	Found by RKF (mg ml^{-1})	Recovery (%)
1	P	0.0303	0.0310	102.3	0.0307	101.4
	R	0.0299	0.0290	96.99	0.0292	97.66
2	P	0.0202	0.0201	99.50	0.0199	98.51
	R	0.0199	0.0200	100.5	0.0202	101.5
3	P	0.0051	0.0053	96.23	0.0051	100.0
	R	0.0498	0.0491	98.59	0.0491	98.59
4	P	0.0202	0.0211	104.5	0.0209	103.5
	R	0.0299	0.0288	96.32	0.0290	97.00
5	P	0.0252	0.0251	99.60	0.0249	98.81
	R	0.0249	0.0243	97.59	0.0245	98.39
6	P	0.0252	0.0258	102.4	0.0256	101.6
	R	0.0249	0.0234	94.00	0.0236	94.78
7	P	0.0303	0.0302	99.67	0.0299	98.68
	R	0.0199	0.0194	97.49	0.0196	98.49
8	P	0.0498	0.0500	100.4	0.0499	100.2
	R	0.0000	−0.0002	–	−0.0001	–
9	P	0.0498	0.0497	99.80	0.0497	99.80
	R	0.0000	0.0002	–	0.0000	–
10	P	0.0000	0.0002	–	0.0000	–
	R	0.0505	0.0494	97.82	0.0494	97.80

given in Table 6 show that the robust Kalman filter is capable of providing results comparable to those of the ordinary Kalman filter in this instance. This is an important prerequisite for robust statistics, as mentioned in the Introduction. As the simulation studies clearly show that the ordinary Kalman filter is non-robust, a robust Kalman filter is highly recommended for cases when the influence of possible outliers should be taken into consideration.

This work was supported by the National Natural Science Foundation of China. The authors thank Dr. Zhi-Liang Li for valuable assistance.

REFERENCES

1 R.-Q. Yu, Introduction to Chemometrics, Hunan Education Publishing House, Changsha, 1991.
2 C.J. Masreliez and R.D. Martin, IEEE Trans. Autom. Control, AC-22 (1977) 361.
3 Y.-M. Liu and R.-Q. Yu, Talanta, 35 (1988) 707.

ANALYTICA CHIMICA ACTA, VOL. 269 (1992)

AUTHOR INDEX

PUBLICATION SCHEDULE FOR 1993

	S'92	O'92	N'92	D'92	J	F
Analytica Chimica Acta	267/1 267/2	268/1 268/2	269/1 269/2	270/1 270/2	271/1 271/2	272/1 272/2
Vibrational Spectroscopy		4/1				4/2

INFORMATION FOR AUTHORS

Manuscripts. The language of the journal is English. English linguistic improvement is provided as part of the normal editorial processing. Authors should submit three copies of the manuscript in clear double-spaced typing on one side of the paper only. *Vibrational Spectroscopy* also accepts papers in English only.

Abstract. All papers and reviews begin with an Abstract (50–250 words) which should comprise a factual account of the contents of the paper, with emphasis on new information.

Figures. Figures should be prepared in black waterproof drawing ink on drawing or tracing paper of the same size as that on which the manuscript is typed. One original (or sharp glossy print) and two photostat (or other) copies are required. Attention should be given to line thickness, lettering (which should be kept to a minimum) and spacing on axes of graphs, to ensure suitability for reduction in size on printing. Axes of a graph should be clearly labelled, along the axes, outside the graph itself. All figures should be numbered with Arabic numerals, and require descriptive legends which should be typed on a separate sheet of paper. Simple straight-line graphs are not acceptable, because they can readily be described in the text by means of an equation or a sentence. Claims of linearity should be supported by regression data that include slope, intercept, standard deviations of the slope and intercept, standard error and the number of data points; correlation coefficients are optional.

Photographs should be glossy prints and be as rich in contrast as possible; colour photographs cannot be accepted. Line diagrams are generally preferred to photographs of equipment.

Computer outputs for reproduction as figures must be good quality on blank paper, and should preferably be submitted as glossy prints.

Nomenclature, abbreviations and symbols. In general, the recommendations of the International Union of Pure and Applied Chemistry (IUPAC) should be followed, and attention should be given to the recommendations of the Analytical Chemistry Division in the journal *Pure and Applied Chemistry* (see also *IUPAC Compendium of Analytical Nomenclature, Definitive Rules*, 1987).

References. The references should be collected at the end of the paper, numbered in the order of their appearance in the text (*not* alphabetically) and typed on a separate sheet.

Reprints. Fifty reprints will be supplied free of charge. Additional reprints (minimum 100) can be ordered. An order form containing price quotations will be sent to the authors together with the proofs of their article.

Papers dealing with vibrational spectroscopy should be sent to: Dr J.G. Grasselli, 150 Greentree Road, Chagrin Falls, OH 44022, U.S.A. Telefax: (+1-216) 2473360 (Americas, Canada, Australia and New Zealand) or Dr J.H. van der Maas, Department of Analytical Molecule Spectrometry, Faculty of Chemistry, University of Utrecht, P.O. Box 80083, 3508 TB Utrecht, The Netherlands. Telefax: (+31-30) 518219 (all other countries).

0003-2670/92/$05.00

This issue is printed on acid-free paper.

PRINTED IN THE NETHERLANDS

COMPREHENSIVE ANALYTICAL CHEMISTRY

edited by **G. Svehla**, *formerly edited by* **C.L. Wilson** *and* **D.W. Wilson**

Volume XXIX
Chemiluminescence Immunoassay

by **I. Weeks**

This is the first work to present the topic as a subject in its own right. In order to provide a complete picture of the subject, overviews are presented of the individual areas of chemiluminescence and immunoassay with particular emphasis on the requirements for interfacing chemiluminescent and immunochemical reactions.

1992 xvi + 294 pages
Price: US $ 151.50 / Dfl. 295.00
Subscription price:
US $ 136.00 / Dfl. 265.00
ISBN 0-444-89035-1

Volume XXVIII
Analysis of Substances in the Gaseous Phase

by **E. Smolková-Keulemansová** *and* **L. Feltl**

The present volume provides a comprehensive description of the state-of-the-art and of future possibilities in the analysis of gaseous substances. In the individual chapters the following themes have been discussed; the theoretical basis for the methods, a description of the instrumentation and the steps necessary in actual analyses and an outline of the principal areas in which each method can be employed.

1991 xiv + 480 pages
Price: US $ 228.50 / Dfl. 400.00
Subscription price:
US $ 205.50 / Dfl. 360.00
ISBN 0-444-89122-6

Volume XXVII
Analytical Voltammetry

edited by **M.R. Smyth** *and* **J.G. Vos**

The aim of this volume is to review the state-of-the-art in analytical voltammetry with regard to theory and instrumentation, and show how these relate to the analysis of inorganic, organometallic, organic and biological molecules.

1992 xxvi + 578 pages
Price: US $ 283.00 / Dfl. 495.00
Subscription price:
US $ 254.00 / Dfl. 445.00
ISBN 0-444-88938-8

Volume XXVI
Radionuclide X-Ray Fluorescence Analysis with Environmental Application

by **J. Tölgyessy, E. Havránek** *and* **E. Dejmková**

This work discusses the use of radionuclide XRFA for solving analytical problems of the environment and information is presented concerning the current state of research and use of radionuclide XRFA in this significant area.

1990 282 pages
Price: US $ 134.50 / Dfl. 235.00
Subscription price:
US $ 120.00 / Dfl. 210.00
ISBN 0-444-98837-8

Distributed in the East European Countries, China, Cuba, Mongolia, North Korea and Vietnam by SLOVART

"...a valuable addition to the well-known series... This book deserves to be recommended to analytical chemists inexperienced in environmental problems and also to environmental scientists planning to apply XRFA to solve their problems, as it gives readily available information."
Analytica Chimica Acta

Volume XII E
Thermal Analysis

edited by **W.W. Wendtlandt**

Part E: Pulse Method of Measuring Basic Thermophysical Parameters

by **L'. Kubicár**

This book provides a systematic analysis of sources of scatter in experimental data, and describes experimental apparatus for measuring specific heats, thermal diffusivities and thermal conductivities in the temperature range 80-1300 K. Information is given on the measurement of thermophysical parameters of selected materials. The work also lists the most important results published so far on the use of the pulse method.

1990 370 pages
Price: US $ 165.50 / Dfl. 290.00
Subscription price:
US $ 151.50 / Dfl. 265.00
ISBN 0-444-98851-3

ORDER INFORMATION

For USA and Canada
ELSEVIER SCIENCE PUBLISHERS
Judy Weislogel
P.O. Box 945
Madison Square Station,
New York, NY 10160-0757
Tel: (212) 989 5800
Fax: (212) 633 3880

In all other countries
ELSEVIER SCIENCE PUBLISHERS
P.O. Box 211
1000 AE Amsterdam
The Netherlands
Tel: (+31-20) 5803 753
Fax: (+31-20) 5803 705

US$ prices are valid only for the USA & Canada and are subject to exchange fluctuations; in all other countries the Dutch guilder price (Dfl.), is definitive. Books are sent postfree if prepaid.

ELSEVIER
SCIENCE PUBLISHERS